UNIVERSITY OF LIVERPOOL

Hydrodeoxygenation of bio-derived oxygenates over bifunctional metal-acid catalysts in the gas phase

Thesis submitted in accordance with the requirements of the University of Liverpool for the degree of Doctor in Philosophy

by

Khadijah Hamed Alharbi

July 2017

Abstract

Hydrodeoxygenation of bio-derived oxygenates over bifunctional metal-acid catalysts in the gas phase

PhD thesis by Khadijah Alharbi

Biomass-derived organic oxygenates, such as ketones, carboxylic acids, alcohols, phenols, ethers and esters, obtained from fermentation, acid-catalysed hydrolysis and fast pyrolysis of biomass are attractive as renewable raw materials for the production of value-added chemicals and bio-fuels. For fuel applications, these oxygenates require reduction in oxygen content to increase their caloric value. Much current research is focused on the deoxygenation of renewable organic oxygenates using heterogeneous catalysis.

The aim of this thesis is to investigate the hydrodeoxygenation (HDO) of organic oxygenates, including aliphatic and aromatic ketones, ethers and esters, using bifunctional metal-acid catalysis in the gas phase to produce value-added chemicals and bio-fuels. The bifunctional catalysts comprise Pt, Ru, Ni and Cu as the metal components and a caesium acidic salt of Keggin-type tungstophosphoric heteropoly acid ($H_3PW_{12}O_{40}$, HPA), $Cs_{2.5}H_{0.5}PW_{12}O_{40}$ (CsPW), as the acid component, with the main focus on the Pt–CsPW catalyst. We also report enhancing effect of Au on the HDO of ketones over Pt-CsPW. A variety of techniques were used to characterise these catalysts. These techniques include BET, TGA, gas chemisorption, ammonia adsorption calorimetry, STEM-EDX, XRD, ICP, elemental analysis (C, H combustion analysis) and FTIR.

The bifunctional catalysed HDO of ketones to form alkanes occurs via a sequence of steps involving hydrogenation of ketone to alcohol on metal sites followed by dehydration of alcohol to alkene on acid sites and finally hydrogenation of alkene to alkane on metal sites.

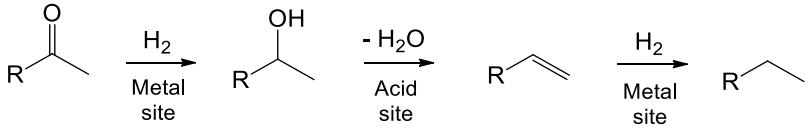

It is demonstrated that the bifunctional HDO pathway is more efficient than the monofunctional metal catalysis. Catalyst activity decreases in the order of metals: Pt > Ru >> Ni > Cu. 0.5%Pt/CsPW is a versatile catalyst for the HDO of aliphatic ketones, giving almost 100% alkane yield at 100 ^{o}C and 1 bar pressure. Evidence is provided that the reaction with Pt/CsPW at 100 ^{o}C is limited by ketone-to-alcohol hydrogenation, whereas at lower temperatures ($\leq$ 60 ^{o}C) by alcohol dehydration resulting in formation of alcohol as the main product. The catalyst composed of a physical mixture Pt/C + CsPW is highly efficient as well, which indicates that the reaction is not limited by migration of intermediates between metal and acid sites in the bifunctional catalyst. Notably, the mixed Pt/C + CsPW shows better performance stability in acetophenone HDO as compared to the Pt/CsPW catalyst, which suffers from deactivation.

We also demonstrate enhancing effect of gold on the activity and stability of Pt/CsPW catalyst in HDO of 3-pentanone. Gold additives increase the turnover rate of 3-pentanone HDO at Pt sites. In addition, the bimetallic catalyst PtAu/CsPW shows the preference of C=O over C=C bond hydrogenation in comparison to the unmodified Pt/CsPW catalyst. STEM-EDX and XRD analysis indicates the presence of bimetallic nanoparticles with a wide range of Pt/Au atomic ratios in the PtAu/CsPW catalysts. The gold enhancing effect on the HDO of ketones over Pt-CsPW can be attributed to PtAu alloy effects (ensemble and ligand effects). Catalyst modification with gold can be a promising methodology to enhance the HDO of biomass-derived feedstock using platinum group metal catalysts.

In the HDO of ethers and esters, including the aromatic ether anisole, the aliphatic diisopropyl ether (DPE) and the aliphatic ester ethyl propanoate (EP), bifunctional metal-acid catalysis is also more efficient in comparison to the corresponding monofunctional metal and acid catalysis. Moreover, it has been found that metal- and acid-catalysed pathways play a different role in these reactions.

Hydrodeoxygenation of anisole is a model for the deoxygenation of lignin. With Pt-CsPW, it occurs with almost 100% yield of cyclohexane under very mild conditions at 60-100 ^{o}C and 1 bar H_2 pressure. In this reaction, Pt-catalysed hydrogenation plays the key role, with a relatively moderate assistance of acid catalysis, further increasing the cyclohexane selectivity. The preferred catalyst formulation is a uniform physical mixture of Pt/C or Pt/SiO_2 with excess CsPW, with a Pt content of 0.1-0.5%, which provides much higher activity and better catalyst stability to deactivation as compared to the Pt/CsPW catalyst prepared by impregnation of platinum onto CsPW. The Pt/C + CsPW mixed catalyst has the highest activity in anisole deoxygenation for a gas-phase catalyst system reported so far. In contrast to anisole, the aliphatic ether DPE decomposes readily over CsPW via acid-catalysed pathway (E1 mechanism) without metal assistance to give propene and isopropanol. Propene selectivity increases with reaction temperature at the expense of isopropanol. Platinum alone (Pt/C), in the absence of CsPW, is inactive in this reaction, either under H_2 or N_2. However, in the presence of Pt-CsPW under H_2, DPE decomposition is significantly accelerated, yielding the more thermodynamically favorable product propane instead of propene.

Decomposition of the EP aliphatic ester is also very efficient via acid-catalysed pathway without metal assistance to yield ethene and propanoic acid. Addition of Pt to CsPW under H_2 causes hydrogenation of ethene to ethane but does not affect the rate of EP decomposition. Nevertheless, the Pt-CsPW bifunctional catalyst under H_2 shows much better performance stability in EP

decomposition in comparison to the CsPW acid catalyst. This can be attributed to reduction of catalyst coking in the presence of Pt and H_2.

Kinetics of the acid-catalysed decomposition of DPE and EP was studied with a wide range of tungsten HPA catalysts. Good linear relationships between the logarithm of turnover reaction rate (TOF) and the HPA catalyst acid strength represented by ammonia adsorption enthalpies were obtained, which can be used to predict the activity of other Brønsted acid catalysts in these reactions.

The main results obtained in this thesis are disseminated in the following publications and conference presentations:

Published papers:

1. K. Alharbi, E. F. Kozhevnikova, I. V. Kozhevnikov, Appl. Catal. A 504 (2015) 457.
2. O. Poole, K. Alharbi, D. Belic, E. F. Kozhevnikova, I. V. Kozhevnikov, Appl. Catal. B 202 (2017) 446.
3. K. Alharbi, W. Alharbi, E. F. Kozhevnikova, I. V. Kozhevnikov, ACS Catal. 6 (2016) 2067.

Poster presentations:

1. K. Alharbi, E. F. Kozhevnikova, I. V. Kozhevnikov, Hydrodeoxygenation of methyl isobutyl ketone (MIBK) over bifunctional metal-acid catalyst in the gas phase, Poster Day, University of Liverpool, Liverpool, UK, 10th April, 2014.
2. K. Alharbi, E. Kozhevnikova, I. V. Kozhevnikov, Hydrodeoxygenation of methyl isobutyl ketone (MIBK) over bifunctional metal-acid catalyst in the gas phase, 4th Northern Sustainable Chemistry (4th NORSC), Huddersfield University, Huddersfield, UK, 23rd October, 2014.
3. K. Alharbi, E. F. Kozhevnikova, I. V. Kozhevnikov, Hydrogenation of ketones over bifunctional Pt-heteropoly acid catalyst in the gas phase, 8th Saudi Students Conference (SSC), Queen Elizabeth II Centre, London, UK, 31st January - 1st February, 2015.
4. K. Alharbi, E. F. Kozhevnikova, I. V. Kozhevnikov, Deoxygenation of ethers and esters over bifunctional Pt−heteropoly acid catalyst in the gas phase, Catalysis fundamentals and practice summer school, University of Liverpool, Liverpool, UK, 20th -24th July, 2015.

5. K. Alharbi, E. F. Kozhevnikova, I. V. Kozhevnikov, Hydrogenation of ester over bifunctional Pt-polyoxometalate and acid catalysts in the gas phase, 9th Saudi Students Conference (SSC), The ICC Birmingham Broad Street, Birmingham, UK, 13th-14th February, 2016.
6. K. Alharbi, M. A. Alotaibi, E. F. Kozhevnikova, I. V. Kozhevnikov, Hydrodeoxygenation of biomass-derived ketones over bifunctional metal-acid catalysts in the gas phase, Designing New Heterogeneous Catalysts: Faraday Discussion, Burlington House, London, UK, 4th-6th April, 2016.

Acknowledgements

The most important acknowledgment of gratitude I wish to express is to my supervisor, Professor Ivan Kozhevnikov, for his excellent guidance, support and encouragement during my study. It was a pleasure working with him.

I would like to express my deepest sense of gratitude for Dr Elena Kozhevnikova for kind assistance and resolution of all technical issues through my laboratory work. Without her assistance, this research could not be performed so smoothly and effectively.

I would like also to thank all member at the University of Liverpool, especially the technical support team in Chemistry Department.

It is a pleasure to record my thanks to all members in my group for their cooperation and sharing knowledge.

I extend my heartfelt gratitude to my parents for their big support and faith in me through my study. Thanks for their love.

I would like to express my deepest appreciate to my mother-in-law, my brother Hani and my best freind Walaa for being with me through my study abroad giving the happiness and motivation to me.

My special thanks to my husband Wael and my kids. Without their constant support and love none of this would have been possible.

Finally, I would like to acknowledge the financial support of the King Abdulaziz University. I also appreciate the financial management of the Saudi Arabia Cultural Bureau in the UK.

Abbreviations

HDO	Hydrodeoxygenation
HPA	Heteropoly acid
HPW	Tungstophosphoric acid ($H_3PW_{12}O_{40}$)
HSiW	Tungstosilicic acid ($H_4SiW_{12}O_{40}$)
CsPW	Caesium salt ($Cs_{2.5}$) of tungstophosphoric acid ($H_3PW_{12}O_{40}$)
POM	Polyoxometalate
BET	Brunauer-Emmett-Teller method
TGA	Thermogravimetric analysis
ICP	Inductively coupled plasma
XRD	X-ray diffraction
TCD	Thermal conductivity detector
STEM	Scanning transmission electron microscopy
EDX	Energy dispersive X-ray emission
FTIR	Fourier transform infrared spectroscopy
GC	Gas chromatography
FID	Flame ionisation detector
MIBK	Methyl isobutyl ketone
MP	Methyl pentane
MP-ol	Methyl pentanol
DIBK	Diisobutyl ketone
EP	Ethyl propanoate
DPE	Diisopropyl ether
TOF	Turnover frequency

Contents

1. Introduction

1.1 Heterogeneous catalysis

1.1.1 Definition and background of catalysis

The word catalysis comes from the Greek prefix of kata-, which means down, and the verb lysein, which means to break. In 1836, Berzelius introduced the word catalysis in his attempt to describe the unusual findings discovered by earlier scientists [1]. By definition, a catalyst is a material that can accelerate the rate of chemical reaction without being substantially consumed in the reaction [2, 3]. A catalyst acts by reducing the activation energy of the rate limiting step providing an alternative pathway to avoid the slowest step in the uncatalysed reaction [4].

Various examples of catalysis have been known since ancient times. Perhaps the earliest example of a catalyst was the use of natural yeasts for the fermentation of the sugar contained in biological material such as grapes to produce wine and beer [5]. Many applications of catalysis were developed during the 19th Century. Table 1.1 exhibits some examples of early large scale catalytic processes with their notable dates [2]. Nowadays, it is estimated that 90% of industrial chemical processes use catalysts at least at one stage; therefore, catalysis is extremely important economically [2, 6].

Table 1.1 Some large scale catalytic processes [2].

Reaction (discoverer)	Catalyst (date)
$2HCl + ½\ O_2 \rightarrow H_2O + Cl_2$ (Deacon)	$CuCl_2$ (1860)
$SO_2 + ½\ O_2 \rightarrow SO_3$ (Phillips)	Pt (1875)
$CH_4 + H_2O \rightarrow CO + 3H_2$ (Mond)	Ni (1888)
$2NH_3 + 5/2O_2 \rightarrow 2NO + 3H_2O$ (Ostwald)	Pt foil (1901)
$C_2H_4 + H_2 \rightarrow C_2H_6$ (Sabatier)	Pt (1902)
$N_2 + 3H_2 \rightarrow 2NH_3$ (Haber)	Fe (1914)

1.1.2 Classification of catalytic systems

In fact, catalytic systems can be divided into two main categories: homogeneous and heterogeneous catalysis [1, 7, 8]. Homogeneous catalysis occurs when the catalyst and reactant are in the same phase and thus no phase boundary exists. This can occur either in the gas phase, for example when using a nitrogen oxide catalyst in the oxidation of sulfur oxide; or in the liquid phase, such as using acid and base catalysts in the mutarotation of glucose. Another type of catalytic system is heterogeneous catalysis, which occurs when the catalyst and reactant are in different phases (gas-solid, liquid-solid or biphasic liquid-liquid).

Most of the large scale industrial catalysis processes are heterogeneous owing to the advantages of easy catalyst regeneration after reaction, less corrosion and easy catalyst separation form the reaction mixture [9-11]. Historically, the earliest research on heterogeneous catalysis can be

traced back to the early 19th Century, when Faraday discovered the first heterogeneously catalysed reaction using platinum for an oxidation reaction [1, 12].

Heterogeneous catalysis in gas-solid and liquid-solid systems is interesting since it presents the opportunity to deposit and immobilize the active substance on the solid surface. More important, however, is the difference between the surface and bulk properties. The surface of a solid material is an abrupt termination of its bulk structure that serves to expose all the surface atoms in an asymmetric environment. These atoms on the surface have lower coordination than the atoms in the bulk, hence the surface atoms are ready for interaction with incoming reactant molecules in order to satisfy their bonding requirements [13]. Since the reaction takes place on the solid surface of the catalyst, the reactivity of the surface atoms is vital in determining the effectiveness of the catalyst and the efficiency of a catalytic process.

1.1.3 Key steps in a heterogeneously catalysed reaction

A gas-phase chemical process occurring over a heterogeneous metal catalyst is illustrated in Figure 1.1. It consists of the following steps [2]:

1) Gas phase diffusion of reactant molecules to the surface of the metal.
2) Adsorption of the molecules to the metal surface.
3) Dissociation of the molecules into atoms may occur on the metal surface (depending on their internal bond strength).
4) Reaction between dissociated molecules at the surface to form a product; this may often be the rate-limiting step.
5) Desorption of the product to the gas phase, where the bond between the product and the surface is broken.

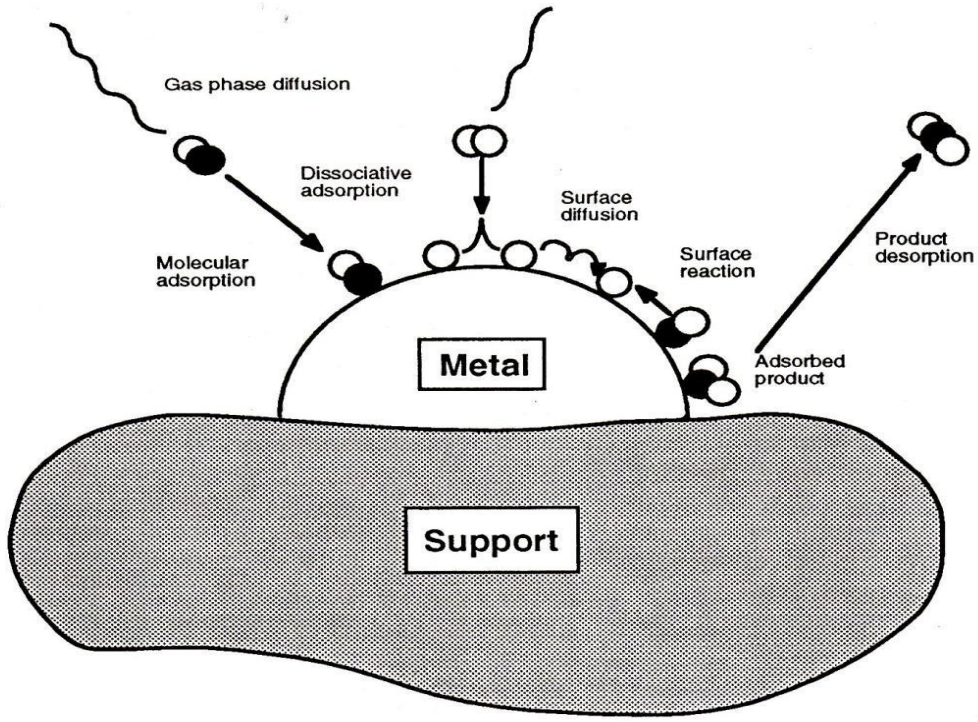

Figure 1.1 Molecular and atomic events occurring in a heterogeneous catalytic reaction on a supported metal catalyst [2].

1.1.4 What makes a good catalyst?

There is a wide range of factors to be taken into account when designing and developing an appropriate catalyst for a particular reaction process [2, 14]. The first property to be considered is the active phase of the catalyst, which is vital for kinetic reaction parameters (represented as a space-time yield). The correct active phase is the fundamental aspect of catalyst preparation. Secondly, the surface area of the catalyst is very important. A high surface area is generally required to produce an optimum yield, although, in some cases, a modest surface area is required to prevent further reactions of the desired products. The longevity and mechanical strength of the catalyst are also very important parameters in catalyst design. If a catalyst is used commercially, stability is important for the catalyst to be considered for further development. Catalyst deactivation can be caused by sintering (reduction of the active phase surface area), or poisoning (reduction of the active site density) e.g. coke formation on some catalysts through organic

reaction. Another factor to be considered in choosing a catalyst is the cost of its production; this must be low compared to the selling price of the product.

1.1.5 Catalysis by metals

Table 1.2 exhibits various examples where metallic catalysts are used in commercial processes. The most common metals used in catalytic processes are the transition metals due to their unfilled d-bands. Almost all metals in the periodic table can be used, however [1, 5].

Table 1.2 Some commercial processes using metal catalysts [5].

Process	**Catalyst**
Ammonia synthesis	Promoted iron
Ammonia oxidation	Pt/Ru gauze
Fisher-Tropsch synthesis	Fe or Co on support
Steam reforming of methane	Ni on support (typically Al_2O_3)
Methanol synthesis	$Cu/Zn/Al_2O_3$
Methanol oxidation	Unsupported silver, BiMo
Reforming of hydrocarbons	Pt/Re/support
Automobile exhaust treatment	$Pt/Pt/CeO_2/Al_2O_3$
Selective reduction of NO_x in flue-gas	V_2O_5/TiO_2/Matrix support
Ethylene oxidation	$Ag/\alpha\text{-}Al_2O_3$
Fat hardening	Ni/Al_2O_3

Although the most common metal catalysts consist of supported metals, there are several examples of processes that can be carried out over pure metals. The most well-known example of an unsupported metallic catalyst is the platinum gauze used for ammonia oxidation. Sintering often occurs in the case of pure metal, however, due to the relatively high temperatures of use,

and therefore stabilization of the metal particles is required to achieve the highest possible surface area. The addition of a promoter can help to achieve this stabilization by anchoring the metal on the surface and avoiding surface migration. In the case of Pt/Rh gauzes for the oxidation of ammonia mentioned above, the surface rearrangement is slowed by the addition of Rh on the surface of Pt. Another example where a promoter is used for metal stabilization is the addition of alumina in the case of Raney nickel [5].

The surface area of the metallic catalyst is important since the reaction rate is usually determined by the rate of the surface reaction. It is therefore vital to create the highest possible accessible metal surface area. For this reason, supported metal catalysts are often used [5].

Preparation methods for supported catalysts have been widely developed to create very small metal crystallites on high surface area supports. There is a wide range of support materials that can be used for catalyst preparation [15]. Single oxides such as alumina (Al_2O_3) or silica (SiO_2), and complex oxides such as silica-alumina or zeolites and active carbons are the most commonly used supports. In fact, the support itself may not only be an inert material in which the metal is placed, it can also enhance catalyst performance [5].

Gold has been long considered to be an inactive catalyst; when a suitable preparation method provides high metal dispersion, however, gold becomes active for various reactions including CO oxidation. An early application of these catalysts was pioneered by Haruta [16] and Hutchings [17] who disclosed the peculiarity of the activity of gold in CO oxidation and other reactions. Since then gold catalysis has become an important topic in the field of catalysis [18].

Recently, several comprehensive reviews and two books have given a good overview of gold nanoparticles as a catalyst [19-23]. Very good reviews were given by Daniel and Astruc and Bond, Louis and Thompson, exhaustively covering all aspects related to the preparation and stabilisation of gold nanoparticles [24].

Generally, gold in heterogeneous catalysis is supported on the outer surface of a solid support. Micro-/meso-porous materials such as silica and metal oxides can be used as hosts in which Au is combined to increase the total surface area and control the selectivity of the process [24].

1.2 Multifunctional catalysis

Nowadays, much attention is being given to the development of cascade (tandem) processes using multifunctional catalysts for the production of organic compounds without intermediate separation. These catalysts contain two or more different active sites working synergistically to effect several chemical transformations in one pot or on a single catalyst bed [25].

Figure 1.2 shows a step-by-step process in which the starting material A is converted to the final product D through a three-step reaction which involves the formation of intermediate products B and C (solid arrows). This process requires the isolation and purification of the intermediates B and C, making the operation both costly and time consuming. These drawbacks can be overcome, however, by using a more efficient and environmentally friendly tandem process with a multifunctional catalyst (broken arrows) [26-28].

A wide range of metal supported bifunctional catalysts are used in heterogeneous catalysis processes, such as hydrogenation, dehydrogenation and hydroisomerisation reactions [29]. Much of the research regarding heterogeneous multifunctional catalysis has concentrated on developing catalysts consisting of transition metals supported on an active support having acidic and/or basic sites for multistage reactions.

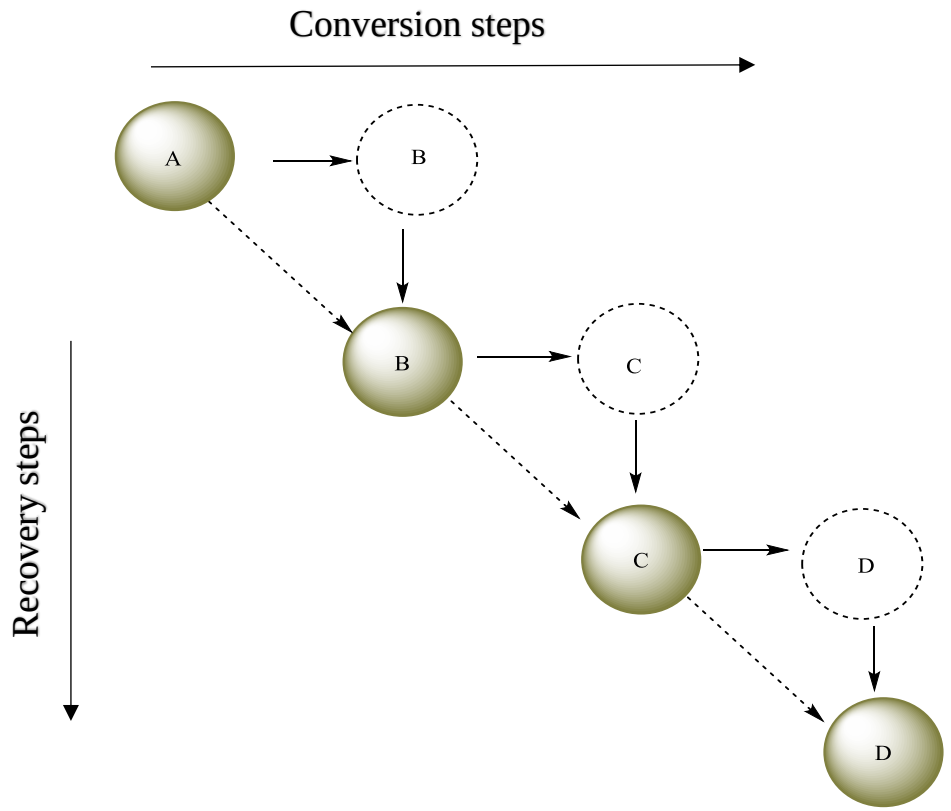

Figure 1.2 Multistage organic synthesis where the starting material A is converted to the desirable product D through B and C intermediates [26]. Broken arrows represent a tandem process to form the final product without recovery steps after each conversion step.

The group VIII transition metals (e.g. Pt, Pd, Ni, Ru) have been shown to be efficient metal catalysts in a number of catalytic processes. For example, platinum can be introduced using different Pt precursors; however, the most commonly used are chloroplatinic acid (H_2PtCl_6) and platinum (II) tetramine ion, $[Pt(NH_3)_4]^{2+}$ [15].

Different preparation procedures are used to introduce metal precursors onto the support, such as impregnation, ion-exchange or co-precipitation, followed by drying and calcination followed by reduction. Calcination has the purpose of decomposing the metal precursor on the support to achieve the highest metal dispersion [15]. The metal dispersion (metal particle size) can be affected by the preparation procedures and type of precursor used, and these, therefore, affect the activity and selectivity of multifunctional metal catalysts.

Bifunctional metal supported acid/base catalysts have been employed for multistep reactions. Early work stated that Ni supported on γ-Al_2O_3 was a good catalyst for the conversion of propylamine into dipropylamine [30]. Pd/KX has been reported for the one-pot synthesis of 2-ethylhexanol from n-butanol [31], while Cu supported on Mg(Al)O mixed oxide is used for the production of isobutanol by coupling MeOH and 2-propanol [32] and a Pd/Mg(Al)O catalyst for one-pot synthesis of 2-methyl-3-phenyl-propanal from benzaldehyde and propanal [33]. Moreover, many bifunctional catalysts, such as Pd/HZSM-5, have been reported for the one-pot synthesis of methyl isobutyl ketone (MIBK) from acetone [34-42]. This process consists of three steps occurring on a single bed containing a bifunctional metal-acid or metal-base catalyst [43]. The first step is the formation of diacetone alcohol (DA) via acid or base catalysed aldol condensation of acetone. In the second step, DA is converted over an acid catalyst to form mesityl oxide (MO) and water. Finally, MO is hydrogenated to produce MIBK over a noble metal catalyst.

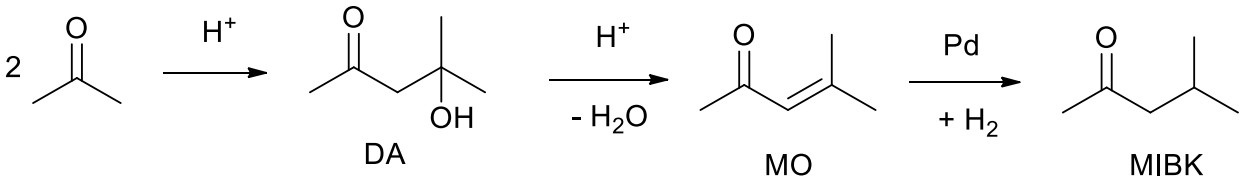

Scheme 1.1 Three-step MIBK synthesis from acetone [42].

1.3 Heteropoly acids

1.3.1 Definition and structure of HPAs

Heteropoly acids (HPAs) contain metal-oxygen cluster polyoxometalate anions and protons as counter cations [44]. The general formula of heteropolyanions is $[X_xM_mO_y]^{q-}$, where x < m, X is the heteroatom or central atom, such as P^{5+}, As^{5+}, Si^{4+}, Ge^{4+} and B^{3+}, and M is a metal ion such

as molybdenum(VI), tungsten(VI), vanadium(V), niobium(V) and, less frequently, tantalum(V) [44].

Heteropolyanions are formed by a self-assembly process in acidified aqueous solution, as shown below (Equation 1.1) [45]:

$$23H^{+} + HPO_4^{2-} + 12WO_4^{2-} \rightarrow [PW_{12}O_{40}]^{3-} + 12\,H_2O \qquad (1.1)$$

The first heteropoly compound was discovered by Berzelius in 1826. Since then, a great number of heteropoly compounds have been synthesised and several assumptions have been made to clarify their structure [46]. The first X-ray crystal structure of HPA (tungstophosphoric acid, $H_3PW_{12}O_{40}$) was reported by Keggin in 1933 [47].

HPAs have been found to possess purely Brønsted acidity; and their acidity is stronger than that of conventional solid acids such as acidic oxides and zeolites. Due to their chemical and physical properties, HPAs have found various applications, primarily in catalysis as well as in other fields [44, 48].

HPAs commonly exist as ionic crystals in the solid state (sometimes amorphous), and are composed of large heteropolyanions (referred to as the primary structure), counter cations, water of crystallisation and other molecules contained within a three-dimensional arrangement. The whole arrangement is referred to as the HPA secondary structure. On top of that, the tertiary structure is a more complex HPA aggregate; this includes the particle size, pore structure and the proton distribution within the particles [49]. This structure hierarchy is illustrated schematically in Figure 1.3.

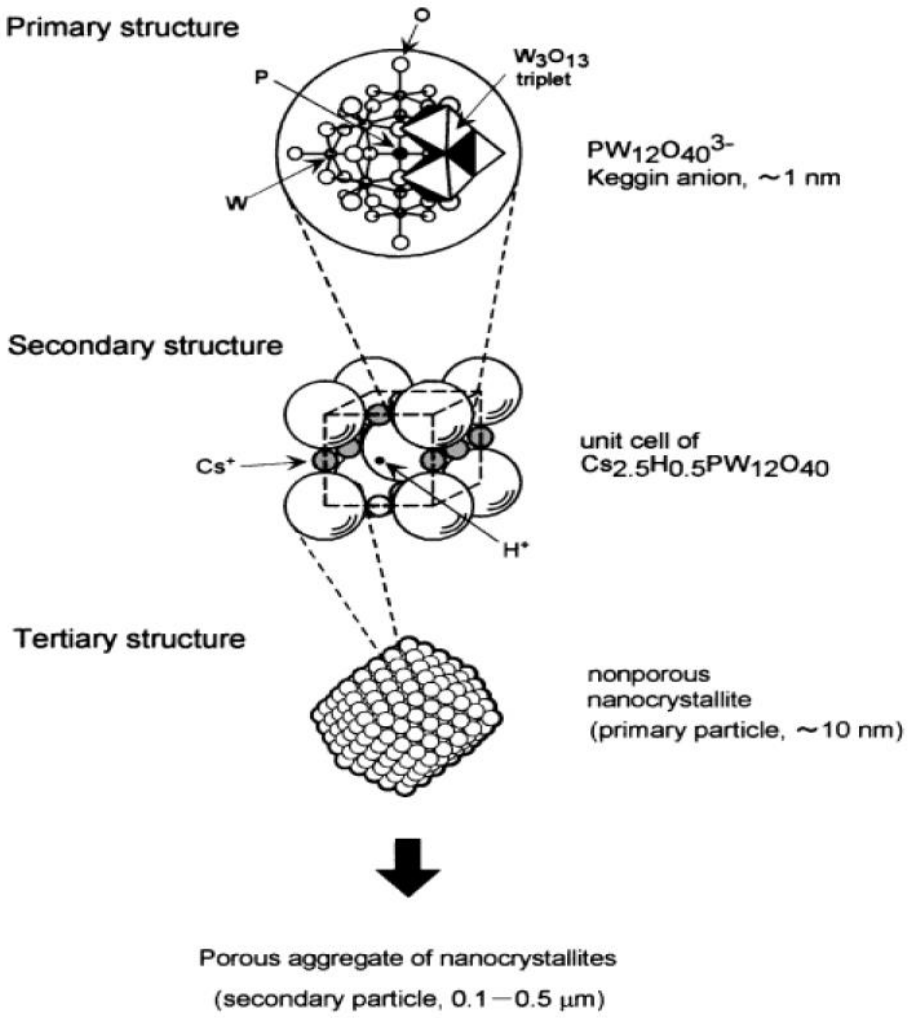

Figure 1.3 Primary, secondary and tertiary structures representing the hierarchical structure of heteropoly acids in the solid state [50].

Structurally, heteropoly acids can be classified into different groups according to the atomic ratio between the metal atom and heteroatom present. The most common classes are represented in Figure 1.4 [51, 52].

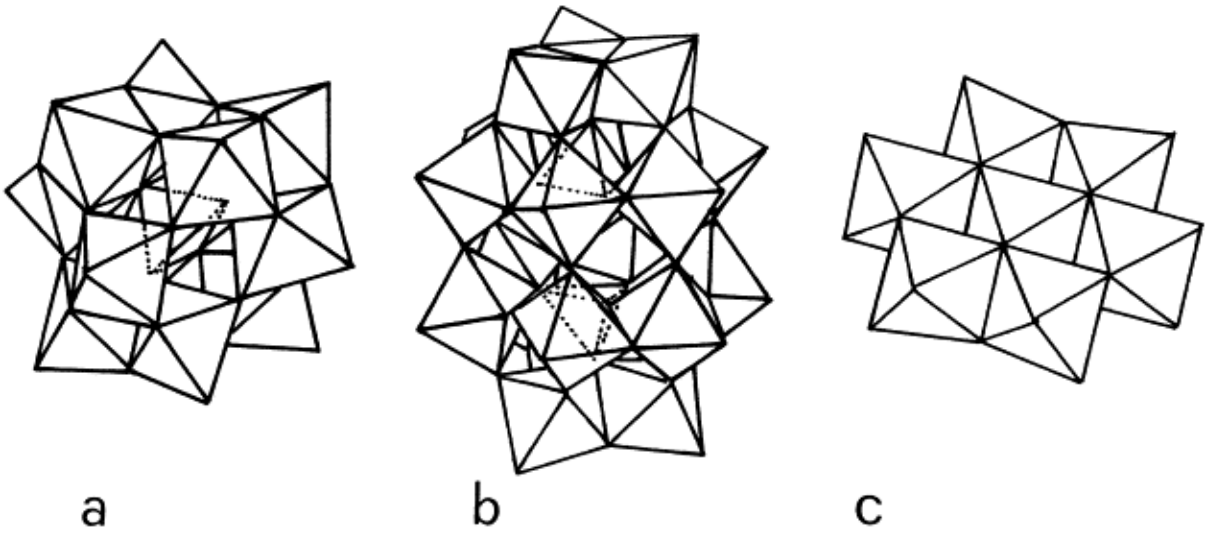

Figure 1.4 Different structural types of HPAs: (a) Keggin, (b) Wells-Dawson and (c) Anderson structures [52].

Table 1.3 Different structures of HPAs.

X/M ratio	Chemical formula (M=Mo or W)	X	Structure name
1:12	$[X^{n+}M_{12}O_{40}]^{(8-n)-}$	P^{5+}, As^{5+}, Si^{4+}, Ge^{4+}	Keggin
1:11	$[X^{n+}M_{11}O_{39}]^{(12-n)-}$	P^{5+}, As^{5+}, Si^{4+}, Ge^{4+}	lacunary Keggin
2:18	$[X_2^{5+}M_{18}O_{62}]^{6-}$	P^{5+}, As^{5+},	Dawson
1:6	$[X^{n+}M_6O_{24}]^{n-}$	Te^{6+}, I^{7+}	Anderson

Heteropolyanions with the Keggin structure are represented by the formula $[XM_{12}O_{40}]^{x-8}$. The Keggin heteropoly compounds (heteropoly acids and heteropoly salts) are more stable and relatively easily available [45, 46]. The Keggin anion is made up of a central tetrahedron (XO_4) surrounded by twelve edge- and corner-sharing metal-oxygen octahedra (MO_6). These octahedra are arranged in four M_3O_{13} groups, with each group being formed by three octahedra sharing

edges with a common oxygen atom which is also shared with the central tetrahedron XO_4, as shown in Figure 1.4 (a) and Figure 1.5 [46]. The structure contains four different types of oxygen atoms (Figure 1.5): twelve terminal $M=O_t$, twelve edge-sharing angular $M-O_{b1}-M$ shared by the octahedra within a M_3O_{13} group, twelve corner-bridging quasi-linear $M-O_{b2}-M$ connecting two M_3O_{13} groups, and four internal $X-O_c-M$. It is possible to distinguish between these oxygen atoms by ^{17}O NMR and fingerprint infrared spectra in the range of 600-1100 cm^{-1} [45, 46, 53].

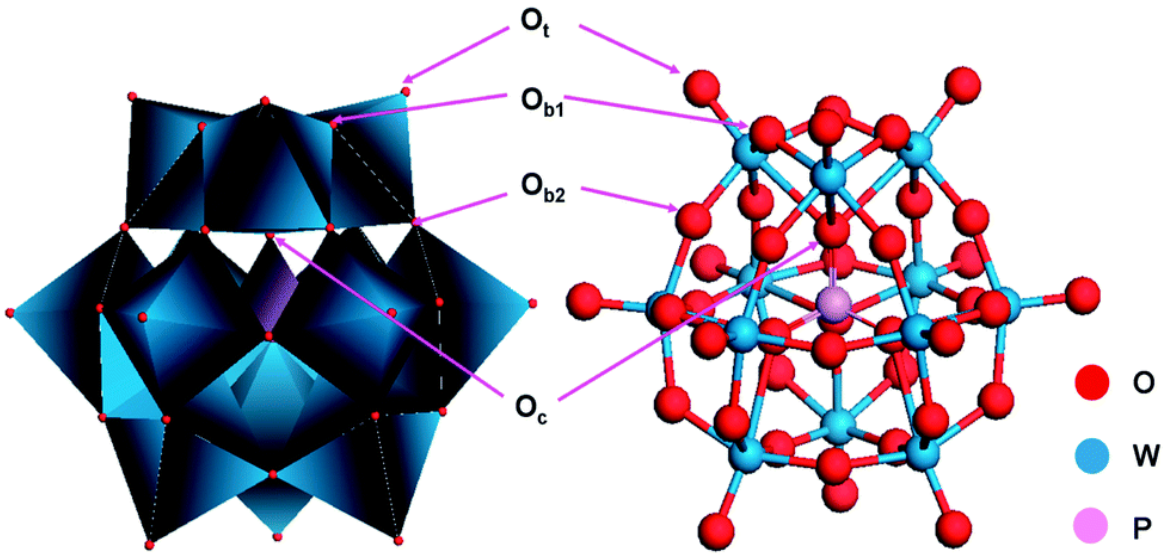

Figure 1.5 Localisation of oxygen atoms in the Keggin structure of $PW_{12}O_{40}^{3-}$ [54].

The most common examples of the Keggin type heteropoly acids are: 12-phosphotungstic acid ($H_3PW_{12}O_{40}$), 12-phosphomolybdic acid ($H_3PMo_{12}O_{40}$), 12-silicotungstic acid ($H_4SiW_{12}O_{40}$) and 12-silicomolybdic acid ($H_4SiMo_{12}O_{40}$). These HPAs are commercially available as crystalline hydrates [45, 46].

1.3.2 Properties of heteropoly acids

1.3.2.1 Thermal stability of HPAs

The thermal stability of heteropoly compounds is a very vital feature for their use in heterogeneous catalysis. Some HPAs have a fairly high thermal stability in the solid state, up to

350 °C, which allows their use as catalysts at moderately high temperatures. Nevertheless, there is a critical issue about their thermal stability regarding catalyst regeneration. For example, burning coke that may form on the catalyst surface may require catalyst thermal stability at least up to 500 ^{o}C [46].

The thermal stability is usually determined by thermogravimetric analysis (TGA), differential thermal analysis (DTA), differential scanning calorimetry (DSC), X-ray diffraction (XRD), infrared spectroscopy (IR) and solid state NMR. HPAs of the Keggin structure are the most stable type of HPA. Their stability can be determined in terms of the decomposition temperature at which all acidic protons are lost (Scheme 1.2) [44, 46, 55].

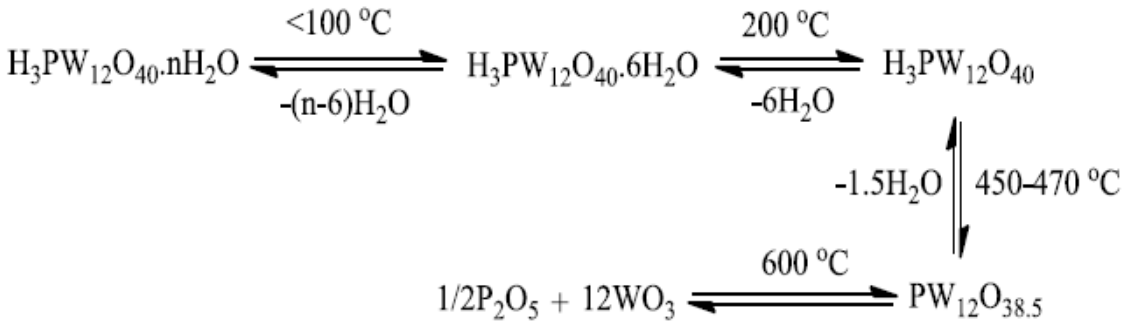

Scheme 1.2 Thermal decomposition of $H_3PW_{12}O_{40}$ hydrate [55].

As estimated by TGA, the decomposition temperature of the Keggin-type PW, SiW, PMo, and SiMo decreases in the following order [46, 55]:

$H_3PW_{12}O_{40}$	>	$H_4SiW_{12}O_{40}$	>	$H_3PMo_{12}O_{40}$	>	$H_4SiMo_{12}O_{40}$
465 ^{o}C		445 ^{o}C		375 ^{o}C		350 ^{o}C

From TGA under transient conditions, $H_3PW_{12}O_{40}$ showed the highest thermal stability of 465 ^{o}C, but under reaction conditions the solid $H_3PW_{12}O_{40}$ catalyst may start to decompose at lower temperatures than those determined by TGA. [46].

1.3.2.2 Acidic properties of HPAs

Reactions catalysed by heteropoly acids take place through the same mechanisms as those catalysed with conventional Brønsted acid catalysts (Equation 1.2). The substrate (S) is protonated by proton transfer from the catalyst, and the ionic intermediate is then converted to yield a reaction product (P) [46]:

$$S + H^+ \rightleftharpoons SH^+ \rightarrow P + H^+ \qquad (1.2)$$

There are two kinds of proton within crystalline heteropoly acids: (i) hydrated protons $[H(H_2O)_n]^+$ and (ii) non-hydrated protons, as represented in Figure 1.6 [46]. The location of protons in HPAs has been the subject of some discussion [56]. The hydrated protons have a high mobility, which causes the extremely high proton conductivity of crystalline heteropoly acid hydrates. The non-hydrated protons, on the other hand, possess considerably less mobility, and Kozhevnikov has suggested that they are in fact localised on the peripheral oxygen atoms in the polyanion [46]. In solid HPAs, both hydrated and non-hydrated protons have a role to play in the formation of the crystal structure, joining the neighbouring heteropoly anions. In crystalline HPA hydrates, bulk protons exist as plane diaquahydrogen ions. These are quasi-symmetrical hydrogen bonded species that serve to link the neighbouring heteropolyanions by forming hydrogen bonds with the terminal W=O oxygens (Figure 1.6 (a) and Figure 1.7) [46].

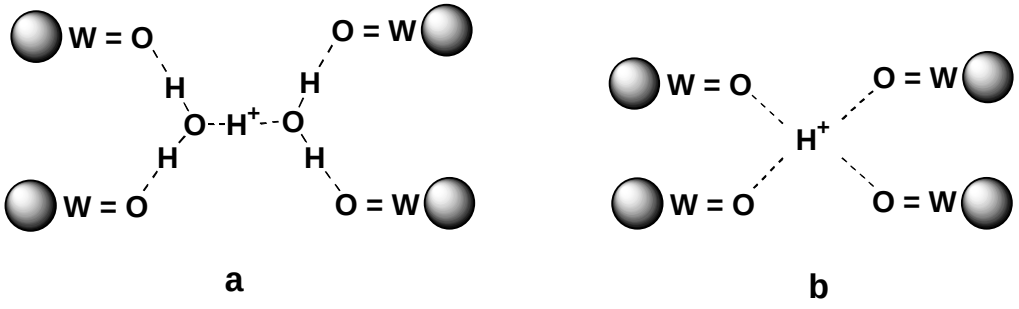

Figure 1.6 Proposed proton sites in (a) $H_3PW_{12}O_{40}\cdot 6\ H_2O$ and (b) dehydrated $H_3PW_{12}O_{40}$ [46].

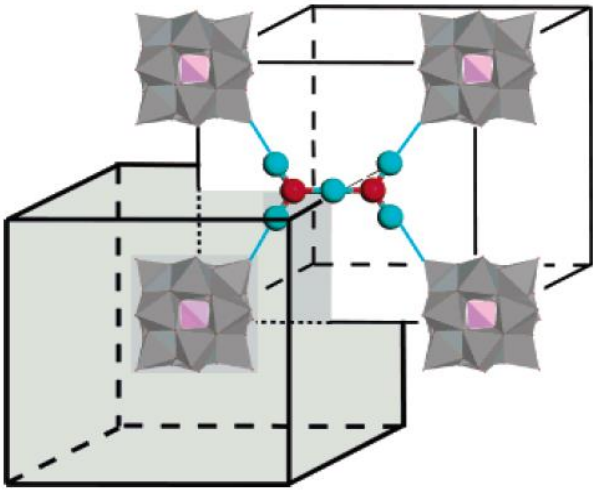

Figure 1.7 $H_3PW_{14}O_{40}.6H_2O$ structure represented as two interpenetrating cubic structures [53].

The surface proton sites in solid HPAs are stronger than the bulk proton sites and thus are vital for heterogeneous acid catalysis. In general, the surface area of crystalline heteropoly acids is very low (< 10 m^2/g) [44-46, 49, 57]. It is suggested that proton sites are localised at the bridging oxygen atoms in the Keggin unit when the HPA is dispersed on the support so as to enhance the HPA's exposed surface area [44].

Heteropoly acids in the solid state possess purely Brønsted acids, and have a stronger acidity, and therefore higher activity, than conventional acids like SiO_2–Al_2O_3, H_3PO_4/SiO_2, and HX and HY zeolites [45, 58, 59].

Thermal desorption of basic molecules reveals the acid properties of solid acids. Okuhara et al. [45] used the thermal desorption of pyridine to compare the acid strength of heteropoly acids and SiO_2-Al_2O_3. At 300 ^oC the pyridine molecules adsorbed on SiO_2-Al_2O_3 are completely desorbed, whereas they remain mostly adsorbed as pyridinium ions on the surface of $H_3PW_{12}O_{40}$ at much higher temperatures. This indicates that the acidity of $H_3PW_{12}O_{40}$ is much stronger than that of SiO_2-Al_2O_3.

Temperature-programmed desorption (TPD) of ammonia can also be used for acid strength characterisation [60-61]. Izumi et al. [61] determined the acid strength of HPA in terms of the temperature of NH_3 desorption which decreased in the following order along with decreasing the acid strength:

$$H_3PW_{12}O_{40} > H_4SiW_{12}O_{40} > H_3PMo_{12}O_{40} > H_4SiMo_{12}O_{40}$$

592 °C 532 °C 463 °C 423 °C

The acid strength of HPAs can be determined more accurately by the calorimetry of NH_3 absorption [63-65]. The order of acid strength thus obtained was the same as that obtained by ammonia TPD [44, 60, 62]. Usually, the activity of heteropoly acid catalysts is consistent with this order both in homogeneous and heterogeneous systems [45, 66].

1.3.3 Supported HPAs

Bulk Keggin HPAs have a very low surface area (< 10 m^2/g) and are highly soluble in polar solvents such as water, alcohols and ethers, which limit their activity as heterogeneous catalysts. These drawbacks can be overcome, however, by supporting HPAs onto high surface area supports, for example silica. The advantage of dispersing HPAs on high surface area supports is that the number of active sites on the surface of HPAs may also increase along with thermal stability, which will enhance their catalytic activity.

The acidity and catalytic activity of supported HPAs greatly depend on the type of support, the HPA loading and the pre-treatment conditions [44, 46]. Generally, acidic and/or neutral supports, such as silica [62], active carbon [67, 68], ion-exchange resin [69], etc., are preferred. In contrast, basic solid supports such as MgO and Al_2O_3 are not suitable for use as supports, because they tend to decompose HPAs due to the instability of HPAs in basic aqueous solutions [51, 66, 70].

Usually, strong interaction is observed between heteropoly acids and their support at low HPA loadings, which decreases the acid strength of the HPA [45]. Frequently, silica is used as a support material for HPAs, which is relatively inert towards HPA. Nevertheless, microcalorimetry of NH_3 adsorption showed that the acid strength of $H_3PW_{12}O_{40}$ decreases when it is loaded on SiO_2 due to the interaction between HPAs and the surface silanol groups, as shown in Figure 1.8 [71-73].

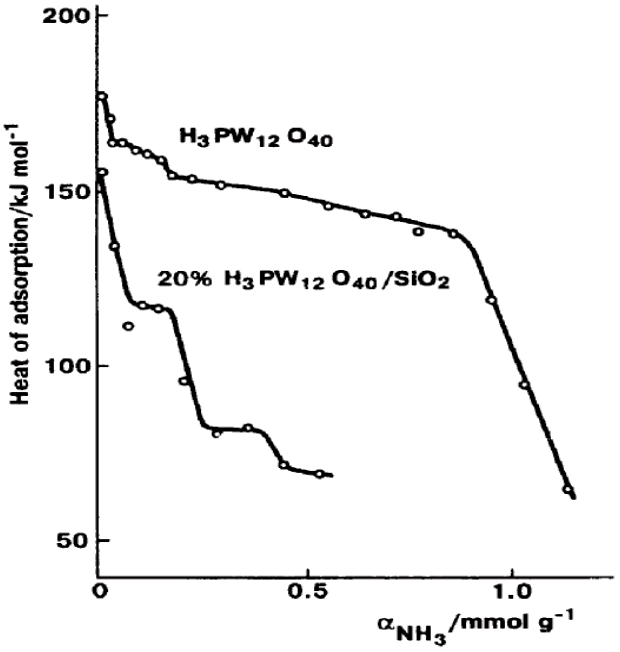

Figure 1.8 Differential heats of NH_3 adsorption onto $H_3PW_{12}O_{40}$ and 20 wt% $H_3PW_{12}O_{40}/SiO_2$ determined at 150 °C after catalyst pre-treatment at 300 ºC /10^{-3} mmHg [71].

1.3.4 Salts of HPAs

The chemical formula of Keggin type HPA salts is $M^1{}_xH_{y-x}M^2M^3{}_{12}O_{40}$, where M^1 is K^+, Cs^+, Rb^+; M^2 is P or Si; M^3 is W or Mo; x is commonly 2.5 and y is 3 or 4 if M^2 is P or Si, respectively. The heteropoly salts are prepared by replacing protons in their parent acids with different metal ions. The nature of the counter cations in HPA salts is very important for their acidity, porosity,

solubility and thermal stability [44, 49, 74]. The HPA salts can be classified according to the size of their counter cations into two groups [75].

Group I: those with small counter cations such as Li^+, Na^+:

- low surface area (under 10 $m^2\ g^{-1}$),
- high solubility in water,
- absorption capability of polar or basic molecules in the solid bulk.

Group II: Large monovalent cations, such as NH_4^+, K^+, Cs^+:

- high surface area (over 100 $m^2\ g^{-1}$),
- water-insoluble,
- unable to absorb polar molecules in the bulk.

The HPA salts with large cations like Cs^+ are water-insoluble and have a surface area exceeding 100 m^2g^{-1} [76, 77]. In contrast to alkali-exchange zeolites, the partially substituted Cs salts of HPA have strong surface acidity [49, 78].

Okuhara et al. have reported the effect of Cs substitution on the surface area of $H_3PW_{12}O_{40}$ (Figure 1.9) [45]. The pore size of $Cs_xH_{3-x}PW_{12}O_{40}$ can be precisely controlled by its Cs content. The number of surface protons decreases when the Cs content, *x,* in $Cs_xH_{3-x}PW_{12}O_{40}$ increases from 0 to 2 due to the reduction in the surface area, but sharply increases when *x* further increases from 2 to 3. The surface area and surface acidity reach a maximum at $x = 2.5$. When *x* increases above 2.5, the surface acidity dramatically reduces since the formal amount of protons becomes very low [45].

HPA salts are normally more stable than their parent acids. For instance, $Cs_{2.5}H_{0.5}PW_{12}O_{40}$ starts to decompose at 500 °C, whereas the parent acid $H_3PW_{12}O_{40}$ decomposes at the relatively lower temperature of 300 °C. The relative stability of HPA salts, meanwhile, depends on the type of

counter cation and increases in the following order: Ba^{2+}, $Co^{2+} < Cu^{2+}$, $Ni^{2+} < H^{+}$, $Cd^{2+} < Ca^{2+}$, $Mn^{2+} < Mg^{2+} < La^{3+}$, $Ce^{3+} < NH_4^{+} < K^{+}$, Tl^{+}, Cs^{+} [49].

The Keggin heteropoly salts are meso-microporous materials which allow other chemical functions, such as metal functionality, to be introduced. The metal particle size and dispersion can be controlled by the metal loading in HPA salts. In this respect, it has been found that introducing 0.5 wt% Pt in $Cs_{2.5}H_{0.5}PW_{12}O_{40}$ did not affect the pore size of this salt, and the platinum particle size was less than 10 Å. The Keggin HPA salt $Cs_xH_{3-x}PW_{12}O_{40}$ (especially when *x* is equal to 2.5) modified with Pt is a promising metal-acid bifunctional catalyst for the conversion of renewable resources to chemicals and fuels [74, 79].

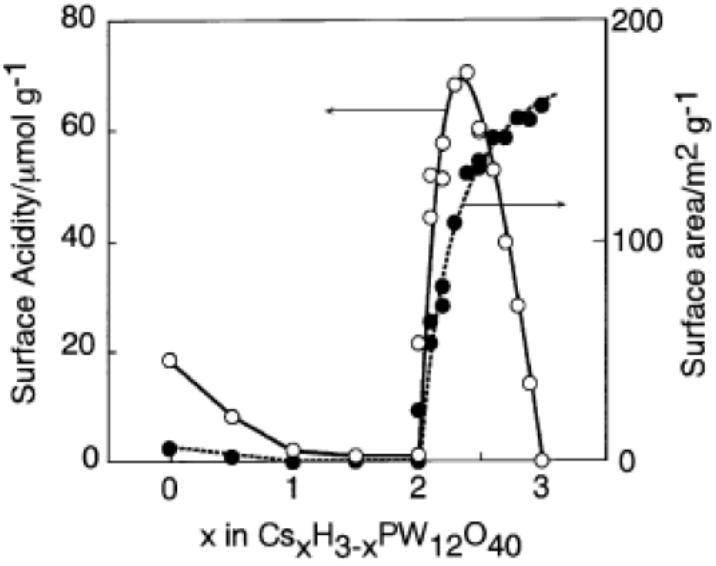

Figure 1.9 Surface area and surface proton density of $Cs_xH_{3-x}PW_{12}O_{40}$ as a function of Cs content [45].

1.3.5 HPAs in heterogeneous catalysis

Heteropoly acids have found numerous applications as catalysts in heterogeneous gas-solid and liquid-solid systems [46, 49, 50, 57, 80]. The most important advantage of heterogeneous systems is that the catalyst can be easily separated from the reaction mixture and reused. There is a critical issue, however, in the form of HPA's relatively low thermal stability regarding catalyst

regeneration; for example, for burning coke that may form on the catalyst surface thus reducing catalyst life [44, 46, 55].

Misono et al. [45, 49, 50] have classified heterogeneous HPA catalysis into three types: surface-type, bulk type I (pseudo-liquid) and bulk type II, as illustrated in Figure 1.10.

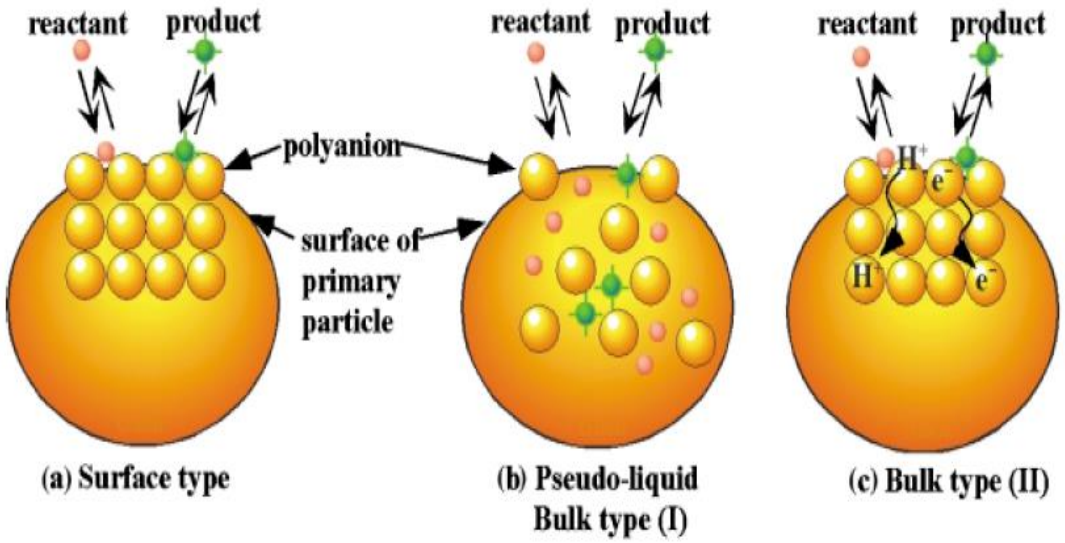

Figure 1.10 Three types of catalysis by solid heteropoly compounds [50].

The surface-type catalysis is a conventional acid or oxidation heterogeneous catalysis which takes place on the surface of a solid catalyst, i.e. on the outer surface and pore walls. The reaction rate in this case is proportional to the catalyst surface area. An example of this type is the oxidation of aldehydes and CO.

The bulk type I occurs in the conversion of a polar substrate (e.g. alcohol) with a bulk solid heteropoly acid or a soluble heteropoly salt (i.e., salts with small metal cations such as Li^+, Na^+, etc.) at low temperature. In this case, the substrate is absorbed into the catalyst bulk, penetrating in between the polyanions and reacting there, so the catalyst performs like a concentrated solution

(pseudoliquid phase). In this type of heterogeneous catalysis, the surface and bulk acid site contribute in the reaction. The reaction rate is proportional to the catalyst volume (catalyst weight). Dehydration of lower alcohols at low temperature is suggested to occur by this mechanism.

The bulk type II catalysis, meanwhile, occurs in oxidation catalysis at high temperatures, accompanied by the migration of redox carriers (protons and electrons) in the solid bulk, and with the whole of that solid bulk taking part in the redox cycle. In this type of catalysis the reaction rate is expected to be proportional to the catalyst weight.

1.3.6 Metal-HPA multifunctional catalysis

The diverse physicochemical properties of HPAs allow for their use as multifunctional catalysts. In addition to the acid and redox properties of HPA, it is possible to introduce other chemical functions such as metal functionality [44-46]. Nevertheless, only a few studies have used HPAs as multifunctional catalysts in multistep reactions [41].

As mention above, some acidic heteropoly salts, e.g. $Cs_xH_{3-x}PW_{12}O_{40}$, possess strong proton acidity and a relatively high surface area. These have therefore been used in metal-acid bifunctional catalysts as an acidic support for some metals [50, 81]. For example, Pd-modified $Cs_{2.5}H_{0.5}PW_{12}O_{40}$ (CsPW) was used for one-pot synthesis of methyl isobutyl ketone (MIBK) from acetone [41]. This reaction occurs in three consecutive steps, as mentioned in section 1.2. Moreover, Ru supported on CsPW has been used to form propanediol by glycerol hydrogenolysis [82]. Alotaibi et al. [83] have studied the deoxygenation of propanoic acid using bifunctional metal-acid catalysis. They reported that Pd and Pt modified CsPW is an efficient catalyst for propanoic acid decarbonylation to produce ethane.

The Pd-$H_3PW_{12}O_{40}/SiO_2$ catalyst has been employed for one-step synthesis of (-)-menthol from citronellal [84]. This process comprises two steps, the production of isopulegol from cyclisation

of (+)-citronellal occurring over acid sites of the heteropoly acid, followed by isopulegol hydrogenation over metal sites (Pd) leading to the formation of menthol, as shown in Scheme 1.3. Supporting Pd-$H_3PW_{12}O_{40}$ on silica is important to ensure heterogeneity of the catalyst and provide a high catalyst surface area.

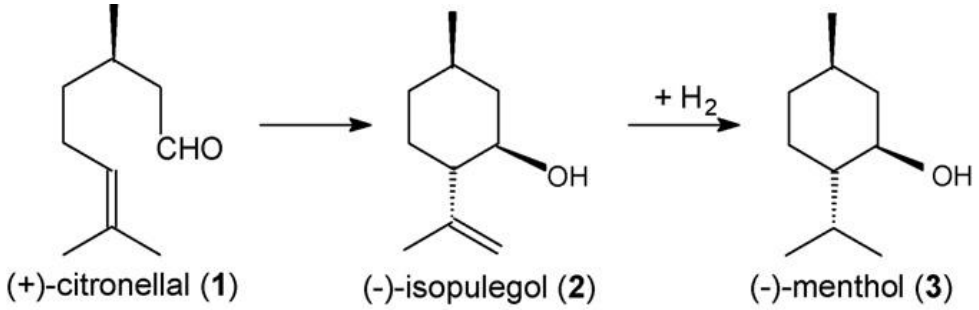

Scheme 1.3 One-step synthesis of (-)-menthol from citronellal over Pd-$H_3PW_{12}O_{40}/SiO_2$ [84].

Kozhevnikov et al. have reported that doping HPAs with platinum group metals enhances catalyst regeneration by coke burning. In Pt- and Pd-modified HPA catalysts only soft coke was formed, and the catalyst could be regenerated by burning coke off at 350 °C without destroying the structure of the HPA [85, 86].

1.4 Synthesis of biofuels from biomass

Before discovering fossil fuels, the world's energy demands were met by using plant biomass. Currently, the main source of energy is fossil fuels, namely coal, natural gas and petroleum. This energy pool was established in the 19th Century and helped to develop the high modern standards of living [87]. Fossil fuels provide over 80% of the world's energy consumption [88]. These days it is important to find alternative sources of energy and raw materials to eliminate the imbalance in fossil fuel sources. In this respect, attention has been given to plant biomass, which, in contrast

to fossil sources, is a renewable energy source. Biofuels produce considerably less greenhouse gas emissions than do fossil fuels and can even be greenhouse gas neutral if efficient processes of conversion of biomass to liquid fuel are developed [87, 89, 90].

The total annual biomass resources reach 1.5 trillion tons [91] and increase annually by 100 billion tons owing to photosynthesis [92]. Only a limited amount of plant biomass is used as an alternative source of energy, however. Nowadays, biomass amounts to about 10-12% of world energy consumption [88]. Experts have predicted that by 2030, 20% of transportation fuel and 25% of chemicals will be produced from biomass [87].

Currently, the production of liquid biofuels is based on the transformation of agricultural plants into bioethanol and biodiesel. In Brazil, ethanol production relies on the juice from sugar cane. In the USA, the main source of ethanol production is starch from corn [93]. These agricultural plants, however, are required in the food industry, which has limited their application in the production of liquid biofuel [94[. It is thought that there is not enough agricultural land available in the world to grow sufficient energy crops to replace conventional fuel with biofuels. Non-edible biomass is an alternative source of biofuel without competing with the food industry [95]. This can be obtained from wood and other plant species (such as Bermuda grass and switchgrass), plant residues (such as cobs, stalks and husks), residues of forest (such as twigs), etc.

The cheapest and most abundant source of biomass is lignocellulose. This is a promising raw material for the production of transportation biofuel. Bio-oil can be produced by pyrolysis or liquefaction of lignocellulose. The conversion of this material to liquid transportation fuel requires the removal of some or all oxygen as CO_2 and H_2O to form molecules with desirable properties for combustion [87, 96].

Lignocellulose is composed of a carbohydrate polymer, cellulose (a crystalline glucose polymer), hemicellulose (a complex amorphous polymer), and lignin (a polyaromatic compound) (Figure 1.11) ([87] and references therein).

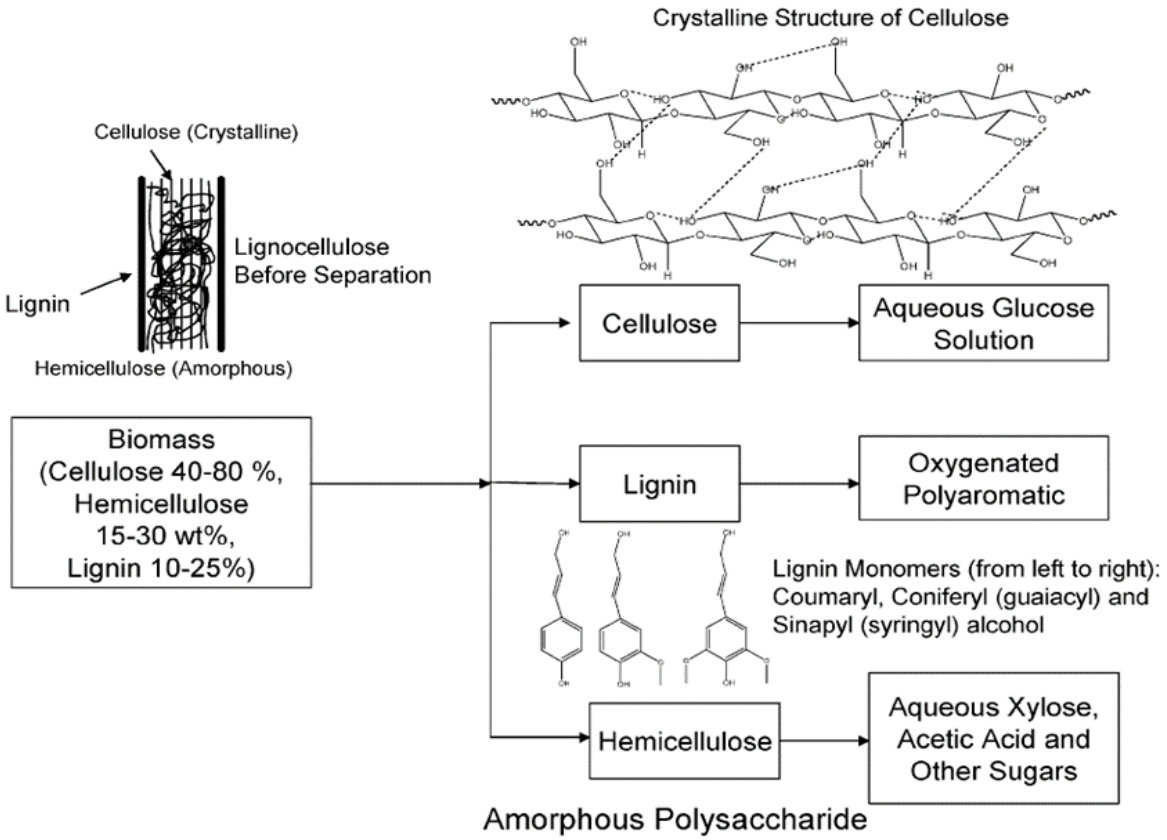

Figure 1.11. Biomass composition [87].

The chemical formula of cellulose is $(C_6H_{10}O_5)_n$, consisting of a linear chain of D-glucopyranose connected via β-1,4-glycosidic linkages, usually in the crystal form with an extended flat 2-fold helical configuration. Hydroxyl groups of glucose form hydrogen bonds that help to maintain and strengthen the flat linear configuration of the chain. This interconnected molecular structure makes cellulose chains completely hydrophobic. A hydrogen bond is formed between the OH groups on the glucose, with oxygen atoms on the same or on a neighbouring chain clasping the chains together and making microfibrils with high tensile strength [87].

Hemicellulose is a sugar polymer that usually constitutes 20-40 wt % of biomass. In contrast to cellulose, which is a polymer of only glucose, hemicellulose is a polymer of five different sugars containing both pentose (usually D-arabinose and D-xylose) and hexose (D-mannose, D-glucose and D-galactose) units. The degree of polymerization of cellulose is approximately 10000 to 15000 units, whereas the polymerization degree of hemicellulose is only 50 to 200 monomer units. This means that hemicellulose decomposes more easily than cellulose. Xylan is the most common type of hemicellulose, and consists of a xylose unit connected via a β-1,4-glycosidic linkage [87].

Lignin is an amorphous polyaromatic hydrophobic compound, which constitutes 10-25 wt% of biomass. Lignin is found in the cell walls of certain biomass, particularly woody biomass. It is a cross-linked three-dimensional polymer formed by a phenylpropane unit. Figure 1.11 shows the three main monomer units of lignin (coumaryl, coniferyl and sinapyl alcohol). Lignins of softwoods are mainly formed from coniferyl alcohol, whereas lignins of hardwoods have both coniferyl and sinapyl alcohol as monomer units. Grass lignin usually consists of all three types of the phenylpropane units. Lignin's complex structure makes it hard to decompose using chemicals and microorganisms. All of these lignocellulose types are found universally in different kinds of biomass and are the most abundant organic matter on the earth [87].

1.5 Deoxygenation of biomass-derived molecules

1.5.1 Introduction

Oxygen-containing organic compounds such as ketones, carboxylic acids, alcohols, phenols, etc., are readily available from natural resources, and are attractive as renewable raw materials for the production of value-added chemicals and bio-fuels [96, 97]. For fuel applications, they require a reduction in oxygen content to increase their caloric value. Much current research is therefore focussed on the deoxygenation of organic oxygenates using heterogeneous catalysis, in particular

for the upgrading of biomass-derived oxygenates obtained from fermentation, hydrolysis and fast pyrolysis of biomass [98-101].

Traditional reduction methods such as Clemmensen and Wolff–Kishner reduction require very drastic reaction conditions and produce large amounts of by-products [102]. Hydrodeoxygenation (using H_2 as the reductant), on the other hand, is considered to be the most effective method for the deoxygenation of oxygen-containing compounds [83, 103-105].

Catalytic bio-oil hydrodeoxygenation involves treating bio-oil at high temperatures and high hydrogen pressure in the presence of a catalyst. Furmisky [106] and Bu et al. [107] have reviewed heterogeneous catalysis for hydrodeoxygenation. Industrially, sulfided CoMo and NiMo catalysts are commonly used for the removal of oxygen, sulfur and nitrogen from petroleum fuels. Noble metals such as Pd, Pt and Ru can also be used for hydrodeoxygenation [87, 107, 108].

Despite the fact that several types of catalysts such as CoMo and NiMo have been used industrially, these catalysts readily undergo deactivation owing to coke deposition. Moreover, these methods involve very drastic reaction conditions (up to 300 °C) [105].

These drawbacks can be overcome by the one-pot strategy using metal-acid bifunctional catalysts. This, however, requires more effort to improve such catalysts in respect to the scope of the substrates, reaction temperature and pressure, as well as the hydrogen consumption [103-105, 109].

1.5.2 Hydrodeoxygenation of biomass-derived ketones

Biomass-derived ketones can be further upgraded by aldol condensation and hydrogenation to produce alkanes that fall in the gasoline/diesel range. The hydrogenation of ketones on supported metal catalysts (e.g. Pt/C and Pd/C) to form alcohols is feasible and well documented [110], however, further hydrogenation to alkanes is rather difficult to achieve on such catalysts [103,

104]. The ketone-to-alkane hydrogenation can be achieved much more easily using bifunctional metal-acid catalysts ([103-105] and references therein).

Ketones can be obtained from the ketonisation of carboxylic acids. In this process, two molecules of a carboxylic acid react to produce ketone (Equation 1.3) [111, 112]. This reaction allows for the partial deoxygenation of carboxylic acids and the further upgrading of their backbone.

$$2\ RCOOH \longrightarrow R_2CO + CO_2 + H_2O \qquad (1.3)$$

A variety of acidic and basic metal oxide and mixed oxide catalysts have been used for ketonisation [111-115]. Basic sites are more favourable for this type of reaction, however [112].

Industrially, aldol condensation is employed for the transformation of acetone into C6, C9 and larger organic molecules such as MIBK and diisobutyl ketone (DIBK) (Scheme 1.4), which are used as solvents in paints, coatings and resins. Many bifunctional catalysts have been reported for the single stage conversion of acetone to MIBK, as described in section 1.2. Multifunctional catalytic systems reported in the literature include Pd supported on cation exchange resins and on zirconium phosphate [116], Pd on zeolites [38], Pd on $Cs_{2.5}H_{0.5}PW_{12}O_{40}$ [41], Pd on ZnCr mixed oxide [40], Pd on MgO/SiO_2 [117], Pt, Pd, Ni and copper on activated carbon [118, 119], Pd on $ALPO_4$-11 and SAPO-11 [39].

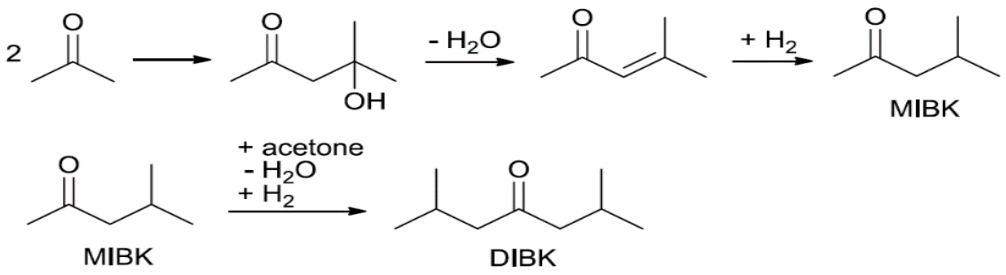

Scheme 1.4 Formation of MIBK and DIBK from acetone [55].

Zaccheria et al. studied the deoxygenation of aromatic ketones into bicyclic ethers in the liquid phase. They used $Cu/SiO_2–Al_2O_3$ in the deoxygenation of fluorenone at 90 ^{0}C and 1 atm H_2. This catalyst showed very low selectivity towards the corresponding methylene formation (48%) but $Cu/SiO_2–ZrO_2$ was found to be an effective catalyst (with 91% selectivity). They also found that acidic support was not necessary, and that the Cu/SiO_2 catalyst was able to reduce aromatic ketones with 100% selectivity [120].

Hydrogenation of acetophenone has been studied by Jiang and co-workers using a Pt_xPd_y/ZrO_2 catalyst, where *x* and *y* correspond to the atomic ratios of Pt and Pd, respectively. Here, the catalyst was used for the solvent-free hydrogenation of ketones at 140 ^{0}C and 60 bar hydrogen [121].

Bimetallic $Pt–Pd/ZrO_2$ catalysts showed excellent catalytic performance in the total removal of oxygen from acetophenone to produce ethylbenzene (EB), but Pd/ZrO_2 exhibited greater EB selectivity (64%) than Pt/ZrO_2 (14%). For bimetallic catalysts, the selectivity toward EB increased as the content of Pd increased, and when the Pt content was increased, the selectivity of $Pt–Pd/ZrO_2$ to phenyl ring hydrogenation products also increased (Scheme 1.5). Overall, it seems that Pd sites favour hydrogenation of the carbonyl group while Pt sites help the phenyl group hydrogenation. Jiang et al. also reported that $Pt_{50}Pd_{50}/ZrO_2$ showed the highest activity (about 85% conversion with 50% EB selectivity) [121].

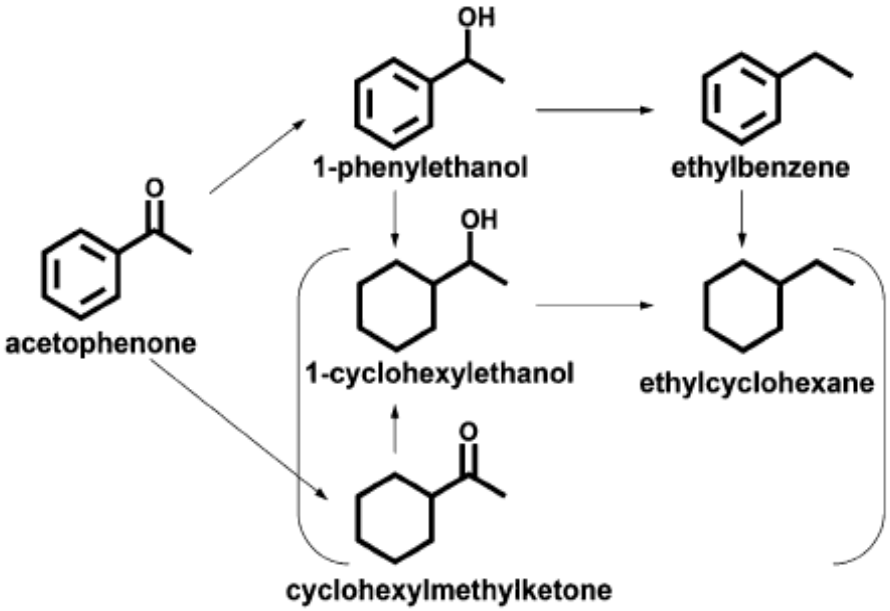

Scheme 1.5 Hydrogenation of acetophenone over bimetallic Pt–Pd/ZrO_2 catalysts [121].

Pt–Pd/ZrO_2 catalysts have also been used in cyclopentanone hydrogenation. During the conversion of cyclopentanone, only cyclopentanol was formed, and no cyclopentane was obtained [121].

Alotaibi et al. [104] investigated a number of metal catalysts (Pd, Pt and Cu) supported on silica and active carbon for MIBK hydrogenation in the temperature range of 100–400 ^{0}C. 10% Pt/C and 10% Pd/C catalysts showed the highest selectivity to 2-methylpentane (87 and 94% respectively) at a temperature as high as 300 ^{0}C, which indicates that further hydrogenation of 2-methylpentanol to 2-methylpentane (2MP) is rather difficult to achieve on such catalysts.

This group has also used bifunctional metal-acid catalysts to study the hydrodeoxygenation of MIBK to produce alkane in one step on a single catalyst bed using platinum metals supported on zeolites such as H-ZSM-5, H-Beta and H-Y. The Pt/H-ZSM-5 catalyst exhibited the best performance, giving >99% selectivity to methylpentanes (2MP/3MP = 83:17) at 100% MIBK conversion at 200 ^{0}C [104].

The hydrodeoxygenation of MIBK has also been studied using bifunctional metal-polyoxometalate catalysts comprising Pt, Pd, Ru, or Cu supported on a Keggin heteropoly salt $Cs_{2.5}H_{0.5}PW_{12}O_{40}$ (CsPW) [103]. At 100 ^{0}C, 0.5%Pt/CsPW catalyst showed very high activity giving ≥99% MIBK conversion with 100% 2MP selectivity. It has been suggested that MIBK-to-2MP hydrogenation over Pt/CsPW at 100 ^{0}C is limited by the first step, i.e., the hydrogenation of MIBK to MP-ol (Scheme 1.6). This is mainly based on the fact that the reaction rate scales with Pt loading, while 2MP selectivity remains constant at ~100% [103].

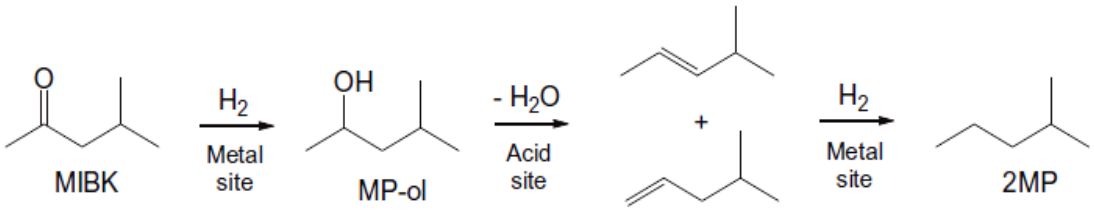

Scheme 1.6 MIBK hydrodeoxygenation via bifunctional metal-acid catalysis [103].

Ketones, such as MIBK, acetone, butanone, cyclohexanone, pentanone, etc., can be hydrogenated to produce alkanes, 2-methylpentane, propane, pentane, etc. C_{5+} alkanes are in the gasoline range and could therefore be blended with the straight-run gasoline, and subjected to standard catalytic reforming [122] to enhance their octane numbers for use through the existing fuel infrastructure.

1.5.3 Hydrodeoxygenation of ethers

While methanol and ethanol have higher octane numbers and are cheaper than their ethers, they have the drawback of being water-miscible, with a low Reid vapour pressure. Since the 1990s, therefore, attention has been drawn to ethers [123].

Presently, all major octane enhancing ethers are obtained from the reaction of the C1 to C3 alcohols with C4 or C5 tertiary olefins (etherification reaction) [123]. Diisopropyl ether (DIPE) can be easily obtained from the base olefin, propylene and water. Commercially, DIPE is only

produced as a by-product of isopropanol manufacture and, to the author's knowledge, no industrial scale commercial plants have thus far been commissioned [123]. Many patents, however, claim to achieve DIPE synthesis using propylene and water as feedstocks in a two-stage process [124], a one stage process [125], or by reactive distillation [126]. Texaco [127], on the other hand, proposed a two stage process of DIPE synthesis using acetone and hydrogen as starting materials. In all these processes, DIPE is eventually formed throw the intermediate isopropanol. The reactions taking place in the system are shown in Scheme 1.7 [123].

$$C_3H_6 + H_2O \Leftrightarrow C_3H_7OH \quad (IPA) \qquad \text{I-A}$$

$$C_3H_6O + H_2 \Leftrightarrow C_3H_7OH \qquad \text{I-B}$$

$$C_3H_7OH + C_3H_6 \Leftrightarrow C_3H_7OC_3H_7 \quad (DIPE) \qquad \text{II-A}$$

$$C_3H_7OH + C_3H_7OH \Leftrightarrow C_3H_7OC_3H_7 + H_2O \qquad \text{II-B}$$

Scheme 1.7 Diisopropyl ether synthesis [123].

Isopropanol is produced as an intermediate either by acetone hydrogenation (step I-B), as in the case with Texaco [127], or by the conventional method of the hydration of propylene (step I-A). After that, this intermediate reacts further to produce diisopropyl ether by either etherification with propylene (step II-A) or by dehydrative etherification (step II-B) [123].

In addition to the more widely studied conversion of cellulose-derived oxygenates, attention has been given to the production of liquid hydrocarbon fuels from lignin-derived components [106, 107, 128-135]. Lignin is a large polyaromatic compound constituting up to 30% biomass; this means that phenolic compounds represent a significant fraction of the biomass of pyrolysis bio-oil. In contrast to the higher oxygen content and shorter carbon chains of the cellulose-derived oxygenates, phenolics have a carbon chain number already in the gasoline range, but their lower

oxygen content means that the deoxygenation process must still preserve the carbon number within the range of gasoline. Methoxy and hydroxy are the most important functional groups of phenolics in bio-oil. The effect of the delocalization of the oxygen lone pair orbital onto the π orbital of the aromatic ring reinforces the bond between C (aromatic) and oxygen of the phenolics, causing a higher energy barrier than that for the C (aliphatic)-O bond for oxygen removal [106]. Challenges still remain, therefore, in terms of finding an efficient catalyst for the deoxygenation of phenolics with maximised carbon retention in liquid fuels [136].

Zhu et al. [130] investigated gas phase transalkylation and hydrodeoxygenation of anisole over a Pt/H-Beta catalyst at 400 ^{o}C and atmospheric pressure. This catalyst showed very high conversion, but suffered from rapid deactivation. They also compared the product gained on the bifunctional catalyst with that produced on two monofunctional catalysts (Pt/SiO_2 and H-Beta). This comparison showed that the acid function accelerates the methyl transfer reaction (transalkylation) from methoxyl to the phenolic ring. The metal function accelerates demethylation, hydrodeoxygenation and hydrogenation in this order. On a Pt/H-Beta catalyst, meanwhile, both hydrodeoxygenation and methyl transfer occurred, resulting in toluene, benzene and xylenes. In comparison with the monofunctional catalysts, bifunctional Pt/H-Beta increases catalyst stability in respect to deactivation and reduces coke deposition.

Hydrodeoxygenation of an aqueous mixture of bio-derived phenolic monomers to hydrocarbon and methanol has also been studied using metal catalysts (Pd and Ni) in the presence of acid (H_3PO_4 or Nafion/SiO_2) at 200 ^{o}C. A Raney Ni catalyst with Nafion/SiO_2 showed good activity and selectivity, with nearly 100% yields. Raney Ni acts as the hydrogenation metal catalyst and Nafion/SiO_2 acts as the Brønsted solid acid for hydrolysis and dehydration [131].

Lee et al. [132] tested the hydrodeoxygenation of lignin monomer guaiacol over bifunctional catalysts comprised of noble metals supported on the acidic matrices, Rh/SiO_2-Al_2O_3 and

Rh/ZrO_2, in the temperature range of 220-310 ^oC. They demonstrated that the selectivity to cyclohexane increases with increasing temperature.

Zhao et al. [133] reported the use of a bifunctional metal-acid catalyst (Pd/C (5 wt%) and H_3PO_4-H_2O (0.5wt%-80 ml)) in aqueous phase hydrodeoxygenation of anisole at 150 ^oC and 5 MPa H_2. The main product was cyclohexanone (80% selectivity) produced by hydrogenation of phenol, which indicates that under the chosen conditions, hydrolysis of anisole to phenol is the dominating reaction.

More recently, Ni-based catalysts were used to study the effect of the metal-support interaction on the selective anisole hydrodeoxygenation to aromatics. Ni-containing (20 wt% loading) catalysts supported on SBA-15, Al-SBA-15, γ-Al_2O_3, microporous carbon, TiO_2 and CeO_2 were tested at 290-310 ^oC, 3 bar hydrogen pressure and space velocity (20.4 and 81.6 h^{-1}). At 310 ^oC and 20.4 h^{-1} space velocity, the Ni/C catalyst showed the best activity and selectivity toward benzene (64% yield) owing to the strong acidity and good metal dispersion. The findings suggest that selecting appropriate catalyst characteristics can promote the selective production of aromatics from biomass in a bio-refinery scheme [134].

Finally, bifunctional Pt supported on HY zeolite showed high activity and selectivity for the hydrodeoxygenation of phenol at 250 ^oC in a fixed-bed reactor and high H_2 pressures forming hydrocarbons, some with enhanced molecular weight [135].

1.5.4 Decomposition of esters

Ethyl propanoate is produced from the esterification of propanoic acid with ethanol. Hydrodeoxygenation can upgrade this ester to enhance fuel properties and to gain synthetic biofuels [137].

Ethyl propanoate is used as a solvent in perfumery and fragrance formulations. It can also be used to manufacture various propanoates for use in pharmaceuticals, antifungal agents, agrochemicals, plasticizers, rubber chemicals, dyes, etc. [137].

Mechanistically, the acid-catalysed decomposition of ethyl propanoate (EP), an aliphatic ester, involves ester protonation to form an oxonium ion followed by acyl−oxygen or alkyl−oxygen bond breaking, which can occur through monomolecular ($A_{AC}1$ or $A_{AL}1$) or bimolecular ($A_{AC}2$ or $A_{AL}2$) pathways (Scheme 1.8). This mechanism is well documented for acid-catalysed hydrolysis of esters in homogeneous solutions [138]. In the gas phase, due to the lack of solvation of cationic intermediates (acylium and primary alkylcarbenium ions), the acid-catalysed EP decomposition yielding an equimolar mixture of propanoic acid and ethene (this will be discussed in more detail in Chapter 6).

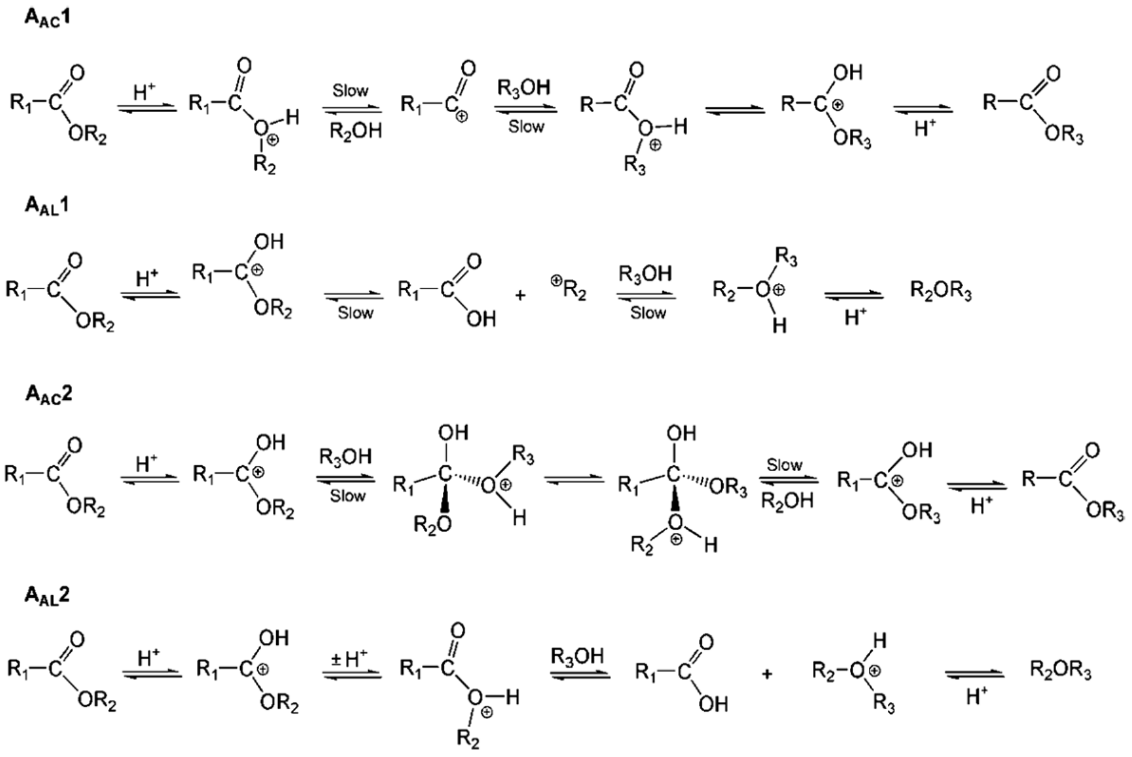

Scheme 1.8 Mechanism of acid ester hydrolysis (when R_3 = H). In the case of R_3 = alkyl, it occurs through transesterification for the A_{AC} mechanism and through etherification for the A_{AL} mechanism [139].

A ruthenium–platinum bimetallic catalyst supported on boehmite and γ-Al_2O_3 was used to study the hydrogenation of ester to produce alcohol in the liquid phase. The effect of surface hydroxyl groups on support and solvent was also reported. In an aqueous solution the Ru–Pt/AlOOH catalyst exhibited better performance than the Ru–Pt/γ-Al_2O_3 in respect to the hydrogenation of methyl propanoate. At 180 ^oC and 5 MPa of H_2 pressure, Ru–Pt/AlOOH catalyst showed very good activity, giving 89 % methyl propanoate conversion with 98% 1-propanol selectivity. The good catalyst performance is attributed to the cooperation between the hydroxyl groups of ALOOH surface and water solvent [140].

Senol et al. [141] have studied the hydrodeoxygenation of aliphatic ester methyl heptanoate in the liquid phase over sulfided NiMo/γ-Al_2O_3 and CoMo/γ-Al_2O_3 catalysts at 250 ^0C and 1.5 MPa of H_2. They also studied the effect of water on the activity of these catalysts. Moreover, they examined the addition of H_2S to the feed, alone and simultaneously with water. They found that under the same conditions the NiMo catalyst showed much higher activity than the CoMo catalyst. They also reported that the addition of water decreased the activity of the catalyst, however, the conversion increased with the addition of H_2S to the same level as that without water addition. The highest ester conversion was obtained when only H_2S was added. In addition, the hydrocarbon yield decreased with an increase in the amount of water, while the concentration of oxygen-containing intermediates increased. The addition of H_2S enhanced the selectivity toward C_6 hydrocarbons, but the catalysts suffered from deactivation.

Zhang et al. [142] investigated the hydrogenation of ethyl acetate to produce ethanol over Ni-based catalysts prepared from Ni/Al hydrotalcites. The highest selectivity (68%) and yield (62%) of ethanol was obtained using a RE1NASH-110-3 catalyst at 250 ℃ and 6 MPa of hydrogen pressure.

The present work demonstrates that Pt/$Cs_{2.5}H_{0.5}PW_{12}O_{40}$ is an efficient catalyst for gas-phase hydrodeoxygenation of a variety of oxygen-containing compounds such as ketones, ethers, and esters in a fixed-bed reactor at temperatures below 100 ^{o}C and ambient H_2 pressure (Chapters 4-6). More recently, Mizuno et al. [105] have applied this catalyst for hydrogenation of ketones, phenols, and ethers in the liquid phase in a batch reactor at 120 ^{o}C and 5 bar H_2 pressure. This catalyst also showed good activity and selectivity under such conditions.

1.6 Objectives and thesis outline

The conversion of biomass-derived oxygenated molecules, such as ketones, ethers, esters, etc., into value-added chemicals and bio-fuels has been attracting increasing attention, as a result of the decline in oil resources and global warming. For fuel applications, these oxygenates require their oxygen content to be reduced so as to increase their caloric value. The aim of this study is to examine the gas phase hydrodeoxygenation of a wide range of oxygenated compounds, ketones, ethers and esters, over bifunctional metal acid catalysis under mild conditions. The metals used include Pt, Ru, Ni and Cu supported on $Cs_{2.5}H_{0.5}PW_{12}O_{40}$ (CsPW), an acidic Cs salt of a Keggin-type heteropoly acid $H_3PW_{12}O_{40}$. Details about the reaction mechanisms are studied, as well as the effect of various catalyst preparation methods.

Another target of this study is to investigate the effect of a gold additive on the activity and performance stability of physically mixed and supported bifunctional catalysts comprising Pt and CsPW in HDO of 3-pentanone in the gas phase.

The catalysts are characterised using various techniques to compare properties that are vital to their use in the reaction. The metals supported on the surface of $Cs_{2.5}PW$ and active carbon are probed using scanning transmission electron microscopy (STEM), X-ray diffraction (XRD) and gas chemisorption for the purpose of determining their dispersion and average particle size. Other

techniques utilised are inductivity coupled plasma (ICP), Fourier transform infrared spectroscopy (FTIR), ammonia adsorption microcalorimetry and element analysis (C, H analysis).

Chapter 1 provides a general introduction to heterogeneous and multifunctional catalysis, along with a brief discussion of the structure and properties of heteropoly acids. Recent literature on the deoxygenation of oxygen-containing organic compounds to form value-added chemicals and biofuels is also covered.

Chapter 2 provides a description of the methods for preparing the bifunctional, acid and bimetallic catalysts, along with the techniques that are used for the characterisation of catalysts and gas phase catalyst reaction testing.

Chapter 3 details the results of the catalyst characterisation techniques, focussing especially on the properties that will have a bearing on the catalytic performance during the hydrodeoxygenation (HDO) of oxygenated compounds.

Chapter 4 investigates the catalytic performance of metal/CsPW catalysts in the HDO of a variety of ketones, including aliphatic ketones and acetophenone in a gas phase reaction operated under mild conditions. This provides insights into the reaction mechanism.

Chapter 5 reports the enhancing effect of gold in the HDO of ketone, 3-pentanone, over a bifunctional Pt/CsPW catalyst in the gas phase.

Chapter 6 explores the deoxygenation and decomposition of a series of ethers and esters, including the aromatic ether anisole, the aliphatic diisopropyl ether (DPE) and the aliphatic ester ethyl propanoate (EP) in the gas phase using bifunctional metal-acid catalysis with the main focus on the Pt−CsPW catalyst. Moreover, the relationship between the turnover reaction rate (turnover frequency) and the HPA acid strength is discussed.

Chapter 7 draws conclusions from the key findings from the previous chapters.

1.7 References

1. G. C. Bond, Heterogeneous Catalysis: Principles and Applications, Clarendon Press, Oxford, 1974.
2. M. Bowker, The Basis and Applications of Heterogeneous Catalysis, Oxford University Press Inc., New York, 1998.
3. B. C. Gates, Catalytic Chemistry, Wiley, Chichester, 1992.
4. M. Michael, Principles of Chemistry, W.W. Norton & Company, 2000.
5. J. R. H. Ross, Heterogeneous Catalysis: Fundamentals and Applications, Elsevier: Amsterdam, 2012.
6. J. M. Thomas, W. J. Thomas, Principles and Practice of Heterogeneous Catalysis, VCH, Weinheim, 1997.
7. O. Deutschmann, H. Knözinger, K. Kochloefl, T. Turek, Heterogeneous Catalysis and Solid Catalysts, Ullmann's Encyclopedia of Industrial Chemistry, Wiley-VCH Verlag GmbH & Co. KGaA, New York, 2000.
8. G. Ertl, H. Knözinger, J. Weitkamp, Handbook of heterogeneous catalysis, Wiley-VCH, Weinheim, 1997.
9. H. Hattori, Mat. Chem. Phys. 18 (1988) 533.
10. W. Keim, Green. Chem. 5 (2003) 105.
11. R. A. Sheldon, H.van Bekkum, Fine Chemicals through Heterogeneous Catalysis, Wiley, Chichester, 2001.
12. S. M. George, Chem. Rev. 95 (1995) 475.
13. K. W. Kolansinski, Surface Science: Foundations of Catalysis and Nanoscience, John Wiley and Sons Inc., West Chester, 2002.
14. G. Ertl, H. Knozinger, J. Weitkamp, Preparation of Solid Catalysts, Wiley-VCH, Germany, 1999.
15. J. R. Anderson, Structure of metallic catalysts, Academic Press, London, 1975.
16. M. Haruta, T. Kobayashi, H. Sano, N. Yamada, Chem. Lett. 405 (1987) 405.
17. G. J. Hutchings, J. Catal. 96 (1985) 292.
18. L. Prati, A. Villa, Catal. 2 (2012) 24.
19. A. S. K. Hashmi, G. J. Hutchings, Angew. Chem., Int. Ed. 45 (2006) 7896.
20. S. A. K. Hashmi, Chem. Rev. 107 (2007) 3180.
21. A. Arcadi, S. Di Giuseppe, Curr. Org. Chem. 8 (2004) 795.

22. E. Jimenez-Nunez, A. M. Echavarren, Chem. Commun. (2007) 333.
23. G. C. Bond, C. Louis, D. T. Thompson, Catalysis by Gold, Imperial College Press, London, 2007.
24. A. Corma, H. Garcia, Chem. Soc. Rev. 37 (2008) 2096.
25. G. H. Brundtland, Our common future: The World Commission on Environment and Development, Oxford University Press, 1987.
26. A. Bruggink, R. Schoevaart, T. Kieboom, Org. Pro. Res. Dev. 7 (2003) 622.
27. J. C. Wasilke, S. J. Obrey, R. T. Baker, G. C. Bazan, Chem. Rev. 105 (2005) 1001.
28. D. E. Fogg, E. N. dos Santos, Coord. Chem. Rev. 248 (2004) 2365.
29. A. Kuhlmann, F. Roessner, W. Schwieger, O. Gravenhorst, T. Selvam, Catal. Today 97 (2004) 303.
30. M. J. F. M. Verhaak, A. J. Vandillen, J. W. Geus, Appl. Catal. A 109 (1994) 263.
31. A. Nissen, G. Heiien, E. Sapper, W. Fliege, A. Wittver, US Patent 4239657, 1980.
32. C. Carlini, M. Marchionna, M. Noviello, A. M. R. Galletti, G. Sbrana, F. Basile, A. Vaccari, J. Mol. Catal. A 232 (2005) 13.
33. D. Tichit, B. Coq, S. Cerneaux, R. Durand, Catal. Today 75 (2002) 197.
34. P. Y. Chen, S. J. Chu, N. S. Chang, T. K. Chuang, L. Y. Chen, Stud. Surf. Sci. Catal. 46 (1989) 231.
35. C. O. Veloso, J. L. F. Monteiro, E. F. Sousaaguiar, Stud. Surf. Sci. Catal. 84 (1994) 1913.
36. W. Nicol, E. L. du Toit, Chem. Eng. Proc. 43 (2004) 1539.
37. P. P. Yang, Y. C. Shang, J. F. Yu, J. Wang, M. L. Zhang, T. G. Wu, J. Mol. Catal. A 272 (2007) 75.
38. P. P. Yang, H. F. Yu, Z. L. Wang, M. P. Xu, Q. S. Liu, X. W. Yang, T. H. Wu, Catal. Comm. 6 (2005) 107.
39. S. M. Yang, Y. M. Wu, Appl. Catal. A 192 (2000) 211.
40. E. F. Kozhevnikova, I. V. Kozhevnikov, J. Catal. 238 (2006) 286.
41. R. D. Hetterley, E. F. Kozhevnikova, I. V. Kozhevnikov, Chem. Commun. (2006) 782.
42. R. D. Hetterley, R. Mackey, J. T. A. Jones, Y. Z. Khimyak, A. M. Fogg, I.V. Kozhevnikov, J. Catal. 258 (2008) 250.
43. F. Winter, A. J. van Dillen, K. P. de Jong, J. Mol. Catal. A 219 (2004) 273.
44. I. V. Kozhevnikov, Chem. Rev. 98 (1998) 171.

45. T. Okuhara, N. Mizuno, M. Misono, Adv. Catal. 41 (1996) 113.
46. I. V. Kozhevnikov, Catalysts for Fine Chemical Synthesis, Catalysis by Polyoxometalates, Wiley, Chichester, 2002.
47. S. Liu, D. Volkmer, D. G. Kurth, J. Clust. Sci. 14 (2003) 405.
48. J. T. Rhule, C. L. Hill, D. A. Judd, Chem. Rev. 98 (1998) 327.
49. N. Mizuno, M. Misono, Chem. Rev. 98 (1998) 199.
50. M. Misono, Chem. Comm. (2001) 1141.
51. R. Wlodarczyk, M. Chojak, K. Miecznikowski, A. Kolary, P. J. Kulesza, R. Marassi, J. Power Sources 159 (2006) 802.
52. F. Cavani, Catal. Today 41 (1998) 73.
53. M. J. Janik, R. J. Davis, M. Neurock, J. Phys. Chem. B 108 (2004) 12292.
54. J. Mater. Chem. A 2 (2014) 7637.
55. I. V. Kozhevnikov, J. Mol. Catal. A 262 (2007) 86.
56. U. B. Mioc, Ph. Colomban, M. Davidovic, J. Tomkinson, J. Mol. Struct. 326 (1994) 99.
57. J. B. Moffat, Metal-Oxygen Clusters: The Surface and Catalytic Properties of Heteropoly Oxometalates, Kluwer, New York, 2001.
58. D. B. Taylor, J. B. Mcmonagle, J. B. Moffat, J. Colloid Interface Sci. 108 (1985) 278.
59. M. Misono, Catal. Rev. Sci. Eng. 30 (1988) 339.
60. T. Okuhara, T. Nishimura, H. Watanabe, M. Misono, J. Mol. Catal. 74 (1992) 247.
61. C. V. Hidalgo, H. Itoh, T. Hattori, M. Niwa, Y. Murakami, J. Catal. 85 (1984) 362.
62. Y. Izumi, R. Hasebe, K. Urabe, J. Catal. 84 (1983) 402.
63. F. Lefebvre, F. X. Liucai, A. Auroux, J. Mater. Chem. 4 (1994) 125.
64. A. Auroux, M. B. Sayed, J. C. Vedrine, Thermochim. Acta. 93 (1985) 557.
65. L. C. Josefowicz, H. G. Karge, E. Vasilyeva, J. B. Moffat, Microporous Mater. 1 (1993) 313.
66. I. V. Kozhevnikov, Russ. Chem. Rev. 56 (1987) 811.
67. Y. Izumi, K. Urabe, Chem. Lett. (1981) 663.
68. M. A. Schwegler, H. van Bekkum, Appl. Catal. 74 (1991) 191.
69. T. Baba, Y. Ono, Appl. Catal. 22 (1986) 321.
70. T. Matsuda, A. Igarashi, Y. Ogino, J. Jpn. Pet. Inst. 23 (1980) 30.

71. G. I. Kapustin, T. R. Brueva, A. L. Klyachko, M. N. Timofeeva, S. M. Kulikov, I. V. Kozhevnikov, Kinet. Katal. 31 (1990) 1017.
72. G. I. Kapustin, T. R. Brueva, Thermochimica Acta. 379 (2001) 71.
73. B. B. Bardin, R. J. Davis, Appl. Catal. 200 (2000) 219.
74. T. Okuhara, Appl. CataL. A 256 (2003) 213.
75. G. Koyano, K. Ueno, M. Misono, Appl. Catal. A 181 (1999) 267.
76. S. Soled, S. Miseo, G. Mc Vicker, W. E. Gates, A Gutierrez, J. Paes, Catal. Today 36 (1997) 441.
77. S. Soled, S. Miseo, G. McVicker, W. E. Gates, A Gutierrez, J. Paes, Chem. Eng. J. 64 (1996) 247.
78. M. Misono, Mater. Chem. Phys. 17 (1987) 103.
79. T. Okuhara, T. Nakato, Catal. Surv. 2 (1998) 31.
80. Y. Izumi, K. Urabe, M. Onaka, Zeolite, Clay and Heteropoly Acid in Organic Reactions, Kodansha/VCH, Tokyo, 1992.
81. T. Okuhara, Chem. Rev. 102 (2002) 3641.
82. A. Alhanash, E. F. Kozhevnikova, I. V. Kozhevnikov, Catal. Lett. 120 (2008) 307.
83. M. A. Alotaibi, E. F. Kozhevnikova, I. V. Kozhevnikov. App. Catal. 447– 448 (2012) 32.
84. K. A. D. Rocha, P. A. Robles-Dutenhefner, E. M. B. Sousa, E. F. Kozhevnikova, I. V. Kozhevnikov, E. V. Gusevskaya, Appl. Catal. A 317 (2007) 171.
85. M. R. H. Siddiqui, S. Holmes, H. He, W. Smith, E. N. Coker, M. P. Atkins, I. V. Kozhevnikov, Catal. Lett. 66 (2000) 53.
86. M. Musawir, E. F. Kozhevnikova, I. V. Kozhevnikov, J. Mol. Catal. A 262 (2007) 93.
87. G. W. Huber, S. Iborra, A. Corma, Chem. Rev. 106 (2006) 4044.
88. K. A. Hossain, Int. J. Renewable Energy Technol. Res.1 (2012) 23.
89. R. L. Lynd, J. H. Cushman, R. J. Nichols, C. E. Wyman, Science. 251 (1991) 1318.
90. C. E. Wyman, Appl. Biochem. Biotechnol. 897 (1994) 45.
91. D. Klemm, B. Heublein, H.-P. Fink, A. Bohn, Angew. Chem. 44 (2005) 2.
92. C. B. Field, M. J. Behrenfeld, J. T. Randerson, P. Falkowski, Science. 281 (1998) 237.
93. S. Tokgoz, A. Elobeid, An Analysis of the Link between Ethanol, Energy, and Crop Markets, Ames, Iowa State University,2006.

94. L. Čuček, M. Martin, I. E. Grossmann, Z. Kravanja, Comp. Chem. Eng. 35 (2011) 1547.
95. D. Bacovsky, M. Dallos, M. Wörgetter, IEA Report 39 (2010) 1.
96. A. Corma, S. Iborra, A. Velty, Chem. Rev. 107 (2007) 2411.
97. E. L. Kunkes, D. A. Simonetti, R. M. West, J. C. Serrano-Ruiz, C. A. Gaertner, J. A. Dumesic, Science 322 (2008) 417.
98. H. Bernas, K. Eranen, I. Simakova, A.-R. Leino, K. Kordas, J. Myllyoja, P. Maki-Arvela, T. Salmi, D. Yu. Murzin, Fuel 89 (2010) 2033.
99. J. G. Immer, M. J. Kelly, H. H. Lamb, Appl. Catal. A 375 (2010) 134.
100. P. T. Do, M. Chiappero, L. L. Lobban, D. Resasco, Catal. Lett. 130 (2009) 9.
101. M. Arend, T. Nonnen, W. F. Hoelderich, J. Fischer, J. Groos, Appl. Catal. A 399 (2011) 198.
102. M. B. Smith, J. March, March's Advanced Organic Chemistry: Reactions, Mechanisms, and Structure, 6th ed., John Wiley & Sons, Inc., Hodoken, New Jersey, 2007.
103. M. A. Alotaibi, E. F. Kozhevnikova, I. V. Kozhevnikov, Chem. Commun. 48 (2012) 7194.
104. M. A. Alotaibi, E. F. Kozhevnikova, I. V. Kozhevnikov, J. Catal. 293 (2012) 141.
105. S. Itagaki, N. Matsuhashi, K. Taniguchi, K. Yamaguchi, N. Mizuno, Chem. Lett.43 (2014) 1086.
106. E. Furimsky, Appl. Catal. A 199 (2000) 147.
107. Q. Bu, H. Lei , A. H. Zacher, L.Wang, S. Ren, J. Liang, Y. Wei, Y. Liu, J. Tang, Q. Zhang, R. Ruan, Bioresour.Technol. 124 (2012) 470.
108. J. Wildschut, F. H. Mahfud, R. H. Venderbosch, H. J. Heeres, Ind. Eng. Chem. Res. 48 (2009) 10324.
109. T. T. Isimjan, Q. He, Y. Liu, J. Zhu, R. J. Puddephatt, D. J. Anderson, ACS Sustainable Chem. Eng. 1 (2013) 381.
110. R. A. Augustine, Heterogeneous Catalysis for the Synthetic Chemist, Marcel Dekker, New York, Inc., N. Y., 1996.
111. A. D. Murkute, J. E. Jackson, D. J. Miller, J. Catal. 278 (2011) 189.
112. M. Renz, European Journal of Organic Chemistry (2005) 979.
113. T. Yokoyama, N. Yamagata, Appl. Catal. A 221 (2001) 227.

114. H. Benaissa, P. N. Davey, E. F. Kozhevnikova, I. V. Kozhevnikov, Appl. Catal. A 351 (2008) 88.
115. H. Benaissa, P. N. Davey, Y. Z. Khimyak, I. V. Kozhevnikov, J. Catal. 253 (2008) 244.
116. H. -J. A. K. Weissermel, Industrial Organic Chemistry, 3rd ed., VCH, Weinheim, 1997.
117. J. J. Gamman, S. D. Jackson, F. A. Wigzell, Ind. Eng. Chem. Res. 49 (2010) 8439.
118. G. Waters, O. Richter, B. Kraushaar-Czarnetzki, Ind. Eng. Chem. Res. 45 (2006) 6111.
119. G. Waters, O. Richter, B. Kraushaar-Czarnetzki, Ind. Eng. Chem. Res. 45 (2006) 5701.
120. F. Zaccheria, N. Ravasio, M. Ercoli, P. Allegrini, Tetrahedron Lett. 46 (2005) 7743.
121. Y.Jiang, R.Buchel, J.Huang, F.Krumeich, S.E.Pratsinis, A.Baiker, ChemSusChem. 5 (2012) 1190.
122. B. G. R. H. A. Wittcoff, Industrial Organic Chemicals, Wiley, N. Y., 1996.
123. F. P. Heese, M. E. Dry, K. P. Moller, Catal. Today 49 (1999) 327-335
124. T. L. Marker, H. U. Hammershaimb, R. Marinangeli, W. H. Keesom, U. G. Bozzano, AIChE Annual Meeting, 1993.
125. T. L. Marker, W. H. Keesom, R. Schmidt, S. Davis, R. Marinangeli, Conference on Clean Air Act and Reformulated Gasolines, 1994.
126. T. L. Marker, G. A. Funk, H. U. Hammershaimb, US Patent 5504258, 1996.
127. R. J. Taylor, Jr., P. E. Dai, J. F. Knifton, US Patent 5583266, 1996.
128. H. Y. Zhao, D. Li, P. Bui, S. T. Oyama, Appl. Catal. A 391 (2011) 305.
129. C. Zhao, J. A. Lercher, ChemCatChem 4 (2012) 64−68.
130. X. L. Zhu, L. L. Lobban, R. G. Mallinson, D. E. Resasco, J. Catal. 281 (2011) 21.
131. C. Zhao, Y. Kou, A. A. Lemonidou, X. Li, J. A. Lercher, Chem. Commun. 46 (2010) 412.
132. C. R. Lee, J. S. Yoon, Y. W. Suh, J. W. Choi, J. M. Ha, D. J. Suh, Y. K. Park, Catal. Commun. 17 (2012) 54.
133. C. Zhao, J. He, A. A. Lemonidou, X. Li, J. A. Lercher, J. Catal. 280 (2011) 8.
134. Y. Yang, C. Ochoa-Hernández, V. A. de la Pe˜na O'Shea, P. Pizarro, J. M. Coronado, D. P. Serrano, Appl. Catal. B 145 (2014) 91.

135. D. Y. Hong, S. J. Miller, P. K. Agrawala, C. W. Jones, Chem. Commun. 46 (2010) 1038.
136. X. Zhu, L. Nie, L. L. Lobban, R. G. Mallinson, D. E. Resasco, Energy Fuels 28 (2014) 4104.
137. S. S. Kanwar, H. K. Verma, R. K. Kaushal, R. Gupta, S. S. Chimni, Y. Kumar, G. S. Chauhan, World J. Microbiol Biotechnol, 21 (2005) 1037.
138. R. A. Y. Jones, Physical and Mechanistic Organic Chemistry, Cambridge University Press, Cambridge, 1979, 227.
139. P. L. Silva, C. M. Silva, L. Guimarães, J. R. Pliego Jr., Theor Chem Acc 134 (2015) 1591.
140. Y. Zhou, H. Fu, X. Zheng, R. Li, H. Chen, X. Li, Catal. Comm. 11 (2009) 137.
141. O. I. Senol, T. R. Viljava, A. O. I. Krause, Catal. Today 106 (2005) 186.
142. B. Zhang, L. Lin , J. Zhuang, Y. Liu, L. Peng, L. Jiang, Molecules 15 (2010) 5139.

2. Experimental

2.1 Introduction

This chapter will describe the experimental techniques that were used in this study. It will begin with the synthesis of the metal-HPA bifunctional catalysts, before moving on to explore the catalyst characterisation techniques used to determine the catalyst's surface and porosity properties, element content, particle sizes, catalyst stability and metal dispersion. Finally, the experimental set up of the reaction studies will be described, in addition to the calculations of the conversion and the product selectivity.

2.2 Materials

MIBK (99%), diisobutyl ketone (80%), acetophenone (≥98%), 2-octanone (98%), cyclohexanone (≥99%), 3-pentanone (≥99%), diisopropyl ether (≥98.5%), ethyl propanoate (99%) and inorganic chemicals used for catalysts preparation were purchased from Aldrich, and anisole (99%) was from Avocado, and 2-butanone (99%) and 2-hexanone (98%) from Acros Organics. Heteropoly acid hydrates, $H_3PW_{12}O_{40}$ (HPW, 99%) and $H_4SiW_{12}O_{40}$ (HSiW, 99.9%) containing 20-28 H_2O molecules per Keggin unit, were purchased from Sigma-Aldrich. The amount of crystallization water in the HPAs was determined by TGA. Carbon-supported platinum 10%Pt/C (7.1% Pt content in dried catalyst from ICP analysis) was from Johnson Matthey. H_2 and N_2 gases (>99%) were supplied by the British Oxygen Company.

Catalyst supports Aerosil 300 silica (surface area S_{BET} = 300 m^2g^{-1}) and P25 titania (anatase/rutile = 3:1, S_{BET} = 44 m^2g^{-1}) were from Degussa.

2.3 Catalyst preparation

2.3.1 Preparation of $Cs_nH_{3-n}PW_{12}O_{40}$

$Cs_{2.5}H_{0.5}PW_{12}O_{40}$ (CsPW) and $Cs_{2.25}H_{0.75}PW_{12}O_{40}$ were prepared according to the literature procedure [1] by adding dropwise the required amount of aqueous solution of Cs_2CO_3 (0.47 M) to an aqueous solution of $H_3PW_{12}O_{40}$ (0.75 M) at 40 ^oC with continuous stirring. The precipitates obtained were aged in aqueous slurry for 24 h at room temperature. The slurry was then slowly evaporated to dryness in a rotary evaporator at 45 ^oC to afford the catalysts as white powder. The catalysts were calcined under vacuum at 150 $^oC/10^{-3}$ kPa for 1.5 h and ground to 45-180 μm particle size.

2.3.2 Preparation of Pt, Ru, Cu, Ni and Au modified CsPW

Bifunctional metal-acid catalysts were prepared by wet impregnation of CsPW with an appropriate metal precursor ($Pt(acac)_2$, H_2PtCl_6, $RuCl_3$, $Ni(NO_3)_2$, $Cu(NO_3)_2$ and $HAuCl_4$) followed by reduction of metal ion to metal with H_2. The metal loadings quoted were confirmed by the ICP-AES elemental analysis; these were in good agreement with the preparation stoichiometries since the preparations did not involve operations such as filtration and washing which could cause metal loss.

2.3.2.1 Preparation of Pt/CsPW

0.5%Pt/CsPW was prepared by stirring CsPW powder with 0.02 M $Pt(acac)_2$ solution in benzene at room temperature for 1 h, followed by slow evaporation of benzene in a rotary evaporator at room temperature [2]. The catalyst was calcined under vacuum at 150 $^oC/10^{-3}$ kPa and then reduced in an oven by a hydrogen flow at 250 ^oC for 2 h. Two other modifications of this catalyst were prepared by impregnation of CsPW with an aqueous solution of H_2PtCl_6, followed by drying in a rotary evaporator at 45 ^oC and the same calcination and reduction procedures. One,

designated as 0.5%Pt/CsPW-I, was prepared by direct wet impregnation of CsPW powder with 0.1 M aqueous solution of H_2PtCl_6 involving stirring the aqueous slurry for 24 h at room temperature, followed by the workup procedure. The other, designated as 0.5%Pt/CsPW-A, was prepared by adding 0.1 M aqueous solution of H_2PtCl_6 to the freshly precipitated aqueous CsPW slurry and ageing the mixture at room temperature with stirring for 24 h, followed by the workup. For comparison with Au/CsPW and Pt/Au/CsPW catalysts, different Pt loadings of Pt/CsPW-I catalyst were used (0.3-6 wt%).

The physical mixture of 7%Pt/C and CsPW containing 0.35% of Pt was prepared by grinding a 1:19 w/w mixture of the two components**.**

10%Pt/SiO_2 was prepared by impregnation of Aerosil 300 silica with $Pt(acac)_2$ from benzene, followed by reduction with H_2 at 250 ^oC for 2 h. The physical mixture 10%Pt/SiO_2 + CsPW containing 0.5% of Pt was prepared by grinding a 1:19 w/w mixture of the two components.

2.3.2.2 Preparation of Ru/CsPW

Two modifications of 5%Ru/CsPW, designated as 5%Ru/CsPW-I and 5%Ru/CsPW-A, were prepared by impregnation of CsPW with 0.1 M aqueous solution of $RuCl_3$ similar to the preparation of 0.5%Pt/CsPW-I and 0.5%Pt/CsPW-A.

2.3.2.3 Preparation of Cu/CsPW

10%Cu/CsPW catalyst, designated as 10%Cu/CsPW-I, was prepared as described elsewhere [2] by stirring CsPW powder with an aqueous solution of $Cu(NO_3)_2.6H_2O$ for 24 h at room temperature, followed by drying in a rotary evaporator at 65 ^oC and calcination at 150 $^oC/10^{-3}$ kPa for 1.5 h. Finally, the sample was reduced in H_2 flow at 400 ^oC for 2 h. Another modification of this catalyst, designated as 10%Cu/CsPW-A, was prepared by adding an aqueous solution of

$Cu(NO_3)_2 \cdot 6H_2O$ to the freshly precipitated aqueous CsPW slurry and ageing the mixture at room temperature with stirring for 24 h, followed by the same workup.

2.3.2.4 Preparation of Ni/CsPW

Two modifications of 10%Ni/CsPW catalyst, designated as 10%Ni/CsPW-I and 10%Ni/CsPW-A, were prepared similarly to the corresponding 10%Cu/CsPW catalysts using $Ni(NO_3)_2 \cdot 6H_2O$ as a precursor.

2.3.2.5 Preparation of Au/CsPW

Au/CsPW was prepared by wet impregnation of CsPW powder with aqueous solutions of $HAuCl_4$. This involved stirring the aqueous slurry at 50 ^oC for 2 h followed by rotary evaporation to dryness and reduction with H_2 flow at 250 ^oC for 2 h. This catalyst had metal loadings between 0.3 – 6 wt%.

2.3.2.6 Preparation of bimetallic Pt/Au/CsPW catalysts

The bimetallic PtAu/CsPW catalysts were prepared similarly; PtAu/CsPW-CI was prepared by co-impregnation, whereas PtAu/CsPW-SI by sequential impregnation of CsPW with H_2PtCl_6 and $HAuCl_4$. The sequential procedure included preparation of Pt/CsPW with reduction by H_2 at 250 ^oC/2 h followed by impregnation of the Pt/CsPW thus made with $HAuCl_4$ aqueous solution and subsequent reduction (H_2/250 ^oC/2 h). In this case, the Pt was treated twice with H_2 at 250 ^oC.

Physically mixed metal-acid bifunctional catalysts 5%Pt/C + CsPW, 5%Au/C + CsPW, 5%Pt/5%Au/C + CsPW, and 5%Pt/10%Au/C + CsPW with 0.5% Pt loading were prepared by grinding a 1:9 w/w mixture of the corresponding two components. 5%Pt/C, 5%Au/C and PtAu/C catalysts were prepared in-house (see below).

2.3.3 Preparation of carbon-supported metal catalysts

Carbon-supported 5%Pt/C and 5%Au/C catalysts were prepared by wet impregnation of Darco KB-B activated carbon with aqueous solutions of H_2PtCl_6 and $HAuCl_4$ at 50 ^oC for 2 h followed by rotary evaporation to dryness and reduction by H_2 flow as above.

Bimetallic PtAu/C catalysts were prepared similarly by wet co-impregnation of the Darco KB-B carbon with H_2PtCl_6 and $HAuCl_4$ (Pt/Au = 1:1 and 1:2 mol/mol); these are hereafter referred to as 5%Pt/5%Au/C-CI and 5%Pt/10%Au/C-CI, respectively. PtAu/C catalysts were also prepared by sequential impregnation either by wet-impregnating the pre-made 5%Pt/C with the required amount of $HAuCl_4$ followed by reduction with H_2 at 250 ^oC/2 h (referred to as 5%Pt/5%Au/C-SI and 5%Pt/10%Au/C-SI) or the other way around by wet-impregnating the pre-made 5%Au/C with H_2PtCl_6.

2.3.4 Preparation of supported hetropoly acid catalysts

Catalyst supports Aerosil 300 silica (surface area S_{BET} = 300 m^2g^{-1}) and P25 titania (anatase/rutile = 3:1, S_{BET} = 44 m^2g^{-1}) were from Degussa. ZrO_2 (S_{BET} = 107 m^2g^{-1}) and Nb_2O_5 (S_{BET} = 187 m^2g^{-1}) were prepared in-house (see below) [3] and calcined at 400 ^oC in air for 5 h.

Supported 15 wt% HPA catalysts were prepared by wet impregnation of the oxide supports with an aqueous HPA solution [3-5]. An oxide support (8.5 g) was mixed with the required amount of aqueous HPW solution. Then the slurry formed was left to age with stirring for 24 h at room temperature. After that, the catalyst was dried in a rotary evaporator. The catalyst was calcined in air for 3 h at a temperature ranged from 100 to 500°C.

15%HPW/SiO_2 catalyst was prepared by wet impregnation [6]. A suspension of 8.5 g Aerosil 300 silica (300 m^2/g) in 60-80 ml aqueous solution, containing a certain amount of heteropoly

acid, was stirred overnight at room temperature. After that, the catalyst was dried in a rotary evaporator. Then the catalyst was calcined under vacuum at 150°C/0.1 kPa for 1.5 h.

Supported hetropoly acid catalysts were kindly provided by Mrs W. Alharbi.

2.3.5 Preparation of Nb_2O_5

Nb_2O_5 (S_{BET} = 187 m^2g^{-1}) was made by the literature method [7]. It was prepared by dissolving a certain amount of $NbCl_5$ powder in ethanol and adding to aqueous solution of ammonia hydroxide (0.3 M) to form a white precipitate of $Nb_2O_5.nH_2O$. The precipitate was filtered off and washed with distilled water many times until chloride free, as tested with $AgNO_3$ (Equation 2.1). Finally, the niobic acid was left overnight in an oven for drying at 100 °C.

$$AgNO_3\,(aq) + Cl^-\,(aq) \longrightarrow AgCl\,(s)\downarrow + NO_3^-\,(aq) \qquad (2.1)$$

2.3.6 Preparation of ZrO_2

ZrO_2 was prepared according to the literature procedure [3]. At room temperature, aqueous ammonium hydroxide (30%) was added dropwise into an aqueous solution of $ZrOCl_2$ (5 g of $ZrOCl_2$ in 42 ml of water) with intense stirring until the pH 10 was reached. After that, the hydrogel produced was left with stirring at room temperature for 24 h and then filtered through a Buchner funnel. Distilled water was used to wash the white precipitate until chloride free, as tested with $AgNO_3$. Finally, the white precipitate was dried in an oven for 24 h at 100 °C.

2.4 Catalyst characterisation techniques

2.4.1 Surface area and porosity analysis

Generally, heterogeneous catalysts are porous materials. The surface area and pore texture of these materials can have significant effect on their activity, selectivity and stability. According to the IUPAC classification, pore sizes are classified into three size groups [8]:

1. Micropores – size < 2 nm, ultramicropores size < 0.7 nm
2. Mesopores – 2 nm < size < 50 nm
3. Macropores – size > 50 nm.

Porous solids have much higher total surface area than the external surface area as a result of the contribution of the porous cavity walls. In general, the total surface area of heterogeneous catalysts is between 1 and 1000 m^2 per gram, and from 0.1-10 m^2 per gram for the external surface area [8].

Nitrogen adsorption at boiling temperature -196 ^oC (77 K) is a very common technique to measure the catalyst surface area and its porous texture [8-11].

A well-defined procedure for determination of the total surface area of porous materials is the Brunauer-Emmett-Teller (BET) method, developed in 1938 [8, 12]. The BET surface area is measured from the BET plot using the relative pressure (P/P_O) usually in the range between 0.05 and 0.35. From the BET isotherm, the monolayer volume of adsorbed nitrogen gas, V_m, and the solid surface area, A_s, are calculated using equation 2.2 and 2.3, respectively:

$$\frac{P}{V(P_0 - P)} = \frac{1}{V_m C} + \frac{C-1}{V_m C}\frac{P}{P_0} \qquad (2.2)$$

In this equation, P is the pressure of adsorbate gas at equilibrium with the surface, P_o is the saturation pressure, V is the adsorbed gas volum and C is the BET constant.

$P/V(P_O - P)$ is plotted against the relative pressure (P/P_O) according to equation 2.2; this plot should give a straight line with the slope $(C-1)/V_mC$ and the intercept $1/V_mC$.

Finally the surface area can be calculated from equation 2.3.

$$A_s = (V_m / 22414)N_a\sigma \qquad (2.3)$$

In this equation, N_a is the Avogadro number ($6.022\ 10^{23}\ mol^{-1}$) and **σ** is the area covered by one nitrogen molecule, 0.162 nm^2 [10].

The BET surface area and porosity of catalysts were determined from nitrogen physisorption measured on a Micromeritics ASAP 2010 instrument at −196 ºC. Before measurement, the samples (typically 0.2 g) were evacuated at 250 ºC for 2 h. After degassing, the sample was allowed to cool to room temperature and reweighted to adjust the sample weight. Then, the sample tube was dipped in liquid nitrogen. Finally, the gas pressure was allowed to reach equilibrium before subsequent dosing and then a series of 55 successive nitrogen doses were applied in order to gain an adsorption isotherm. The surface analyser used is shown in Figure 2.1.

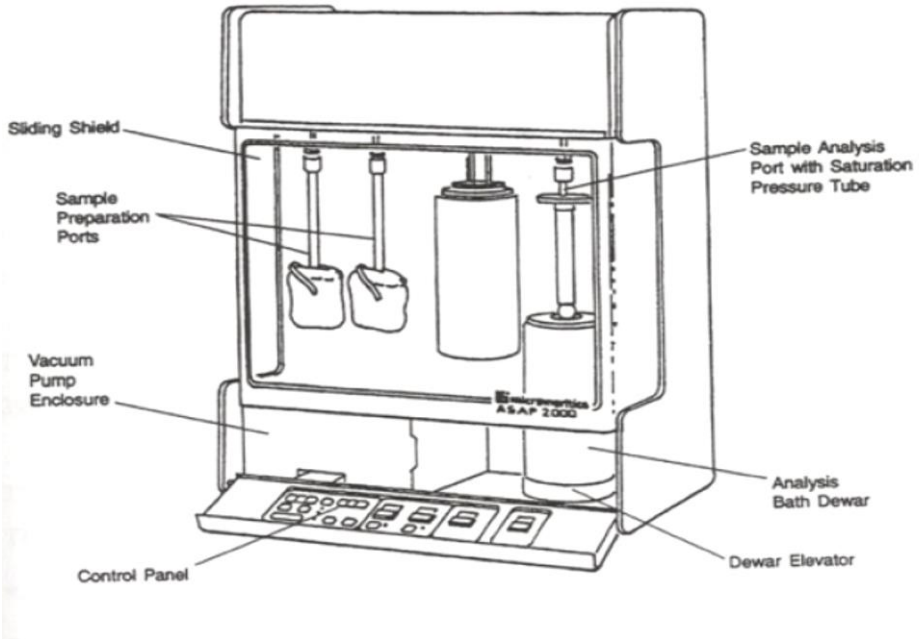

Figure 2.1 Micromeritics ASAP 2010 analyser utilised to determine the surface area and porosity of catalysts [13].

2.4.2 Inductively coupled plasma atomic emission spectroscopy (ICP-AEC)

ICP-AEC is an important technique for elemental analysis of catalyst samples. Solid samples are dissolved in a liquid, usually an acidic solution. Then, a plasma source (a gas mixture of positive ions and electrons created by heating gases such as argon at ≈6000 K) is used to ionize molecules and excite them to higher energy levels. Once they have returned to the ground state, they emit light with characteristic emission lines [14]. The intensity of the light can tell how much of each element is contained within the sample, whereas the wavelengths tell which elements are present. The spectral intensity of elements is proportional to the concentration of these elements in the sample, so the intensity produced can be compared to a standard curve to calculate the concentrations of the elements in the sample.

In this study, ICP spectroscopy was used to quantify metal content in the doped CsPW and active carbon. This experiment was kindly performed on a Spectro Ciros emission spectrometer by G. Miller at Liverpool University in Chemistry Department.

2.4.3 Powder X-ray diffraction (XRD)

XRD diffraction is one of the most important characterization technique used to study the phase structure of solid materials. The wavelengths of X-rays are equivalent to the atom spacing in crystals, so they are able to go through these materials, resulting in characteristic diffraction patterns. There are different factors that affect the scattering angle of X-rays which obeys the Bragg's law (Equation 2.4) [15].

$$n\lambda = 2d\sin\theta \qquad (2.4)$$

In Equation 2.4, n is the reflection order (an integer value), λ is the X-ray wavelength, d is the lattice planar spacing, θ is the angle of diffraction.

The X-ray diffractogram can provide valuable information including the crystallinity of solid materials, the dimensions and symmetries of the unit cell and the average particle size, which can be determined from the Scherrer equation (2.5):

$$t = 0.9\lambda/B\cos\theta \qquad (2.5)$$

Here t is the particle thickness, λ is the incident X-ray wavelength, B is the full-width at half maximum of the diffraction peak and θ is the diffraction angle. In this work, Pt, Au and Cu metal particle size was measured using this method [16].

In this work, powder X-ray diffraction (XRD) of catalysts were recorded on a PANalytical Xpert diffractometer with a CuKα radiation (λ= 1.542 Å). XRD patterns were attributed using the JCPDS database.

2.4.4 H_2 chemisorption

It is important to be able to determine the metal dispersion on the surface of the catalyst support in order to understand the activity of supported metal catalysts. The catalyst activity usually increases as the metal dispersion increases. For practical reasons, gas adsorption techniques are commonly used to determine the metal dispersion [17]. Metal dispersion is defined as the ratio of the total number of metal atoms which are at the surface of the metal particles to the total number of metal atoms in the catalyst. The metal particle size can be calculated from the dispersion of the metal atoms [18].

The metal dispersion of Pt and Ru in our catalysts was measured in a flow system by hydrogen chemisorption using the hydrogen-oxygen titration pulse method, which is a more sensitive and convenient analytic method to determine metal dispersion in supported metal catalysts [19, 20]. This technique has previously been used for dispersion measurement of Pd [20], Pt [19], Ru [21] and Rh [22].

In this study M/CsPW catalysts were reduced in hydrogen flow at 250 °C for 2 h to convert

metal precursor to M^0. A catalyst sample (50 mg) reduced by hydrogen was pre-exposed to air at room temperature for 1 h to allow O_2 to adsorb onto the metal atoms on the catalyst surface (M_S) at an M_S/O ratio of 1:1. Then the sample was placed in a glass sample tube connected to a Micromeritics TPD/TPR 2900 instrument equipped with a thermal conductivity detector (TCD) and stabilised at a specified temperature under nitrogen flow (Figure 2.2). The hydrogen-oxygen titration was carried out at room temperature for Pt catalysts and at 100 °C for Ru catalysts. 20 µl pulses of pure H_2 (heated to 75°C) were injected in the N_2 flow in 3 min intervals until the catalyst was saturated with hydrogen. The metal dispersion, D, defined as the fraction of metal (M) at the surface, $D = M_s/M_{total}$, was calculated assuming the stoichiometry of H_2 adsorption (Equation 2.5) [19, 20]:

$$M_sO + 1.5\ H_2 \rightarrow M_sH + H_2O \qquad (2.6)$$

Figure 2.2 Micromeritics TPD/TPR 2900 analyzer used for conducting H_2 chemisorption experiments.

The hydrogen volume adsorbed onto the surface of the catalyst was determined through integrating areas under peaks displayed on the screen which were detected by TCD. Pulses were repeated until no more adsorption was occurred, then the total volume of hydrogen adsorbed at 75 ºC (348 K) was calculated. Equations 2.7-2.10 were used to calculate the dispersion and average M particle diameter [23].

$$V_{348K}\ (\mu l) = \Sigma\ \{20 - [(PA_{ads}/PA_{av})\ x\ 20] \quad (2.7)$$

In equation 2.7, V_{348K} is the total volume adsorbed of H_2 (µL) at 75 ºC (348 K), PA_{ads} is the peak area of adsorbed H_2, PA_{av} is the mean average peak area of blank H_2 injections in the absence of catalyst.

$$V_{273\ K}\ (\mu l) = V_{348K} \times (273/348) \quad (2.8)$$

In equation 2.8, $V_{273\ K}$ is the total volume (µL) of adsorbed H_2 at 0 ºC (273 K).

$$D = \frac{V_{273}(ml) \times A_r(g/mol)}{M_{cat}(g) \times 22414(ml/mol) \times C_M \times 1.5} \quad (2.9)$$

In equation 2.9, D is the metal dispersion, A_r is the relative atomic mass of M, m_{cat} is the mass of catalyst used (g), 22414 represents the volume of one mole of H_2 gas at 0 ºC (273 K), C_M is the concentration of M as a fraction of the catalyst mass, and 1.5 is the stoichiometry of H_2 adsorbed onto M.

The average diameter of metal particles, d, was obtained from the empirical equation 2.10 [20].

$$d\ (nm) = 0.9/D \quad (2.10)$$

2.4.5 CO chemisorption

In this study Pt dispersion for the commercial 7%Pt/C catalyst was determined by pulse chemisorption of CO on a Micromeritics TPD/TPR 2900 apparatus at 50 ºC in He flow (20 mg catalyst sample, 50 µL pulses of pure CO, adsorption stoichiometry Pt_s:CO = 1).

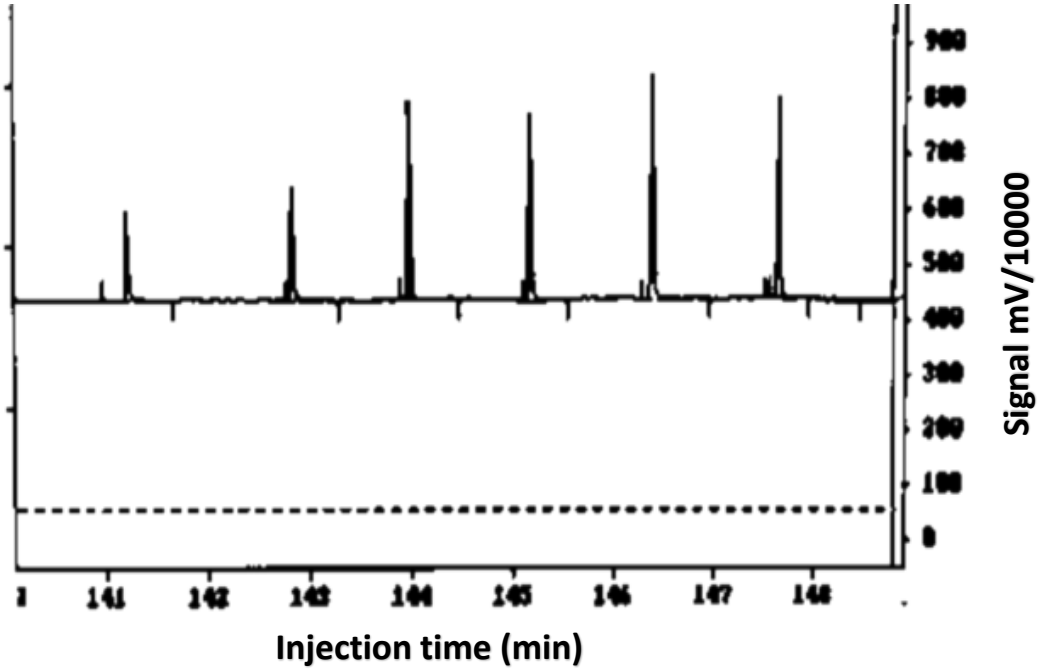

Figure 2.3 CO pulse adsorption on the surface of 7%Pt/C, with CO signals detected during the pulsation.

2.4.6 Thermogravimetric analysis (TGA)

Thermogravimetric analysis (TGA) is commonly used to investigate the changes that accompany the programmed heating of the sample. The change in the mass of the material may refer to chemical or physical changes, which can be determined as percentage value. A TGA instrument consists of a sensitive balance comprising a pan loaded with the sample, which is then placed inside a programmed furnace (Figure 2.4). TGA curves display the change in the weight in relation to the changes in temperature. This weight loss curve provides information about changes in the sample composition, thermal stability and kinetic parameters for the chemical reactions in the sample. A derivative thermogravimetric (DTG) weight loss curve can be used to show the point at which weight loss is most apparent [24].

In this study, a Perkin Elmer TGA 7 instrument was used to conduct the thermogravimetric experiments. In these experiments, the temperature was increased from room temperature to 700

ºC with a rate of heating of either 10 or 20 ºC/ min, under continuous N_2 flow. Figure 2.5 shows an example of TGA for HPW hydrate.

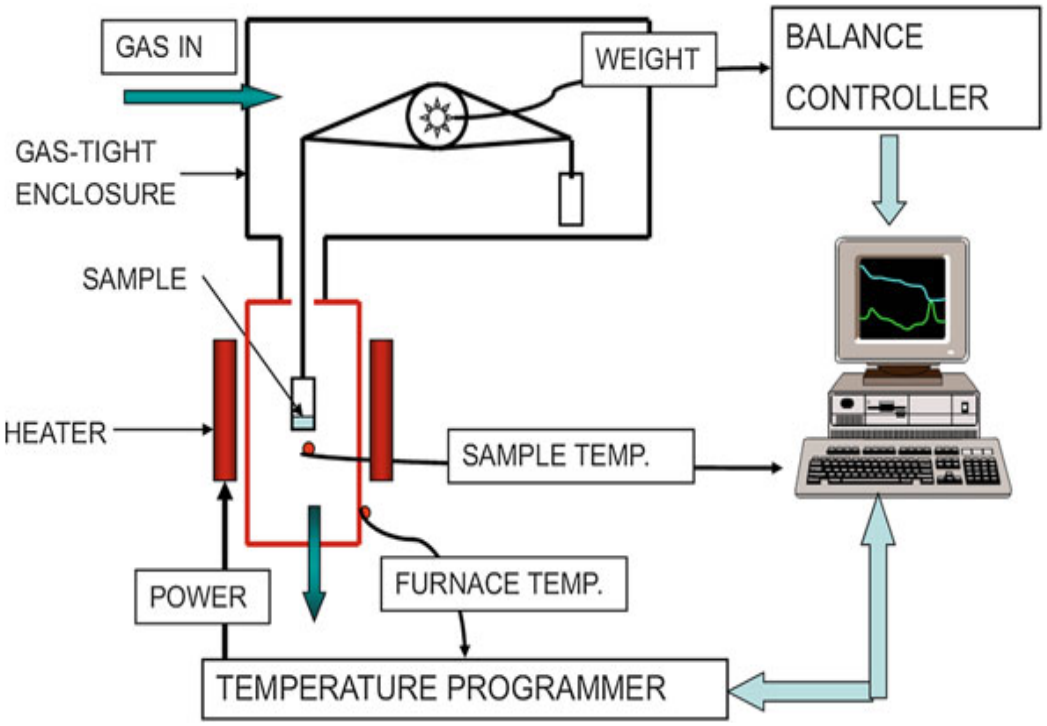

Figure 2.4 Diagram of TGA instrument [25].

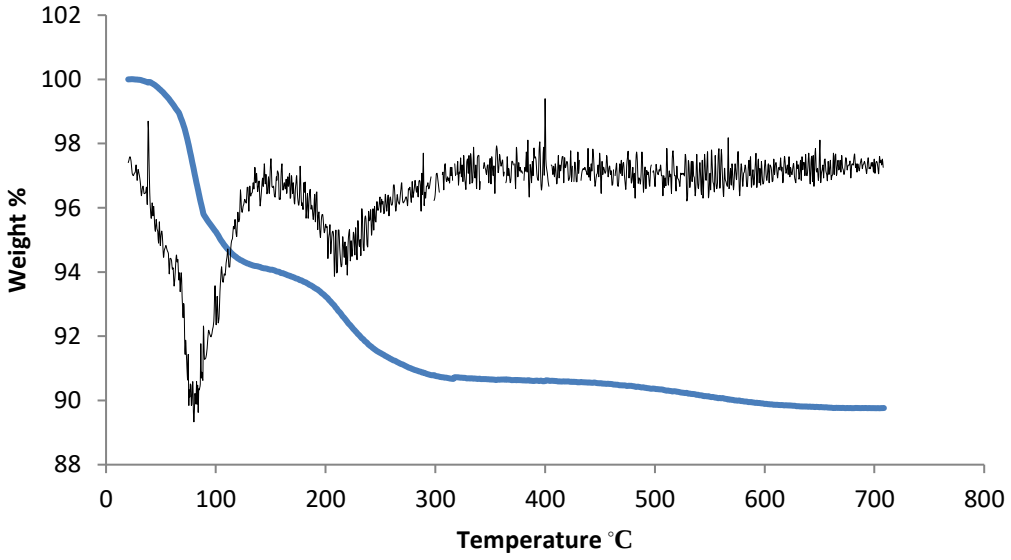

Figure 2.5 TG/DTG for HPW hydrate.

2.4.7 Elemental analysis

In this study carbon and hydrogen content in spent catalysts was determined with the aim of studying the influence of coke on catalyst performance. This determination was carried out using combustion analysis, which was performed on a Thermo Flash EA 1112 series analyser in the Chemistry Department at Liverpool University.

2.4.8 Microcalorimetry

Calvet calorimeters proved to be very valuable tools for the measurement of heats of chemical reactions. In this work, a Setaram C80 heat flux Calvet type microcalorimeter was utilized to measure the heat of ammonia adsorption by solid HPA catalysts. The setup includes two vessels, one for the sample and one for the reference, that are placed in the calorimetric block (Figure 2.6), which functions as a heat sink.

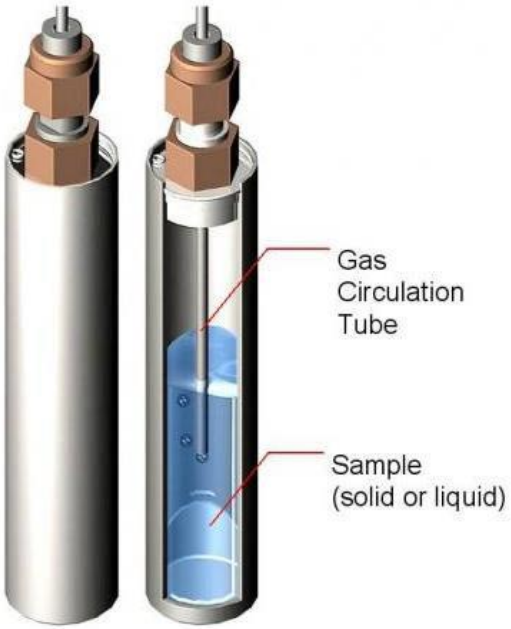

Figure 2.6 Setaram C80 calorimeter gas vessel [26].

Each catalyst sample (0.5-1 g) was pre-treated at 150 ^{o}C in a dry nitrogen atmosphere (20 mL/min) for 90 minutes. Once equilibrium attained, the experiment was initiated by successive pulses of gaseous ammonia (0.5 mL, 0.02 mmol) into the N_2 flow using a stainless steel loop fitted in a 10 port Valco valve, and ammonia was injected every 30 minutes. The amount of ammonia adsorbed onto the catalyst was calculated by difference between the initial amount of ammonia and the amount of ammonia broken through the sample cell.

Ammonia adsorption measurement was kindly performed by Mrs W. Alharbi.

2.4.9 Scanning transmission electron microscopy (STEM) with energy dispersive X-ray emission (EDX) microanalysis

STEM-EDX was used in this study to analyse supported Pt, Au and PtAu catalysts: Pt/CsPW, Au/CsPW and PtAu/CsPW.

The STEM-EDX measurements were kindly performed by Dr D. Belic.

2.4.9.1 STEM

A focussed beam of electrons is tunnelled between the tip of a probe and the surface of the sample, generating an electrical signal. The electron probe can be scanned over the sample, allowing a computer-generated image to be created of the sample surface in a raster pattern. STEM experiments are carried out under a high vacuum to reinforce the signal. The mean surface particle diameter, d_{sp}, is defined as $\Sigma n_i d_i^3 / \Sigma n_i d_i^2$, where n_i is the number of metal particles of a dimeter d_i [27].

2.4.9.2 EDX

To develop a map of the surface, an energy dispersive X-ray emission detector (EDX) is placed close to the sample grid in STEM. EDX is used to identify and assess the particular elements and their relative proportions in STEM images. When the STEM electron beam passes throw the sample, electrons from lower energy “inner” electron shells may be excited and ejected from that

energy state, leaving holes. These holes are filled by electrons from higher energy "outer" shells, and in doing so, emit X-rays with an energy that is representative of the difference in energy between the two electron shells where the transition occurs. The X-ray emission lines produced are characteristic of the elements contained within the sample [27].

STEM imaging and EDX analysis of catalysts was carried out on an aberration-corrected JEOL JEM 2100FCs instrument operated at 200 kV, equipped with an EDAX Octane T Optima 60 windowless silicon drift detector. For STEM analysis, the samples were prepared by scooping up the powder catalyst by a TEM grid (holey carbon film on 300 Ni mesh, Agar Scientific) followed by shaking to remove excess material from the grid.

2.4.10 Fourier transform infrared spectroscopy (FTIR).

Infrared spectroscopy is a widely used technique for the determination of solid catalyst structures [12, 15, 28, 29]. Infrared radiation, approximately in the region 400-4000 cm^{-1} can be used to investigate the fundamental vibration of sample chemical bonds. The chemical bonds absorb the infrared radiation, bending and stretching them. The frequency of the radiation required to excite the vibrational modes, and the intensity of absorption, depends on the strength and chemical environment of the bonds. The infrared radiation scans the sample and when absorption occurs, the transmitted infrared beam is weakened. The resulting spectrum (the intensity is plotted against wave number (λ)) can be presented in either absorption or transmission mode. In this technique, diffusely scattered light can be directly collected from the catalyst with a mirror which is then passed to a detector (Figure 2.7). This method can be applied for sampling catalyst powders.

Fourier transform infrared spectroscopy of adsorbed pyridine has been widely used to study Lewis and Bronsted acid sites on the catalyst surface [3, 30-32].

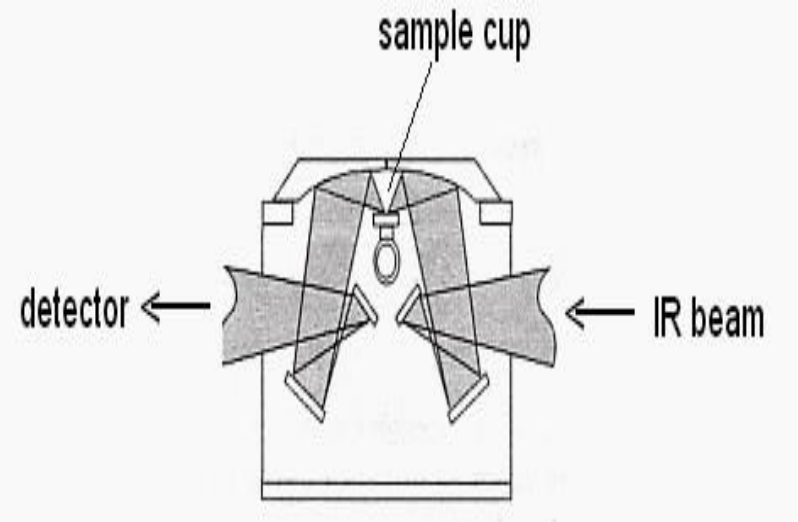

Figure 2.7 Schematic of the diffuse reflectance accessory [33].

A Nicolet NEXUS FTIR spectrometer was used in this study to confirm the stability of HPA catalysts and to examine the presence of Lewis acid and Bronsted sites by adsorption of pyridine.

The investigation of the Keggin structure for fresh and spent HPA catalysts was carried out in the range of 500-1200 cm^{-1}. The investigation of Lewis and Bronsted acid sites was performed in the region of 1450 and 1540 cm^{-1}, respectively. Catalyst preparation involved degassing of samples under vacuum for 1.5 h at 150 °C, then careful grinding to make a diffusely scattering matrix by mixing 0.025 g of catalysts with 0.475 g of potassium bromide (20 wt %). Such matrix results in lower absorption and thus greater beam throughput, enhancing analysis resolution.

2.5 Catalytic reaction studies

2.5.1 Hydrodeoxygenation of biomass-derived ketones

The hydrogenation of ketones was carried out in the gas phase in flowing H_2. The catalysts were tested at 60-100 ^oC under atmospheric pressure in a Pyrex fixed-bed down-flow reactor (9 mm internal diameter) fitted with an on-line gas chromatograph (Varian Star 3400 CX instrument with a 30 m x 0.25 mm HP INNOWAX capillary column (column A) and a flame ionisation

detector). For more accurate hydrocarbon analysis, a 60 m x 0.32 mm GSGasPro capillary column (column B) was utilised which provides better separation for C_1-C_3 hydrocarbons. The temperature in the reactor was controlled by a Eurotherm controller using a thermocouple placed at the top of the catalyst bed. The gas feed contained a variable amount of ketone in H_2 as a carrier gas. The ketone was fed by passing H_2 carrier gas flow controlled by a Brooks mass flow controller through a stainless steel saturator, which held the liquid ketone at appropriate temperature to maintain the chosen reactant partial pressure. The downstream gas lines and valves were heated to 180 ^oC to prevent substrate and product condensation. The gas feed entered the reactor at the top at a flow rate of 20-100 mL min^{-1}. The reactor was packed with 0.2 g catalyst powder of 45-180 μm particle size. In some cases, to reduce conversion a smaller amount of catalyst was used as a homogeneous mixture with silica of a total weight of 0.2 g. Prior to reaction, the catalysts were pre-treated in H_2 for 1 h at the reaction temperature unless stated otherwise. The dehydration of 2-methyl-4-pentanol was studied similarly, except using N_2 as a carrier gas instead of H_2. Once reaction started, the downstream gas flow was analysed by the on-line GC to obtain reactant conversion and product selectivity. Reactant conversion (X), product yields (Y_p) and product selectivities ($S_{p,s}$) were calculated using equations (2.11-2.13). The mean absolute percentage error in conversion and selectivity was ≤ 10% and the carbon balance was maintained within 95%.

$$Y_p = \frac{S_p \times K_g \times A}{S_r + (\sum S_p \times K_g \times A)} \times 100 \qquad (2.11)$$

$$X = \sum Y_p \qquad (2.12)$$

$$S_{p,s} = \frac{Y_p}{X} \times 100 \qquad (2.13)$$

In equations (2.11-2.13): S_r is the area count of unreacted substrate, S_p is the product peak area, K_g is the calibration factor of product relative to the substrate, A is the product stoichiometry factor relative to the substrate and (ΣS_P x K_g x A) is the summation for all products in reaction.

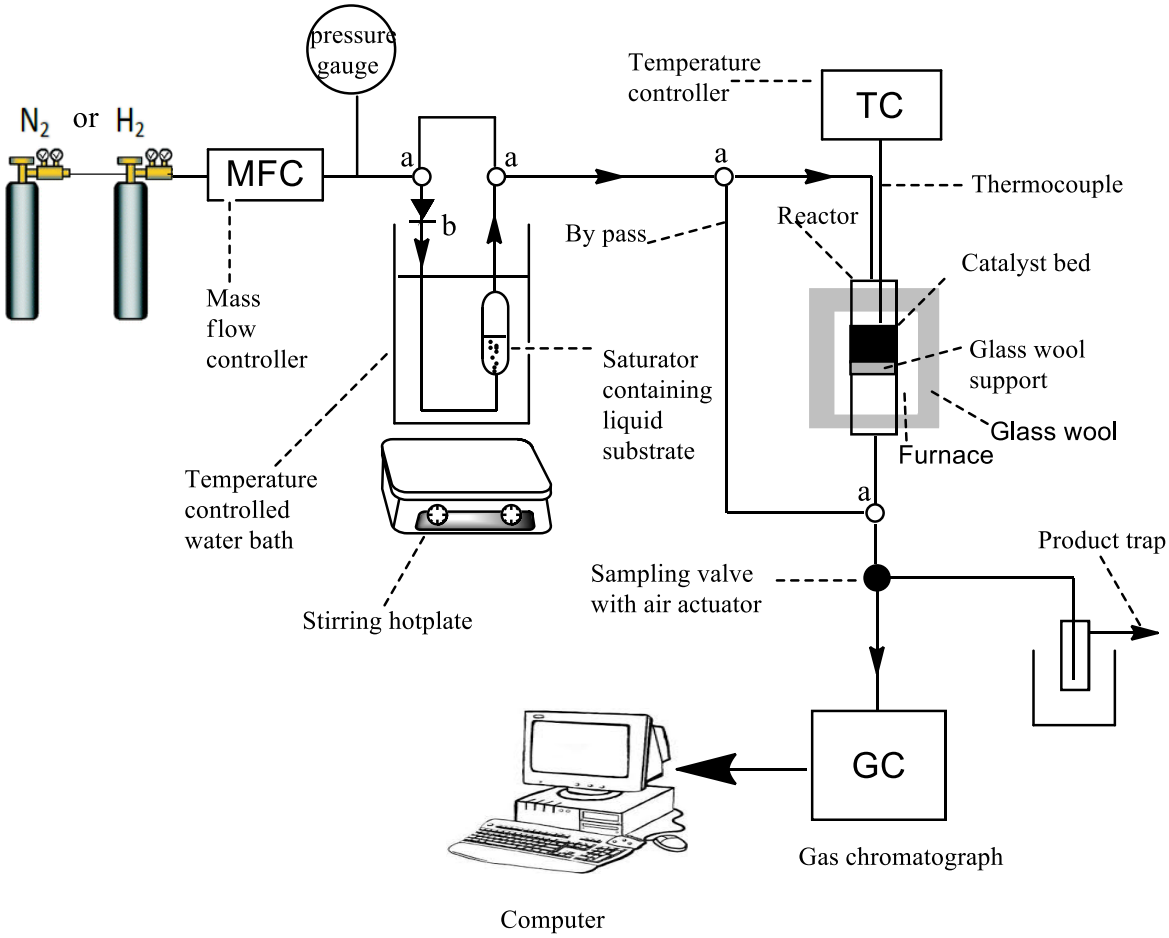

Figure 2.8 Equipment setup for gas-phase reaction, where (a) 3-way valve, (b) check valve (non return).

The activation energy of MIBK conversion over Pt/CsPW catalysts was measured using the Arrhenius equation (2.14) at the temperature between 80-110°C under differential conditions within the conversion range < 10%.

$$k = Ae^{\frac{-E_a}{RT}} \qquad (2.14)$$

Here k is the rate constant of the reaction, A is the pre-exponential factor, E_a is the activation energy, R is the universal gas constant and T is the absolute temperature in Kelvin. E_a can be determined from the straight line gained from a plot of ln k against 1/T using following equation:

$$\ln k = \ln A - \frac{E_a}{RT} \qquad (2.15)$$

2.5.2 Deoxygenation of ethers and esters

Deoxygenation (decomposition) of anisole, diisopropyl ether (DPE) and ethyl propanoate (EP) ester was carried out in the gas phase in flowing H_2 or N_2. The catalysts were tested under atmospheric pressure in the same reactor which was used in hydrodeoxygenation of ketones. The substrates were fed by passing the carrier gas flow controlled by a Brooks mass flow controller through a stainless steel saturator, which held the liquid substrate at appropriate temperature (±1 ^oC) to maintain the chosen reactant partial pressure. The downstream gas lines and valves were heated to 150 ^oC to prevent substrate and product condensation. The gas feed entered the reactor at the top at a flow rate of 20 mL min^{-1}. The reactor was packed with 0.20 g catalyst powder of 45-180 μm particle size. Prior to reaction, the catalysts were pre-treated in situ for 1 h at the reaction temperature. Reactant conversion, product selectivity and activation energy were calculated using equations 2.11-2.15.

2.6 Product analysis

2.6.1 Gas chromatography

Gas chromatography is very common technique used in analytical chemistry to separate mixtures of volatile compounds. The mobile phase is a carrier gas, such as helium, argon, hydrogen or nitrogen, which mixes with the volatile compounds and is then passed through a column containing a solid or liquid stationary phase [15]. This stationary phase separates the mixture passing through it, with the products progressing through to the detector at different times depending on their boiling points and solubility.

Although different types of detector can be utilised, the flame ionization detector (FID) is often used for analysing organic compounds (Figure 2.9). Within the FID detector, the effluent from the column is heated with a high temperature flame created by mixing H_2 and air, which then

ionises solute molecules having low ionisation potential. The amount of charge formed is proportional to the concentration of ions derived from the solutes. The current is then amplified using the built-in computer and a chromatogram is produced on an external computer. A schematic diagram of a gas chromatograph is provided in Figure 2.10.

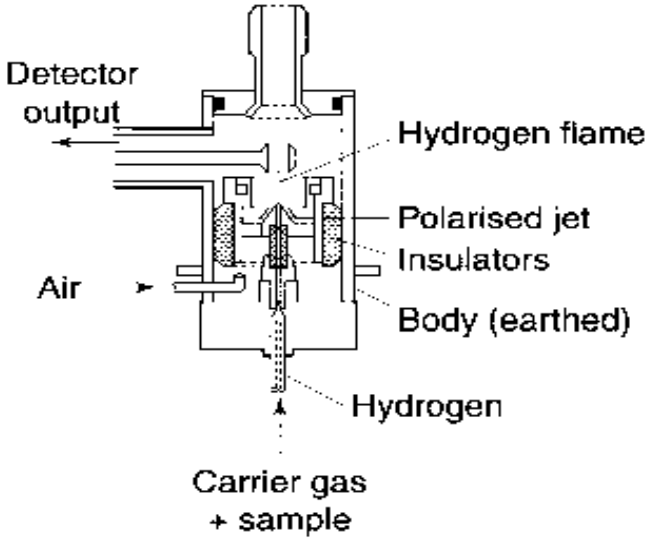

Figure 2.9 Flame ionization detector (FID) [34].

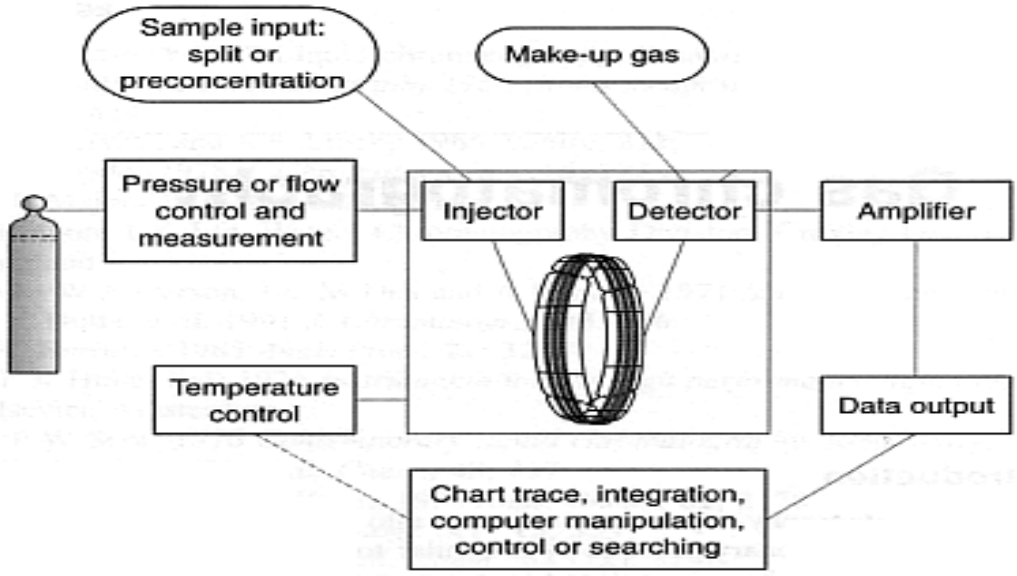

Figure 2.10 Diagrammatical representation of gas chromatograph set up [34].

2.6.2 GC calibration

In this study, all components in a mixture of volatile compounds were quantified using the internal standard method. Calibration factors were determined by preparing a series of solutions with a different concentration of analyte and a constant concentration of the standard which were diluted in a solvent, and the molar ratio of the analyte (M) to the internal standard (M_O) was plotted against the peak area ratio of the two components (S/S_O) (equation 2.16). The gradient of the straight line obtained is the calibration factor K.

$$M/M_o = K \times S/S_o \qquad (2.16)$$

The calibrations were carried out using decane and dodecane as GC standards and toluene, methanol and acetone as solvents.

Table 2.1 Molecular weights, boiling points, retention times and calibration factors for all components involved in the gas phase hydrodeoxygenation of MIBK, acetone and DIBK.

Compound	M wt ($g\ mol^{-1}$)	Boiling point (°C)	Retention time (min)	K (rel. to decane)	K (rel.to corresponding ketones (MIBK, acetone and DIBK)
MIBK[a]	100	117	3.0	1.85	1.00
2-Methylpentane[a]	86	60	1.2	1.86	1.01
4-Methyl-2-pentanol[a]	102	131	4.4	1.77	0.96
2-Methyl-3-pentanol[a]	102	131	4.3	1.44	0.78
Acetone[b]	58	56	1.7	5.00	1.00
Iso-Propanol[b]	60	83	2.3	4.75	0.95
Propane[b]	44	-42	1.2	3.33	0.67
DIBK[c]	142	168	4.6	1.59	1.00
2,6-Dimethylheptane[c]	128	135	1.7	1.33	0.84
2,6-Dimethyl-4-heptanol[c]	144	179	6.0	1.30	0.82

a) Acetone was used as a solvent.

b) Calibration factors were estimated using decane as a standard related to the effective carbon-atom number.

c) Toluene was used as a solvent.

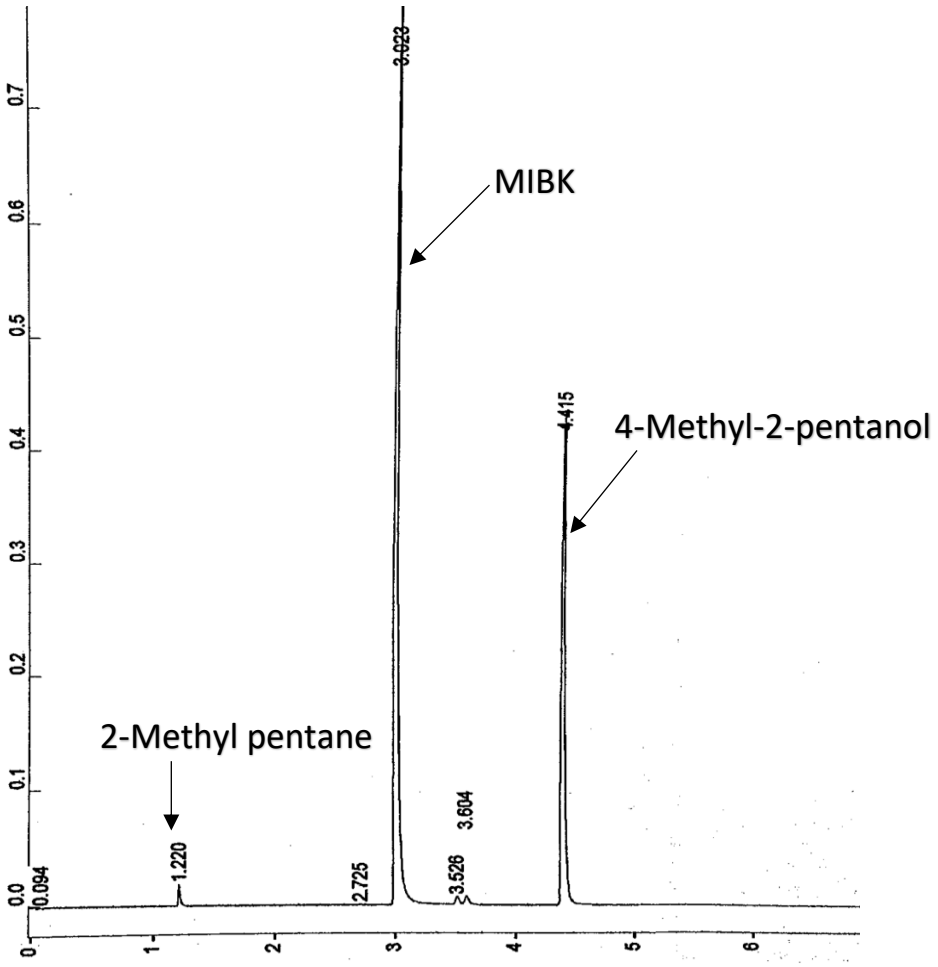

Figure 2.11 GC trace for MIBK hydrodeoxygenation over 0.5%Pt/CsHPW at 40 °C.

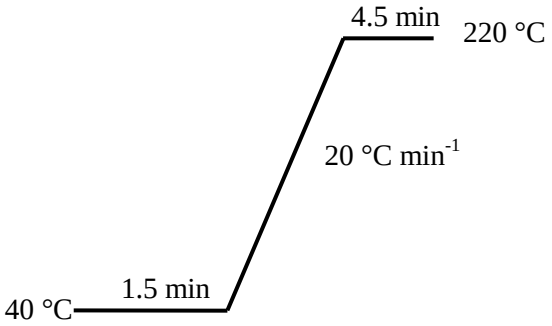

Injector temperature = 250 °C

Detector temperature = 250 °C

Figure 2.12 Conditions of GC analysis using column A for all reactions studied.

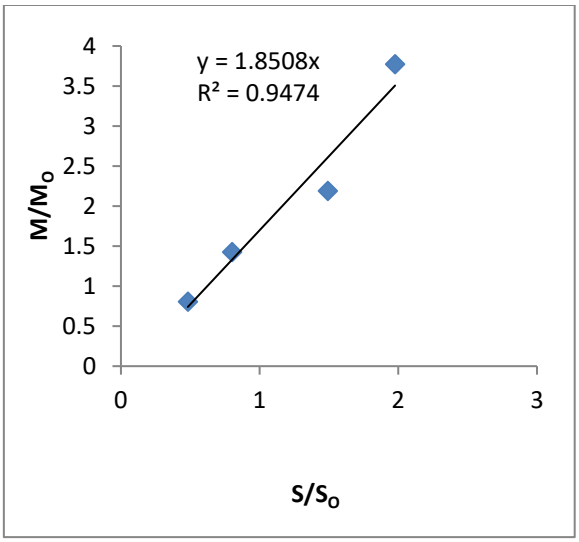

Figure 2.13 Calibration of MIBK.

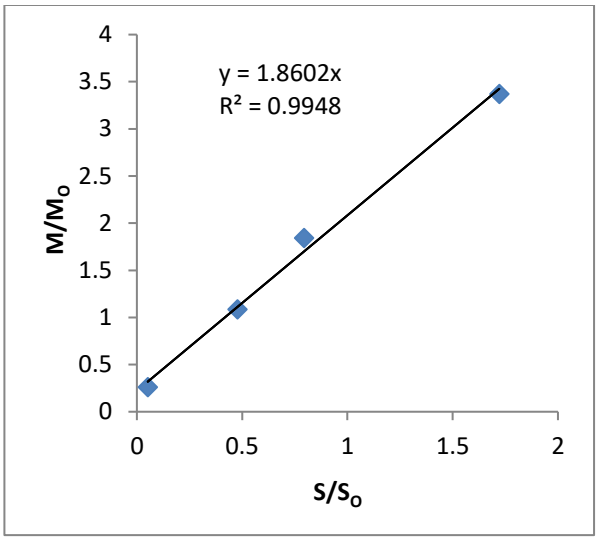

Figure 2.14 Calibration of 2-methyl pentane.

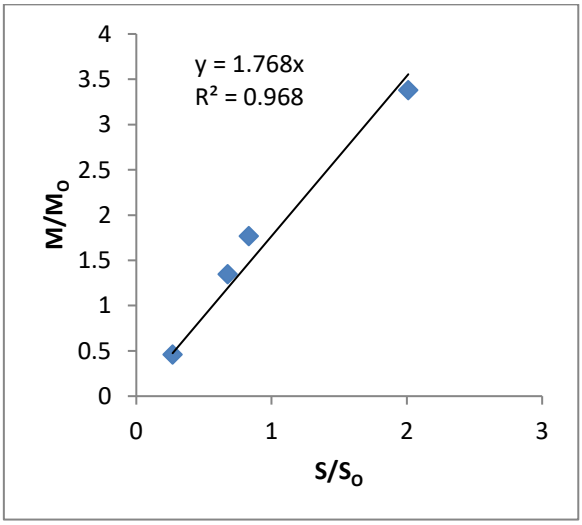

Figure 2.15 Calibration of 4-methyl-2-pentanol.

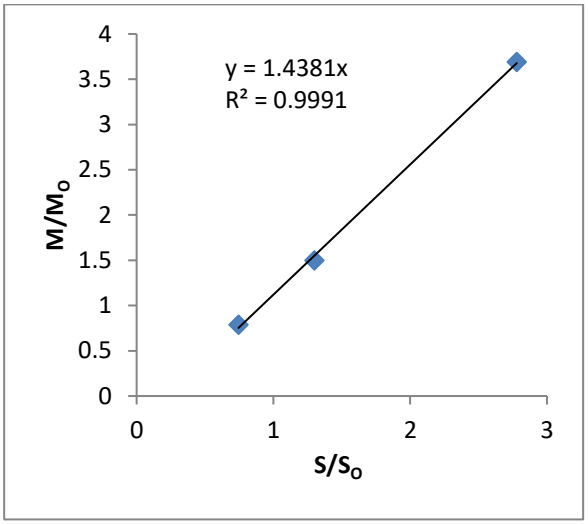

Figure 2.16 Calibration of 2-methyl-3-pentanol.

Table 2.2 Molecular weights, boiling points, retention times and calibration factors for all components involved in the gas phase hydrodeoxygenation of 3-pentanone, 2-hexanone, cyclohexanone, 2-octanone, 2-butanone and acetophenone.

Compound	M wt ($g\ mol^{-1}$)	Boiling point (°C)	Retention time (min)	K (rel. to dodecane)	K (rel.to corresponding ketones)
3-Pentanone[a]	86	101	2.7	1.51	1.00
Pentane[a]	72	36	1.2	1.36	0.90
3-Pentanol[a]	88	115	3.9	1.22	0.81
2-Hexanone[a]	100	128	3.7	1.88	1.00
2-Hexanol[a]	102	140	4.9	1.41	0.75
Hexane[b]	86	69	1.2	1.52	0.81
Cycloheanone[c]	98	156	5.7	2.44	1.00
Cyclohexanol[b]	100	162	6.6	1.70	0.70
Cyclohexane[b]	84	81	1.4	1.98	0.81
2-Octanone[c]	128	173	5.6	1.60	1.00
2-Octanol[c]	130	195	6.6	1.36	0.85
Octane[b]	114	126	1.6	1.54	0.96
2-Butanone[d]	72	80	2.3	4.00	1.00
2-Butanol[d]	74	99	3.2	3.70	0.93
Butane[d]	58	0	1.2	3.00	0.75
Acetophenone[a]	120	202	8.7	1.22	1.00
Ethylcyclohexane[a]	112	132	2.0	1.46	1.20
Ethylbenzene[a]	106	136	4.0	1.13	0.93

a) Acetone was used as a solvent.

b) Toluene was used as a solvent.

c) Methanol was used as a solvent.

d) Calibration factors were estimated using dodecane as a standard related to the effective carbon-atom number.

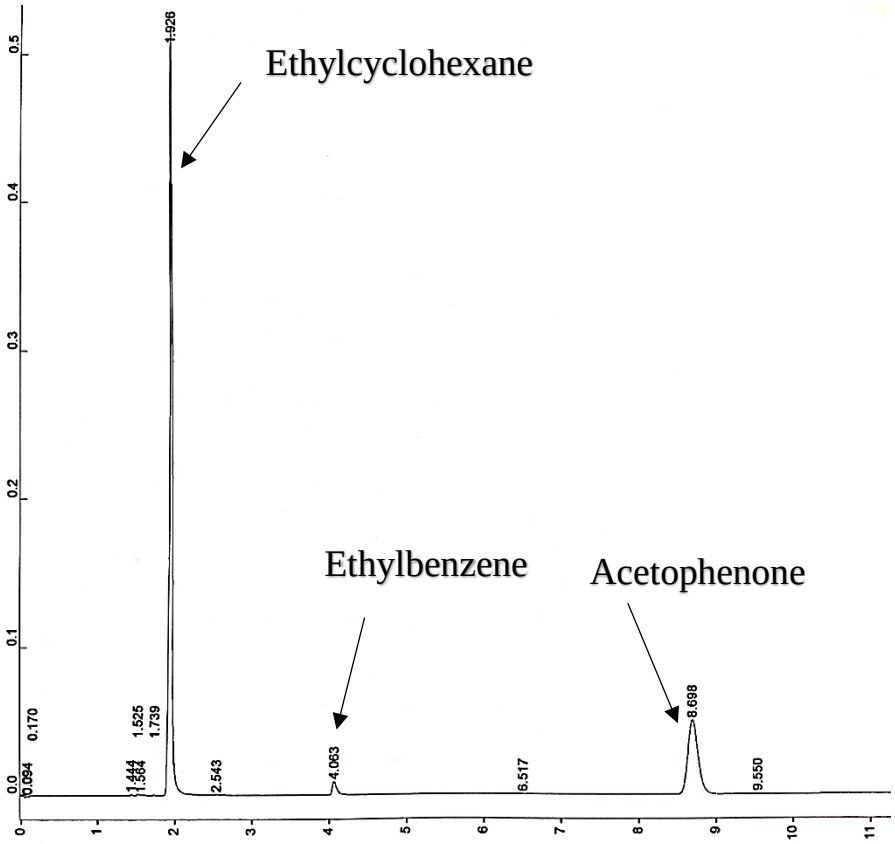

Figure 2.17 GC trace for acetophenone hydrodeoxygenation over 7%Pt/C+CsPW(1:19) at 100˚C.

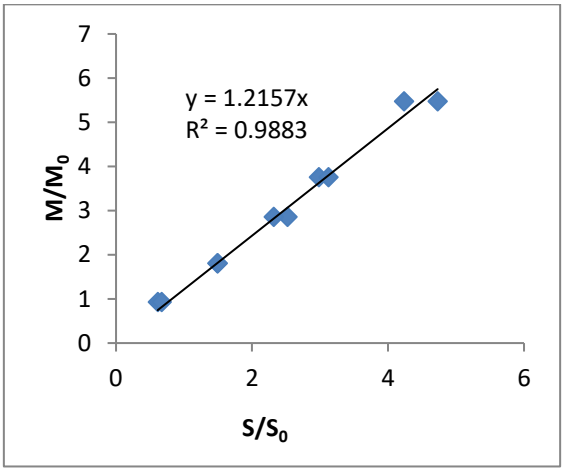

Figure 2.18 Calibration of acetophenone.

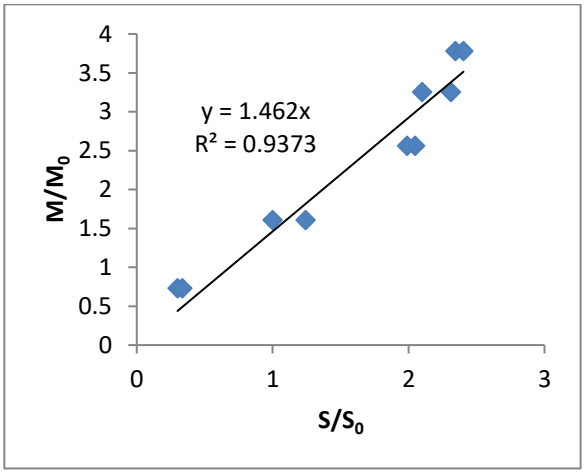

Figure 2.19 Calibration of ethylcyclohexane.

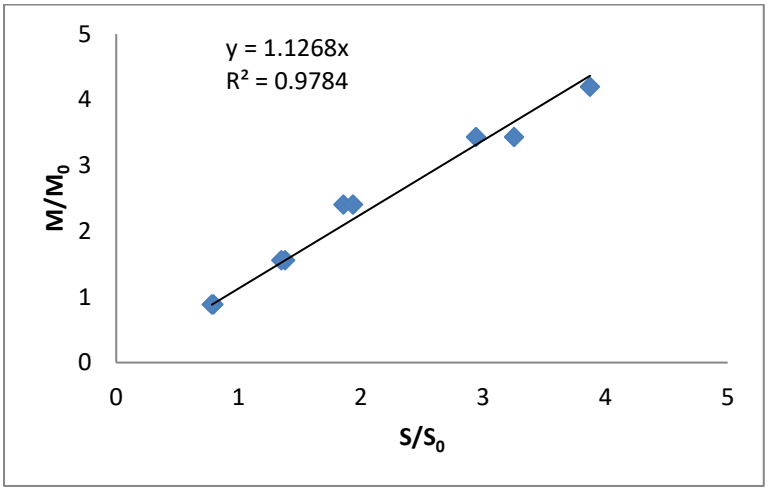

Figure 2.20 Calibration of ethylbenzene.

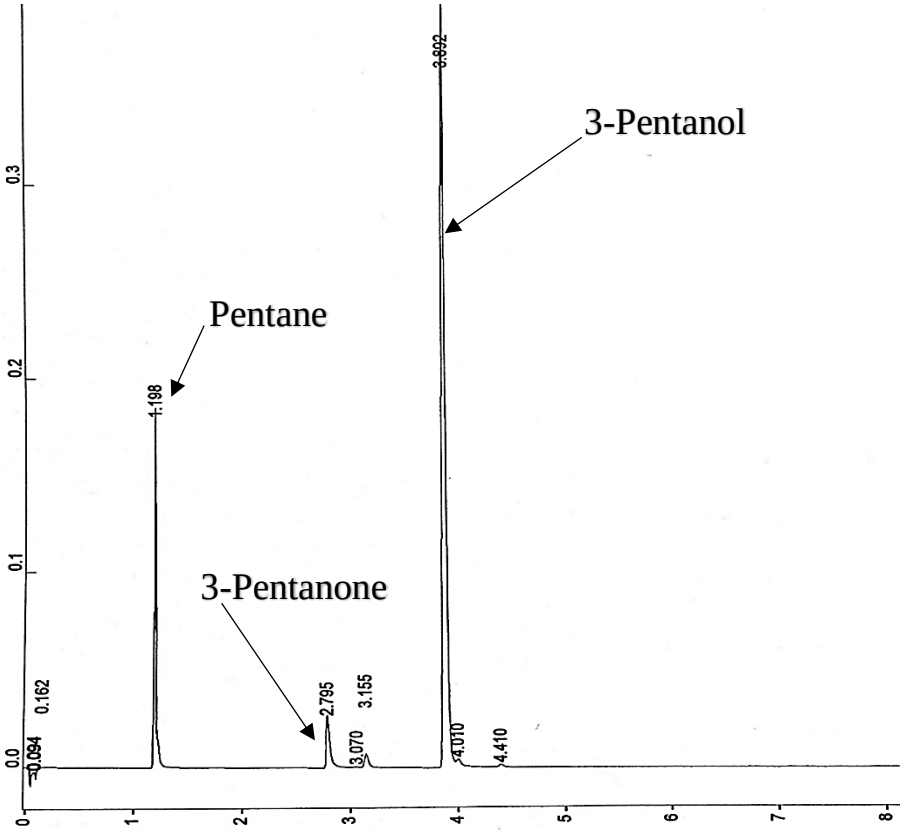

Figure 2.21 GC trace for 3-pentanone hydrodeoxygenation over 0.5%Pt/CsHPW at 60˚C.

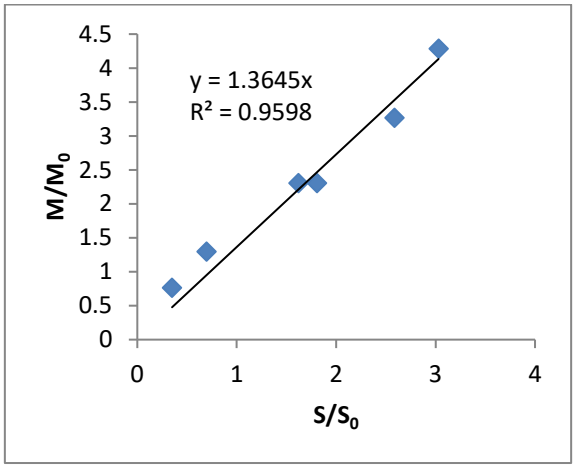

Figure 2.22 Calibration of pentane.

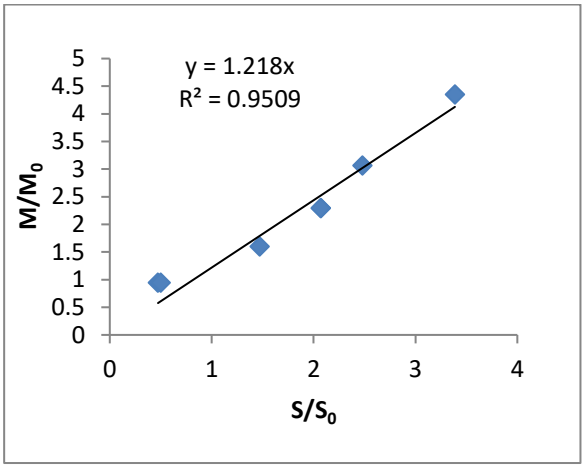

Figure 2.23 Calibration of 3-pentanol.

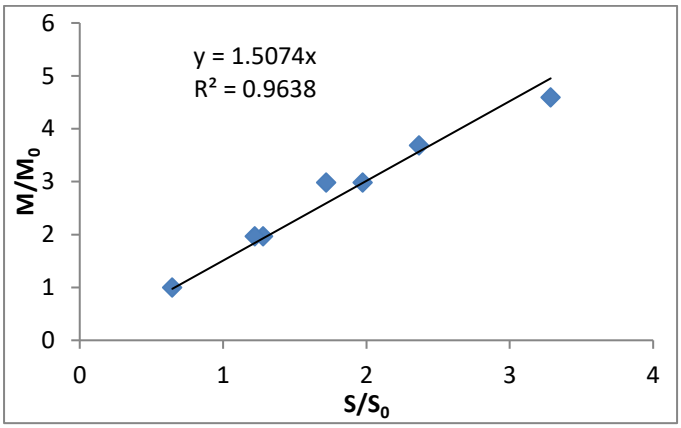

Figure 2.24 Calibration of 3-pentanone.

Table 2.3 Retention times and calibration factors for all components involved in conversion of ethyl propanoate.

Compound	M wt (g mol^{-1})	Boiling point (◦C)	Retention time (min)	K (rel. to decane)	K (rel. to ethyl propanoate)
Ethyl propanoate[a]	102	99	2.5	2.21	1.00
Propanoic acid[b]	74	141	7.4	4.88	2.21
C_2 [ethane+ethane]	30	-89	4.7-4.8[c]	5.00[d]	2.26

a) Acetone was used as a solvent.

b) Toluene was used as a solvent.

c) Retention times using column B.

d) Calibration factors were estimated using decane as standard related to the effective carbon-atom number.

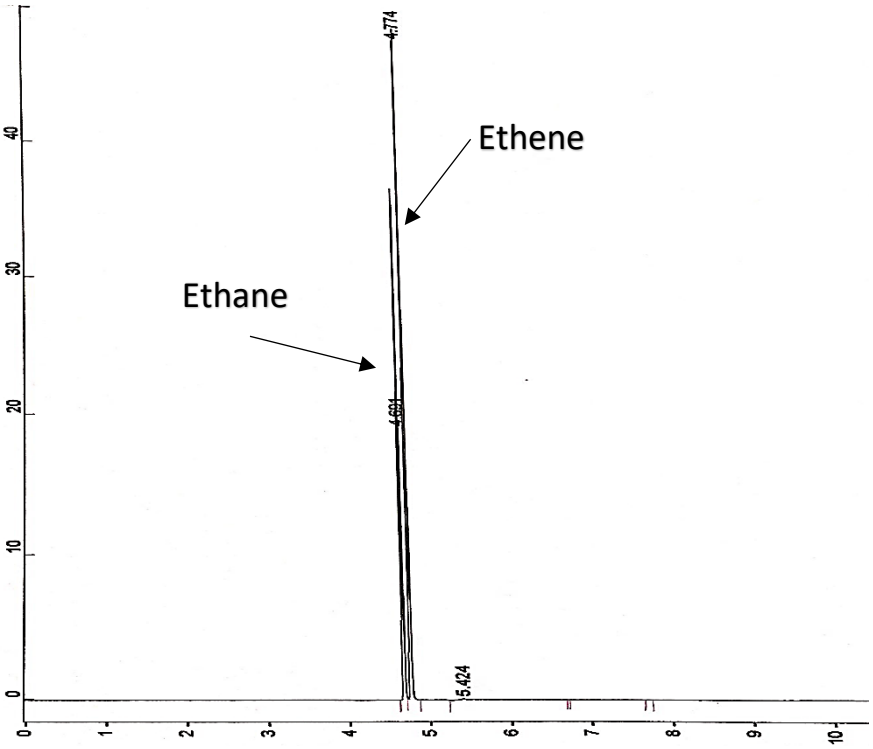

Figure 2.25 GC trace for ethyl propanoate hydrodeoxygenation over CsHPW at 180ºC under H_2 using column B.

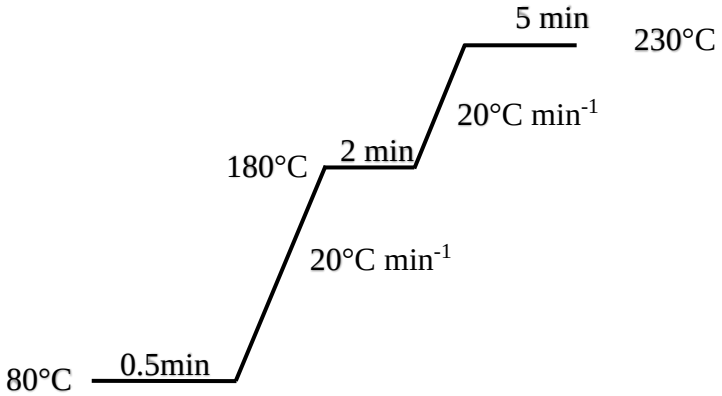

Figure 2.26 Condition of column B of GC analysis for all reactions studied.

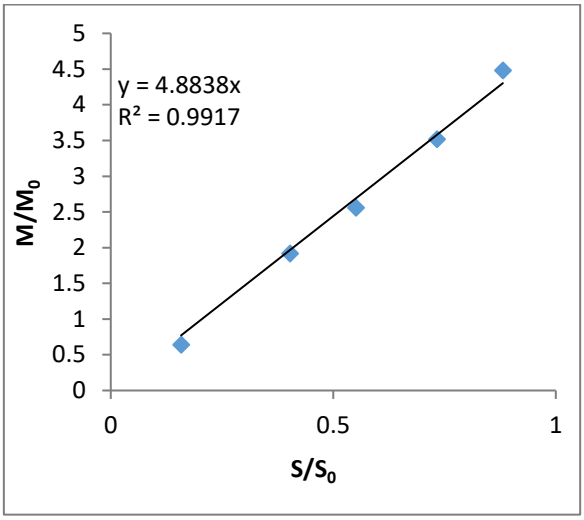

Figure 2.27 Calibration of propanoic acid.

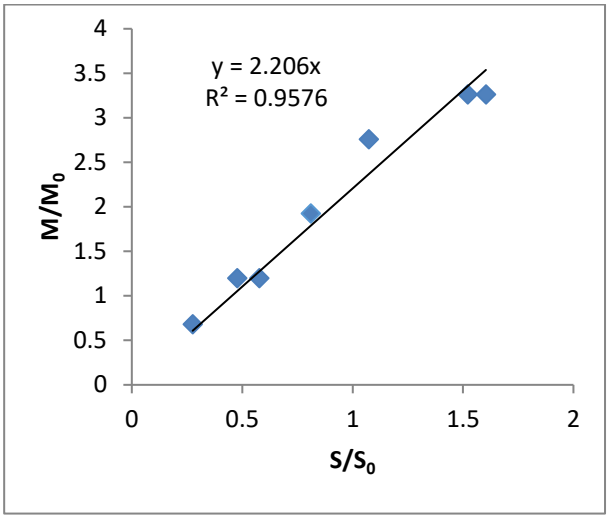

Figure 2.28 Calibration of ethyl propanoate.

Table 2.4 Retention times and calibration factors for all components involved in conversion of anisole.

Compound	M wt (g mol^{-1})	Boiling point (◦C)	Retention time (min)	K (rel. to dodecane)	K (rel. to anisole)
Anisole[a]	108	154	6.1	1.00	1.00
Cyclohexane[b]	84	81	1.4	1.98	1.98
Methanol[b]	32	65	2.1	12.9	12.9
Cyclohexanol[b]	100	162	6.7	1.70	1.70
Benzene[a]	78	80	2.4	1.16	1.16
Toluene[a]	92	111	3.4	1.06	1.06

a) Acetone was used as a solvent.

b) Toluene was used as a solvent.

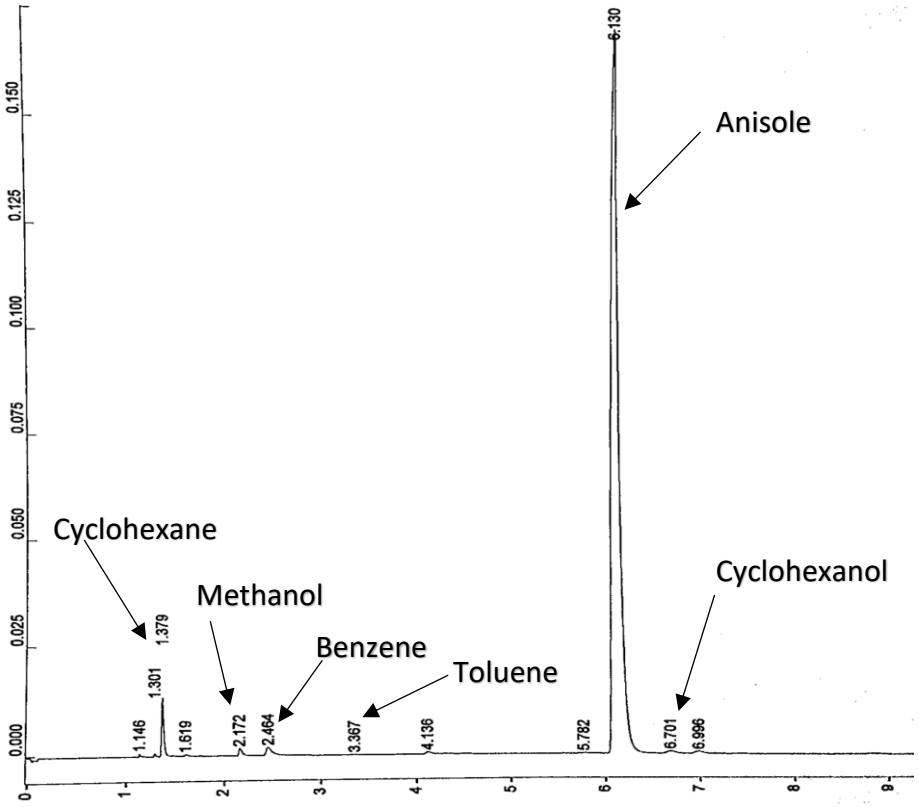

Figure 2.29 GC trace for anisole hydrodeoxygenation over 10%Cu +CsPW at 100◦C.

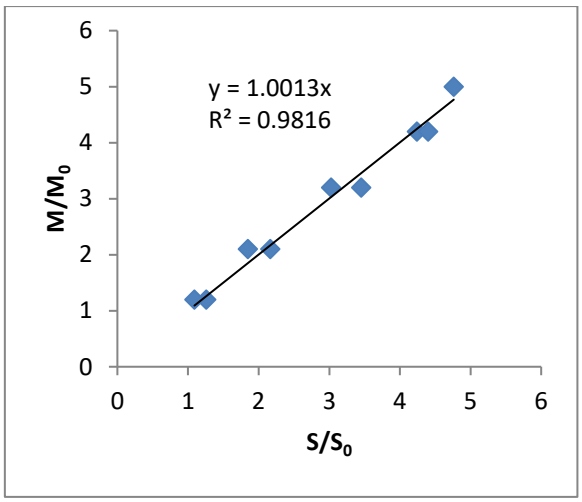

Figure 2.30 Calibration of anisole.

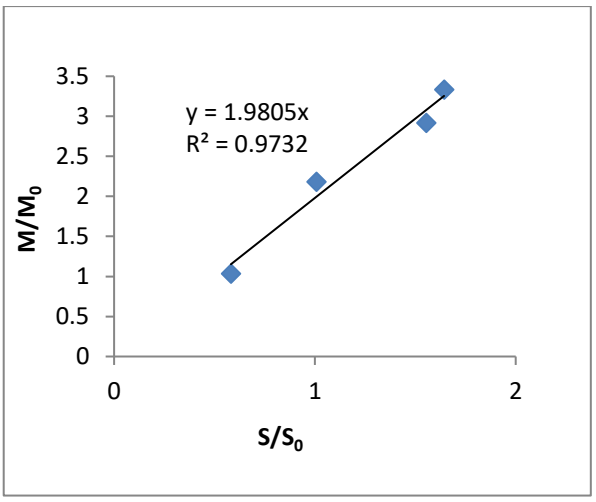

Figure 2.31 Calibration of cyclohexane.

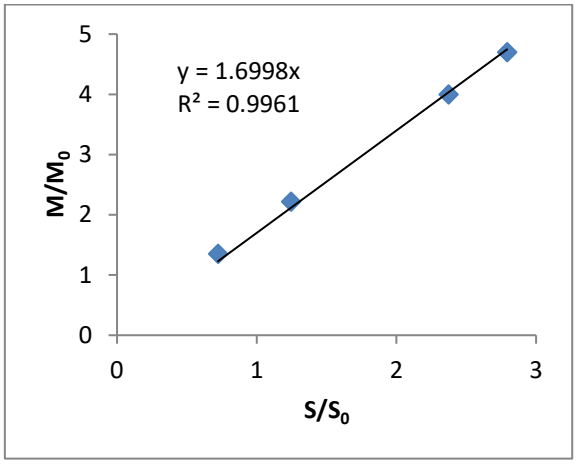

Figure 2.32 Calibration of cyclohexanol.

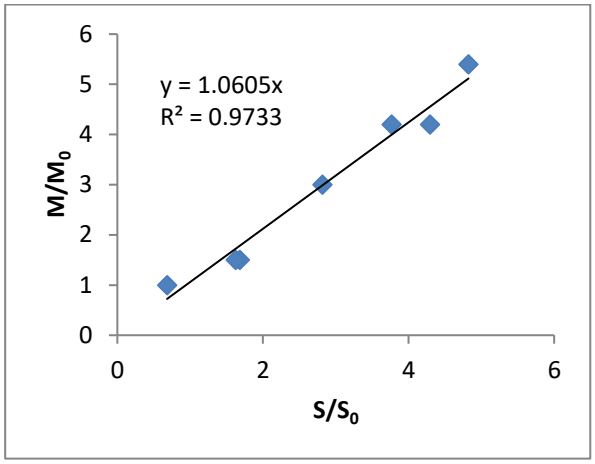

Figure 2.33 Calibration of toluene.

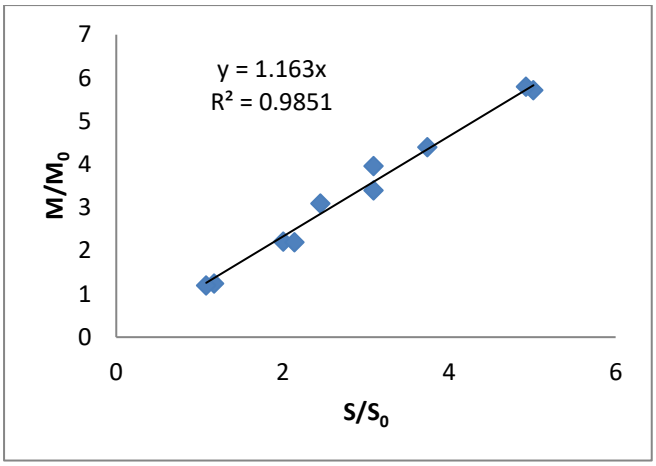

Figure 2.34 Calibration of benzene.

Table 2.5 Retention times and calibration factors for all components involved in conversion of diisopropyl ether.

Compound	M wt (g mol-1)	Boiling point (°C)	Retention time (min)	K (rel. to decane)[a]	K (rel. to diisopropyl ether)
Diisopropyl ether	102.18	69	1.3	2.00	1.00
Iso-Propanol	60.10	83	2.3	4.44	2.22
C_3	44.10	-42	5.4-5.9[b]	3.33	1.67

a) Calibration factors were estimated using decane as standard related to the effective carbon-atom number.

b) Retention times using column B.

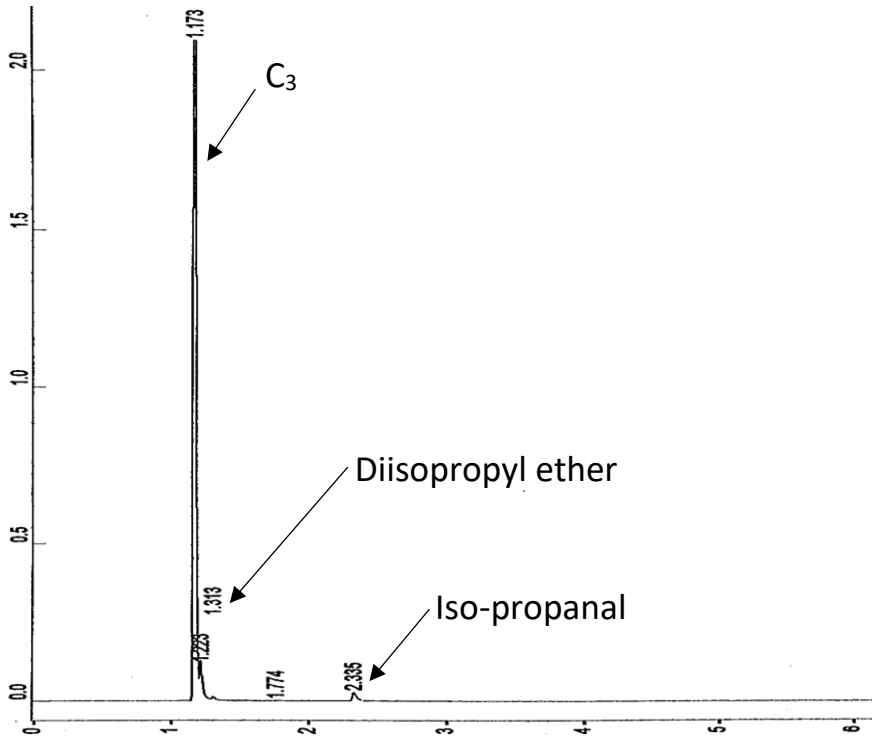

Figure 2.35 GC trace for diisopropyl ether hydrodeoxygenation over 7%Pt/C+CsPW [1:19] at 110 ◦C under H_2 using column A.

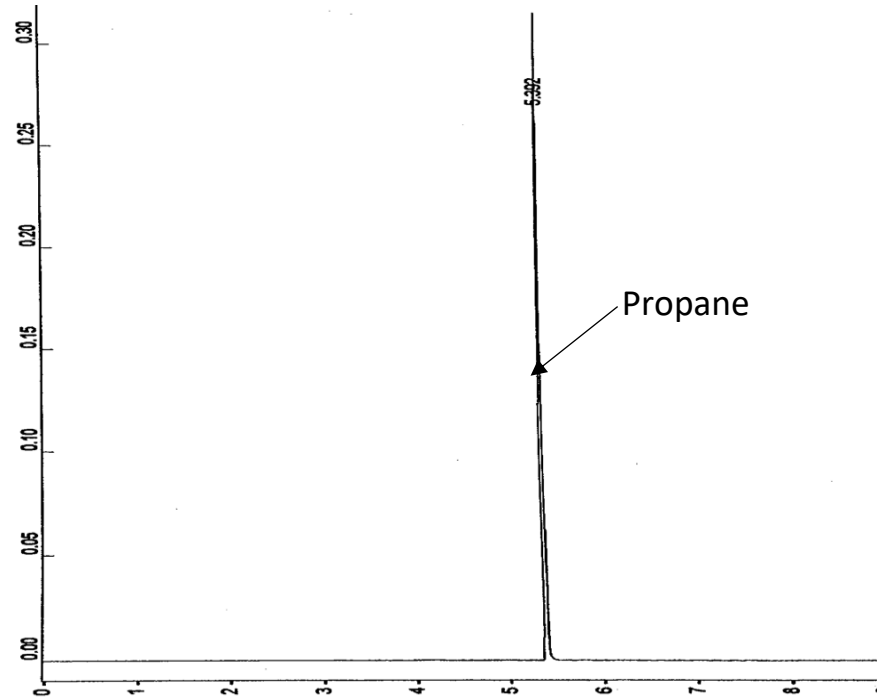

Figure 2.36 GC chromatogram for light hydrocarbon from hyrodeoxygenation of diisopropyl ether over 7%Pt/C+CsPW [1:19] at 110◦C under H_2 using column B.

2.7 References

1. Y. Izumi, M. Ono, M. Kitagawa, M. Yoshida, K. Urabe, Microporous Mater. 5 (1995) 255.
2. M. A. Alotaibi, E. F. Kozhevnikova, I. V. Kozhevnikov, Appl. Catal. A 447-448 (2012) 32.
3. A. M. Alsalme, P. V. Wiper, Y. Z. Khimyak, E. F. Kozhevnikova, I. V. Kozhevnikov, J. Catal. 276 (2010) 181.
4. G. C. Bond, S. J. Frodsham, P. Jubb, E. F. Kozhevnikova, I. V. Kozhevnikov, J. Catal. 293 (2012) 158.
5. W. Alharbi, E. Brown, E. F. Kozhevnikova, I. V. Kozhevnikov, J. Catal. 319 (2014) 174.
6. E. F. Kozhevnikova, I. V. Kozhevnikov, J. Catal. 224 (2004) 164.
7. N. Uekawa, T. Kudo, F. Mori, Y. J. Wu, K. Kakeawa, J. Colloid Interface Sci. 264 (2003) 378.
8. G. Leofanti, M. Padovan, G. Tozzola, B. Venturelli, Catal. Today. 41 (1998) 207.
9. J. M. Thomas, W. J. Thomas, Principles and Practice of Heterogeneous Catalysis, VCH, 1997.
10. G. Attard, C. Barnes, Surfaces, Oxford University Press, 1998.
11. R. A. van Santen, P. W. N. M. van Leeuwen, J.A. Moulijn, B.A. Averill (Eds.) Catalysis: An Integrated Approach, Elsevier, 2000.
12. S. Brunauer, P. H. Emmett, E. Teller, J. Am. Chem. Soc. 60 (1938) 309.
13. A. A. Mirzaei, PhD thesis, University of Liverpool, 1998.
14. D. Kealey, D. J. Haines, Analytical Chemistry, 1st ed., Bio scientific, Oxford, 2002.
15. P. W. Atkins, Physical Chemistry, Oxford University Press, 1998.
16. A. W. Burton, Zeolite Characterization and Catalysis: A Tutorial (2009) 1.
17. J. H. Sinfelt, Rev. Mod. Phys. 51 (1979) 569.
18. G. Bergeret, P. Gallezot, Handbook of Heterogeneous Catalysis, Wiley-VCH Verlag GmbH & Co. KGaA, Weinheim, Germany, 2008.
19. J. E. Benson, M. Boudart, J. Catal. 4 (1965) 704.
20. J. E. Benson, H. S. Hwang, M. Boudart, J. Catal. 30 (1973) 146.
21. K. C. Taylor, J. Catal. 38 (1975) 299.
22. S. E. Wanke, N. A. Dougharty, J. Catal. 24 (1972) 367.
23. PD/TPR 2900 analyser, Operator's Manual, VI.02, April 1993.

24. P. Patnaik, Dean's Analytical Chemistry Handbook, 2nd ed., 2004.
25. E. A. Varella, Conservation Science for the Cultural Heritage: Applications of Instrumental Analysis, Vol. 79, Springer-Verlag Berlin Heidelberg, 2013.
26. http://www.setaram.com/C80-Cells.htm.
27. B. Imelik, J. C. Vedrine, Catalyst Characterization, Physical Techniques for Solid Materials, Plenum Press, New York, 1994.
28. F. W. Fifield, D. Kealy, Principles and Practice of Analytical Chemistry, (5th ed) Blackwell Science Ltd, 2000.
29. L. M. Harwood, C. J. Moody, J. M. Percy, Experimental Organic Chemistry: Standard and Microscale, Blackwell Science, 2001.
30. F. Al-Wadaani, E. F. Kozhevnikova, I. V. Kozhevnikov, J.Catal. 257 (2008) 199.
31. T. Pham, D. Shi, D. Resasco, Topics in Catalysis. 57 (2014) 706.
32. V. V. Costa, H. Bayahia, E. F. Kozhevnikova, E. V. Gusevskaya, I. V. Kozhevnikov, ChemCatChem. 6 (2014) 2134.
33. E. F. Kozhevnikova, PhD thesis, University of Liverpool, 2004.
34. J. Mendham, R. C. Denney, J. D. Barnes, M. J. K. Thomas, Vogel's Textbook of Quantitative Chemical Analysis, Pearson Education Ltd., 2000.

3. Catalyst characterisation

3.1 Introduction

This chapter will present and discuss the results of catalysts characterisation. The catalyst's surface and porosity properties are investigated by BET. The metals supported on the surface of $Cs_{2.5}PW$ and active carbon are probed using XRD and gas chemisorption for the purpose of determining the dispersion and average particle size. Catalyst stability, catalyst composition and the strength and nature of acidic sites are also investigated using ICP, TGA, FTIR and ammonia adsorption microcalorimetry.

3.2 Thermogravimetric analysis

TGA was utilized to determine the content of water in catalysts and to access their thermal stability. Moreover, this technique was also used to characterise the composition of metal precursors that were used to prepare metal-modified CsPW catalysts.

Previous studies showed that, the CsPW is insoluble in water and stable up to 600 °C, which means that it has higher thermal stability than the parent HPW [1, 2]. The thermal analysis of CsPW, 0.5%Pt/CsPW and 5%Ru/CsPW are presented in Figures 3.1-3.3. The experiment was carried with a rate of heating of 20 °C per minute, under continuous N_2 flow, and 0.015-0.025 g of the sample weight pretreated at 150°C and 0.5 Torr pressure.

It can be seen in Figure 3.1 that approximately 3% loss in the weight occurred in the temperature range up to 300 °C for CsPW catalyst corresponding to the loss of 3 to 4 molecules of water per Keggin unit as physisorbed water and/ or crystallisation water [3]. More weight loss occurred at around 580°C owing to the deprotonation of the catalyst and corresponds to 0.25 H_2O molecules per Keggin unit. This is shown in Equation 3.1.

$$Cs_{2.5}H_{0.5}PW_{12}O_{40} \longrightarrow Cs_{2.5}PW_{12}O_{39.75} + 0.25\ H_2O \qquad (3.1)$$

TGA profiles of 0.5%Pt/CsPW and 5%Ru/CsPW-I are shown in Figure 3.2 and 3.3, respectively. The weight loss of these catalysts is less than the parent CsPW. This is probably the result of the reduction at 250°C of these catalysts before TGA analysis.

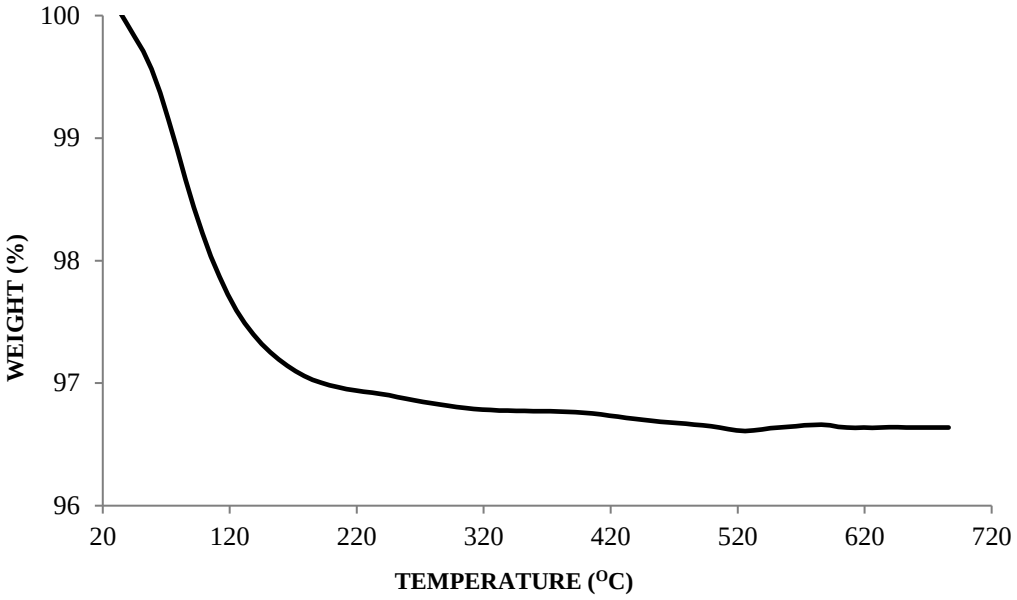

Figure 3.1 TGA of CsPW calcined under vacuum at 150°C for 1.5 h.

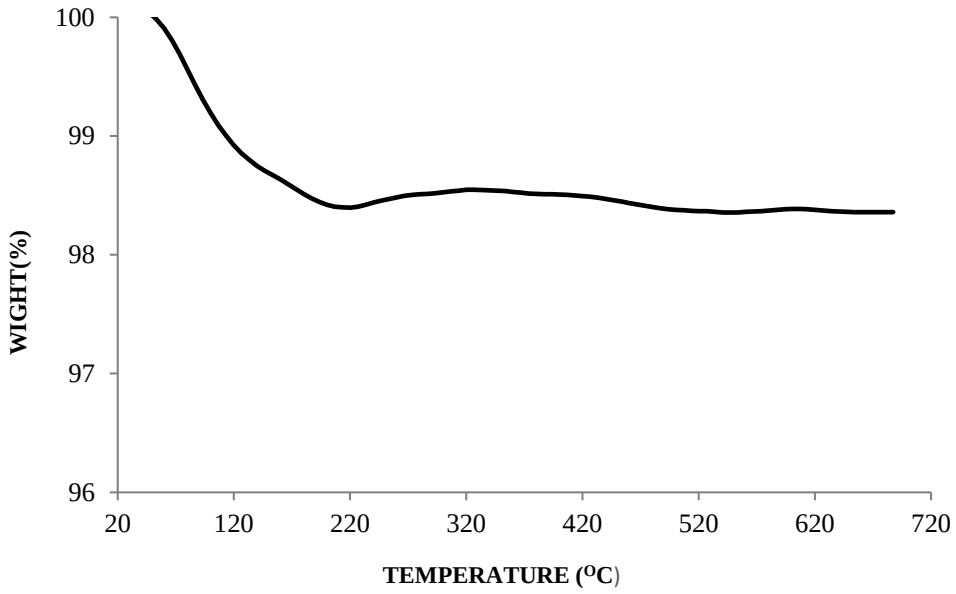

Figure 3.2 TGA analysis of 0.5%Pt/CsPW reduced at 250 °C in H_2 for 2 h.

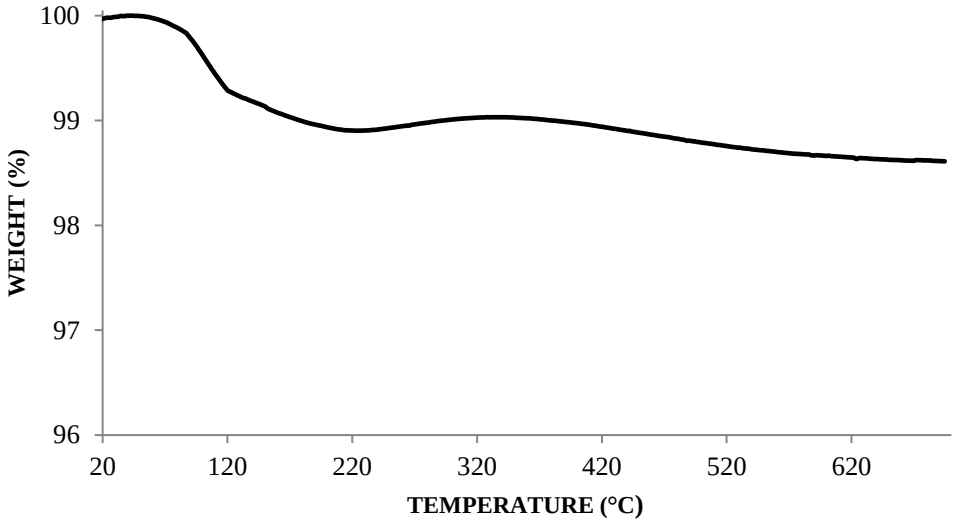

Figure 3.3 TGA analysis of 5.0%Ru/CsPW-I reduced at 250°C in H_2 for 2 h.

3.3 Surface area and porosity studies

Nitrogen adsorption at -196 ºC represents the most widely used method to measure the catalyst surface area and its porous texture. The nitrogen isotherm is obtained by plotting the volume of nitrogen adsorbed against its relative pressure. Isotherm shape depends on the porous texture of the catalyst. As exhibited in Figure 3.4, there are six types of isotherm that can be distinguished according to IUPAC classification, but only types I, II, IV, and VI are generally found in catalyst characterisation [4-6].

Type I, II and VI isotherms are representative of microporous, macroporous and uniform ultramicroporous solids, respectively. Type IV isotherm is attributed to mesoporous materials, and it is this isotherm that will be explained in more detail because of its relevance to the catalysts prepared in this study.

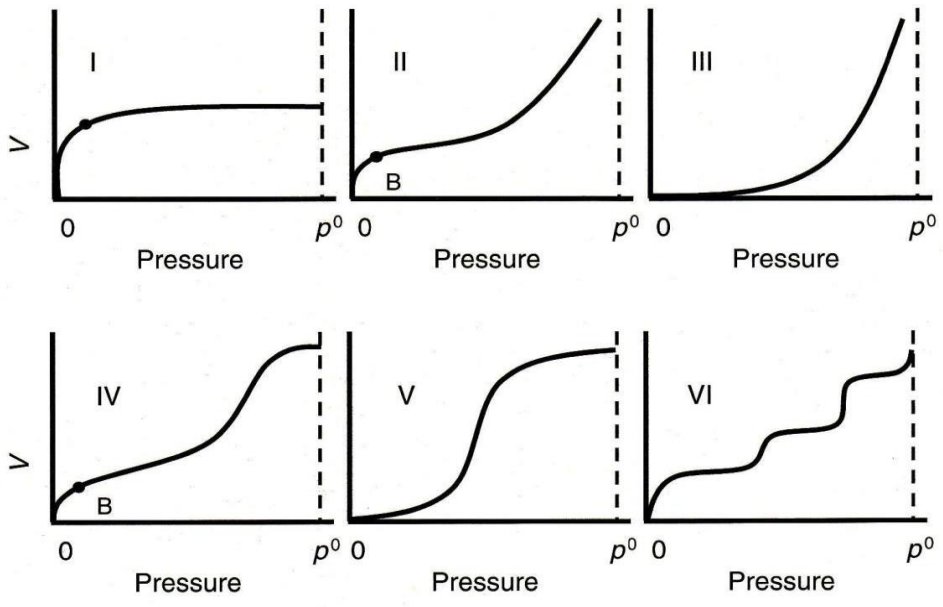

Figure 3.4 The six types of adsorption isotherms [4].

On a mesoporous solid (type IV) a monolayer adsorption occurs at low pressure, while at high relative pressures a multilayer adsorption takes place until condensation occurs, giving a sharp adsorption volume increase. Adsorption continues on the external catalyst surface as mesopores are completely saturated [4, 5]. HPA catalysts belong to this class of solid.

After saturation is reached, desorption of the adsorbed nitrogen takes place in the opposite process to that of adsorption. For mesoporous solids, this process occurs at a pressure lower than that for adsorption, leading to a hysteresis loop. There are four hysteresis types that are recognised for solid catalyst, which are displayed in Figure 3.5 [5].

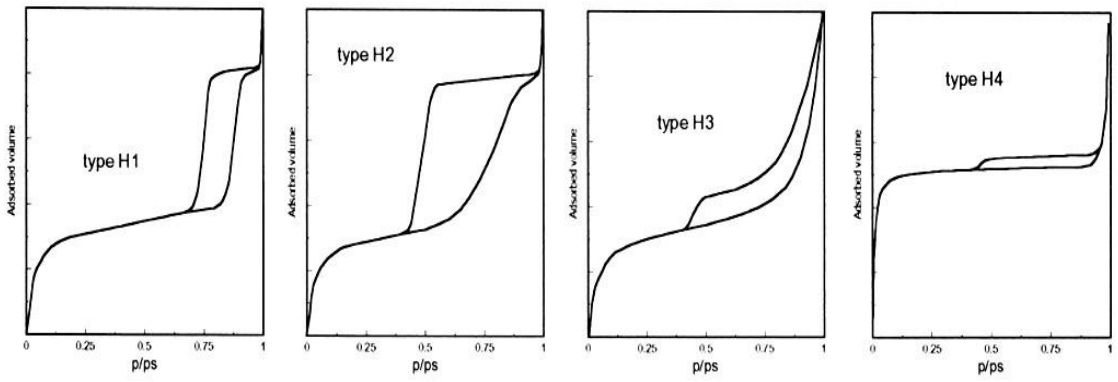

Figure 3.5 The four hysteresis shapes usually found by N_2 adsorption [5].

Types H1 and H2 hysteresis are associated with solid materials that consist of particles crossed by nearly cylindrical channels in shape, or of spheroidal aggregates or agglomerates. Pores of uniform size and shape give H1 hysteresis, while H2 hysteresis occurs in non-uniform pores. These hysteresises are due to a different size of pore mouth and pore body (this is in the case of ink-bottle-shaped pores) and/or a differences in adsorption and desorption behavior close to cylindrical through pores. Most common mesoporous materials such as HPAs usually show type H1 or H2 hysteresis [5].

Types H3 and H4 hysteresis isotherms occur when the sample pores are uniform and non-uniform in size and shape, respectively. These two hysteresis loops are usually formed when solid

materials consist of aggregates or agglomerates of particles creating slit-shaped pores (plates or edged particles like cubes). Typical examples of this hysteresis category are shown by active carbon and zeolites [5].

When solid materials have blind cylindrical, wedge-shaped and cone-shaped pores, no hysteresis loop is observed. However, we can only observe materials with much reduced hysteresis loops due to their irregular pores [5].

The general method for the measurement of surface area and porosity is described in Section 2.4.1. The Brunauer-Emmett-Teller (BET) method was used to calculate the total catalyst surface area [7], while the Barrett, Joyner and Halenda (BJH) method was used to determine pore size distribution and total pore volumes [8].

The surface area of water-soluble bulk HPW is very low, in the range of 1-10 m^2/g [1, 9, 10]. However, salts of HPA with large cations, such as Cs^+, are water insoluble and have a surface area > 100 $m^2\ g^{-1}$ [1, 11]. Table 3.1 and 3.2 show the BET surface area and porous texture of the bifunctional metal−acid and acid catalysts, respectively, used in this work. Previous studies showed that the introduction of metal into the structure reduces the surface area to a small extent, which is the evidence of metal situated on the catalyst surface [12, 13]. To examine the effect of catalyst preparation on catalyst activity the preparation procedure was varied regarding the use of different metal precursors and impregnation conditions (see Section 2.3). The metal loading of Pt and Ru was 0.5 and 5%, respectively, and 10% for Cu and Ni catalysts due to lower catalytic activity of Ru, Cu and Ni compared to Pt. As can be seen from Table 3.1, the catalyst preparation procedure had little effect on the catalyst texture, whereas the metal loading had significant effect on the catalyst surface area. The catalysts had surface areas between 35 and 144 m^2g^{-1} and low porosities typical of CsPW-based catalysts. 0.5% Pt and 5% Ru catalysts had the surface areas above 100 m^2g^{-1}, whereas 10% Ni and Cu catalysts had lower surface areas, 74-93 m^2g^{-1} for Ni and 35 m^2g^{-1} for Cu catalysts. As can be seen in Table 3.2, supporting

HPA onto high surface area supports increases the surface area of HPA catalysts, as compared to bulk HPAs. These catalysts are mesoporous solids with an average pore diameter calculated to be in the range of 22-185 Å.

Table 3.1 Texture of metal catalysts from N_2 adsorption.

Catalyst	S_{BET}[a] (m^2g^{-1})	Pore volume[b] (cm^3g^{-1})	Pore size[c] (Å)
0.5%Pt/CsPW	128	0.100	30
0.5%Pt/CsPW-I	108	0.091	34
0.5%Pt/CsPW-A	144	0.085	24
5.0%Ru/CsPW-I	103	0.088	34
5.0%Ru/CsPW-A	116	0.084	29
10%Cu/CsPW-I	35	0.044	51
10%Cu/CsPW-A	35	0.023	27
10%Ni/CsPW-I	93	0.090	39
10%Ni/CsPW-A	74	0.049	26
7%Pt/C	801	0.580	29

a) BET surface area.
b) Single point total pore volume.
c) Average BET pore diameter.

Table 3.2 Texture of acid catalysts from N_2 adsorption [14].

Catalysts[a]	S_{BET}[b] (m^2g^{-1})	Pore volume[c] (cm^3g^{-1})	Pore size[d] (Å)
$H_3PW_{12}O_{40}$	2	0.04	81
$H_4SiW_{12}O_{40}$	9	0.02	71
$Cs_{2.25}H_{0.75}PW_{12}O_{40}$	128	0.07	22
$Cs_{2.5}H_{0.5}PW_{12}O_{40}$	132	0.10	29
15%HPW/Nb_2O_5	126	0.11	34
15%HPW/ZrO_2	109	0.09	36
15%HPW/TiO_2	45	0.20	174
15%HPW/SiO_2	202	1.00	169
15%HSiW/SiO_2	221	1.02	185

a) HPA catalysts calcined under vacuum at 150 °C for 1.5 h. ZrO_2 and Nb_2O_5 supports were prepared in-house and calcined at 400 °C in air for 5 h.
b) BET surface area.
c) Single point total pore volume.
d) Average BET pore diameter.

Figure 3.6 and Figure 3.7 exhibit the BET isotherm and the pore size distribution of CsPW respectively. It can be seen that, CsPW exhibited a type IV isotherm, in agreement with previous studies [2, 5, 9, 15]. This type of isotherm is typical of mesoporous materials (2 nm < pore diameter < 50 nm). In this case an H2 hysteresis loop was observed, indicating the presence of mesopores of non-uniform shape. The mesopore-size distribution of CsPW gained form the BJH method showed a sharp peak at around 40 Å diameter (Figure 3.7) in good agreement with that reported previously by Okuhara [2]. The pore size distribution created using the N_2 adsorption technique employed in this study was not capable to account for micropores. However, the steep

increase in N_2 adsorption at low pressure ($P/P_0 < 0.1$) from the adsorption isotherm suggests the existence of micropores in this catalyst as well [2].

Figures 3.8-3.16 represent the effect of metal loading on the adsorption isotherm of CsPW. Different preparation procedures and metal precursors were used. However, no obvious change in the N_2 adsorption isotherms of Metal-CsPW catalysts was observed.

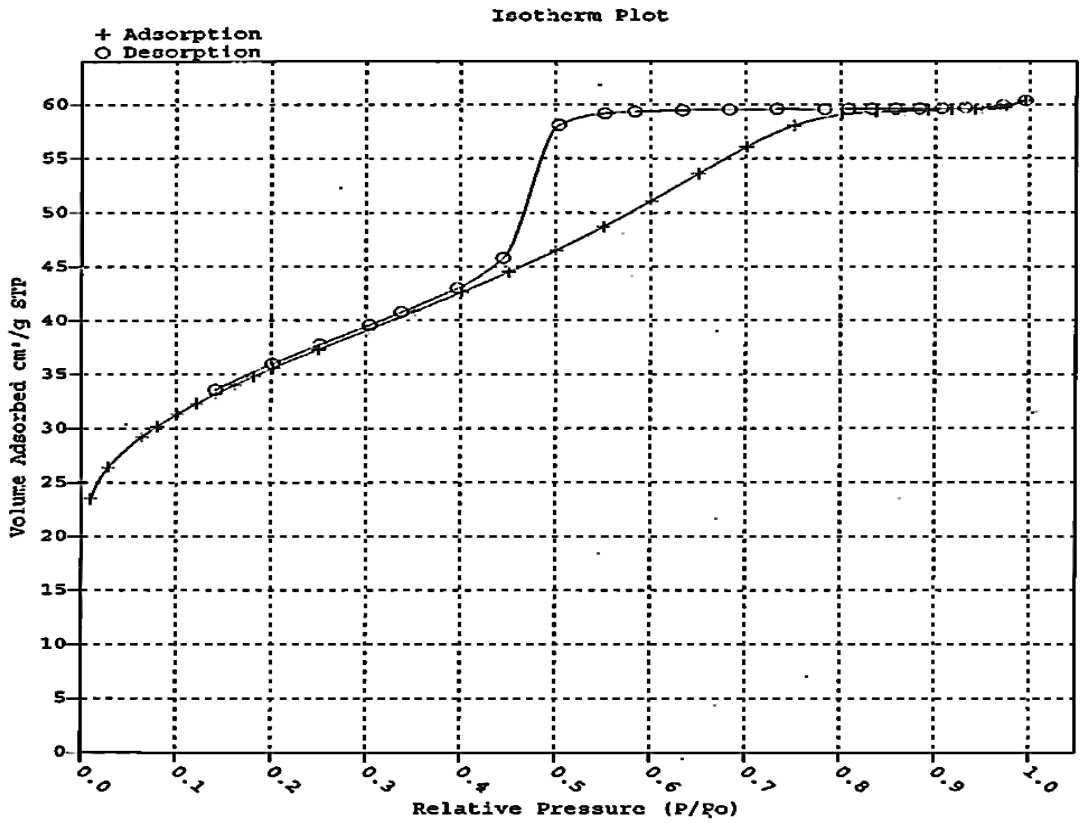

Figure 3.6 N_2 adsorption-desorption isotherms on CsPW.

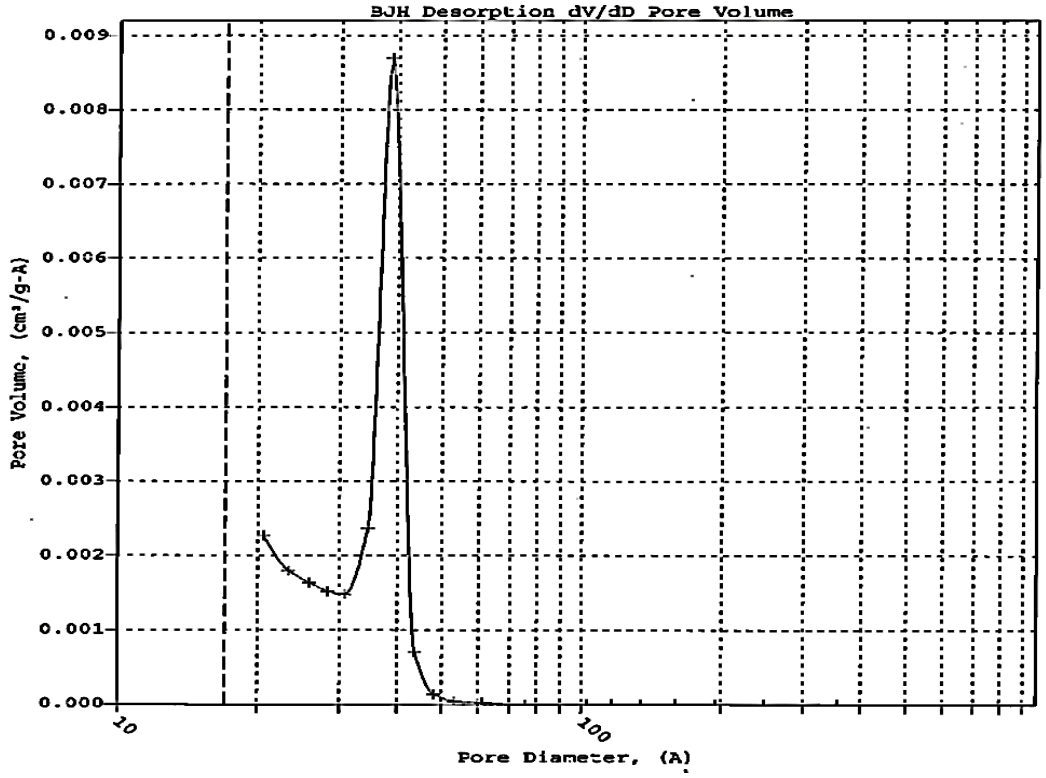

Figure 3.7 Pore size distribution of CsPW.

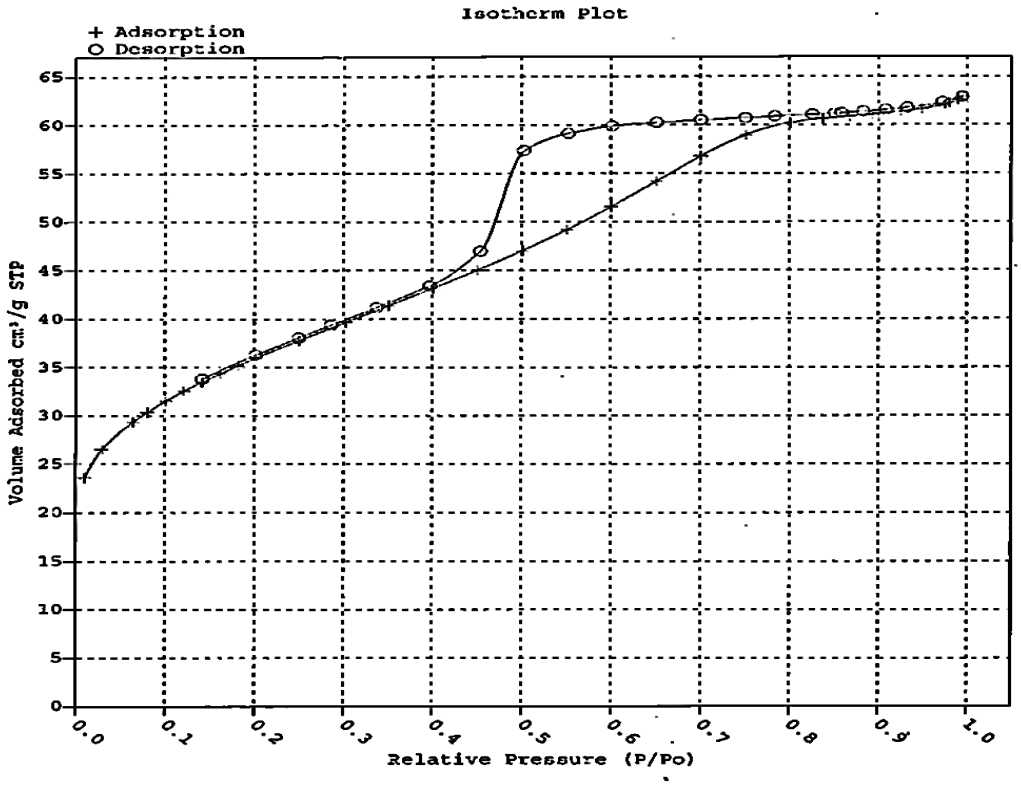

Figure 3.8 N_2 adsorption-desorption isotherms on 0.5%Pt/CsPW.

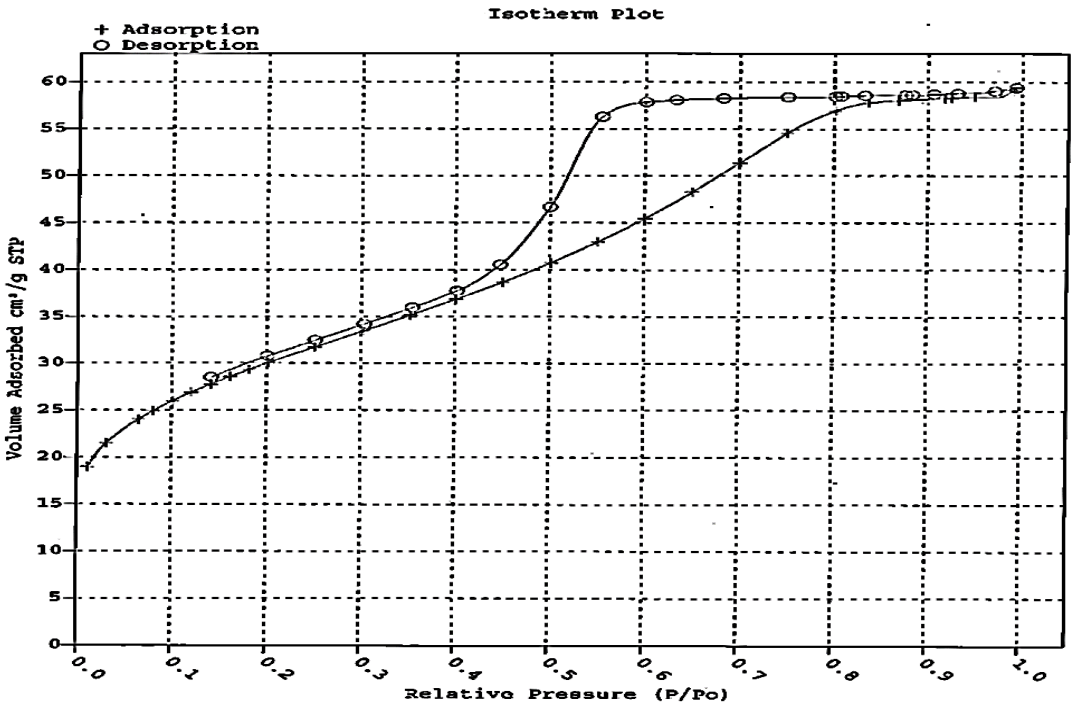

Figure 3.9 N_2 adsorption-desorption isotherms on 0.5%Pt/CsPW-I.

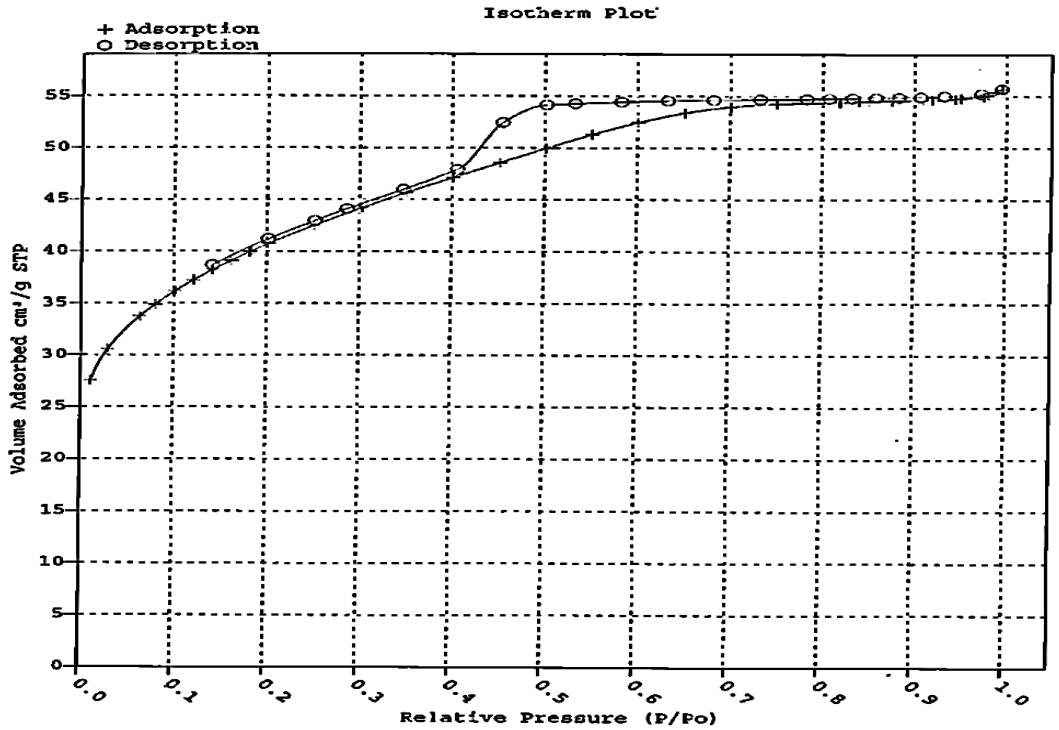

Figure 3.10 N_2 adsorption-desorption isotherms on 0.5%Pt/CsPW-A.

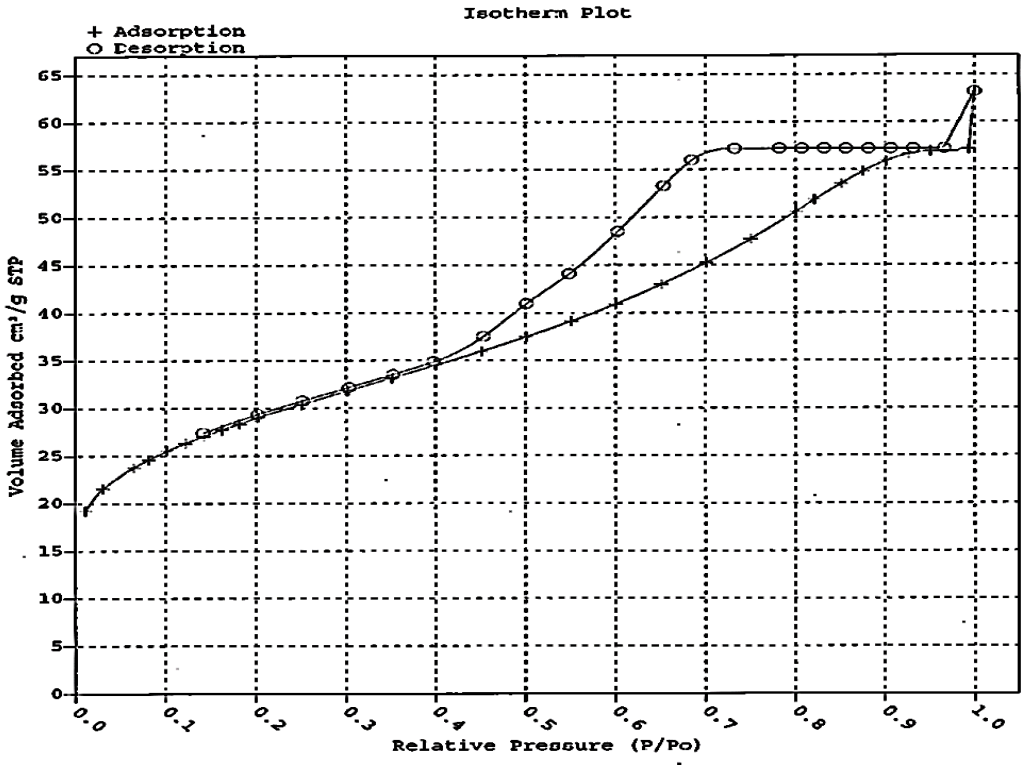

Figure 3.11 N_2 adsorption-desorption isotherms on 5%Ru/CsPW-I.

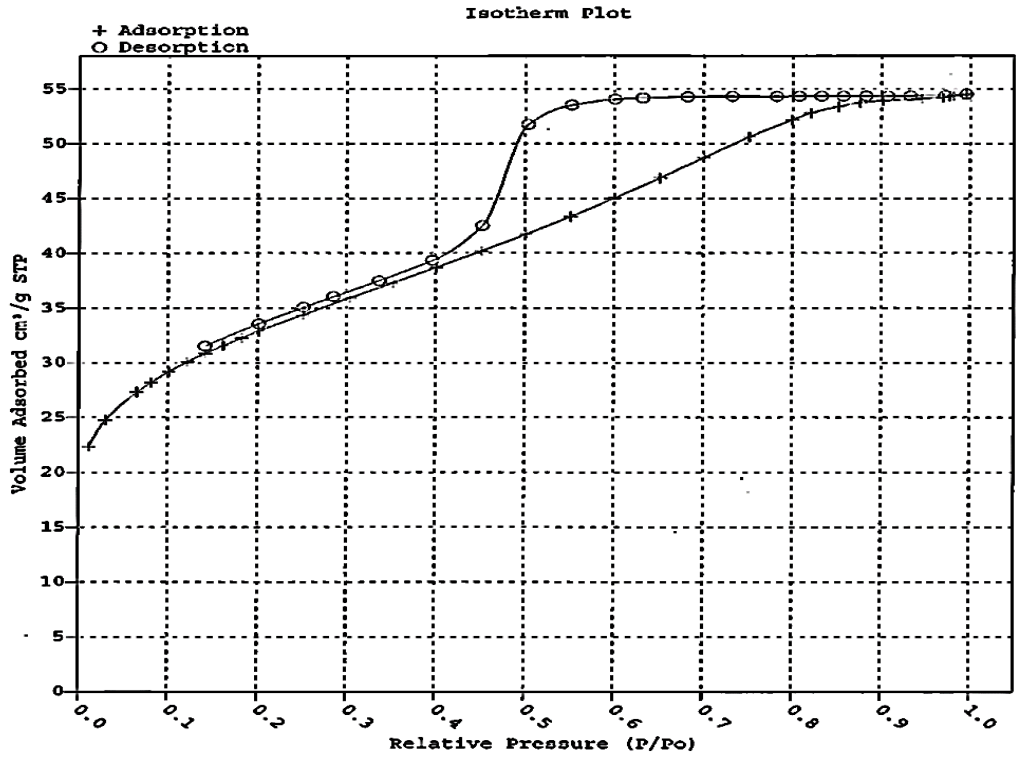

Figure 3.12 N_2 adsorption-desorption isotherms on 5%Ru/CsPW-A.

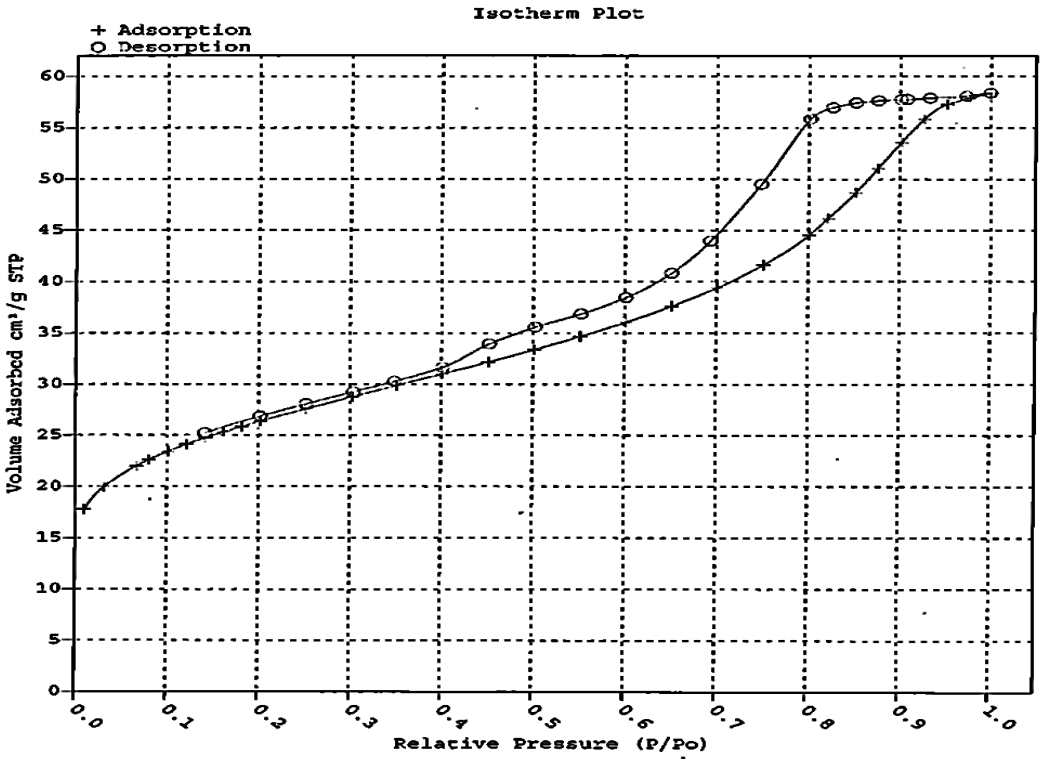

Figure 3.13 N_2 adsorption-desorption isotherms on 10%Ni/CsPW-I.

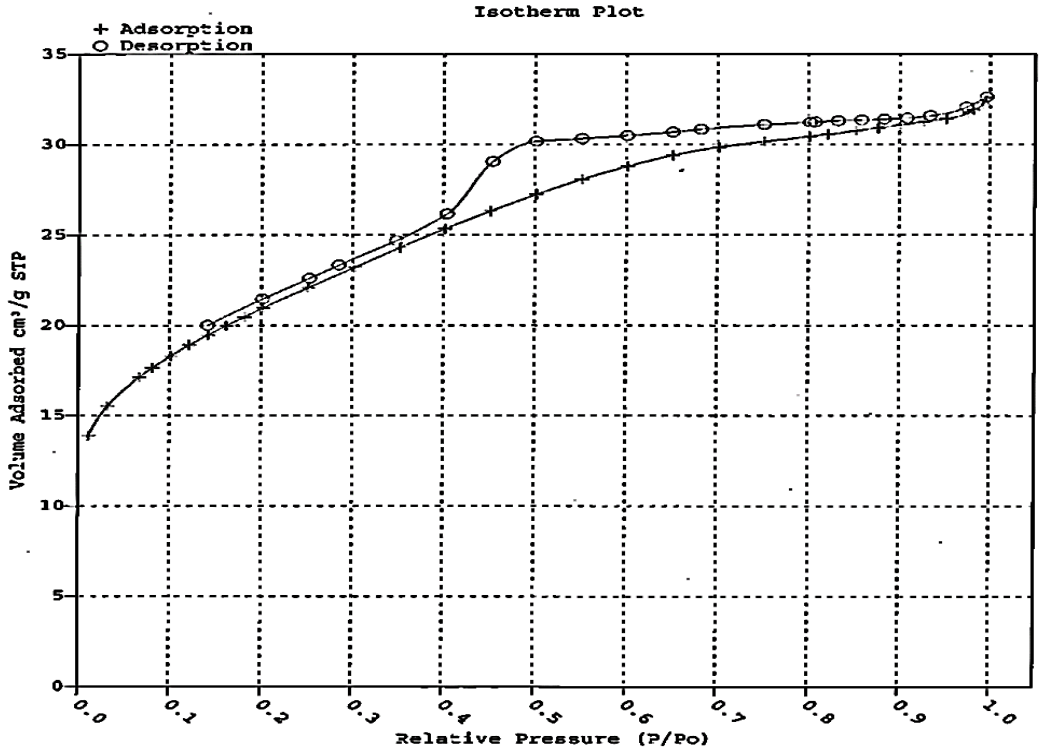

Figure 3.14 N_2 adsorption-desorption isotherms on 10%Ni/CsPW-A.

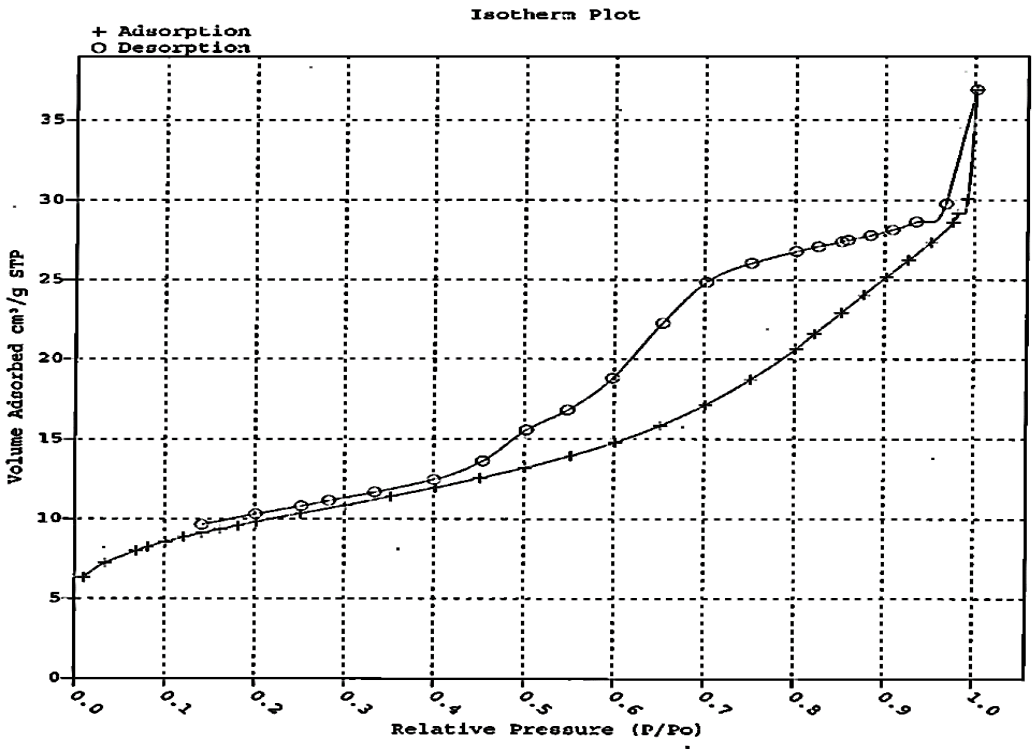

Figure 3.15 N_2 adsorption-desorption isotherms on 10%Cu/CsPW-I.

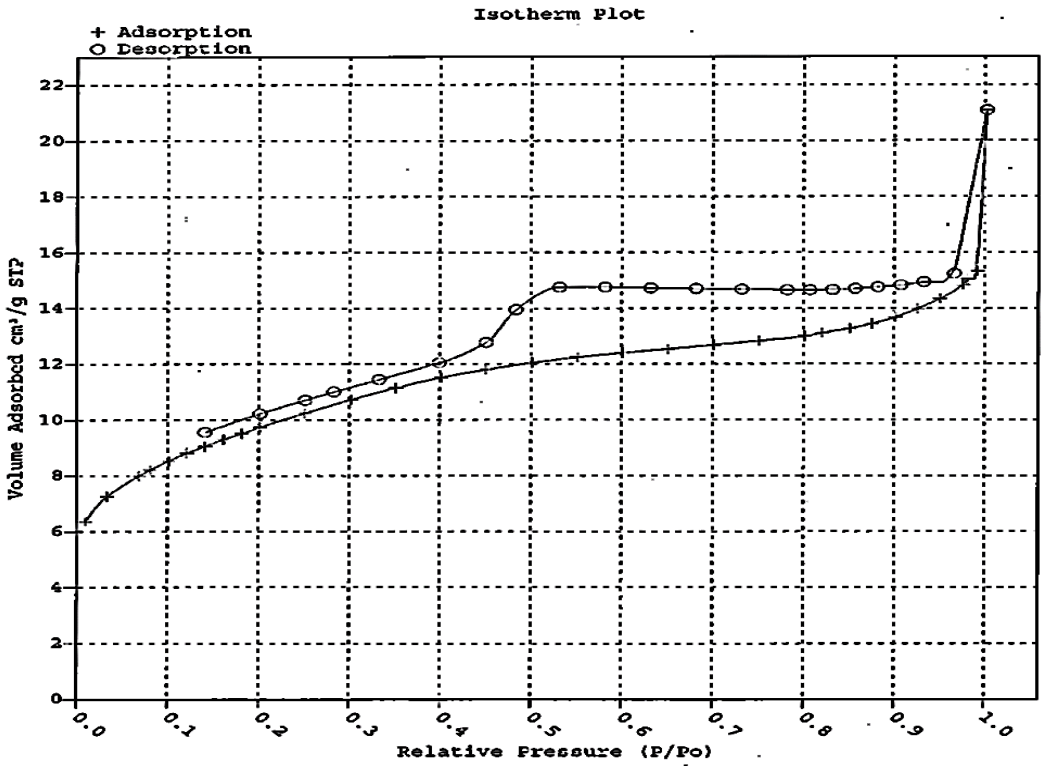

Figure 3.16 N_2 adsorption-desorption isotherms on 10%Cu/CsPW-A.

3.4 Metal dispersion of bifunctional catalysts

0.5% Pt-, 5% Ru-, 10% Ni and 10% Cu-modified CsPW catalysts were used in the gas phase hydrodeoxygenation of ketones, ethers and esters. The dispersions of the Pt- and Ru-modified CsPW catalysts were determined using the pulse H_2 chemisorption method. However, the dispersions of 10% Cu/CsPW and 7% Pt/C were measured using XRD and CO chemisorption, respectively. The general procedure for determination of metal dispersion using gas chemisorption is described in detail in Sections 2.4.4 and 2.4.5.

Table 3.3 Particle size and dispersion of metals on CsPW.

Catalyst[a]	D[b]	d[c] (nm)
0.5%Pt/CsPW	0.46	2.0[d]
0.5%Pt/CsPW-I	0.10	9.0[d]
0.5%Pt/CsPW-A	0.11	8.2[d]
5.0%Ru/CsPW-I	0.048	19[d]
5.0%Ru/CsPW-A	0.054	17[d]
10%Cu/CsPW-I	0.019[f]	59[e]
10%Cu/CsPW-A	0.012[f]	88[e]
7%Pt/C	0.44[g]	2.0[d]

a) The metal loadings quoted were confirmed by the ICP-AES elemental analysis.
b) Metal dispersion in catalysts as determined from H_2 chemisorption.
c) Metal particle diameter.
d) Values obtained from the equation d (nm) = 0.9/D [16].
e) From XRD.
f) Values obtained from the equation D = 1.1/d (nm) [17].
g) Form CO chemisorption.

Table 3.3 shows the metal dispersion, D, and metal particle diameter, d, in the catalysts. For Pt/CsPW and Ru/CsW catalysts, these were determined from H_2 titration and for Cu/CsPW from

XRD. The results for 0.5%Pt/CsPW catalysts demonstrate a strong effect of catalyst preparation on the metal dispersion. The use of $Pt(acac)_2$ as a platinum source and benzene as a solvent for impregnation gave a Pt dispersion D = 0.46 corresponding to a Pt particle diameter d = 2.0 nm. This dispersion was much higher than that obtained by impregnation with H_2PtCl_6 from aqueous solution, i.e. D = 0.10 – 0.11 (d = 8.2 – 9.0 nm) for the Pt/CsPW-I and Pt/CsPW-A catalysts. The mode of impregnation from aqueous media, i.e. with or without ageing of the Pt^{II} – CsPW aqueous slurry, practically did not affect the Pt dispersion and particle size. The same was observed for the Ru/CsPW-I and Ru/CsPW-A. On the other hand, Cu/CsPW-A had larger Cu particles (88 nm), hence a lower Cu dispersion, than Cu/CsPW-I (59 nm) (Table 3.4).

For 7%Pt/C catalyst, Pt dispersion and particle size were determined from CO chemisorption (D = 0.44±0.07, d = 2.0 nm, average of three measurements); these values are in agreement with many literature reports. It should be noted that H_2 titration overestimated Pt dispersion for this catalyst to give a value of D = 1.2±0.1. This may be explained by hydrogen spillover onto the carbon support, which has been reported previously ([18] and references therein). XRD was also unable to determine correctly the size of Pt particles. 7%Pt/C exhibited a clear pattern of the Pt *fcc* phase, with 39.8 (111), 46.3 (200) and 67.5 (220) reflections (Figure 3.21, Section 3.6), from which the particle size was estimated to be d = 28±5 nm (average of three measurements, D = 0.032). This implies that the XRD was biased towards larger Pt particles.

Pt/CsPW, Au/CsPW and bimetallic Pt/Au/CsPW catalysts with metal loading between 0.3-6 wt% were used to study the enhancing effect of gold in the hydrodeoxygenation of 3- pentanone. An accurate assessment of metal dispersion was obtained from hydrogen adsorption. Moreover, STEM and XRD were used to estimate metal particle size for some of these catalysts.

Table 3.4 shows the results of H_2/O_2 titration of CsPW-supported Pt and PtAu catalysts, which was carried out at room temperature by the pulse method in flow system. Under such conditions,

CsPW did not adsorb any hydrogen, in agreement with the previous report [19]. No hydrogen adsorption was observed on the Au/CsPW either, which is also in agreement with the literature [20-22]. Hence the adsorption of H_2 observed on the PtAu catalysts was attributed entirely to platinum. Pt dispersion, *D*, in 0.32%Pt/CsPW was found to be 0.61 and predictably reduced to 0.19 in 5.8%Pt/CsPW, which corresponds to a Pt particle size of 1.5 and 4.7 nm in these catalysts, respectively. The PtAu/CsPW catalysts prepared by co-impregnation showed a small reduction trend in Pt dispersion in comparison with the unmodified Pt/CsPW catalysts, although the difference was within the experimental error. This may be explained by PtAu alloying. Notably, the Pt dispersion in the 0.32%Pt/0.36%Au/CsPW-SI catalyst prepared by sequential Au-after-Pt impregnation dropped significantly down to 0.30 (Table 3.4). This may be the reason for the less efficient performance of this catalyst as compared to the co-impregnation catalyst 0.28%Pt/0.35%Au/CsPW-CI (see Chapter 5).

Table 3.4 H_2/O_2 titration of catalysts.

Catalyst[a]	H_2/Pt_{total} (mol/mol)	D[b]	d[c] (nm)
0.32%Pt/CsPW-I	0.91±0.13	0.61±0.09	1.5
0.28%Pt/0.35%Au/CsPW-CI[d]	0.83±0.09	0.55±0.06	1.6
0.32%Pt/0.36%Au/CsPW-SI[e]	0.45±0.09	0.30±0.06	3.0
5.8%Pt/CsPW-I	0.28±0.07	0.19±0.05	4.7
5.6%Pt/4.3%Au/CsPW-CI[d]	0.26±0.03	0.17±0.02	5.3
2.6%Au/CsPW	0[f]		≤10
CsPW	0[f]		

a) Metal loadings obtained from ICP-AES analysis.
b) Pt dispersion determined as an average from three H_2/O_2 titration measurements assuming negligible H_2 adsorption on gold.
c) Metal particle diameter: for Pt from the equation d (nm) = 0.9/D, for Au from STEM.
d) Catalysts prepared by co-impregnation of H_2PtCl_6 and $HAuCl_4$ followed by reduction with H_2 at 250 ^oC/2 h.
e) Catalyst prepared by sequential impregnation of H_2PtCl_6 then $HAuCl_4$, with Pt(IV) reduced to Pt(0) with H_2 at 250 ^oC/2 h prior to $HAuCl_4$ impregnation, then the Pt^oAu^{III}/CsPW was reduced with H_2 at 250 ^oC/2 h.
f) No H_2 adsorption observed.

3.6 X-ray diffraction

Powder XRD patterns were recorded for metal-modified CsPW catalysts. The Scherrer equation was used to determine metal particle size of these catalysts. Several researchers have reported the XRD pattern for CsPW which was found to be similar to the parent HPW [2, 23]. Figure 3.17 shows the results of powder XRD analysis of CsPW-supported metal catalysts. The XRD of 0.5%Pt/CsPW displays only the well-known pattern of crystalline CsPW [2]; it did not reveal any Pt metal phase, which is probably due to the fine dispersion and low concentration of Pt in

the catalyst. 10%Cu/CsPW-I and 10%Cu/CsPW-A exhibited sharp XRD pattern of Cu metal, with (111) and (200) reflections at 43.1 and 50.3°, respectively, in agreement with the standard values 43.3 and 50.4° (JCPDS, copper 04-0836). From these, a mean diameter of 59 - 88 nm for Cu particles was obtained using the Scherrer equation. Previously, the Kozhevnikov group measured the Cu dispersion using different techniques, such as XRD, TEM and N_2O adsorption [19]. TEM and XRD gave very close results. However, N_2O titration gave agreement with TEM and XRD only by careful optimisation of N_2O concentration, titration temperature and the length of exposure. The problem is that oxidation of Cu with N_2O is not restricted to the outermost Cu layer. Consequently, XRD is as a more reliable and less time consuming technique for measuring the Cu dispersion. The XRD of 10%Ni/CsPW-I and 10%Ni/CsPW-A did not reveal any Ni metal phase (Figure 3.17), which prevented the determination of Ni dispersion in these catalysts. The absence of Ni phase may be explained by Ni oxidation to NiO on exposure of these catalysts to air [24]. It should be noted, however, that no XRD pattern of NiO was observed either (Figure 3.17), which may be explained by fine dispersion of the NiO in our catalysts.

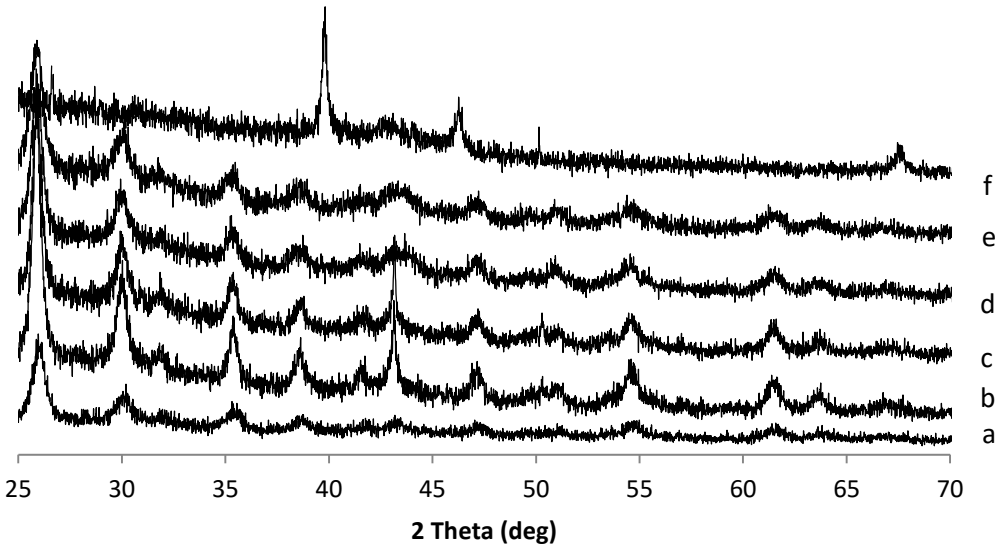

Figure 3.17 XRD patterns (CuKα radiation) for fresh catalysts: (a) 0.5%Pt/CsPW, (b) 10%Cu/CsPW-I, (c) 10%Cu/CsPW-A, (d) 10%Ni/CsPW-I, (e) 10%Ni/CsPW-A, (f) 7%Pt/C.

3.7 Fourier transform infrared spectroscopy (FTIR)

FTIR technique was utilised in this study to investigate the Keggin structure of fresh and spent HPA catalysts. Also it was used to study the Lewis and Bronsted acid sites on the catalyst surface. The general method of FTIR measurements is described in Section 2.4.10.

3.7.1 Keggin structure

IR active bands of the Keggin anion are found in the region between 1200 and 500 cm^{-1} [10, 25]. Choi *et al.* [26] reported infrared bands of bulk HPW and CsPW after calcination at 300^0C for 2 h at 984 cm^{-1} (terminal W=O), 1080 cm^{-1} (P-O in the central tetrahedron), 897, and 812 cm^{-1} (W-O-W) related to asymmetric vibrations in the Keggin polyanion. Figure 3.18 exhibits the DRIFT spectrum of the CsPW catalyst.

In this study, we examined the fresh and spent 0.5%Pt/CsPW catalysts to investigate any possible change in the catalyst structure after MIBK hydrodeoxygenation at 100^0C under H_2 in the gas phase (Figure 3.19). These two spectra show absorption bands of Keggin structure before and after use which indicate the stability of this catalyst structure under the reaction conditions. Moreover, the infrared spectra of CsPW and 7%Pt/C+CsPW (1:19) spent catalysts after diisopropyl ether hydrogenation show no sign of structural changes (Figure 3.20 and 3.21).

We also investigated the structure stability of spent 7% Pt/C+CsPW(1:19) after gas phase ethyl propanoate reaction under H_2 at 200 ^{0}C (Figure 3.22). This catalyst also exhibited the well-known IR spectrum of the Keggin anion at 1079, 987, 889 and 809 cm^{-1}, matching the spectrum of the fresh CsPW catalyst (Figure 3.18).

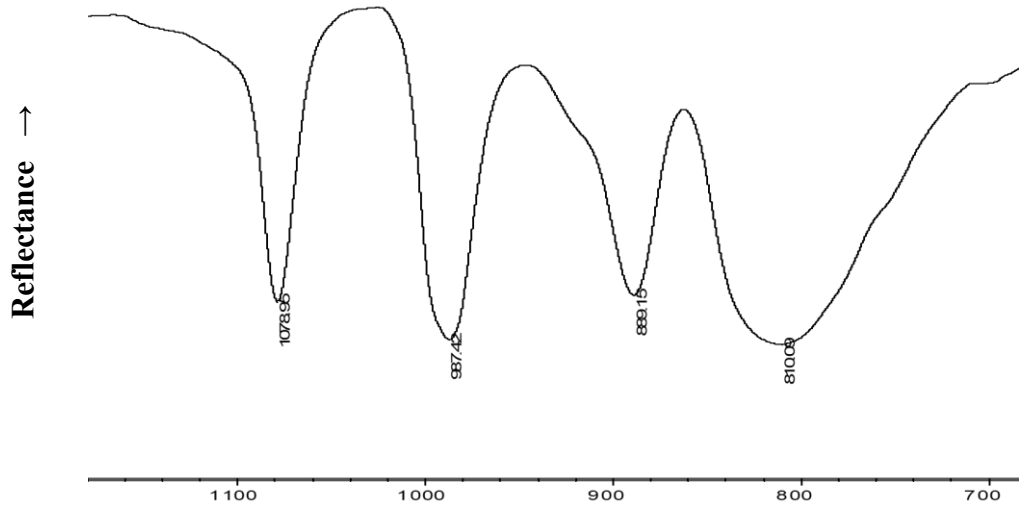

Figure 3.18 DRIFT spectra for fresh CsPW catalyst.

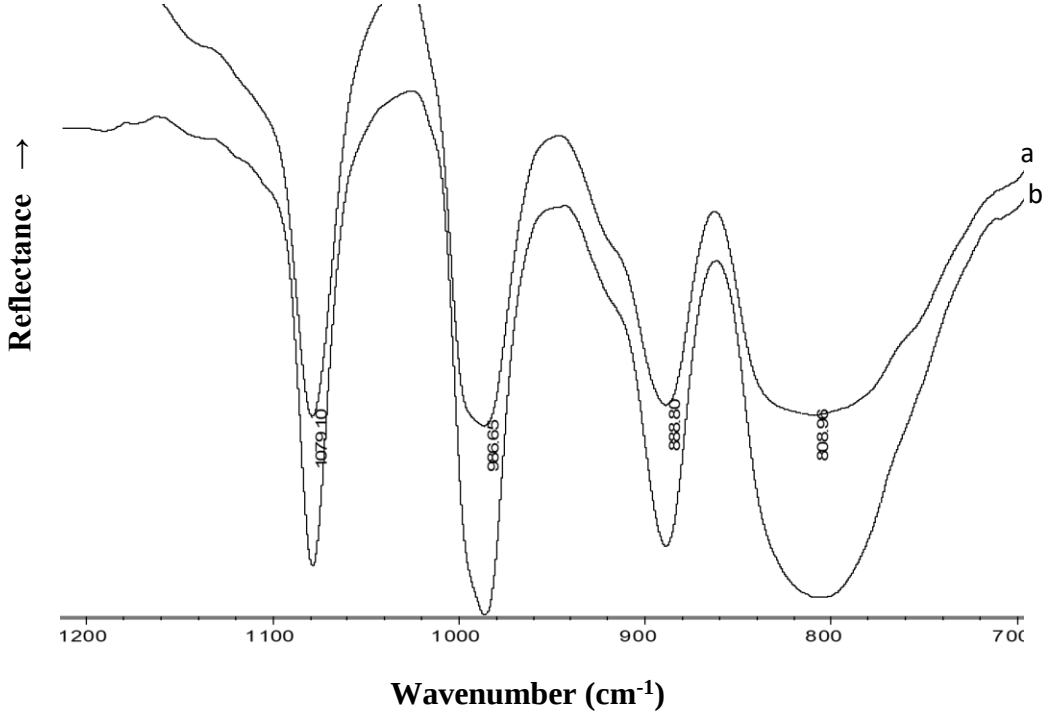

Figure 3.19 DRIFT spectra for (a) fresh and (b) spent 0.5%Pt/CsPW catalyst after MIBK hydroxygenation at 100 ^{0}C under H_2, catalyst reduced under H_2 at 250 ^{0}C for 1.5 h.

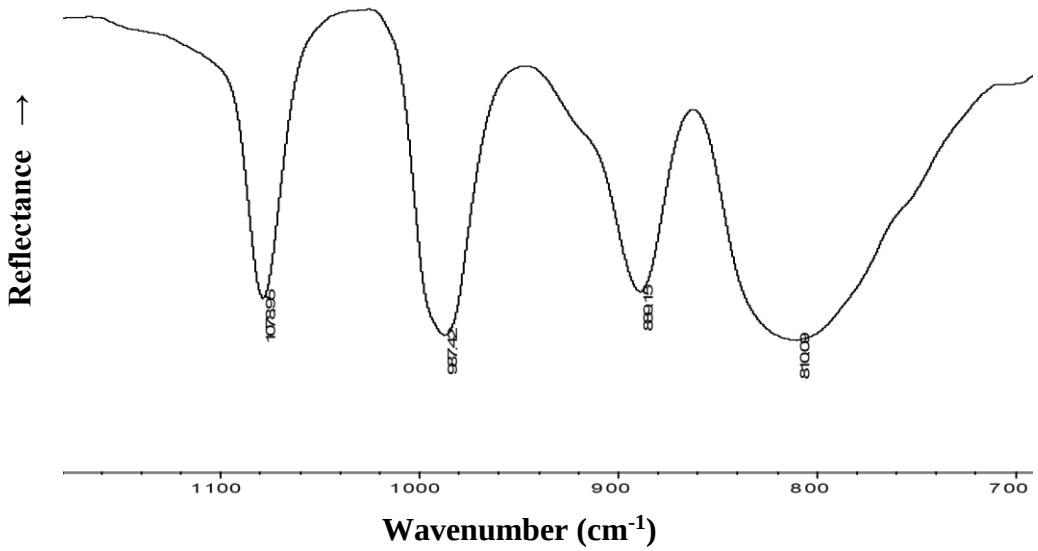

Figure 3.20 DRIFT spectra for spent CsPW catalyst after diisopropyl ether hydroxygenation at 150 ^{0}C under N_2.

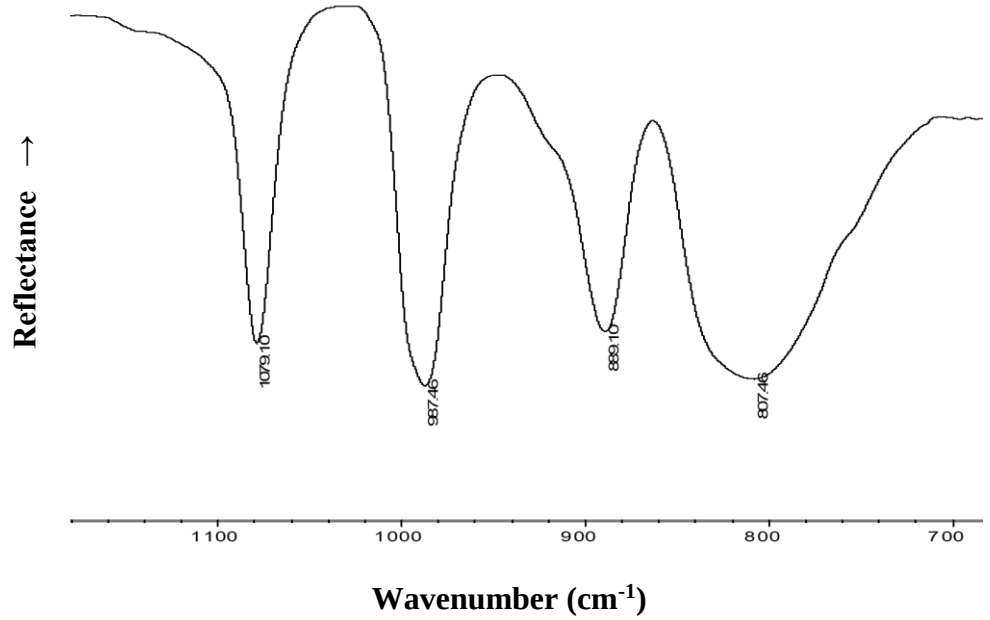

Figure 3.21 DRIFT spectra for spent 7%Pt/C+CsPW(1:19) catalyst after diisopropyl ether hydroxygenation at 110 ^{0}C under H_2.

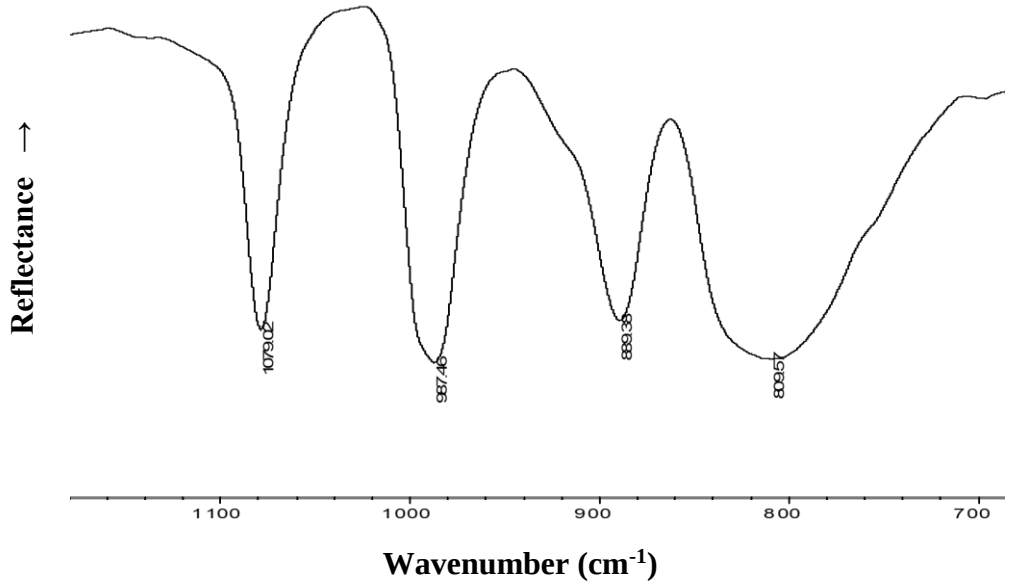

Figure 3.22 DRIFT spectra for spent 7%Pt/C+CsPW(1:19) catalyst after ethyl propanoate hydroxygenation at 200 ^{0}C under H_2.

3.7.2 Pyridine adsorption

Adsorption of pyridine as a base on surface acid sites is fundamental technique used for characterisation of the nature of surface acid sites in heterogeneous catalysis [27-31]. Pyridine chemisorbs on Brønsted and Lewis acid sites and displays a vibration at around 1540, 1490 and 1450 cm^{-1} which are attributed to Brønsted, Brønsted and Lewis and Lewis acidic sites, respectively [32].

The FTIR of pyridine adsorption was utilised in this study to characterise the nature of the acidity of CsPW and 0.5%Pt/CsPW catalysts. Previous studies showed that bulk HPW and CsPW, pre-treated below 300°C, possess a very strong Brønsted acidity [1, 10]. From the DRIFT spectra (Figure 3.23), both CsPW and 0.5%Pt/CsPW catalysts have both Lewis and Brønsted acid sites as confirmed by IR bands at 1450 and 1540 cm^{-1} respectively. This is in agreement with previous studies [28]. Modification of CsPW with Pt may reduce the strength Brønsted sites, which could be expected due to the interaction between the metal and acid sites [33, 34].

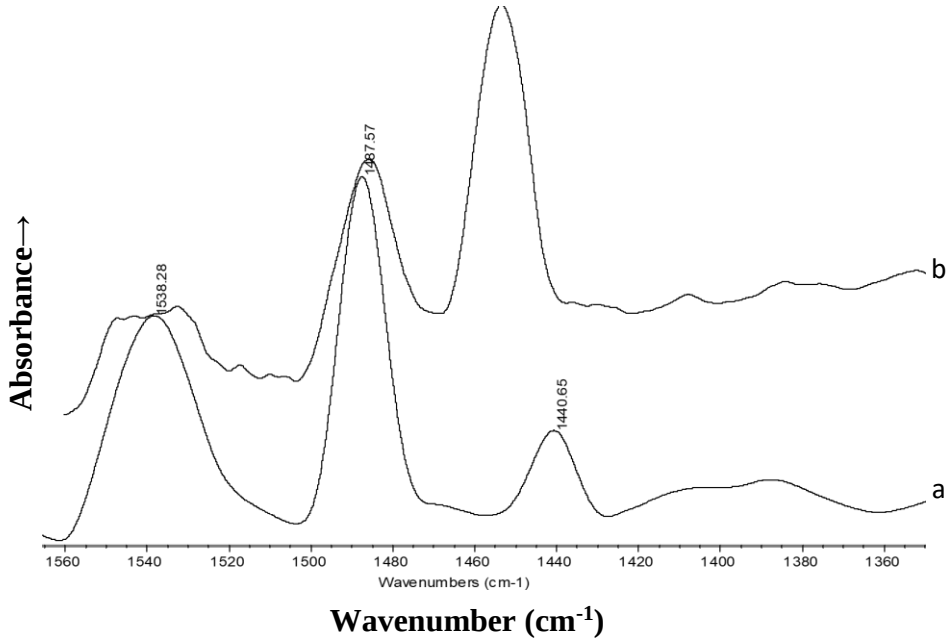

Figure 3.23 DRIFT spectra of adsorbed pyridine on (a) CsPW and (b) 0.5%Pt/CsPW catalysts.

3.8 Microcalorimetry of ammonia adsorption

The acid strength of supported and bulk acid catalysts was measured using ammonia adsorption microcalorimetry technique. Specifically, we looked at the correlation between the turnover reaction rate (turnover frequency) of ethyl propanoate (EP) and diisopropyl ether (DPE) decomposition and the HPA acid strength, which can be used to predict the activity of acid catalysts in these reactions. Solid acid catalysts under study are based on Keggin-type tungsten HPAs, $H_3PW_{12}O_{40}$ and $H_4SiW_{12}O_{40}$, and possess predominantly Brønsted acid sites. Previously, the effect of HPA catalyst acid strength on turnover rate of alcohols dehydration has been studied [14, 35, 36]. In cited references, these catalysts have been thoroughly characterised using XRD, FTIR, FTIR of adsorbed pyridine, ^{31}P MAS NMR and NH_3 adsorption calorimetry, and their properties have been discussed in detail [14, 35-37]. Experimental procedure of ammonia adsorption is detailed in Section 2.4.8. The acid strength of the catalysts under study decreases in the order (Table 3.5): $H_3PW_{12}O_{40}$ > $H_4SiW_{12}O_{40}$ > $Cs_{2.5}H_{0.5}PW_{12}O_{40}$ > $Cs_{2.25}H_{0.75}PW_{12}O_{40}$ >

15%$H_3PW_{12}O_{40}/SiO_2 \approx$ 15%$H_4SiW_{12}O_{40}/SiO_2$> 15%$H_3PW_{12}O_{40}/TiO_2$ > 15%$H_3PW_{12}O_{40}/Nb_2O_5$ > 15%$H_3PW_{12}O_{40}/ZrO_2$. This order is in line with the catalytic activity (see Chapter 6).

Table 3.5 Initial enthalpy of ammonia adsorption at 150 °C.

Catalysts[a]	ΔH_{NH3} (kJ mol^{-1})
$H_3PW_{12}O_{40}$	-197
$H_4SiW_{12}O_{40}$	-171
$Cs_{2.25}H_{0.75}PW_{12}O_{40}$	-162
$Cs_{2.5}PW_{12}O_{40}$	-164
15%HPW/Nb_2O_5	-132
15%HPW/ZrO_2	-121
15%HPW/TiO_2	-143
15%HPW/SiO_2	-154
15%HSiW/SiO_2	-154

[a] All HPA catalysts calcined at 150 °C under vacuum for 1.5 h; in-house made supports ZrO_2 and Nb_2O_5 calcined at 400 °C in air for 5 h [14].

3.9 Conclusion

This chapter has provided the results of catalyst characterization. The nitrogen physisorption technique was used for measuring surface area and porosity of catalysts. All the bifunctional metal−acid and acid catalysts were mesoporous solids with average pore diameters of 22-185 Å. For bifunctional metal acid catalysts, catalyst preparation procedure had little effect on the

catalyst texture, whereas the metal loading had significant effect on the catalyst surface area. Supporting HPA onto high surface area supports increases the catalyst surface area.

Gas chemisorption was used to determine the dispersion and particle size of Pt and Ru on CsPW. However, XRD was used the determine the particle size of Cu

FTIR showed that CsPW and its modified metal catalysts retained their primary Keggin structure in all reaction conditions used in this study. FTIR of pyridine adsorption indicated Brønsted and Lewis sites of CsPW and Pt/CsPW catalysts.

Ammonia adsorption microcalorimetry was used to determine the initial enthalpy of NH_3 adsorption, $\Delta H_,$ for HPA catalysts. Their ΔH values are in the range from -121 to -197 kJ/mol.

3.10 References

1. I. V. Kozhevnikov, Catalysts for Fine Chemical Synthesis, Catalysis by Polyoxometalates, Wiley 2002.
2. T. Okuhara, H. Watanabe, T. Nishimura, K. Inumaru, M. Misono, Chem. Mater. 12 (2000) 2230.
3. N. Essayem, G. Coudurier, M. Fournier, J. C. Vedrine, Catal. Lett. 34 (1995) 223.
4. G. Rothenberg, Catalysis: Concepts and Green Applications, Wiley-VCH, Weinheim, 2008.
5. G. Leofanti, M. Padovan, G. Tozzola, B. Venturelli, Catal. Today 41 (1998) 207.
6. S. J. Gregg, K. S. W. Sing, Adsorption, Surface Area and Porosity, Academic Press, London, 1982.
7. S. Brunauer, P. H. Emmett, E. Teller, J. Am. Chem. Soc. 60 (1938) 309.
8. L. G. Joyner, E. P. Barrett, R. Skold, J. Am. Chem. Soc. 73 (1951) 3155.
9. N. Mizuno, M. Misono, Chem. Rev. 98 (1998) 199.
10. T. Okuhara, N. Mizuno, M. Misono, Adv. Catal. 41 (1996) 113.
11. I. V. Kozhevnikov, Chem. Rev. 98 (1998) 171.
12. K. Na, T. Okuhara, M. Misono, J. Catal. 170 (1997) 96.
13. E. F. Kozhevnikova, E. Rafiee, I. V. Kozhevnikov, Appl. Catal. A. 260 (2004) 25.
14. W. Alharbi, E. I. Kozhevnikova, I. V. Kozhevnikov, ACS Catal. 5 (2015) 7186.
15. T. Nakato, Y. Toyoshi, M. Kimura, T. Okuhara, Catal. Today 52 (1999) 23.
16. J. E. Benson, H. S. Hwang, M. Boudart, J. Catal. 30 (1973) 146.
17. A. Dandekar, M. A. Vannice, J. Catal. 178 (1998) 621.
18. G. Bergeret, P. Gallezot, in: G. Ertl, H. Knözinger, F. Schüth, J. Weitkamp (Eds.), Handbook of Heterogeneous Catalysis, 2, Wiley-VCH, New York, 2008.
19. M. A. Alotaibi, E. F. Kozhevnikova, I. V. Kozhevnikov, Appl. Catal. A 447-448 (2012) 32.
20. C. Hoang-Van, G. Tournier, S. J. Teichner, J. Catal. 86 (1984) 210.
21. J. E. Benson, M. Boudart, J. Catal. 4 (1965) 704.
22. E. Bus, J. A. van Bokhoven, Phys. Chem. Chem. Phys. 9 (2007) 2894.
23. J. A. Dias, E. Caliman, S. C. L. Dias, Micropor. Mesopor. Mat. 76 (2004) 221.
24. M. L. Toebes, J. H. Bitter, A. J. van Dillen, K. P. de Jong, Catal. Today 76 (2002) 33.
25. J. B. Moffat, Metal-Oxygen Clusters. The Surface and Catalytic Properties of Heteropoly Oxometalates, Kluwer, New York, 2001.

26. S. M. Choi, Y. Wang, Z.M. Nie, J. Liu, C. H. F. Peden, Catal. Today 55 (2000) 117.
27. B. M. Devassy, S. B. Halligudi, J. Catal. 236 (2005) 313.
28. B. M. Devassy, F. Lefebvre, S. B. Halligudi, J. Catal. 231 (2005) 1.
29. H. Sachsenroder, E. Brunner, M. Koch, H. Pfeifer, B. Staudte, Microporous Mater. 6 (1996) 341.
30. A. A. Khasin, T. M. Yur'eva, L. M. Plyasova, G. N. Kustova, H. Jobic, A. Ivanov, Y. A. Chesalov, V. I. Zaikovskii, A. V. Khasin, L. P. Davydova, V. N. Parmon, Russ. J. Gen. Chem. 78 (2008) 2203.
31. K. Okumura, K. Yamashita, M. Hirano, M. Niwa, J. Catal. 234 (2005) 300.
32. B. H. Davis, R. A. Keogh, S. Alerasool, D. J. Zalewski, D. E. Day, P. K. Doolin, J. Catal. 183 (1999) 45.
33. D. Kubicka, N. Kumar, T. Venalainen, H. Karhu, I. Kubickova, H. Osterholm, D. Yu. Murzin, J. Phys. Chem. B 110 (2006) 4937.
34. V. Nieminen, M. Kangas, T. Salmi, D. Yu. Murzin, Ind. Eng. Chem. Res. 44 (2005) 471.
35. A. M. Alsalme, P. V. Wiper, Y. Z. Khimyak, E. F. Kozhevnikova, I. V. Kozhevnikov, J. Catal. 276 (2010) 181.
36. W. Alharbi, E. Brown, E. F. Kozhevnikova, I. V. Kozhevnikov, J. Catal. 319 (2014) 174.
37. G. C. Bond, S. J. Frodsham, P. Jubb, E. F. Kozhevnikova, I. V. Kozhevnikov, J. Catal. 293 (2012) 158.

4. Hydrogenation of ketones over bifunctional Pt-heteropoly acid catalyst in the gas phase

4.1 Introduction

Biomass-derived organic oxygenates such as ketones, carboxylic acids, alcohols, phenols, etc., readily available from natural resources, are attractive as renewable raw materials for the production of value-added chemicals and bio-fuels, as a result of the decline in oil resources and global warming [1, 2]. Today the main targets of biofuels are diesel, gasoline and jet fuel. Commercially, bioethanol and fatty acid alkyl esters are used as biogasoline and biodiesel. However, the drawbacks of this first generation of biofuels are their low stability, low energy density and competition with food production. These drawbacks can be overcome by developing next generation biofuels that do not conflict with food production and totally match with petroleum based transportation fuels composed of hydrocarbons [3, 4]. Generally, biomass derived organic compounds contain a large amount of oxygen and have low energy density. For fuel applications, they require reduction in oxygen content to increase their caloric value. Much attention is given to deoxygenation of organic oxygenates using heterogeneous catalysis, in particular for the upgrading of biomass-derived oxygenates obtained from fermentation, hydrolysis and fast pyrolysis of biomass [5-9].

Biomass-derived ketones can be further upgraded by aldol condensation and hydrogenation to produce alkanes that fall in the gasoline/diesel range. The hydrogenation of ketones to produce alcohols is feasible and is catalysed by supported metal catalysts (e.g. Pt/C and Pd/C) [10]; however, further hydrogenation to alkanes is rather difficult to achieve on such catalysts [11, 12]. In combination with acid catalysts (bifunctional metal-acid catalysts), the production of alkane

from ketone can be achieved much easier ([11-13] and references therein). This process occurs via a sequence of steps involving hydrogenation of ketone to alcohol on metal sites followed by dehydration of secondary alcohol to alkene on acid sites and finally hydrogenation of alkene to alkane on metal sites (Scheme 4.1). Although alkenes have higher octane number than alkanes, alkanes are more favourable for fuels because of their higher stability. Consequently, using metal-acid bifunctional catalysts is one of the most promising approaches for complete hydrodeoxygenation (HDO) [3].

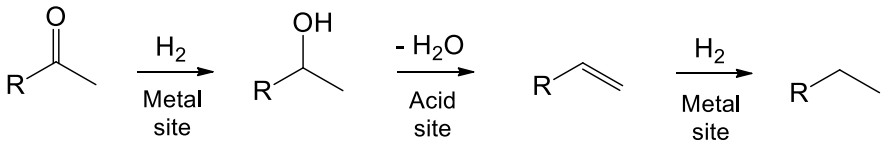

Scheme 4.1 Ketone hydrogenation via bifunctional metal-acid catalysis.

Previously, Kozhevnikov group have reported that platinum on acidic supports, namely Pt on zeolite HZSM-5 [11] and acidic caesium salt of tungstophosphoric heteropoly acid $Cs_{2.5}H_{0.5}PW_{12}O_{40}$ (CsPW) [12], are active bifunctional catalysts for hydrogenation of methyl isobutyl ketone (MIBK) to the corresponding alkane 2-methylpentane (MP) in the gas phase. 0.5%Pt/CsPW, possessing very strong Brønsted acidity in addition to Pt metal sites, has been found to be particularly efficient catalyst giving 100% yield of MP at 100 ^{o}C and 1 bar pressure without alkane isomerisation [12]. They have also proved the bifunctional metal-acid catalysis mechanism (Scheme 4.1) for MIBK hydrodeoxygenation [12]. Recently, Mizuno et al. [13] have applied this catalyst for hydrogenation of ketones, phenols and ethers in the liquid phase at 120 ^{o}C and 5 bar H_2 pressure.

In this chapter, we investigate the hydrogenation (hydrodeoxygenation) of a variety of ketones including aliphatic ketones and acetophenone in the gas phase using bifunctional metal-acid catalysts comprising Pt, Ru, Ni and Cu supported on CsPW. Firstly, methyl isobutyl ketone (MIBK) hydrogenation was studied in more detail using metal (Pt, Ru, Ni, Cu) modified CsPW

catalysts. Then the most efficient catalyst, 0.5%Pt/CsPW, was used to study the hydrogenation of aliphatic ketones and acetophenone. It is demonstrated that 0.5%Pt/CsPW is a highly efficient and versatile catalyst for the ketone-to-alkane hydrogenation, and an insight into the reaction mechanism is gained.

4.2 Hydrogenation of MIBK over CsPW-supported metal catalysts

The hydrogenation of MIBK was carried out in the gas phase in flowing H_2. The catalysts were tested at 60-100 ^oC under atmospheric pressure in a Pyrex fixed-bed down-flow reactor (9 mm internal diameter) fitted with an on-line gas chromatograph (Varian Star 3400 CX instrument with a 30 m x 0.25 mm HP INNOWAX capillary column and a flame ionisation detector) described in Chapter 2.

The catalysts studied together with their characterisation data are shown in Table 3.1 and 3.3 in Chapter 3. To examine the effect of catalyst preparation on catalyst activity the preparation procedure was varied regarding the use of different metal precursors and impregnation conditions (Chapter 2 section 2.3). The metal loading of Pt, Ru was 0.5% and 5%, respectively, and 10% for Cu and Ni catalyst due to lower catalytic activity of Ru, Cu and Ni compared to Pt. Previous H_2-TPR, XRD, and FTIR studies have shown that CsPW in Pt/CsPW and Pd/CsPW catalysts is resistant to reduction by H_2 below 600°C, and the primary (Keggin) structure of CsPW is retained in CsPW-supported Pt, Pd, and Cu catalysts after H_2 treatment at 400°C [14].

The hydrogenation of methyl isobutyl ketone (MIBK) was studied in more detail using CsPW-supported Pt, Ru, Ni and Cu catalysts in order to optimise catalyst preparation and to gain an insight into the reaction mechanism. Representative results are shown in Table 4.1. CsPW alone in the absence of metal exhibited very low activity at 80-100 ^oC. As found previously [12], non-acidic metal catalysts, such as Pt/C and Ru/C, are active in hydrogenation of MIBK to alcohol,

2-methyl-4-pentanol (MP-ol), at 100 ^{o}C, but further hydrogenation to alkane, 2-methypentane (MP), becomes feasible only at temperatures as high as 300 ^{o}C. In contrast, bifunctional metal-acid catalyst 0.5%Pt/CsPW, prepared from $Pt(acac)_2$ in benzene solution, showed excellent activity in MIBK hydrogenation, giving 100% MP yield at 100 ^{o}C and 1 bar pressure (Table 4.1). No MP isomerisation was observed at this temperature. It can be seen that both 0.5%Pt/CsPW-I and 0.5%Pt/CsPW-A, prepared from H_2PtCl_6 in aqueous solution, were less active than the 0.5%Pt/CsPW catalyst (cf. MIBK conversions at 60 and 80 ^{o}C). This may be explained by the higher Pt dispersion in 0.5%Pt/CsPW (Table 3.3 in Chapter 3) and the presence of chloride in 0.5%Pt/CsPW-I and 0.5%Pt/CsPW-A. Reaction selectivity was greatly affected by the temperature. At 60 ^{o}C, MP-ol was the main product, whereas at 100 ^{o}C, MP was formed in almost 100% yield, in agreement with the previous report [12]. This suggests the change of the rate-limiting step with increasing the temperature (see below).

5%Ru/CsPW-I and 5%Ru/CsPW-A exhibited close activities in MIBK hydrogenation (Table 4.1). These catalysts matched 0.5%Pt/CsPW in activity and selectivity at 100 ^{o}C, but at a ten times higher metal loading, in agreement with the previous report [12], yet they were considerably less active than 0.5%Pt/CsPW at lower temperatures 60-80 ^{o}C. Ni/CsPW and Cu/CsPW catalysts were much less active, showing a moderate activity at 350 ^{o}C, with Ni being more active than Cu. The mode of preparation of these catalysts, i.e. with or without ageing of CsPW and metal precursor aqueous slurry, had little effect on their performance. It should be noted that since the non-metal doped CsPW support also showed some catalytic activity (Table 4.1) the activity of Ni/CsPW and Cu/CsPW could to some extent be attributed to the CsPW rather than to the Ni and Cu. Therefore, the activity of the catalysts studied in terms of MIBK conversion per unit metal weight decreased in the order: Pt > Ru >> Ni > Cu. The 0.5%Pt/CsPW catalyst, prepared from $Pt(acac)_2$ as a platinum source in benzene solution, showed the best performance in the MIBK-to-MP hydrogenation.

Table 4.1 Hydrogenation of MIBK over bifunctional metal-acid catalysts.[a]

Catalyst	Temperature (°C)	Conversion (%)	Selectivity (mol%)		
			MP	MP-ol	Other[b]
CsPW	80	1	27	0	73
	100	3	22	0	78
0.5%Pt/CsPW	60	76	13	80	7
	80	97	42	50	8
	100	100	100	0	0
0.5%Pt/CsPW-I	60	32	41	49	10
	80	88	89	11	0
	100	98	98	0	2
0.5%Pt/CsPW-A	60	59	16	84	0
	80	94	29	63	8
	100	100	100	0	0
5%Ru/CsPW-I	60	36	24	76	0
	80	71	75	25	0
	100	96	100	0	0
5% Ru/ CsPW-A	60	31	8	92	0
	80	66	29	67	4
	100	90	98	2	0
10%Ni/CsPW-I	350	24	93	0	7
10%Ni/CsPW-A	350	19	95	0	5
10%Cu/CsPW-I	350	9	93	2	5
10%Cu/CsPW-A	350	4	97	0	3

a) Reaction conditions: 0.2 g catalyst, 3.6% MIBK in H_2 flow, 1 bar pressure, 20 mL min^{-1} flow rate, 2 h time on stream, catalyst pre-treatment at 100 °C/1 h in H_2 flow.

b) C_1-C_5 cracking products, mainly propene and butenes, together with small amount of C_{6+} condensation products.

Table 4.2 compares the performances of bifunctional catalyst 0.5%Pt/CsPW having metal and acid sites in a rather close proximity to each other and the corresponding 1:19 w/w physical mixture of 7%Pt/C and CsPW containing 0.35% of Pt, in which metal and acid sites are a longer distance apart. It can be seen that these two catalysts give very similar MIBK conversions in the temperature range of 60 – 100 ^{o}C. This indicates that the reaction is not limited by migration of intermediates between metal and acid sites in the bifunctional catalyst [15], hence the metal and acid sites are not required to be located in close proximity for the reaction to occur. It should be noted, however, that the 0.5%Pt/CsPW catalyst produced more by-products (C_1-C_5 hydrocarbons and C_{6+} condensation products) than the mixed 7%Pt/C + CsPW catalyst (Table 4.2).

Table 4.2 Hydrogenation of MIBK over Pt/CsPW and Pt/C+CsPW catalysts.[a]

Catalyst	Temperature (^{o}C)	Conversion (%)	Selectivity (mol%)		
			MP	MP-ol	Other[b]
0.5%Pt/CsPW	60	94	12	81	7
	80	99	60	29	11
	100	100	100	0	0
7%Pt/C+CsPW[c]	60	91	17	81	2
	80	97	90	10	1
	100	99	100	0	0

a) Reaction conditions: 0.2 g catalyst, 3.6% MIBK in H_2 flow, 1 bar pressure, 20 mL min^{-1} flow rate, 2 h time on stream, catalyst pre-treatment at reaction temperature for1 h in H_2 flow.

b) C_1-C_5 cracking products, mainly propene and butenes, together with small amount of C_{6+} condensation products.

c) Physical mixture of 7%Pt/C + CsPW (0.35% Pt content).

The time course shown in Figure 4.1 demonstrates stable catalytic activity of 0.5%Pt/CsPW in MIBK hydrogenation for 2.5 h on stream. Previously, extended stability tests showed no catalyst deactivation at least for 14 h on stream [12].

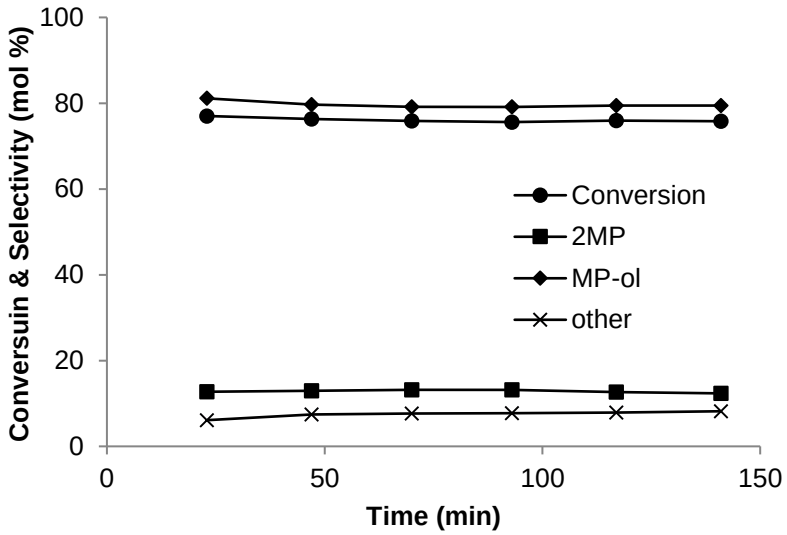

Figure 4.1 MIBK hydrogenation over 0.5%Pt/CsPW (0.2 g catalyst, 60 ^{o}C, 3.6% MIBK in H_2 flow, 1 bar pressure, 20 mL min^{-1} flow rate, catalyst pre-treatment at 100 ^{o}C/1 h in H_2 flow).

The activation energy of MIBK hydrogenation over 0.5%Pt/CsPW was determined under differential conditions. To fit these conditions, the catalyst sample was reduced to 0.025 g diluted with 0.175 g SiO_2, and the flow rate was increased to 100 mL min^{-1}. The reaction obeys the Arrhenius equation with an activation energy E_a = 69 kJ mol^{-1} in the temperature range 80 – 110 ^{o}C where MP is by far the main reaction product (Figure 4.2). The high activation energy indicates that the reaction occurred under kinetic control. This is supported by the Weisz-Prater analysis [16] of the reaction system. Assuming spherical catalyst particles and Knudsen diffusion regime, the Weisz-Prater criterion was calculated to be $C_{WP} = 1.2 \cdot 10^{-2} < 1$ indicating no internal diffusion limitations [17]. Other results reported previously [12], such as the close to zero reaction order in MIBK and DIBK conversion scaling almost linearly with the Pt loading in the catalyst, are also in agreement with reaction occurring under kinetic control.

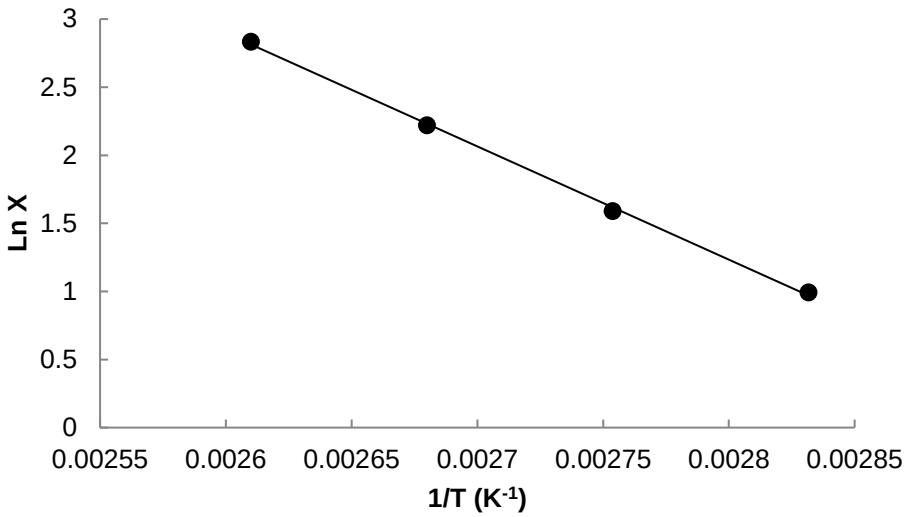

Figure 4.2 Arrhenius plot for MIBK hydrogenation over 0.5%Pt/CsPW (0.025 g catalyst diluted with 0.175 g SiO_2, 3.6% MIBK in H_2 flow, 1 bar pressure, 100 mL min^{-1} flow rate, MIBK conversion range X = 3 – 17%).

4.3 Dehydration of 2-methyl-4-pentanol over CsPW

The dehydration of the secondary alcohol MP-ol is the second step in MIBK hydrogenation through the bifunctional metal-acid-catalysed pathway (Scheme 4.1). It was studied to obtain knowledge about the rate-limiting step in the MIBK hydrogenation.

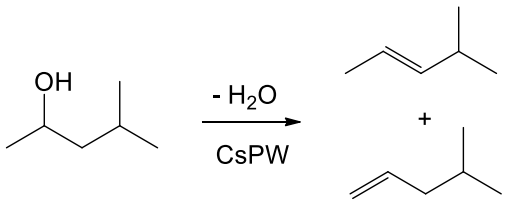

Scheme 4.2 Dehydration of 2-methyl-4-pentanol over CsPW.

MP-ol dehydration over CsPW was found to yield two 2-methylpentene isomers with high selectivity (Scheme 4.2). MP-ol conversion increased with increasing the temperature to reach 100% above 80 ^{o}C (Table 4.3). The reaction was found to be close to zero order in MP-ol (0.15 order) in the MP-ol partial pressure range of 1 – 3 kPa (Figure 4.3). Previously, zero order in

alcohol has been observed for isopropanol dehydration over CsPW [18]. The activation energy of MP-ol dehydration was found to be E_a = 130 kJ mol^{-1} in the temperature range of 60 – 80 ^{o}C (determined under differential conditions at MP-ol conversion X = 0.8 – 12%).

Table 4.3 Dehydration of MP-ol over CsPW.[a]

Temperature (^{o}C)	Conversion (%)	Selectivity (mol%)	
		2-Methylpentene	Other
40	3	79	21
60	43	97	3
80	99	100	0
100	100	100	0

a) Reaction conditions: 0.2 g catalyst, 1.6% MP-ol in N_2 flow, 1 bar pressure, 20 mL min^{-1} flow rate , 3 h time on stream, catalyst pre-treatment at reaction temperature for 1 h in N_2 flow.

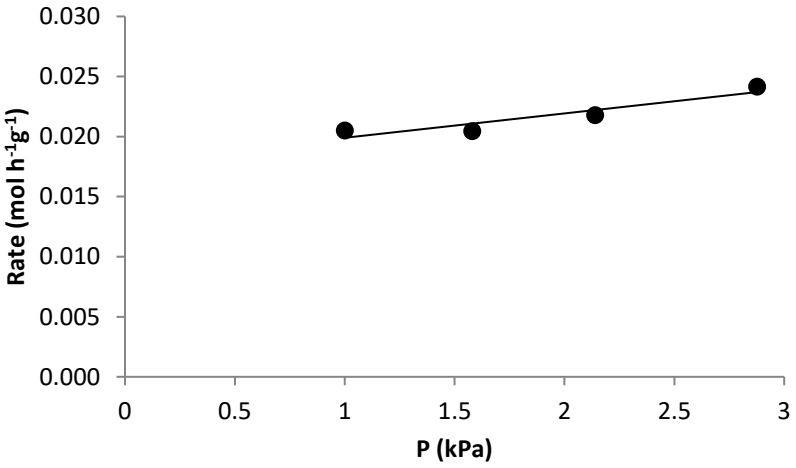

Figure 4.3 Effect of MP-ol partial pressure on the rate of MP-ol dehydration over CsPW (0.025 g catalyst diluted with 0.175 g SiO_2, 80 ^{o}C, 1 bar pressure, 100 ml min^{-1} N_2 flow rate, X = 8 – 20%).

Previously, it has been suggested that MIBK-to-MP hydrogenation over Pt/CsPW at 100 ^{o}C is limited by the first step, i.e., hydrogenation of MIBK to MP-ol (Scheme 4.1). This is mainly based on the fact that reaction rate scales with Pt loading, while MP selectivity remains constant ~100% [12]. The results on MP-ol dehydration obtained here fully support this view. First, the MP-ol dehydration is fast at 100 ^{o}C; and second, it has much higher activation energy that the MIBK-to-MP hydrogenation. Consequently, at lower temperatures, ~60 ^{o}C, MIBK-to-MP hydrogenation appears to be limited by MP-ol dehydration, resulting in formation of MP-ol as the main product. At higher temperatures, ~100 ^{o}C, the MP-ol dehydration step, having higher activation energy, becomes faster than the MIBK-to-MP-ol hydrogenation step. The latter becomes the rate-limiting step, which results in high MP selectivity. The last step in Scheme 1, i.e., 2-methylpentene hydrogenation, appears to be fast, which is supported by the absence of 2-methylpentenes in the products of MIBK hydrogenation. Alkene hydrogenation is known to be significantly exothermic and fast, especially on Pt catalysts ([19] and references therein). The heat of hydrogenation of 4-methyl-1-pentene has been reported to be -121 kJ mol^{-1} [19]. Therefore, hydrogenation of ketones to alkenes rather than to alkanes via metal-acid bifunctional pathway on a single catalyst bed is not feasible. This could be better achieved by a consecutive two-step process with ketone-to-alcohol hydrogenation on a metal catalyst as the first step followed by alcohol dehydration on an acid catalyst as the second step.

4.4 Hydrogenation of aliphatic ketones over Pt/CsPW

Table 4.4 shows the results for hydrogenation of C_3-C_9 aliphatic ketones over 0.5%Pt/CsPW. It can be seen that these ketones reacted very similarly to MIBK. At 60 ^oC, alcohols were the main products, except for the higher C_8-C_9 ketones 2-octanone and diisobutyl ketone, which gave mainly the corresponding alkanes. The latter indicates that the corresponding C_8-C_9 alcohols were easier to dehydrate over CsPW as compared to the alcohols related to the lower ketones. At 100 ^oC, all ketones gave the corresponding alkanes in high yields 87 – 100%. Therefore, 0.5%Pt/CsPW is a versatile bifunctional catalyst for the gas-phase hydrogenation of aliphatic ketones to alkanes.

Table 4.4 Hydrogenation of aliphatic ketones over 0.5%Pt/CsPW.[a]

Ketone	Temperature (°C)	Conversion (%)	Selectivity (mol%)		
			Alkane	Alcohol	Other[b]
Acetone	60	62	5	70	25
	100	98	87	9	4
2-Butanone	60	99	5	77	19
	100	100	99	0	1
3-Pentanone	60	94	21	76	3
	100	100	100	0	0
2-Hexanone	60	98	21	63	11
	100	100	99	0	1
MIBK	60	96	18	77	5
	100	100	100	0	0
Cyclohexanone	60	92	28	72	0
	100	99	99	0	1
2-Octanone[c]	60	41	68	27	5
	100	95	98	0	2
Diisobutyl ketone	60	40	93	4	3
	100	99	93	0	7

a) Reaction conditions: 0.2 g catalyst, 2.0% ketone in H_2 flow, 1 bar pressure, 20 mL min^{-1} flow rate, 3 h time on stream, catalyst pre-treatment at 100 °C/1 h in H_2 flow.

b) C_1-C_5 cracking products together with small amount of ketone condensation products.

c) 5 h time on stream.

4.5 Hydrogenation of acetophenone over Pt/CsPW

Acetophenone is an example of aromatic ketone, and its hydrogenation is more complicated than that of aliphatic ketones regarding the reaction selectivity and catalyst stability. The hydrogenation of acetophenone through bifunctional metal-acid-catalysed pathway can be represented by Scheme 4.3.

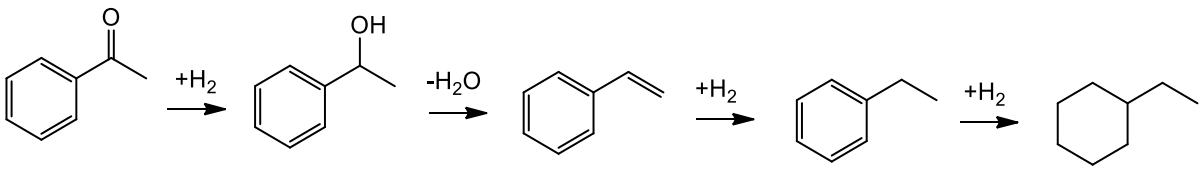

Scheme 4.3 Hydrogenation of acetophenone via bifunctional metal-acid catalysis.

Two bifunctional catalysts were tested at 100 ^{o}C: 0.5%Pt/CsPW and 1:19 w/w mixture of 7%Pt/C and CsPW. The results are shown in Table 6. Both catalysts gave ethylcyclohexane and ethylbenzene as the main products. It should be noted that no 1-phenylethanol and styrene was observed amongst the products, which can be explained by their high reactivity. Thus, 1-phenylethanol is known to be dehydrated much easier than aliphatic secondary alcohols [20]. Initially, 0.5%Pt/CsPW gave 98% selectivity to ethylcyclohexane at 74% acetophenone conversion (73% yield). However, this catalyst suffered from deactivation, resulting in significant loss in conversion and ethylcyclohexane selectivity over time on stream. After 6 h, the conversion dropped to 59%, and ethylcyclohexane selectivity to 19% in favour of ethylbenzene (81%). In contrast, the 7%Pt/C + CsPW mixed catalyst showed very little deactivation with time, yielding 74-77% of ethylcyclohexane and only 3-5% of ethylbenzene over 5 h on stream (Table 4.5). The poor stability of 0.5%Pt/CsPW to deactivation may be due

to blocking Pt sites by adsorption of acetophenone and/or ethylbenzene on the neighbouring strong proton sites of CsPW.

Table 4.5 Hydrogenation of acetophenone.[a]

Catalyst	TOS[b] (h)	Conversion (%)	Selectivity (mol%)	
			Ethylcyclohexane	Ethylbenzene
0.5%Pt/CsPW	3	74	98	2
0.5%Pt/CsPW	5	67	61	39
0.5%Pt/CsPW	6	59	19	81
7%Pt/C+CsPW[c]	3	80	96	4
7%Pt/C+CsPW[c]	5	79	94	6

a) Reaction conditions: 100 ^{o}C, 0.2 g catalyst, 0.5% acetophenone in H_2 flow, 1 bar pressure, 20 mL min^{-1} flow rate, 3 h time on stream, catalyst pre-treatment at 100 ^{o}C/1 h in H_2 flow.

b) Time on stream.

c) Physical mixture of 0.02 g 7%Pt/C + CsPW (0.35% Pt content).

4.6 Conclusions

In this work, we have investigated the gas-phase hydrogenation of a wide range of ketones to alkanes, including hydrogenation of aliphatic ketones and acetophenone, using bifunctional metal-acid catalysis. The bifunctional catalysts comprise Pt, Ru, Ni and Cu metals supported on acidic caesium salt of tungstophosphoric heteropoly acid $Cs_{2.5}H_{0.5}PW_{12}O_{40}$ (CsPW). The reaction occurs via a sequence of steps involving hydrogenation of ketone to alcohol on metal sites followed by dehydration of alcohol to alkene on acid sites and finally hydrogenation of alkene to alkane on metal sites. Catalyst activity has been shown to decrease in the order: Pt > Ru >> Ni > Cu. 0.5%Pt/CsPW has been demonstrated to be versatile catalyst for the hydrogenation of aliphatic ketones, giving almost 100% alkane yield at 100 ^{o}C and 1 bar pressure. Evidence has

been provided that the reaction with Pt/CsPW at 100 ^{o}C is limited by ketone-to-alcohol hydrogenation, whereas at lower temperatures ($\leq$ 60 ^{o}C) by alcohol dehydration resulting in alcohol formation as the main product. The catalyst comprising of a physical mixture of 7%Pt/C + CsPW has been found to be highly efficient as well, which indicates that the reaction is not limited by migration of intermediates between metal and acid sites in the bifunctional catalyst. The mixed 7%Pt/C + CsPW catalyst shows better performance stability in acetophenone hydrogenation compared to the impregnated Pt/CsPW catalyst, which suffers from deactivation.

4.7 References

1. A. Corma, S. Iborra, A. Velty, Chem. Rev. 107 (2007) 2411.
2. E. L. Kunkes, D. A. Simonetti, R. M. West, J. C. Serrano-Ruiz, C. A. Gaertner, J. A. Dumesic, Science 322 (2008) 417.
3. Y. Nakagawa, S. Liu, M. Tamura, K. Tomishige, ChemSusChem 8 (2015) 1114.
4. S. Lestari, P. Maki-Arvela, J. Beltramini, G. Q. Max Lu, D. Y. Murzin, ChemSusChem 2 (2009) 1109.
5. M. Snare, I. Kubickova, P. Maki-Arvela, K. Eranen, D. Yu. Murzin, Ind. Eng. Chem. Res. 45 (2006) 5708.
6. H. Bernas, K. Eranen, I. Simakova, A.-R. Leino, K. Kordas, J. Myllyoja, P. Maki-Arvela, T. Salmi, D. Yu. Murzin, Fuel 89 (2010) 2033.
7. J. G. Immer, M. J. Kelly, H. H. Lamb, Appl. Catal. A 375 (2010) 134.
8. P. T. Do, M. Chiappero, L. L. Lobban, D. Resasco, Catal. Lett. 130 (2009) 9.
9. M. Arend, T. Nonnen, W. F. Hoelderich, J. Fischer, J. Groos, Appl. Catal. A, 399 (2011) 198.
10. R. A. Augustine, Heterogeneous Catalysis for the Synthetic Chemist, Marcel Dekker, Inc., N. Y., 1996.
11. M. A. Alotaibi, E. F. Kozhevnikova, I. V. Kozhevnikov, J. Catal. 293 (2012) 141.
12. M. A. Alotaibi, E. F. Kozhevnikova, I. V. Kozhevnikov, Chem. Commun. 48 (2012) 7194.
13. S. Itagaki, N. Matsuhashi, K. Taniguchi, K. Yamaguchi, N. Mizuno, Chem. Lett. 43 (2014) 1086.
14. M. A. Alotaibi, E. F. Kozhevnikova, I. V. Kozhevnikov, Appl. Catal. A 447–448 (2012) 32.
15. P. B. Weisz, Adv. Catal. 13 (1962) 137.
16. P. B. Weisz, C. D. Prater, Adv. Catal. 6 (1954) 143.
17. K. Alharbi, E. F. Kozhevnikova, I. V. Kozhevnikov, Appl. Catal. A 504 (2015) 457.
18. G. C. Bond, S. J. Frodsham, P. Jubb, E. F. Kozhevnikova, I. V. Kozhevnikov, J. Catal. 293 (2012) 158.
19. G. C. Bond, Metal-Catalysed Reactions of Hydrocarbons, Springer, N. Y., 2005, Chapter 7.
20. C. K. Ingold, Structure and Mechanism in Organic Chemistry, 2nd ed., Bell, London, 1969.

5. Hydrodeoxygenation of 3-pentanone over bifunctional Pt-heteropoly acid catalyst in the gas phase: enhancing effect of gold

5.1 Introduction

As shown in Chapter 4 and reported in other studies [1-5], platinum on acidic supports, especially, Pt on heteropoly acids (HPA), is a highly active bifunctional metal-acid catalyst for hydrodeoxygenation (HDO) of a wide range of oxygenates in the gas and liquid phases under mild conditions. On the other hand, bimetallic PdAu and PtAu catalysts have attracted much attention because of their enhanced performance in comparison to monometallic Pd and Pt catalysts [6-17] (and references therein). Bimetallic enhancement of catalyst performance has been attributed to Au alloying through geometric (ensemble) and electronic (ligand) effects of the constituent elements [16, 17]. The ensemble effect, often considered to be more important one [17], can cause structural modifications in the surface metal atom geometry to generate specific isolated surface sites that are highly active for certain reactions. The ligand effect can alter the strength of metal-adsorbate bonds as a result of electronic perturbations of platinum group metal due to heteronuclear metal-metal bond formation, which can also lead to increased catalyst activity in certain reactions. Bimetallic PdAu catalysts have been extensively investigated and employed for many important applications, including, among others, the industrial vinyl acetate synthesis [11, 12], low-temperature CO oxidation [13, 14], and direct H_2O_2 synthesis from H_2 and O_2 [7]. PtAu bimetallics have been widely used for electrocatalysis in fuel cells [15], but scarcely documented for environment-friendly synthetic applications.

The challenge addressed in this chapter is to study the enhancing effect of Au on the gas-phase HDO of a ketone, 3-pentanone, over bifunctional metal-acid catalysts comprising Pt as the metal component and a caesium acidic salt of tungstophosphoric HPA, $Cs_{2.5}H_{0.5}PW_{12}O_{40}$ (CsPW), as the acid component. This catalyst has been shown to be highly efficient in a wide range of HDO reactions [1-5]; it has the highest activity in the HDO of anisole [3] and aliphatic ketones [2] (Chapter 4) for a gas-phase catalyst system reported so far. The HDO of ketones via bifunctional metal-acid catalysis occurs through a sequence of steps involving hydrogenation of ketone to secondary alcohol on metal sites followed by dehydration of the alcohol to alkene on acid sites and finally hydrogenation of the alkene to alkane on metal sites (Scheme 5.1) [1-3]. The bifunctional metal-acid catalysed pathway has been demonstrated to be much more efficient compared to the monofunctional metal-catalysed ketone-to-alkane hydrogenation [1, 2] (Chapter 4). It is now demonstrated that modification of the Pt/CsPW catalyst with gold increases the turnover rate of ketone hydrogenation at Pt surface sites and decreases the rate of catalyst deactivation. These effects, however, are dependent on the catalyst formulation and preparation technique. It is suggested that the catalyst enhancement is caused by PtAu alloying. STEM-EDX and XRD analysis of the PtAu/CsPW catalysts indicates the presence of bimetallic PtAu nanoparticles with a wide range of Pt/Au atomic ratios.

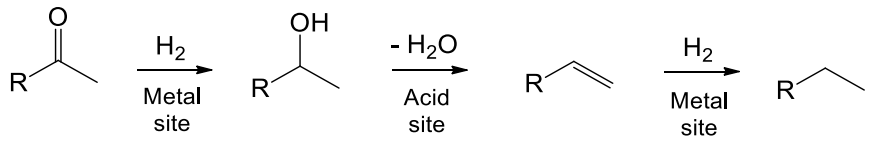

Scheme 5.1 Ketone hydrodeoxygenation via bifunctional metal-acid catalysis.

Hydrodeoxygenation of 3-pentanone was carried out in the gas phase in flowing H_2. The catalysts were tested under atmospheric pressure in a Pyrex fixed-bed down-flow microreactor (9 mm internal diameter) fitted with an on-line gas chromatograph (Varian Star 3400 CX instrument

with a 30 m x 0.25 mm HP INNOWAX capillary column and a flame ionization detector) described in Chapter 2. Reaction rates (R) were determined as $R = XF/W$ (in mol $g_{cat}^{-1}h^{-1}$), where X is the conversion of 3-pentanone. Turnover frequencies (TOF) were calculated from the reaction rates using Pt dispersion obtained from hydrogen chemisorption.

5.2 Effect of gold on HDO of 3-pentanone

As demonstrated in Chapter 4, the HDO of aliphatic ketones, including 3-pentanone, over 0.5%Pt/CsPW readily occurs via bifunctional metal-acid catalysed pathway (Scheme 5.1) with up to 100% alkane yield in a fixed-bed microreactor under mild conditions (60-100 ^{o}C, 1 bar H_2 pressure). Supported Pt/CsPW and physically mixed Pt/C + CsPW catalysts with the same Pt loading exhibit comparable activities in the HDO of aliphatic ketones. The alkane/alcohol product ratio increases with reaction temperature as the result of rate-limiting step change in the HDO process (Scheme 5.1). 3-Pentanone HDO over 0.5%Pt/CsPW occurs with 80% selectivity to 3-pentanol at 60 ^{o}C and 100% selectivity to pentane at 100 ^{o}C (Chapter 4).

In this chapter, we examined the effect of Au additives on activity and performance stability of physically mixed and supported bifunctional catalysts comprising Pt and CsPW with different relative amounts of metal and acid components in the HDO of 3-pentanone under kinetically controlled conditions (<100% ketone conversion) in the temperature range of 40 – 80 ^{o}C and W/F = 400 g h mol^{-1}. The catalyst preparation procedure is explained in detail in Chapter 2, but briefly summarized here for clarity. The bimetallic PtAu/CsPW catalysts were prepared by two different methods, co-impregnation and sequential impregnation of CsPW with H_2PtCl_6 and $HAuCl_4$ and designated as PtAu/CsPW-CI and PtAu/CsPW-SI respectively. Gold, indeed, was found to have profound effect on the performance of Pt – CsPW catalysts, subject to catalyst formulation and preparation method.

Addition of Au to Pt/C (Pt/Au = 1:1 and 1:2 atomic ratio) in mixed catalysts Pt/C + CsPW (1:9 w/w, 0.5% Pt loading), did not improve catalyst activity. On the contrary, a decrease in 3-pentanone conversion was observed regardless of catalyst preparation method, i.e., co-impregnation or sequential impregnation. Thus, the unmodified 5%Pt/C + CsPW (1:9 w/w) catalyst gave 70% 3-pentanone conversion with 91% 3-pentanol selectivity at 40 ^{o}C, whereas the Au-modified 5%Pt/5%Au/C + CsPW catalyst with the same Pt loading gave 66% and 82%, respectively (Table 5.1). Both catalysts showed stable conversion for 4 h on stream. In the absence of Pt, gold-only catalyst 5%Au/C + CsPW (1:9 w/w) had a negligible activity with only 2% ketone conversion (Table 5.1). Likewise, CsPW alone was totally inert in this reaction at 40-80 ^{o}C (Chapter 4).

Table 5.1 3-Pentanone HDO over mixed PtAu/C + CsPW (1:9 w/w) bifunctional catalysts[a]

Catalyst[b]	Conversion	Selectivity (mol%)		
	(%)	Pentane[c]	3-Pentanol	Other[d]
5%Pt/C	70	8	91	1
5%Au/C	2			
5%Pt/5%Au/C-SI[e]	66	17	82	1
5%Pt/10%Au/C-SI[e]	32	20	77	3
5%Pt/5%Au/C-SI[f]	29	30	67	3
5%Pt/10%Au/C-SI[f]	25	40	58	2
5%Pt/5%Au/C-CI[g]	19	46	51	3
5%Pt/10%Au/C-CI[g]	40	15	83	2

a) Reaction conditions: 0.2 g catalyst weight, 40 ^{o}C, 1.0% concentration of 3-pentanone in H_2 flow, 20 ml min^{-1} flow rate, catalyst pre-treatment at 40 ^{o}C in H_2 for 1 h, 4 h time on stream.

b) Pt/C, Au/C, and PtAu/C physically mixed with CsPW 1:9 w/w (0.5% Pt loading).

c) Also included cis- and trans-2-pentene at a 5 – 8 pentane/pentene molar ratio.

d) Mainly C_1-C_4 hydrocarbon cracking products.

e) Catalyst prepared by sequential impregnation by wet-impregnating the pre-made 5%Pt/C with the required amount of $HAuCl_4$ followed by reduction with H_2 at 250 ^{o}C/2 h.

f) Catalysts prepared by sequential impregnation by wet-impregnating the pre-made 5%Au/C and 10% Au/C with H_2PtCl_6.

g) Catalysts prepared by co-impregnation of the Darco KB-B carbon with H_2PtCl_6 and $HAuCl_4$ followed by reduction with H_2 at 250 ^{o}C/2 h.

Next, we looked at a different formulation of the PtAu – CsPW catalysts, with Pt and Au directly supported on the acidic support CsPW. In these catalysts, Pt and Au sites were in close proximity to strong proton sites in CsPW also interacting with the ionic surface of CsPW polyoxometalate, which had profound effect on catalyst performance, i.e., catalyst activity and its resistance to deactivation.

Figure 5.1 shows 3-pentanone HDO over unmodified supported catalyst 0.32%Pt/CsPW as well as the corresponding Au-modified catalysts 0.32%Pt/0.36%Au/CsPW-SI and 0.28%Pt/0.35%Au/CsPW-CI prepared by sequential impregnation and co-impregnation of Pt and Au, respectively. The results clearly demonstrate enhancement of catalyst performance by Au additives. First, the co-impregnated catalyst PtAu/CsPW-CI, despite its slightly lower Pt loading, gives a higher ketone conversion as compared to the unmodified Pt/CsPW, while the PtAu/CsPW-SI and Pt/CsPW are almost neck and neck. Second, all three catalysts exhibit deactivation on stream; nevertheless, both Au-modified catalysts deactivate slower than the unmodified Pt/CsPW. It is conceivable that catalyst deactivation is caused by coking originated from oligomerization of alkene intermediates (Scheme 5.1) on the strong proton sites of CsPW. This is supported by propene oligomerization and coking over supported $H_3PW_{12}O_{40}$ [18, 19]. Faster deactivation rate of the supported catalysts in comparison with the mixed ones (PtAu/C + CsPW) can be explained by the close proximity between the Pt and H^+ active sites in the supported catalysts. Also deactivation of the supported catalysts may be increased due to their lower Pt loading and higher Pt dispersion (Chapter 3, Table 3.4).

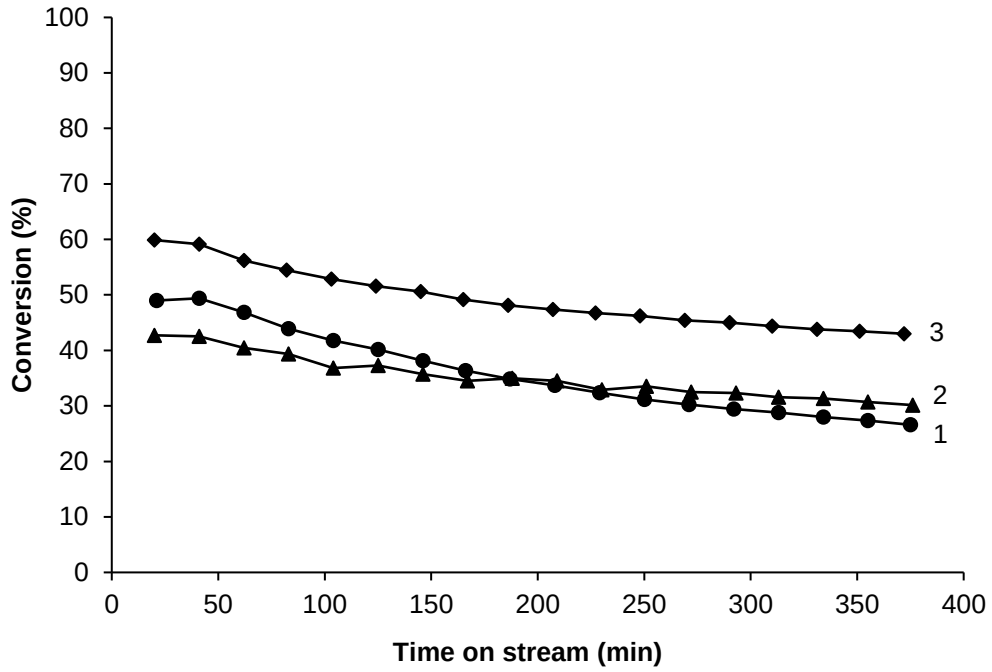

Figure 5.1 3-Pentanone HDO over (1) 0.32%Pt/CsPW, (2) 0.32%Pt/0.36%Au/CsPW-SI and (3) 0.28%Pt/0.35%Au/CsPW-CI (0.20 g catalyst weight, 40 ^{o}C, ambient pressure, 1.0% concentration of 3-pentanone in H_2 flow, 20 mL min^{-1} flow rate, catalyst pre-treatment at 40 ^{o}C/1 h in H_2 flow).

Table 5.2 presents product selectivity for the supported catalysts, which provides an important insight into the mechanism of Au enhancement. The products contained n-pentane, n-pentenes (1-pentene, cis- and trans-2-pentene), and 3-pentanol; no products of skeletal isomerization was observed, which can be explained by low reaction temperature. It should be noted that skeletal isomerization of n-hexane over Pt/HPA/SiO_2 catalysts has been reported at 200 ^{o}C [20, 21]. All three CsPW-supported catalysts, unmodified and Au-modified, had the same 3-pentanol selectivity of 11%. However, pentane/pentene selectivities differed significantly. The Pt/CsPW and PtAu/CsPW-SI, that showed similar performance (Figure 5.1), had rather similar selectivities to pentane (56-62%) and pentenes (27-33%). In contrast, the more active co-impregnated catalyst PtAu/CsPW-CI gave significantly more pentenes (52%) at the expense of pentane (37%). This indicates that the Au enhancement of catalyst activity observed for the PtAu/CsPW-CI is largely

due to the increased C=O hydrogenation activity, whereas hydrogenation of the alkene C=C double bond appears to be impeded by the Au additives. It is worth noting that the preference of Au catalysts to hydrogenation of the C=O bond over C=C bond has been documented previously, for example, for selective hydrogenation of unsaturated aldehydes to unsaturated alcohols [22, 23], despite the opposite thermodynamic preference [22]. Conversely, Pt alone will preferably hydrogenate the C=C bond [22].

Table 5.2 HDO of 3-pentanone over Pt/CsPW and PtAu/CsPW.[a]

Catalyst	Conv.[b]	Selectivity (%)				
	(%)	pentane	1-C_5H_{10}	trans-2-C_5H_{10}	cis-2-C_5H_{10}	3-pentanol
0.32%Pt/CsPW	36	56	<1	15	18	11
0.32%Pt/0.36%Au/CsPW-SI[c]	35	62	<1	13	14	11
0.28%Pt/0.35%Au/CsPW-CI[d]	49	37	<1	23	29	11

a) Reaction conditions: 0.20 g catalyst weight, 40 ^oC, ambient pressure, 1.0 % concentration of 3-pentanone in H_2 flow, 20 mL min^{-1} flow rate, catalyst pre-treatment at 80 ^oC/1 h in H_2 flow, 6 h time on stream.
b) Average 3-pentanone conversion over 6 h time on stream.
c) Catalyst prepared by sequential impregnation of H_2PtCl_6 then $HAuCl_4$, with Pt(IV) reduced to Pt(0) with H_2 at 250 ^oC/2 h prior to $HAuCl_4$ impregnation, then the Pt^oAu^{III}/CsPW was reduced with H_2 at 250 ^oC/2 h.
d) Catalysts prepared by co-impregnation of H_2PtCl_6 and $HAuCl_4$ followed by reduction with H_2 at 250 ^oC/2 h.

Much more profound effect of Au on catalyst stability was observed in the HDO reaction at 80 ^oC, i.e., under stronger deactivating conditions (Figure 5.2). Initially, all three CsPW-supported catalysts exhibited almost 100% 3-pentanone conversion with 100% pentane selectivity. In 6.5 h on stream, the unmodified Pt/CsPW lost 70% of its initial activity and its pentane selectivity reduced to 95% in favor of 3-pentanol formation. The Au-modified PtAu/CsPW-SI prepared by sequential impregnation lost half of its activity (49% conversion and 98% pentane selectivity at

7 h time on stream). The best performance stability was displayed by the co-impregnated catalyst PtAu/CsPW-CI, which showed 88% conversion and 100% pentane selectivity after 7 h on stream. Combustion analysis of spent catalysts indicated that catalyst deactivation rate was in line with the amount of coke formed, which decreased in the order (C content, %): 2.6 (Pt/CsPW) > 2.5 (PtAu/CsPW-SI) > 2.2 (PtAu/CsPW-CI).

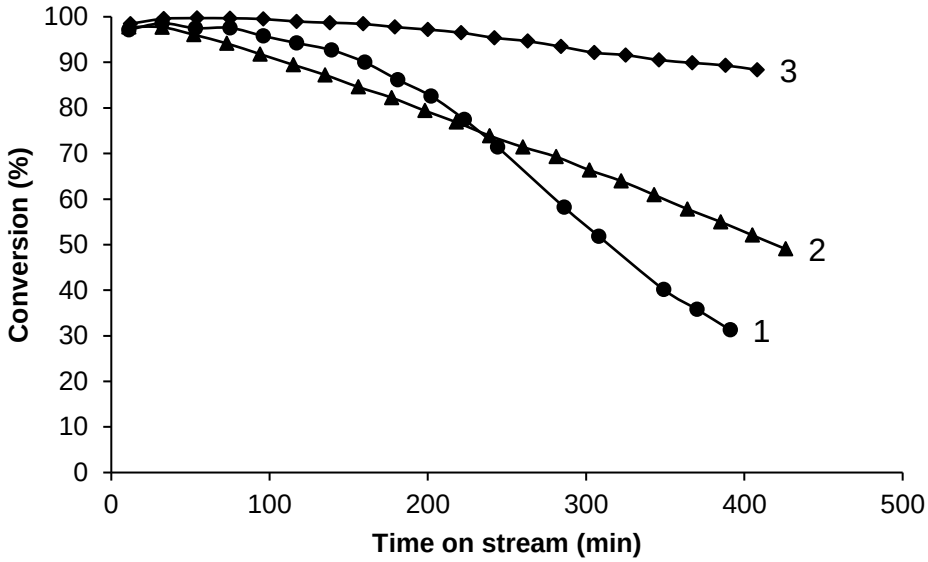

Figure 5.2 3-Pentanone HDO over (1) 0.32%Pt/CsPW, (2) 0.32%Pt/0.36%Au/CsPW-SI and (3) 0.28%Pt/0.35%Au/CsPW-CI (0.20 g catalyst weight, 80 ^{o}C, ambient pressure, 1.0% concentration of 3-pentanone in H_2 flow, 20 mL min^{-1} flow rate, catalyst pre-treatment at 80 ^{o}C/1 h in H_2 flow).

Metal dispersion obtained from hydrogen adsorption showed that Pt dispersion in PtAu/CsPW-CI catalyst was found to be higher in comparison with PtAu/CsPW-SI catalyst (Chapter 3, Table 3.4). This may be the reason for less efficient performance of the catalysts prepared by sequential impregnation compared with the catalyst prepared by co-impregnation of metal precursors.

Further, the effect of Au was tested in a series of bifunctional metal-acid catalysts with various relative amounts of metal (Pt) and acid (CsPW) components to compare unmodified Pt/CsPW catalysts with Au-modified co-impregnated PtAu/CsPW-CI catalysts that showed greater enhancement of catalyst performance.

Figure 5.3 shows the HDO of 3-pentanone at 40 ^{o}C over catalysts with reduced acid function. These catalysts comprised 5.4%Pt/CsPW and 5.3%Pt/3.3%Au/CsPW-CI diluted 1:7 w/w by SiO_2 (0.7% Pt loading). These reactions predictably yielded 3-pentanol as the main product (95-97% selectivity, Figure 5.4) due to slowing down the alcohol dehydration step (Scheme 5.1). The unmodified Pt/CsPW catalyst gave 58% average ketone conversion over 4 h on stream, with a slight catalyst deactivation. The Au-modified catalyst, PtAu/CsPW-CI, again demonstrated significant enhancement of catalyst activity to exhibit a stable 95% ketone conversion.

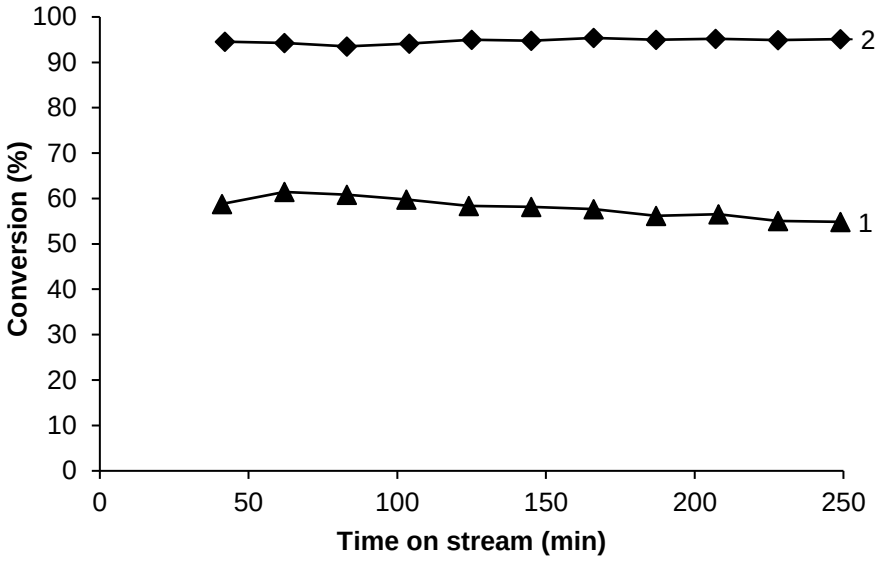

Figure 5.3 3-Pentanone HDO over (1) 5.4%Pt/CsPW and (2) 5.3%Pt/3.3%Au/CsPW-CI diluted 1:7 w/w by SiO_2 to 0.7% Pt loading (0.20 g catalyst weight, 40 ^{o}C, ambient pressure, 1.0% 3-pentanone concentration in H_2 flow, 20 mL min^{-1} flow rate, catalyst pre-treatment at 40 ^{o}C/1 h in H_2 flow).

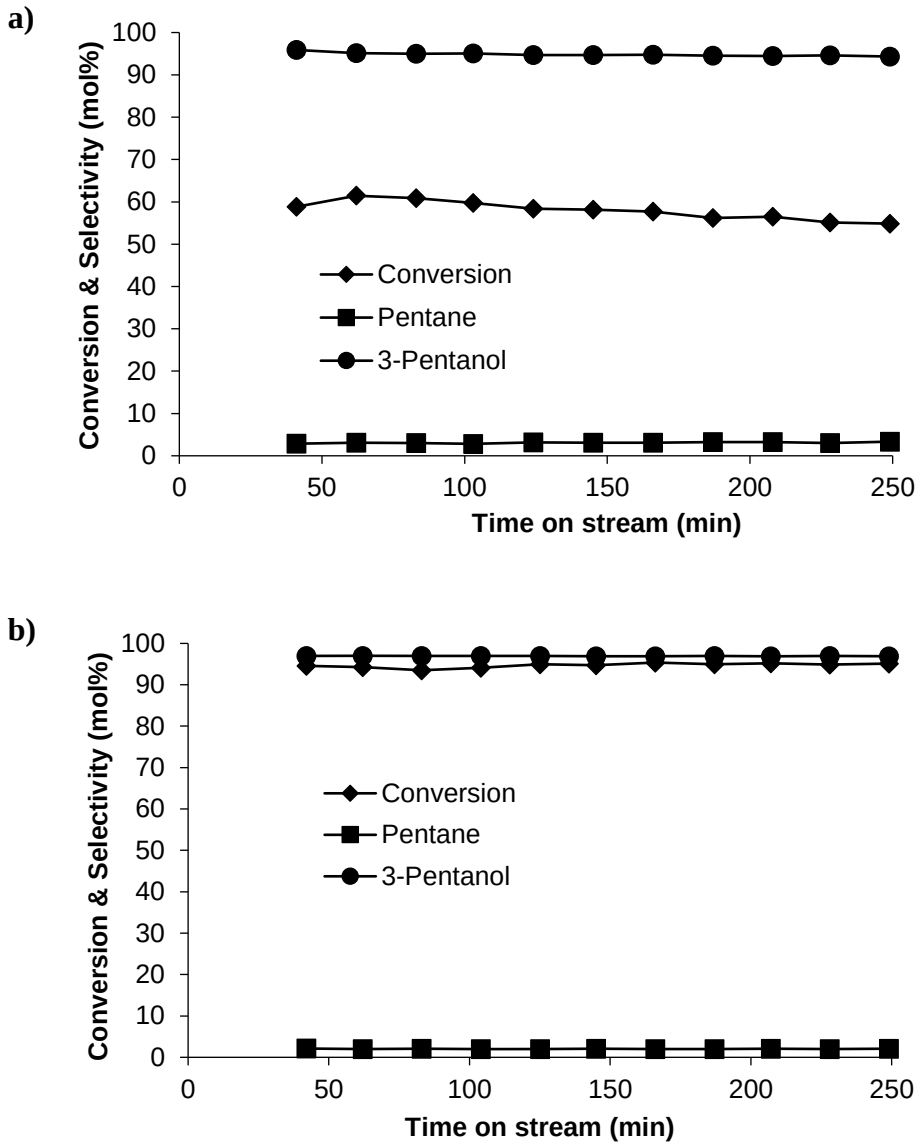

Figure 5.4 3-Pentanone hydrogenation over (**a**) 5.4%Pt/CsPW and (**b**) 5.3%Pt/3.3%Au/CsPW-CI diluted 1:7 w/w by SiO_2 (0.20 g catalyst weight, 40 ºC, ambient pressure, 1.0% concentration of 3-pentanone in H_2 flow, 20 mL min^{-1} flow rate, catalyst pre-treatment at 40 ºC/1 h in H_2 flow).

Selectivity (**a**): 3-pentanol, 95%; n-pentane, 3%; other (not shown), 2%; average conversion, 58%; (**b**): 3-pentanol, 97%; n-pentane, 2%; other (not shown), 1%; average conversion, 95%. In both cases, cis- and trans-2-pentene, <0.3%.

The reaction with similar catalysts, but with increased acid function, is shown in Figure 5.5. In this case, 5.8%Pt/CsPW and 5.6%Pt/4.3%Au/CsPW-CI catalysts were diluted 1:19 w/w with

CsPW (0.3% Pt loading). As a result, reaction selectivity changed dramatically to yield mainly C_5 hydrocarbons, i.e., pentane and pentenes (91% selectivity, C_5H_{12}/C_5H_{10} = 16 mol/mol for Pt/CsPW and 86%, C_5H_{12}/C_5H_{10} = 6.6 for PtAu/CsPW-CI). The increased catalyst acidity led to an increase in catalyst deactivation rate (cf. Figure 5.3), and again the Au enhancement of catalyst stability is clearly visible. Along with reducing the rate of catalyst deactivation, addition of Au increased the average ketone conversion from 21% for Pt/CsPW to 45% for PtAu/CsPW-CI over 6 h time on stream (Figure 5.5). Again, from the pentane/pentene product ratio, the preference of PtAu catalyst for the C=O over C=C hydrogenation can be clearly seen, as compared to the unmodified Pt catalyst (C_5H_{12}/C_5H_{10} = 16 and 6.6 mol/mol for Pt/CsPW and PtAu/CsPW-CI, respectively). It should be noted that the Au-only catalyst, 2.6%Au/CsPW + CsPW (1:19 w/w), showed only negligible activity (~1% ketone conversion).

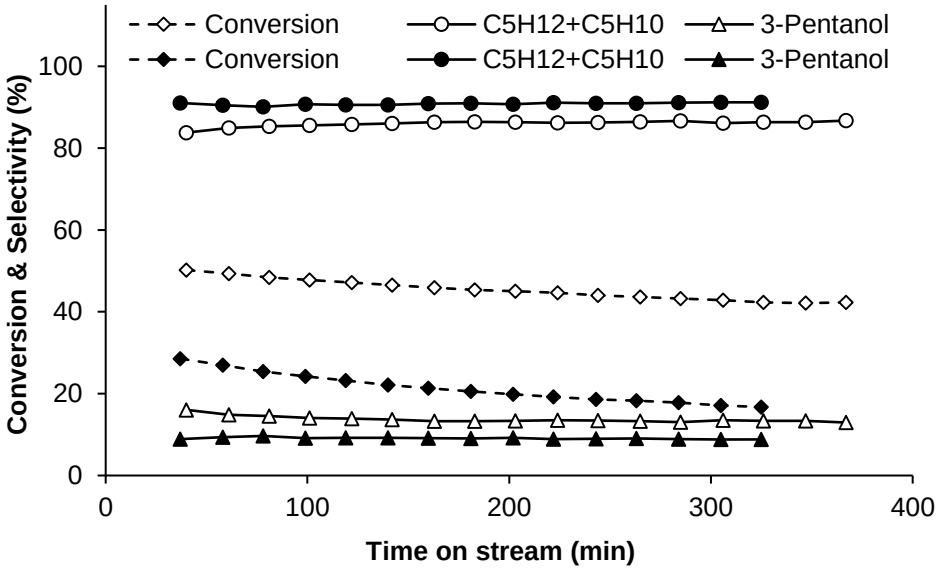

Figure 5.5 3-Pentanone HDO over 5.8%Pt/CsPW (solid markers) and 5.6%Pt/4.3%Au/CsPW-CI (open markers) diluted 1:19 w/w by CsPW to 0.3% Pt loading (0.20 g catalyst weight, 40 ^oC, ambient pressure, 1.0% concentration of 3-pentanone in H_2 flow, 20 mL min^{-1} flow rate, catalyst pre-treatment at 40 ^oC/1 h in H_2 flow).

Finally, the effect of Au was examined under very strong deactivating conditions at 80 ^{o}C using bifunctional catalysts with greatly increased acid function over metal function. In this case, 5.8%Pt/CsPW and 5.6%Pt/4.3%Au/CsPW-CI were diluted by CsPW 1:79 w/w to 0.07% Pt loading. The results are shown in Figure 5.6. Initially, in this system pentane was the only product (~100% selectivity). In the course of reaction, the unmodified Pt/CsPW was severely deactivated losing practically all its activity in 6 h on stream. Its selectivity was also changed to form 3-pentanol at the expense of pentane. The Au-modified catalyst was also deactivating, but at a much slower rate, with its pentane selectivity only slightly changing from 100 to 94%. The amount of coke formed in the Au-modified catalyst (2.8%) was smaller than in the Pt/CsPW (3.1%), which is in agreement with the stability of these catalysts.

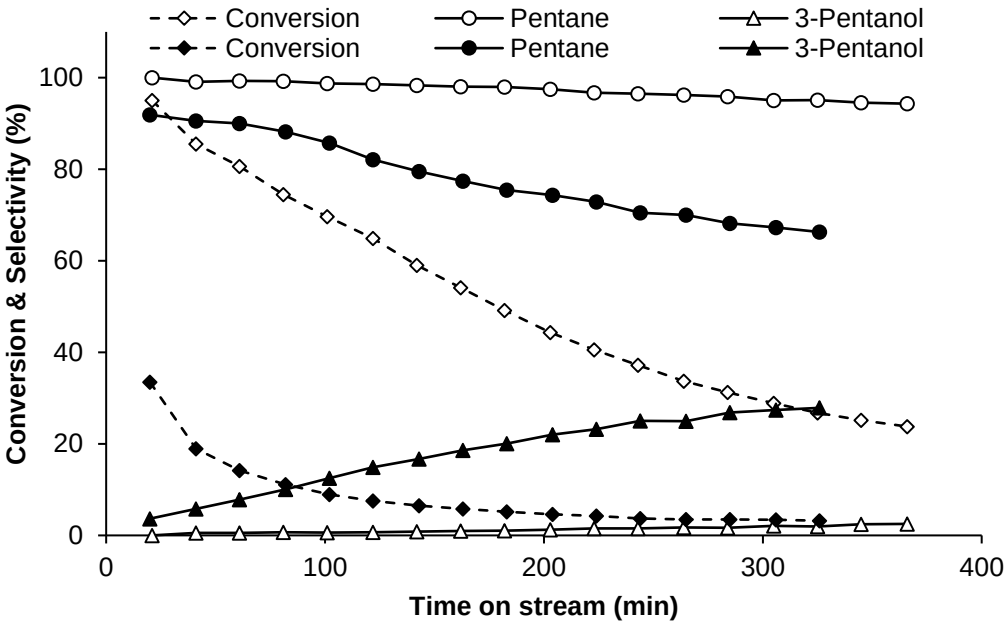

Figure 5.6 3-Pentanone HDO over 5.8%Pt/CsPW (solid markers) and 5.6%Pt/4.3%Au/CsPW-CI (open markers) diluted 1:79 w/w by CsPW to 0.07% Pt loading (0.20 g catalyst weight, 80 ^{o}C, ambient pressure, 1.0% concentration of 3-pentanone in H_2 flow, 20 mL min^{-1} flow rate, catalyst pre-treatment at 80 ^{o}C/1 h in H_2 flow).

Therefore, the modification of Pt/CsPW catalyst with gold increases its activity (ketone conversion) in the HDO of 3-pentanone and decreases the rate of catalyst deactivation, although the gold itself is inert in this reaction. The activity enhancement also indicates the preference of the PtAu/CsPW catalysts toward hydrogenation of C=O bond over C=C bond in comparison with the unmodified Pt/CsPW. The Au enhancement appears to be strongly dependent on catalyst formulation as well on the catalyst preparation method. Carbon-supported Pt and Au physically mixed with CsPW solid acid failed to show any enhancement, whereas the metals directly supported onto CsPW did display the enhancement effect. This indicates importance of close proximity between metal and proton active sites in the bifunctional metal-acid catalysts. This might also indicate a special role of the acidic CsPW polyoxometalate support, however there is no direct evidence for that as yet. PtAu catalysts prepared by co-impregnation of metal precursors showed stronger enhancement effect in comparison with the catalysts prepared by sequential impregnation. It is conceivable that Pt-Au alloying was the cause of the enhancement of catalyst performance as the result of the ensemble and ligand effects of Au on the Pt active sites [16, 17]. In this respect, the co-impregnation is expected to be more favorable for Pt-Au alloying than the successive impregnation.

5.3 Catalyst characterisation

This includes investigation of metal nanoparticles in Pt/CsPW and PtAu/CsPW catalysts by X-ray powder diffraction (XRD) and scanning transmission electron microscopy–energy dispersive X-ray spectroscopy (STEM-EDX). The STEM-EDX and XRD analysis of the PtAu/CsPW catalysts indicated the presence of PtAu bimetallic nanoparticles, which may be the cause of catalyst performance enhancement.

Supported bimetallic catalysts, while preferred for practical use, have a drawback, which is the lack of homogeneity of metal nanoparticles regarding their composition, size, and shape [17].

The method of preparation of the CsPW-supported PtAu catalysts chosen in this work involves formation of metal nanoparticles at a gas-solid interface upon reduction of a solid pre-catalyst with H_2 at 250 ^oC. This would favor formation of supported PtAu alloys of a random composition together with various Pt-alone and Au-alone nanoparticles, rather than specific core-shell bimetallics often formed in solution in the presence of a protective agent preventing aggregation [17].

5.3.1 X-ray diffraction

X-ray powder diffraction (XRD) has been widely used for the characterization of supported Au alloy catalysts [17]. XRD patterns for unmodified 5.8%Pt/CsPW and Au-modified 5.6%Pt/4.3%Au/CsPW-CI catalysts are shown in Figure 5.7a. These are dominated by the well-known bcc pattern of crystalline CsPW [24] and also clearly display the fcc pattern of Au (38.2^o [111] and 44.4^o [200]) and Pt (39.8^o [111] and 46.2^o [200]) metal nanoparticles. As expected, this indicates coexistence of Pt-alone and Au-alone particles and possibly PtAu bimetallic particles with diffraction pattern falling in between the corresponding diffractions of the pure metals [17]. The latter, however, is obscured by the intense pattern of CsPW in Figure 3.22a. Nevertheless, the normalized difference XRD (Figure 5.7b) shows a broad diffraction peak in the range of 38-40^o between the diffractions of pure Pt and Au, which could be attributed to PtAu alloys. It should be noted that Pt peaks appear broader than Au peaks (Figure 5.7a), which indicates higher dispersion of Pt particles. Accurate analysis of metal particle size is difficult due to the dominance of the CsPW pattern. Rough estimate from the [111] peaks using the Scherrer equation gave 60 and 30 nm volume-average particle size for Au and Pt, respectively, which may be biased toward larger metal particles.

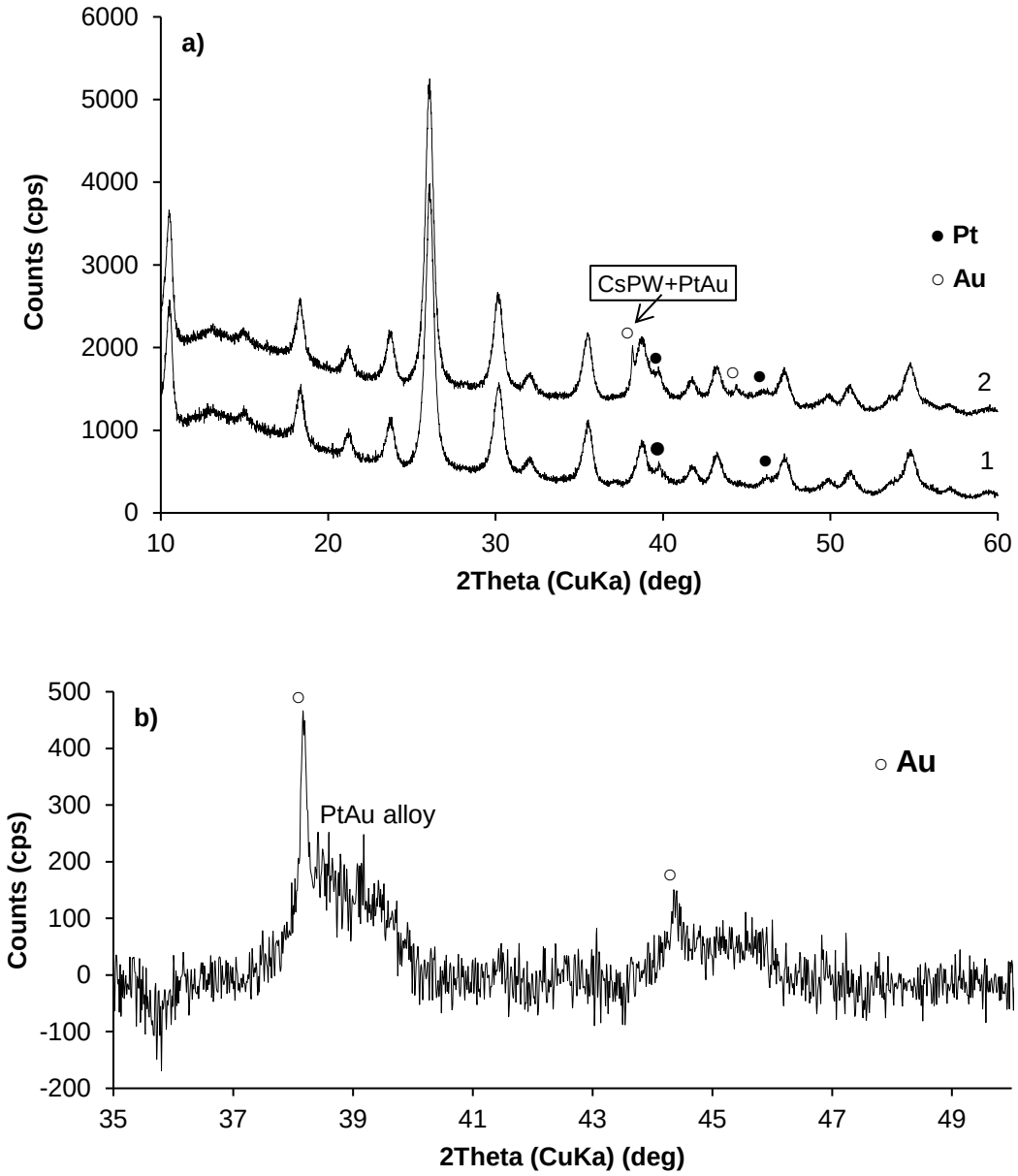

Figure 5.7 XRD: (a) 5.8%Pt/CsPW (1) and 5.6%Pt/4.3%Au/CsPW-CI (2); (b) close-up normalized difference (2)-(1) XRD spectrum revealing a broad [111] fcc PtAu alloy peak in the range 38-40^{o} and possibly a weaker [200] PtAu alloy peak in the range 44-46^{o}.

5.3.2 STEM-EDX

Scanning transmission electron microscopy (STEM) and energy dispersive X-ray spectroscopy (EDX) have been used extensively for the characterization of PdAu [7, 17, 25] and PtAu [15] nanoparticles. Figure 5.8 shows the high-angle annular dark field (HAADF) STEM images of

the three catalysts 5.8%Pt/CsPW, 2.6%Au/CsPW and 5.6%Pt/4.3%Au/CsPW-CI with metal nanoparticles indicated as bright spots on the darker background. As gold, platinum and tungsten all have similar atomic number *Z* (74, 78, and 79 for W, Pt, and Au, respectively), the strong background of CsPW containing 70 wt% of W in these catalysts makes it difficult to discern smaller Pt and Au particles from the *Z*-contrast HAADF images. Due to this, no accurate determination of the metal particle size distribution could be made. Figure 5.8a (sample 5.8%Pt/CsPW) shows platinum particles with a size of ≤ 12 nm. Figure 5.8b (sample 2.6%Au/CsPW) shows oval shaped gold particles sized up between 4 and 25 nm, with an average gold particle size estimated to be ≤ 10 nm. Particles of a similar size and shape can be seen in Figure 5.8c (sample 5.6%Pt/4.3%Au/CsPW-CI), which is suggestive of a PtAu alloying on the catalyst surface (see the EDX analysis below). It can be seen that individual nanoparticles in this catalyst exhibit well-defined low-index facets with a lattice spacing of 2.3±0.1 Å consistent with [111] interplanar distances in fcc Au or Pt (Figure 5.8d).

The EDX analysis of a large number of metal nanoparticles in the 5.6%Pt/4.3%Au/CsPW-CI catalyst showed that all these particles contained both platinum and gold in different Pt/Au atomic ratios varying from 0.5 to 7.7 (Figure 5.9 and Figure 5.10). This may indicate PtAu alloying in this catalyst. EDX elemental mapping showed that Pt and Au maps covered the same areas of PtAu/CsPW catalyst particles (Figure 5.11), indicating formation of a non-uniform PtAu particles, with local variations in Pt/Au atomic ratio.

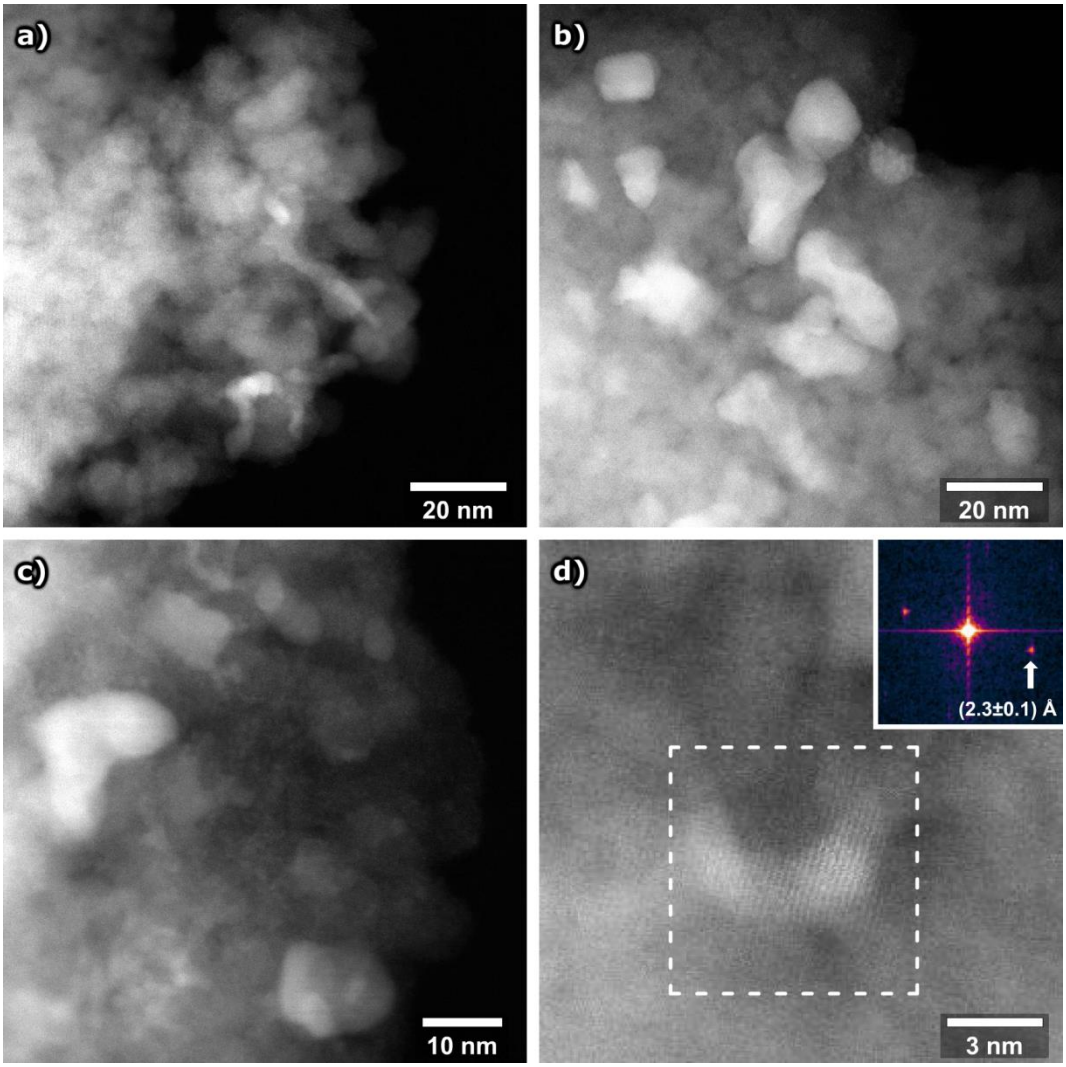

Figure 5.8 HAADF-STEM images of catalyst samples, showing metal nanoparticles as bright spots: (a) 5.8%Pt/CsPW, (b) 2.6%Au/CsPW, and (c) 5.6%Pt/4.3%Au/CsPW-CI; a high-resolution image (d) of sample 5.6%Pt/4.3%Au/CsPW-CI, with fast Fourier transform (FFT) of the marked area given in the inset, revealing the crystalline structure of the metal nanoparticle.

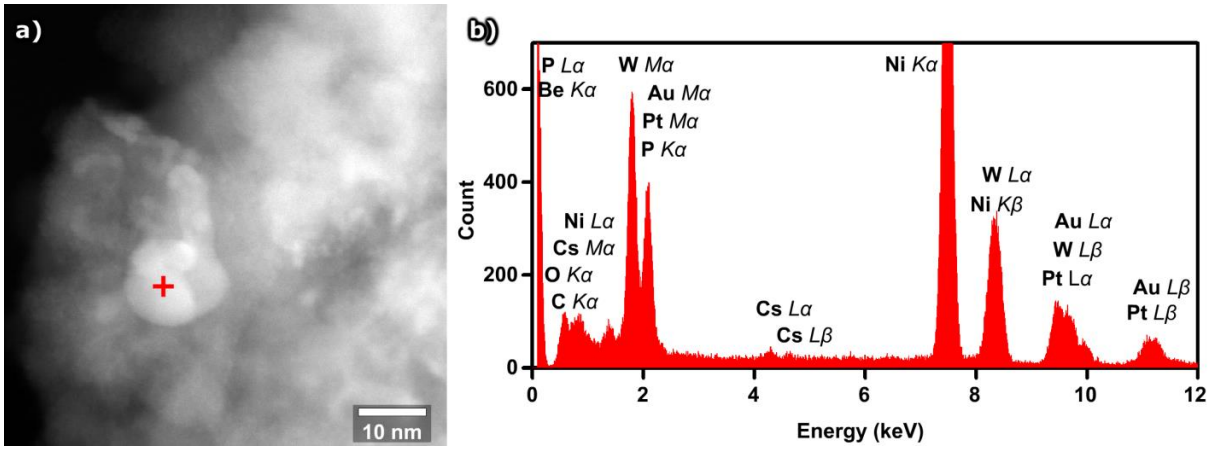

Figure 5.9 (a) HAADF-STEM image of 5.6%Pt/4.3%Au/CsPW-CI catalyst sample, with the cross on a 12 nm PtAu nanoparticle marking the spot where EDX analysis was performed; (b) the corresponding EDX spectrum, revealing the atomic ratio Pt/Au = 7.7, indicating that the probed alloy nanoparticle is Pt-rich.

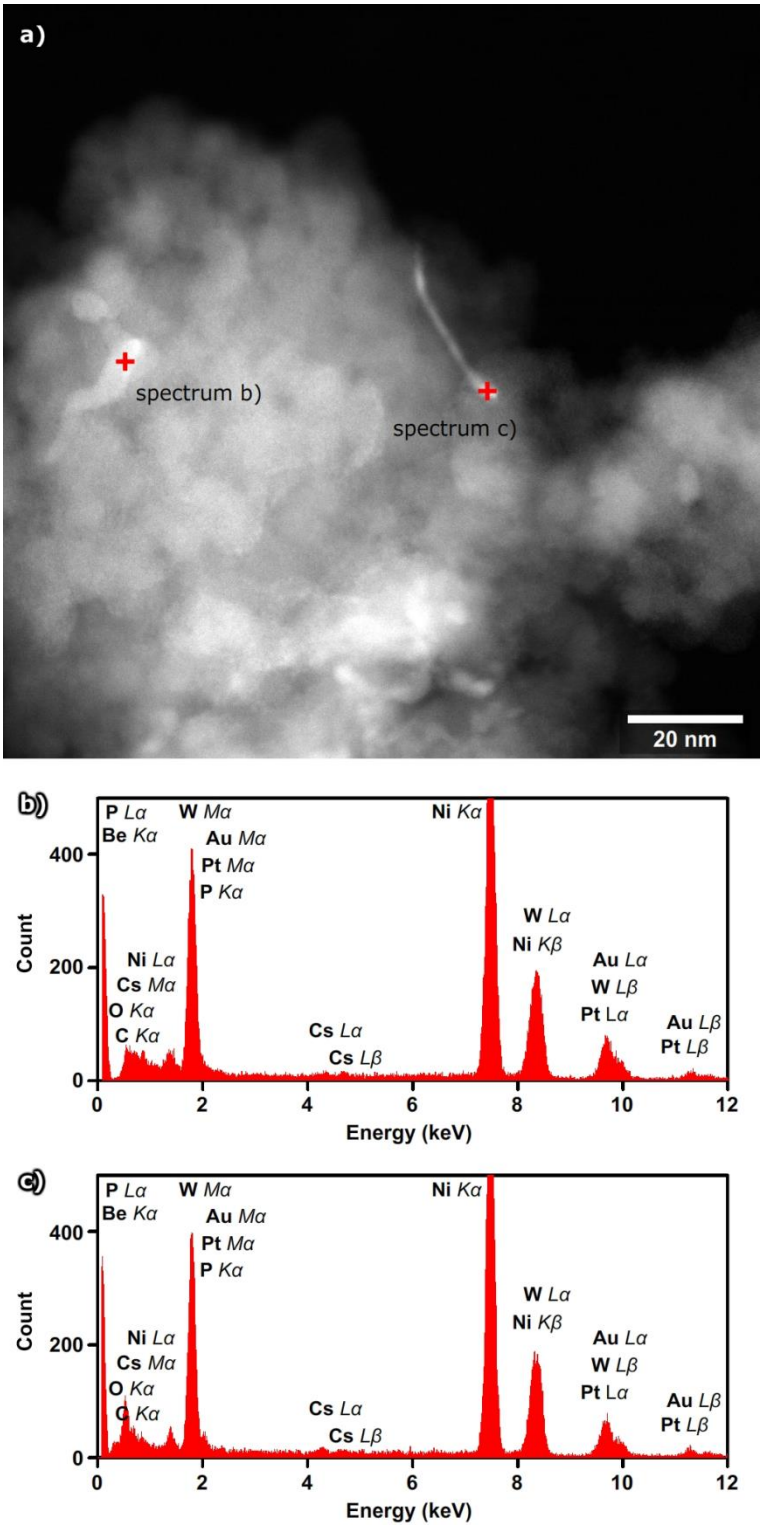

Figure 5.10 STEM-EDX analysis of 5.6%Pt/4.3%Au/CsPW-CI catalyst: (a) HAADF-STEM image showing two PtAu nanoparticles marked with crosses that were investigated by EDX; (b, c) the corresponding EDX spectra, revealing the atomic ratio Pt/Au ≈ 0.5 in both spots.

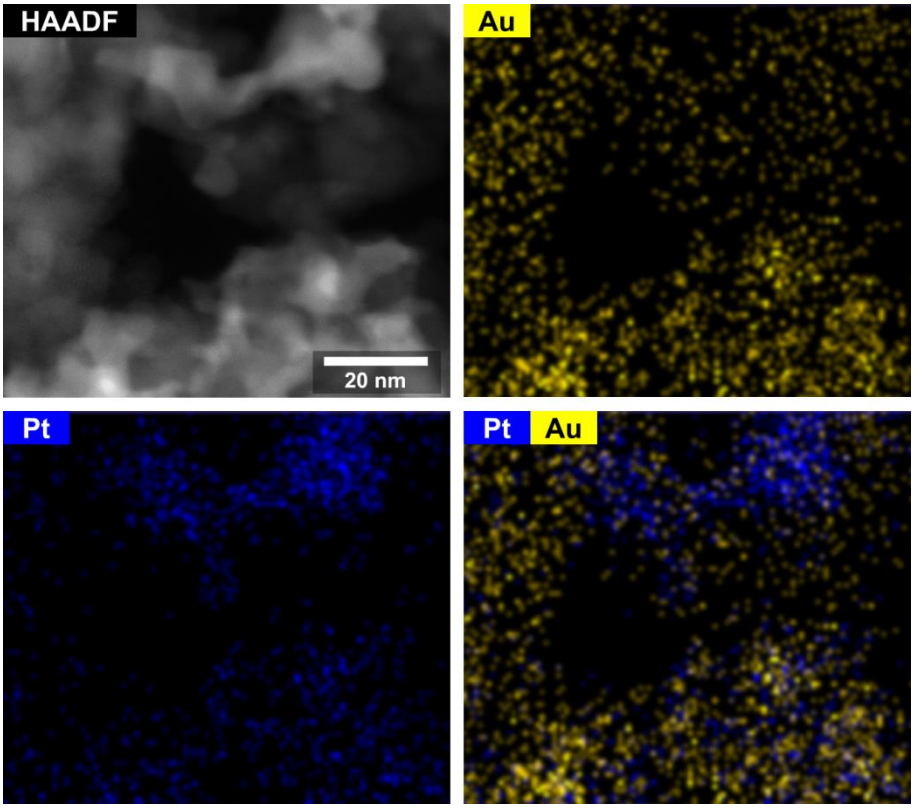

Figure 5.11 HAADF-STEM image of 5.6%Pt/4.3%Au/CsPW-CI catalyst and the corresponding STEM-EDX elemental maps showing the spatial distribution of Au (yellow) and Pt (blue) in the sample. Note the upper part seem to be relatively Pt rich, whereas the bottom part is Au rich, indicating non-uniform alloying.

5.4 Turnover rates

The turnover frequencies (TOF) of 3-pentanone conversion over Pt and PtAu catalysts were calculated from the reaction rate using the Pt dispersion obtained from hydrogen chemisorption (Chapter 3, Table 3.4). This allowed us to estimate the effect of gold on the intrinsic activity of Pt surface sites. As the gold alone was practically inactive, the catalyst activity can be attributed entirely to the Pt sites. Previously, it has been shown that ketone HDO over Pt/CsPW catalyst is zero order in ketone and near first order in Pt loading [2]. The HDO of 3-pentanone over 5.6%Pt/4.3%Au/CsPW-CI was also found to be zero order in ketone, as the initial reaction rate practically did not change upon increasing ketone concentration in the feed from 1.0 to 2.0% (Table 5.3, last two entries). This means that 3-pentanone conversion is equivalent to the reaction

rate constant, which allows obtaining TOF values from non-differential conversions. Table 5.3 shows the TOF values thus obtained for Pt/CsPW and PtAu/CsPW catalysts at 40 ^{o}C, which were calculated from the results presented in Figure 5.1 and Figure 5.5 using initial 3-pentanone conversion (varied between 29 and 60%) and Pt dispersion from Table 3.4 in Chapter 3. These results show that the turnover rate at Pt sites in the gold-free Pt/CsPW catalysts is weakly dependent on Pt dispersion, decreasing 2-fold with a 3-fold increase in the Pt dispersion within the range of 0.32 – 5.8% Pt loading. Gold additives increase the intrinsic activity of Pt surface sites. More specifically, addition of Au to Pt/CsPW in a Pt/Au molar ratio of about 1:1 and a gold loading of 0.35 – 4.3% increases the turnover rate at the Pt sites almost 2-fold regardless of the Pt particle size. This may indicate that Au enhancement of Pt hydrogenation activity is structure insensitive, as may be expected for catalytic hydrogenation [26].

Table 5.3 Turnover rates for Pt/CsPW and PtAu/CsPW catalysts at 40 ^{o}C.[a]

Catalyst	D[b]	d[c] (nm)	Initial conversion	Initial rate (mol $g_{cat}^{-1}h^{-1}$)	TOF (h^{-1})
0.32%Pt/CsPW	0.61	1.5	0.490	$1.23 \cdot 10^{-3}$	0.63
0.28%Pt/0.35%Au/CsPW-CI	0.55	1.6	0.599	$1.50 \cdot 10^{-3}$	0.97
0.32%Pt/0.36%Au/CsPW-SI	0.30	3.0	0.427	$1.07 \cdot 10^{-3}$	1.1
5.8%Pt/CsPW	0.19	4.7	0.286	$1.43 \cdot 10^{-2}$	1.3
5.6%Pt/4.3%Au/CsPW-CI	0.17	5.3	0.502	$2.51 \cdot 10^{-2}$	2.6
5.6%Pt/4.3%Au/CsPW-CI[d]	0.17	5.3	0.225	$2.25 \cdot 10^{-2}$	2.3

a) Calculated form the results shown in Figure 5.1 and Figure 5.5 obtained at 1.0% concentration of 3-pentanone in H_2 flow.
b) Pt dispersion (Chapter 3, Table 3.4).
c) Pt particle diameter (Chapter 3, Table 3.4).
d) At 2.0% concentration of 3-pentanone in H_2 flow, other conditions as in Figure 5.5.

5.5 Conclusions

In this chapter, we have demonstrated the enhancing effect of gold on activity and stability of Pt/CsPW bifunctional metal-acid catalyst in hydrodeoxygenation (HDO) of 3-pentanone. Addition of gold to Pt/CsPW has been found to increase both catalyst hydrogenation activity (turnover rate at Pt sites) and catalyst stability to deactivation, although the Au alone without Pt is almost totally inert. The bimetallic catalyst PtAu/CsPW shows the preference of C=O over C=C bond hydrogenation in comparison with the unmodified Pt/CsPW catalyst. The Au enhancement has been found to be dependent on catalyst formulation as well as catalyst preparation method. Carbon-supported Pt and Au physically mixed with CsPW solid acid do not improve catalyst activity. On the other hand, the different formulation of PtAu-CsPW catalyst, with the metals directly supported on acidic support CsPW, does show the enhancement effect. PtAu catalyst prepared by sequential Au-after-Pt impregnation shows less enhancement effect in comparison with the catalysts prepared by co-impregnation.

STEM-EDX and XRD analysis indicates the presence of bimetallic nanoparticles with a wide range of Pt/Au atomic ratios in the PtAu/CsPW catalysts. The catalyst enhancement can be attributed to the two previously documented Au alloy effects, i.e., ensemble and ligand effects [16, 17]. These effects can modify the geometry and electronic state of Pt active sites to enhance their activity toward C=O bond hydrogenation and reduce catalyst poisoning. Overall, the results obtained confirm the view that the addition of Au is a promising methodology to enhance the HDO of biomass-derived feedstock using platinum group metal catalysts [16, 17].

5.6References

1. M. A. Alotaibi, E. F. Kozhevnikova, I. V. Kozhevnikov, J. Catal. 293 (2012) 141.
2. M. A. Alotaibi, E. F. Kozhevnikova, I. V. Kozhevnikov, Chem. Commun. 48 (2012) 7194.
3. K. Alharbi, W. Alharbi, E. F. Kozhevnikova, I. V. Kozhevnikov, ACS Catal. 6 (2016) 2067.
4. S. Itagaki, N. Matsuhashi, K. Taniguchi, K. Yamaguchi, N. Mizuno, Chem. Lett. 43 (2014) 1086.
5. S. Zhu, X. Gao, Y. Zhu, Y. Zhu, X. Xiang, C. Hu, Y. Li, Appl. Catal. B 140-141 (2013) 60.
6. C. Hoang-Van, G. Tournier, S. J. Teichner, J. Catal. 86 (1984) 210.
7. G. J. Hutchings, Chem. Commun. 2008, 1148.
8. K. Q. Sun, Y. C. Hong, G. R. Zhang, B. Q. Xu, ACS Catal. 1 (2011) 1336.
9. D. Tongsakul, S. Nishimura, K. Ebitani, ACS Catal. 3 (2013) 2199.
10. K. Sun, A. R. Wilson, S. T. Thompson, H. H. Lamb, ACS Catal. 5 (2015) 1939.
11. Y. F. Han, J. H. Wang, D. Kumar, Z. Yan, D. W. Goodman, J. Catal. 232 (2005) 467.
12. E. K. Hanrieder, A. Jentys, J. A. Lercher, J. Catal. 333 (2016) 71.
13. J. Xu, T. White, P. Li, C. He, J. Yu, W. Yuan, Y. F. Han, J. Am. Chem. Soc. 132 (2010) 10398.
14. L. B. Ortiz-Soto, O. S. Alexeev, M. D. Amiridis, Langmuir 22 (2006) 3112.
15. R. N. Singh, R. Awasthi, C. S. Sharma, Int. J. Electrochem. Sci. 9 (2014) 5607.
16. B. Coq, F. Figueras, J. Mol. Catal. A 173 (2001) 117.
17. F. Gao, D. W. Goodman, Chem. Soc. Rev. 41 (2012) 8009.
18. M. R. H. Siddiqui, S. Holmes, H. He, W. Smith, E. N. Coker, M. P. Atkins, I. V. Kozhevnikov, Catal. Lett. 66 (2000) 53.
19. I. V. Kozhevnikov, S. Holmes, M. R. H. Siddiqui, Appl. Catal. A 214 (2001) 47.
20. W. Knaeble, R. T. Carr, E. Iglesia, J. Catal. 319 (2014) 283.
21. T. Pinto, P. Arquilliere, G. P. Niccolai, F. Lefebvre, V. Dufaud, New J.Chem. 39 (2015) 5300.
22. P. Claus, Appl. Catal. A 291 (2005) 222.
23. A. S. K. Hashmi, Chem. Rev. 107 (2007) 3180.
24. T. Okuhara, H. Watanabe, T. Nishimura, K. Inumaru, M. Misono, Chem. Mater. 12 (2000) 2230.
25. K. Sun, A. R. Wilson, S. T. Thompson, H. H. Lamb, ACS Catal. 5 (2015) 1939.

26. R. A. van Santen, M. Neurock, in: G. Ertl, H. Knözinger, F. Schüth, J. Weitkamp (Eds.), Handbook of Heterogeneous Catalysis, 3, Wiley−VCH, 2008, p. 1415.

6. Deoxygenation of ethers and esters over bifunctional Pt-heteropoly acid catalyst in the gas phase

6.1 Introduction

As stated before by Alotaibi et al. [1, 2] and shown in Chapter 4, platinum on acidic supports, namely Pt on zeolite HZSM-5 and the acidic caesium salt of tungstophosphoric heteropoly acid $Cs_{2.5}H_{0.5}PW_{12}O_{40}$ (CsPW), are highly active bifunctional metal-acid catalysts for hydrogenation (hydrodeoxygenation) of a wide range of aliphatic and aromatic ketones in the gas phase under mild conditions to yield the corresponding alkanes.

Here, we investigate the deoxygenation and decomposition of a series of ethers and esters, including the aromatic ether anisole, the aliphatic diisopropyl ether (DPE) and the aliphatic ester ethyl propanoate (EP) in the gas phase using bifunctional metal-acid catalysis. The bifunctional catalysts comprise Pt, Ru, Ni and Cu as the metal components and CsPW as the acid component, with the main focus on the Pt–CsPW catalyst. It is demonstrated that bifunctional metal-acid catalysis in the presence of H_2 is more efficient for ether and ester deoxygenation than the corresponding monofunctional metal and acid catalysis. Also it is found that metal- and acid-catalysed pathways play a different role in these reactions.

Deoxygenation (decomposition) of anisole, DPE and EP ester was carried out in the gas phase in flowing H_2 or N_2 under atmospheric pressure in a Pyrex fixed-bed down-flow reactor as described in Chapter 2.

Information about bifunctional metal-acid and the acid catalysts used in this work is given in Tables 3.1-3.3 and 3.5 (Chapter 3) including their texture (surface area, pore volume and pore

diameter), metal dispersion and acid strength (initial enthalpy of ammonia adsorption). Solid acid catalysts under study are based on Keggin-type tungsten HPAs, $H_3PW_{12}O_{40}$ and $H_4SiW_{12}O_{40}$, and possess predominantly Brønsted acid sites. Previously, these catalysts have been thoroughly characterised using XRD, FTIR, FTIR of adsorbed pyridine, ^{31}P MAS NMR and NH_3 adsorption calorimetry, and their properties have been discussed in detail [3-6]. H_2-TPR, XRD and FTIR studies have shown that CsPW in bifunctional catalysts Pt/CsPW and Pd/CsPW is resistant to reduction by H_2 below 600 ^oC, and the primary (Keggin) structure of CsPW is retained in CsPW-supported Pt, Pd and Cu catalysts after treatment with H_2 at 400 ^oC [7], which confirms their stability under reaction conditions used in this study.

6.2 Hydrogenation of anisole

6.2.1 Catalyst performance

Catalytic hydrogenation of anisole is a model for hydrodeoxygenation of lignin; it has been extensively studied using both homogeneous and heterogeneous catalysis [8-14] (and references therein). Representative results for hydrogenation of anisole are given in Table 6.1. Different catalysts are compared at 100 ^oC and 1 bar H_2 pressure. In anisole conversion over bifunctional catalysts comprising Pt and CsPW, Pt-catalysed hydrogenation was found to play the key role, with a relatively moderate assistance of acid catalysis from CsPW. In the absence of Pt, acid-catalysed conversion of anisole with CsPW was low (19%), yielding mainly phenol (entry 1). In contrast, Pt-catalysed hydrogenation of anisole, over Pt/C in the absence of CsPW, occurred readily with 100% conversion and 83% selectivity to cyclohexane, also giving 12% of toluene by-product (entry 2). The bifunctional Pt-CsPW catalyst comprising a uniform physical mixture 7%Pt/C + CsPW (0.35% Pt content) prepared by grinding a mixture of the two components gave 100% anisole conversion with 98-100% cyclohexane selectivity at 80-100 ^oC, i.e., almost 100% cyclohexane yield (entries 3, 4), with stable activity for 20 h on stream as shown in Figure 6.1.

This catalyst was highly active even at 60 ^{o}C giving 100% anisole conversion with 90% cyclohexane selectivity (Table 6.1, entry 5). Similar results were obtained when using a mixture of 10%Pt/SiO_2 + CsPW with 0.5% Pt content (entry 6), which exhibited stable performance for at least 6 h on stream. Methanol was also formed in these reactions with 80-99% selectivity based on converted anisole (not shown in Table 6.1). The Pt/C + CsPW catalyst with Pt content reduced to as low as 0.1% showed the same high activity (entry 7). Its activity was dropped only when the Pt content was further reduced to 0.02% (entries 8, 9, Figure 6.2). Therefore, it is evident that the Pt metal sites play the primary role in anisole hydrogenation; however, the acid (proton) sites of CsPW also make significant contribution further enhancing the selectivity to cyclohexane up to 100%. The Pt/C + CsPW catalyst is more active in comparison with previously reported catalysts such as Raney Ni and supported Ni, copper-chromite, Mo carbide, Pt/H-Beta, etc., which operate in the gas or liquid phase at temperatures of 150-400 ^{o}C and elevated H_2 pressures [11-14] (and references therein). Our catalyst compares favorably with the homogeneous polyoxometalate-stabilized Rh(0) nanocluster, which holds the record lifetime/activity of 2600 TON (turnover numbers) in anisole hydrogenation to methoxycyclohexane (91% yield at 22 ^{o}C, 3 bar H_2 pressure, 144 h reaction time; reaction in propylene carbonate solution containing $HBF_4 \cdot Et_2O$ as an acid promoter) [8]. Our Pt/C + CsPW catalyst is capable of at least 1700 TON at 100 ^{o}C, 1 bar H_2 and 20 h on stream (Figure 6.1, Table 6.1), without any problem of catalyst recovery and reuse.

Table 6.1 Hydrogenation of anisole over bifunctional catalysts in the gas phase.[a]

Entry	Catalyst	Temp. (°C)	Conversion[b] (%)	Selectivity[b] (%)	
				Cyclohexane	Other[c]
1	CsPW	100	19 (3)	12	88 (60% PhOH)
2	7%Pt/C+SiO_2 (1:9 w/w)	100	100 (6)	83	17 (12% PhMe)
3	7%Pt/C+CsPW (1:19 w/w)	100	100 (20)	98	2
4	7%Pt/C+CsPW (1:19 w/w)	80	100 (4)	100	0
5	7%Pt/C+CsPW (1:19 w/w)	60	100 (3)	90	10 (9% MePh)
6	10%Pt/SiO_2+CsPW (1:19 w/w)	100	100 (3)	99	1
7	7%Pt/C+CsPW+SiO_2 (1:19:60 w/w)	100	100 (6)	98	2
8	7%Pt/C+CsPW+SiO_2 (1:19:400 w/w)	100	55 (3)	91	9 (4% PhMe)
9	7%Pt/C+CsPW+SiO_2 (1:19:400 w/w)	100	40 (6)	89	11 (4% PhMe)
10	0.5%Pt/CsPW (acac)	100	20 (2)	19	81 (41% PhOH)
11	0.5%Pt/CsPW (H_2PtCl_6)[d]	100	87 (2)	89	11 (5% cyclohexanol)
12	5%Ru/CsPW[d]	100	64 (2)	86	14 (9% PhH)
13	5%Ru/CsPW[d]	100	23 (4)	85	15 (5% PhH)
14	10%Cu/CsPW[d]	100	7 (3)	63	37 (8% cyclohexanol)
15	10%Ni/CsPW[d]	100	10 (3)	22	78 (40% PhOH)

a) Reaction conditions: 0.20 g catalyst weight, 0.50% anisole concentration in H_2 flow, 20 ml min^{-1} flow rate, catalyst pre-treatment at 100 °C for 1 h in H_2 flow.

b) Anisole conversion and product selectivity at the time on stream given in round brackets (in hours); selectivity to methanol (80-99%) not shown.

c) Other: phenol, cyclohexanol, benzene, toluene and unidentified products.

d) Bifunctional metal-acid catalysts were prepared by direct wet impregnation of CsPW with an appropriate metal precursor (H_2PtCl_6, $RuCl_3$, $Ni(NO_3)_2$, $Cu(NO_3)_2$, designated in Chapters 3 and 4 M/CsPW-I.

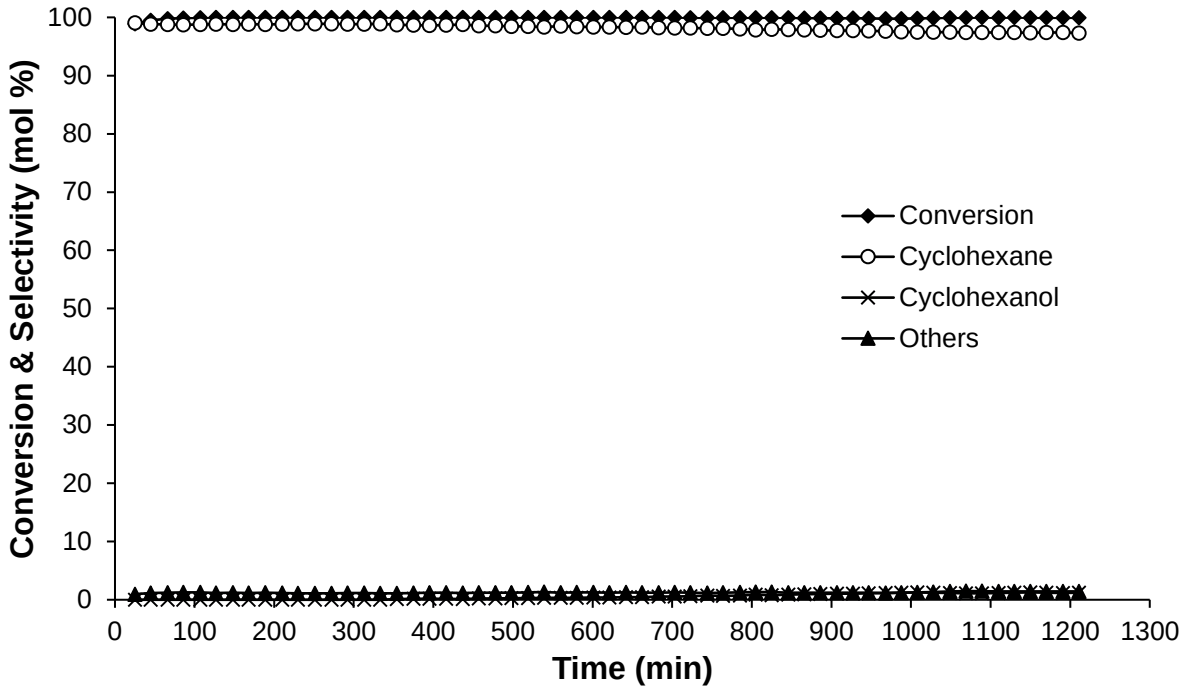

Figure 6.1 Anisole hydrogenation over bifunctional catalyst 7%Pt/C+CsPW (1:19 w/w, 0.35% Pt content) (100 ^{o}C, 0.20 g catalyst weight, 0.50% anisole concentration in H_2 flow, 20 mL min^{-1} flow rate, catalyst pre-treatment at 100 ^{o}C/1 h in H_2 flow. Methanol is not shown; its selectivity was close to 100%.

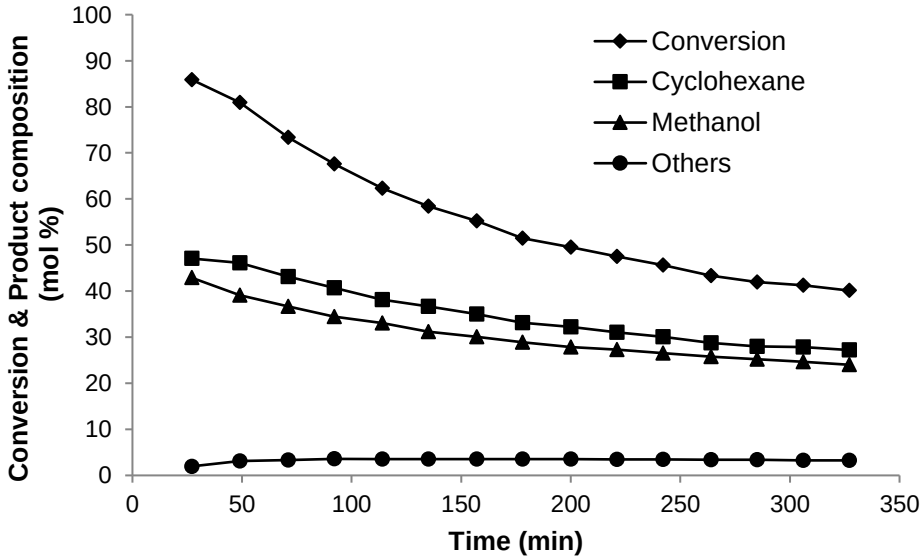

Figure 6.2 Anisole hydrogenation over bifunctional catalyst 7%Pt/C+CsPW+SiO_2 (1:19:400 w/w) (100 ^{o}C, 0.20 g catalyst weight, 0.50% anisole concentration in H_2 flow, 20 mL min^{-1} flow rate, catalyst pre-treatment at 100 ^{o}C/1 h in H_2 flow (20 mL min^{-1}).

6.2.2 Effect of catalyst formulation and preparation on the catalyst performance

It was found that catalyst performance depended greatly on catalyst formulation and preparation. The Pt/C + CsPW physical mixture was found to be much more active as well as more resistant to deactivation than the Pt/CsPW catalyst prepared by impregnation of CsPW with a Pt precursor. Moreover, the type of Pt precursor and the conditions of impregnation were also important for the performance of catalysts thus made. Thus, 0.5%Pt/CsPW prepared by impregnation of CsPW with $Pt(acac)_2$ from benzene solution, denoted Pt/CsPW(acac), was less active and less stable to deactivation than the same catalyst prepared by impregnation with H_2PtCl_6 from aqueous solution and denoted Pt/CsPW(H_2PtCl_6) (cf. Table 6.1, entries 10 and 11). This may be explained by very different Pt dispersion in these catalysts: 0.46 in Pt/CsPW(acac) and 0.10 in Pt/CsPW(H_2PtCl_6) (Table 3.3). It is conceivable that the latter catalyst with larger Pt particles is more stable to catalyst deactivation, hence its higher catalytic activity. The higher activity and better performance stability of the Pt/C + CsPW mixture compared with the supported Pt/CsPW catalyst may be explained assuming that the former catalyst having Pt and proton sites farther apart suffers less from deactivation (coking) than the latter one with the active sites in close proximity. This also indicates fast migration of reaction intermediates between metal and acid sites in the mixed catalyst. Previously, similar behavior, although less pronounced, has been observed for hydrogenation of acetophenone over Pt/C + CsPW and Pt/CsPW. However, in hydrogenation of aliphatic ketones these two catalysts showed similar performance (Chapter 4).

Bifunctional catalysts containing other metals supported on CsPW were also tested for hydrogenation of anisole (Table 6.1, entries 12-15). All these catalysts suffered from catalyst deactivation. Thus 5%Ru/CsPW gave 64% anisole conversion at 2 h time on stream, which reduced to 23% at 4 h on stream (entries 12 and 13). Catalyst activity (anisole conversion per metal weight) was found to decrease in the order of metals: Pt >> Ru > Ni > Cu. The same order

of activity has been found for ketone hydrogenation (Chapter 4). Catalyst deactivation can be attributed to catalyst coking. Table 6.2 shows the amount of carbon in spent catalysts over anisole hydrogenation at 100 °C.

Table 6.2 C and H combustion analysis for spent M/CsPW catalysts used in the gas phase hydrogenation of anisole at (100 °C, 3-4 h).

Catalyst	C (%)	H (%)
0.5%Pt/CsPW (acac)	4.20	0.37
0.5%Pt/CsPW (H_2PtCl_6)	4.77	0.47
5% Ru/CsPW	4.46	0.51
10%Pt/SiO_2 +CsPW +SiO_2(1 / 19 / 400 w/w)	1.55	0.38
CsPW	2.86	0.30

6.2.3 Proposed mechanism of anisole hydrogenation over Pt-CsPW

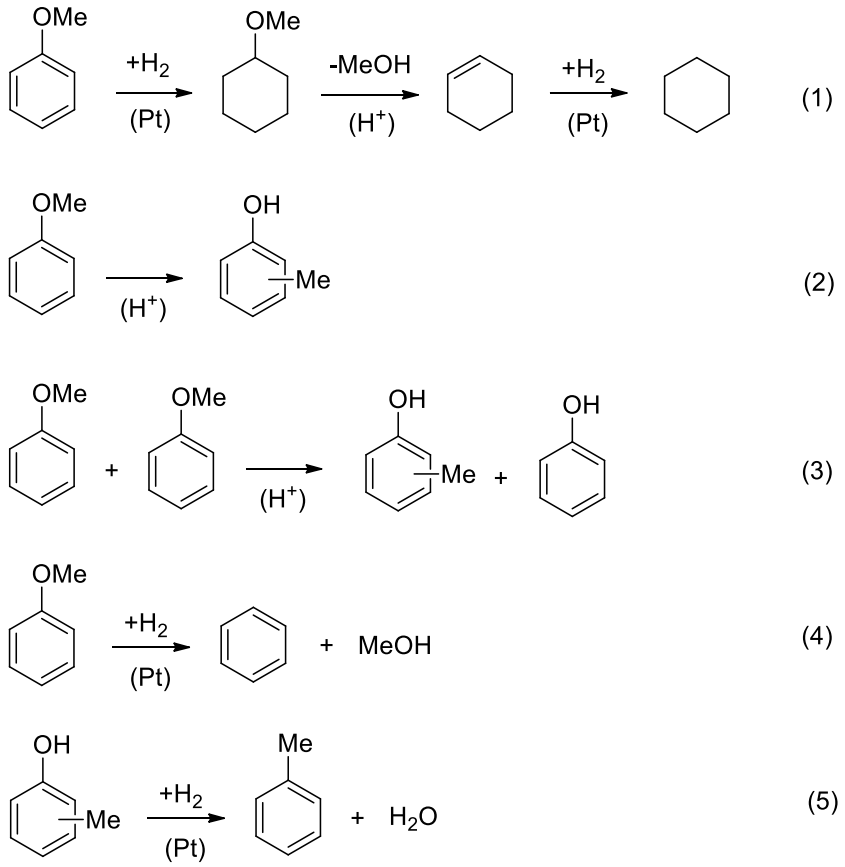

Scheme 6.1 Reaction network for anisole hydrogenation over Pt-CsPW bifunctional catalyst.

In most cases, cyclohexane was the main reaction product (Table 6.1). Among other products found were methanol, phenol, toluene, benzene and cyclohexanol, in agreement with previous reports [11-14]. Reaction network for anisole hydrogenation has been discussed elsewhere [8-14]. It can be represented by Scheme 6.1, which includes metal-catalysed hydrogenation of aromatic ring (Equation 1), acid-catalysed intra- and intermolecular migration of methyl group (Equations 2 and 3) and hydrogenolysis of Ar–OH and Ar–OMe bonds on metal sites to yield benzene and toluene (Equations 4 and 5). The last reaction has been shown to occur readily on metal complexes and metal nanoclusters [8-10]. Acid-catalysed intra- and intermolecular migration of methyl group in anisole has been reported previously, for example, over HY zeolite [15]. As regards the positive effect of acid sites on cyclohexane selectivity in anisole

hydrogenation over the Pt/C + CsPW catalyst, it can be attributed to the acid-catalysed elimination of methanol from methoxylcyclohexane to form cyclohexene followed by its hydrogenation to cyclohexane (Equation 1).

6.3 Decomposition of diisopropyl ether

6.3.1 Reaction mechanism over Pt-CsPW

Decomposition of the aliphatic diisopropyl ether, DPE, over Pt-CsPW in the presence of hydrogen can be represented by Equations (6) – (8). These involve the acid-catalysed reactions of DPE decomposition (6) and isopropanol dehydration (7) to yield propene and the Pt-catalysed hydrogenation of propene to propane (8).

$$(iPr)_2O \rightleftharpoons iPrOH + C_3H_6 \quad (6)$$

$$iPrOH \rightleftharpoons C_3H_6 + H_2O \quad (7)$$

$$C_3H_6 + H_2 \longrightarrow C_3H_8 \quad (8)$$

Scheme 6.2 Decomposition of the aliphatic diisopropyl ether over Pt-CsPW.

With CsPW, possessing strong Brønsted acid sites, reactions (6) and (7) are known to proceed readily in the gas phase, probably through the mechanism of E1 elimination [3, 4] (Scheme 6.3). These reactions are reversible and controlled by equilibrium; their Gibbs free energies (ΔG) are 14.1 and -0.8 kJ mol^{-1} for (6) and 7.9 and -4.7 kJ mol^{-1} for (7) in the gas phase at 25 and 110 ^{o}C, respectively (the thermodynamic data are given bellow in Table 6.4). In contrast, reaction (8) is thermodynamically favorable with ΔG = -86.4 kJ mol^{-1} at 25 ^{o}C and -75.3 kJ mol^{-1} at 110 ^{o}C (Table 6.4). Therefore, it may be expected that with Pt-CsPW bifunctional catalyst under H_2 the decomposition of DPE will be driven forward to form propane as the thermodynamically favorable product.

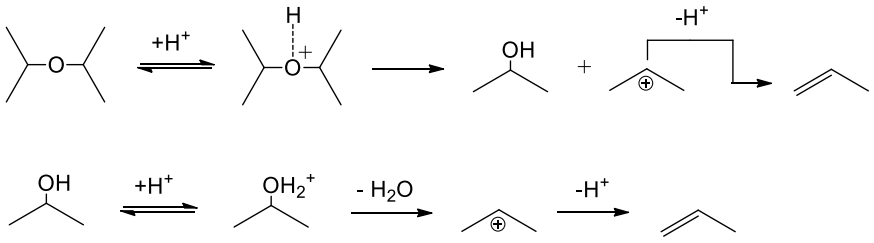

Scheme 6.3 Mechanism of E1 elimination of DPE and isopropanol.

6.3.2 Thermodynamics of DPE decomposition [16]

Thermodynamic analysis included the flowing reactions:

$(iPr)_2O = iPrOH + C_3H_6$ (A)

$(iPr)_2O = 2\ C_3H_6 + H_2O$ (B)

$(iPr)_2O + 2\ H_2 = 2\ C_3H_8 + H_2O$ (C)

$iPrOH = C_3H_6 + H_2O$ (D)

$C_3H_6 + H_2 = C_3H_8$ (E)

Initial thermodynamic data at standard conditions (Table 6.3) were taken from the literature [17-21].

Table 6.3 Initial thermodynamic data (298.15 K, 1 bar, ideal gas).

Compound	$\Delta_f G^o$ kJ mol^{-1}	$\Delta_f H^o$ kJ mol^{-1}	S^o J mol^{-1}K^{-1}	$C_p{}^o$ J mol^{-1}K^{-1}	References
H_2	0	0	130.68	28.82	[17]
C_3H_8	-23.56	-103.85	270.20	73.60	[18]
C_3H_6	62.84	20.42	266.60	64.31	[19]
H_2O	-228.6	-241.80	188.8	36.6	[20]
iPrOH		-272.6	310.0	89.0	[21]
$(iPr)_2O$		-319.0	400[a]	155[a]	[20]

a) Estimated from values for similar compounds.

Table 6.4 Thermodynamic parameters for DPE decomposition at 298.15 and 383.15 K.[a]

Reaction	ΔH^{298} kJ mol^{-1}	ΔS^{298} J mol^{-1}K^{-1}	ΔC_p^{298} J mol^{-1}K^{-1}	ΔG^{298} kJ mol^{-1}	ΔG^{383} kJ mol^{-1}	K_p^{383}	x^{383}
(A)	66.8	176.6	-1.7	14.1	-0.81	1.29 bar	0.75
(B)	118.0	322.0	10.2	22.0	-5.47	5.57 bar^2	0.84
(C)	-130.5	67.8	-28.8	-150.7	-156.1	1.91 10^{21}	1.00
(D)[b]				7.9	-4.7		
(E)[b]				-86.4	-75.3		

a) Undiluted ideal gas system at 1 bar pressure.

b) ΔG values calculated from those for reactions (A) – (D).

Equations (6.1 - 6.7) used for the calculations of thermodynamic parameters for DPE decomposition are given below, where K_p is the equilibrium constant and x is the equilibrium conversion of DPE. ΔC_p was assumed to be independent of temperature, i.e., $\Delta C_p^T = \Delta C_p^{298}$. The results are presented in Table 6.4 for undiluted ideal gas system. In fact, our reaction system was diluted with nitrogen, [DPE] = 5.0%. Dilution with inert gas is equivalent to reduction of total pressure P, which shifts equilibria (A) and (B) towards products. As a result, equilibrium conversion x will increase. Thus, for reaction (A), x = 0.75 for undiluted system and 0.98 for our diluted system ([DPE] = 5.0%) at 383.15 K (110 ^{o}C). For reaction (B) in diluted system x = 1. Reaction (C) is volume neutral, i.e., independent of P.

$$\Delta H^T = \Delta H^{298} + \Delta C_p^{298}(T - 298.15) \quad (6.1)$$

$$\Delta S^T = \Delta S^{298} + \Delta C_p^{298} \ln(T/298.15) \quad (6.2)$$

$$\Delta G^T = \Delta H^T - T\Delta S^T \quad (6.3)$$

$$K_p = \exp\{-\Delta G/RT\} \quad (6.4)$$

$$K_p = x^2P/(1-x^2) \text{ for reaction (A), where } P \text{ is the pressure} \quad (6.5)$$

$$x = \sqrt{K_p/(P + K_p)} \quad (6.6)$$

$$K_p = 4x^3P^2/(1-x)(1+2x)^2 \text{ for reaction (B)} \quad (6.7)$$

6.3.3 Decomposition of diisopropyl ether over CsPW and Pt/CsPW

Table 6.5 shows the results for DPE decomposition in the gas phase catalysed by CsPW and Pt-CsPW under N_2 and H_2. In the acid-catalysed reaction with CsPW under N_2, ether conversion increased from 6.3 to 96% with increasing the temperature from 50 to 200 ^oC to give propene and isopropanol as the products. In this temperature range, propene selectivity increased from 60 to 99% at the expense of isopropanol, indicating the growing contribution of reaction (7) in the decomposition process as the temperature increased (Figure 6.3). As expected, ether conversion and product selectivity practically did not change when the CsPW-catalysed reaction was carried out under H_2 instead of N_2 (Table 6.5).

Last entries in Table 6.5 show the DPE decomposition in the presence of the bifunctional catalyst Pt-CsPW under H_2 at 110 ^oC; the catalyst was applied as the uniform 1:19 w/w physical mixture of 7%Pt/C and CsPW (0.35% Pt content). Pt alone applied as Pt/C + SiO_2 under H_2 in the absence of CsPW was inactive in DPE decomposition; nor had the Pt any effect in the reaction with Pt/C + CsPW under N_2. However, in the reaction with Pt/C + CsPW under H_2, the conversion of DPE greatly increased (from 53 to 99%), giving propane as the main product with 93% selectivity. Therefore, although DPE decomposed readily without metal assistance via the acid-catalysed pathway (E1 mechanism) to give propene and isopropanol, the process was greatly accelerated in the presence of Pt under H_2 via the bifunctional metal-acid-catalysed pathway due to shifting process equilibrium to yield propane, the more thermodynamically favorable product.

Table 6.5 Decomposition of diisopropyl ether in the gas phase.[a]

Catalyst	Temperature (°C)	Conversion[b] (%)	Selectivity[b] (mol %)		
			Propene	Isopropanol	Other[c]
CsPW	50	6.3	60	40	0
CsPW	70	19	62	38	0
CsPW	110	54	66	33	1
CsPW	110[d]	56	65[e]	35	0
CsPW	150	97	98	1	1
CsPW	170	97	98	1	1
CsPW	200	96	99	0	1
7%Pt/C+SiO_2[f]	110[d]	~1			
7%Pt/C+CsPW[f]	110	53	64	36	0
7%Pt/C+CsPW[f]	110[d]	99	93[g]	2	5[h]

a) Reaction conditions: 0.20 g catalyst weight, 5.0% diisopropyl ether concentration in N_2 flow, 20 ml min^{-1} flow rate, catalyst pre-treatment at reaction temperature for 1 h in N_2 flow (20 mL min^{-1}), 4 h time on stream.

b) Average conversion and product selectivity for 4 h time on stream.

c) Other: acetone, hexene and hexane.

d) Reaction under H_2; catalyst pre-treatment at reaction temperature for 1 h in H_2 flow.

e) 5% propane + 95% propene.

f) Uniform physical mixture of 7%Pt/C with CsPW or SiO_2 (1:19 w/w), 0.35% Pt content.

g) 100% propane.

h) Hexane.

6.3.4 Effect of temperature on DPE decomposition over CsPW

Figure 6.3 shows how the gas phase reaction results vary with increasing temperature (50-200 ºC) for CsPW catalysts. The reactions were carried out for a period of 4 h, at the same conditions described above. The conversion of DPE increase with increasing in temperature producing propene and isopropanol. The selectivity toward propene increased with increasing temperature reached 99% at 150-200 ºC.

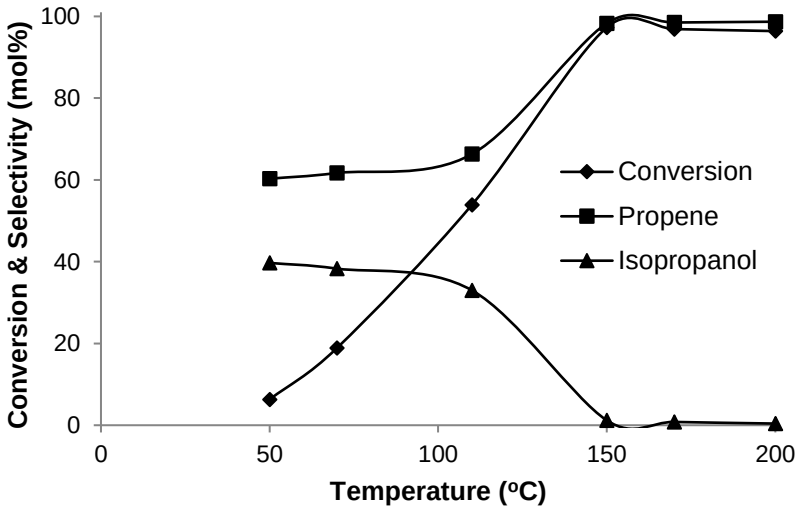

Figure 6.3 Effect of temperature on diisopropyl ether decomposition catalysed by CsPW (0.20 g catalyst weight, 5.0% diisopropyl ether concentration in N_2 flow, 20 mL min^{-1} flow rate).

6.3.5 Catalyst performance stability over CsPW

CsPW catalyst showed no deactivation in extended catalyst stability test for 21 h time on stream (Figure 6.4).

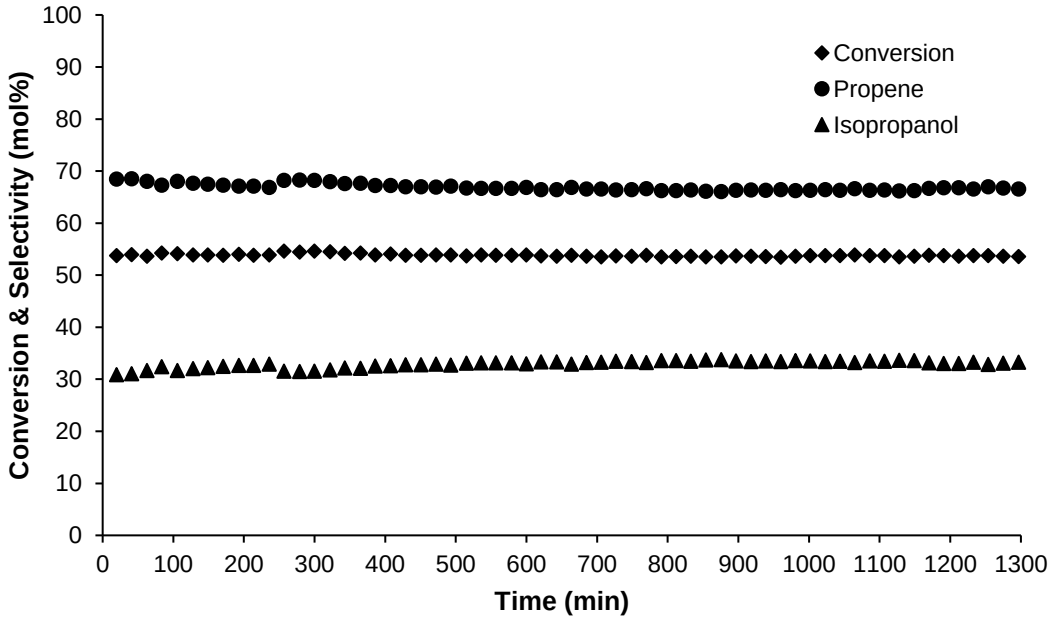

Figure 6.4 Diisopropyl ether decomposition over CsPW (0.20 g catalyst weight, 110 ^{o}C, 5.0% diisopropyl ether concentration in N_2 flow, 20 mL min^{-1} flow rate, catalyst pre-treatment at 110 ^{o}C/1 h in N_2 flow).

6.3.6 Kinetic studies

Kinetic studies showed that the CsPW-catalysed reaction was first order in DPE in the DPE partial pressure range of 1-5 kPa (Figure 6.5); these results were obtained under differential conditions, i.e., at DPE conversion <10%. The reaction had an apparent activation energy E_a = 50 kJ mol^{-1} in the temperature range of 50-70 ^{o}C. The latter indicates that DPE decomposition was not limited by mass transport. The absence of pore diffusion limitations was also backed up by the Weisz-Prater analysis [22] of the reaction system.

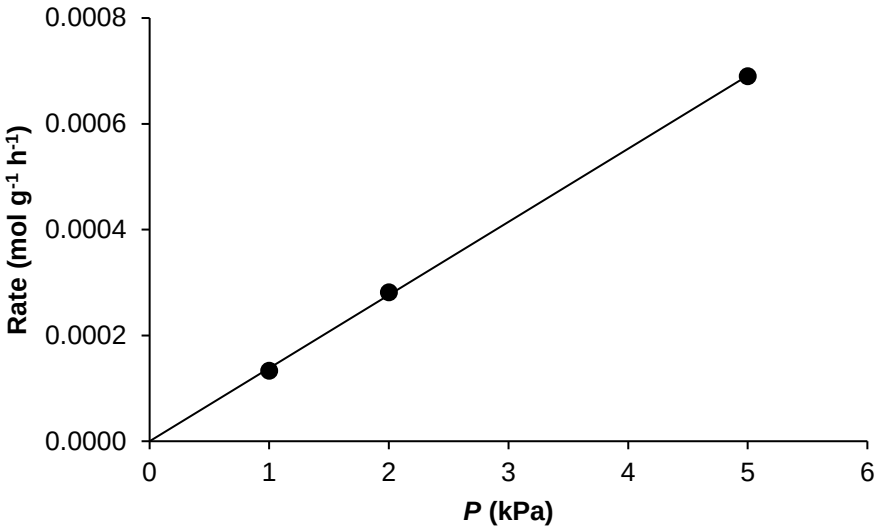

Figure 6.5 Effect of diisopropyl ether partial pressure on the rate of diisopropyl ether decomposition over CsPW (0.20 g catalyst weight, 50 ^{o}C, 20 ml min^{-1} flow rate).

The activity of a wide range of Keggin-type tungsten HPA catalysts listed in Table 3.2 was tested in the acid-catalysed decomposition of DPE at 50 ^{o}C; the reaction rates and turnover frequencies (TOF) obtained are given in Table 6.6. TOF is vital measurement used to determine the catalyst efficiency based on knowledge of catalyst active sites [23].

$$\mathrm{TOF} = \frac{\text{change of molecules of reactant or product}}{\text{time} \times \text{active site}}$$

In this work, the TOF values (h^{-1}) were calculated per surface proton site from the values of DPE conversion (X) measured under differential conditions (X < 0.1). The required densities of accessible proton sites were estimated as described elsewhere [3-6]. The protons of our supported HPA catalysts, which contained HPW or HSiW at sub-monolayer coverage, assumed to be equally accessible for the reaction (o.16 mmol g^{-1} for supported 15% HPA and 0.21 mmol g^{-1} for 15% HSiW). This has been proved in earlier studies by titration of silica-supported HPW with NH_3 [24] and pyridine [25]. For bulk HPW, HSiW and Cs salts of HPW, which have been

demonstrated to catalyse alcohol dehydration through the surface type mechanism [3-6], the number of protons on surface was measured using a Keggin unit cross section of 144 $Å^2$ and the catalyst surface areas from Table 3.2, Chapter 3: HPW (5.6 m^2g^{-1}, 0.019 mmol(H^+) g^{-1}), HSiW (9.0 m^2g^{-1}. 0.042 mmol(H^+) g^{-1}), $Cs_{2.5}H_{0.5}PW$ (132 m^2g^{-1}, 0.076 mmol(H^+) g^{-1}) and $Cs_{2.25}H_{0.75}PW$ (128 m^2g^{-1}, 0.11 mmol(H^+) g^{-1}). The TOF values thus obtained indicate a strong effect of catalyst acid strength on the turnover reaction rate (see ΔH values in Table 3.5 in Chapter 3).

Table 6.6 Rates of DPE decomposition over HPA catalysts.[a]

Catalyst	Conversion[b]	10^4 Rate[c] mol $h^{-1}g^{-1}$	TOF[d] h^{-1}
15%HPW/ZrO_2	0.0565	7.06	4.53
15%HPW/Nb_2O_5	0.0384	4.80	3.08
15%HPW/TiO_2	0.0539	6.74	4.32
15%HPW/SiO_2	0.0672	8.40	5.39
$Cs_{2.5}H_{0.5}PW$	0.0576	7.20	9.48
$Cs_{2.25}H_{0.75}PW$	0.0795	9.94	8.95
HSiW	0.0528	6.60	15.9
HPW	0.0479	5.99	30.9

a) Reaction conditions: 50 °C, 0.20 g catalyst weight, 5.0% DPE concentration in N_2 flow, 20 mL min^{-1} flow rate, 4 h time on stream.
b) Average conversion for 4 h time on stream.
c) Rate = *XF/W*, where *X* is the conversion, *F* is the molar flow rate of DPE and *W* is the catalyst weight.
d) TOF calculated as the reaction rate per surface proton site.

Figure 6.6 shows a fairly good linear relationship (R^2 = 0.871) between the activity of HPA catalysts in DPE decomposition, ln (TOF), and their acid strength represented by the initial enthalpy of ammonia adsorption, ΔH_{NH3} (Table 3.5). Both supported HPA catalysts, bulk Cs salts of HPW and bulk HPAs (HPW and HSiW) obeyed this plot. This indicates that all these HPA catalysts operate through the same mechanism of surface catalysis [26, 27] including the bulk HPAs, for which another, namely a bulk catalysis mechanism, has hitherto been suggested [28]

(for more discussion on the bulk and surface catalysis mechanisms see [5, 6]). This relationship can be used to predict the activity of other Brønsted acid catalysts in DPE decomposition from their ΔH_{NH3} values and vice versa.

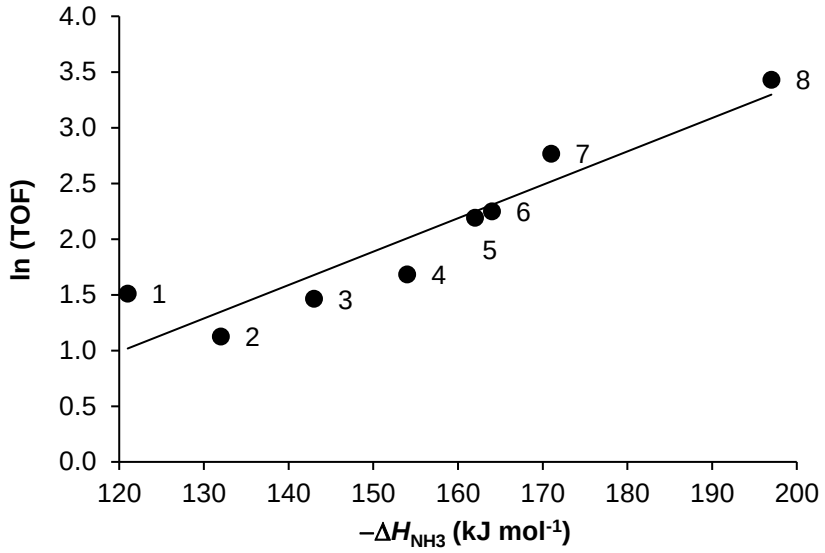

Figure 6.6 Plot of ln (TOF) (TOF in h^{-1}) for diisopropyl ether decomposition versus catalyst acid strength (50 °C, 0.20 g catalyst weight, 5.0% diisopropyl ether concentration in N_2 flow, 20 mL min^{-1} flow rate): (1) 15%HPW/ZrO_2, (2) 15%HPW/Nb_2O_5, (3) 15%HPW/TiO_2, (4) 15%HPW/SiO_2, (5) $Cs_{2.25}H_{0.75}PW$, (6) $Cs_{2.5}H_{0.5}PW$, (7) HSiW, (8) HPW.

6.4 Decomposition of ethyl propanoate

6.4.1 Mechanism of acid catalysed decomposition of ethyl propanoate

Mechanistically, the acid-catalysed decomposition of ethyl propanoate, EP, an aliphatic ester, involves ester protonation to form oxonium ion followed by acyl-oxygen or alkyl-oxygen bond breaking, which can occur through monomolecular ($A_{AC}1$ or $A_{AL}1$) or bimolecular ($A_{AC}2$ or $A_{AL}2$) pathways. This mechanism is well documented for acid-catalysed hydrolysis of esters in homogeneous solutions [28]. In the gas phase, due to the lack of solvation of cationic intermediates (acylium and primary alkylcarbenium ions), the acid-catalysed EP decomposition yielding equimolar mixture of propanoic acid and ethene (see below) is likely to proceed via an

$A_{AL}2$ mechanism with the alkyl-oxygen bond breaking assisted by a catalyst base site followed by proton elimination (Scheme 6.4).

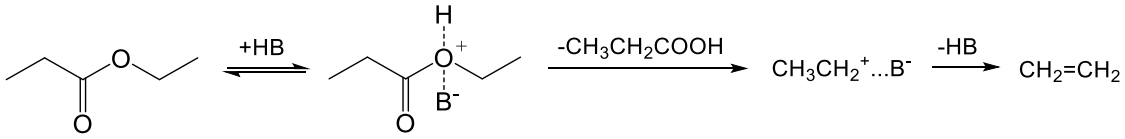

Scheme 6.4 $A_{AL}2$ mechanism of acid-catalysed decomposition of ethyl propanoate (HB is the catalyst acid site with the conjugate base B).

6.4.2 Decomposition of EP over CsPW and Pt/CsPW

Table 6.7 shows our results for EP decomposition catalysed by CsPW and Pt-CsPW in H_2 and N_2 flow. The reaction with CsPW under N_2 yielded equimolar mixtures of ethene and propanoic acid. As expected, EP conversion increased with temperature; at 180 ^oC, the average EP conversion was 81% in 4 h on stream.

Table 6.7 Decomposition of ethyl propanoate in the gas phase.[a]

Catalyst	Temperature (°C)	Conversion[b] (%)	Product composition[b,c] (mol %)			
			C2	PA	EP	Other
CsPW	130[d]	11	10[e]	10	79	1
CsPW	180	88	49	45	6	0
CsPW	180[d]	81	46[e]	43	11	0
7%Pt/C+SiO_2[f]	180	0.6				
7%Pt/C+CsPW[f]	100	3.0				
7%Pt/C+CsPW[f]	150	31	26	23	50	1
7%Pt/C+CsPW[f]	170	77[g]	45	43	12	0
7%Pt/C+CsPW[f]	180	92	50	46	4	0
7%Pt/C+CsPW[f]	180[d]	80	46[h]	43	11	0
7%Pt/C+CsPW[f]	200	97	54	45	1	0

a) Reaction conditions: 0.20 g catalyst weight, 0.85% ethyl propanoate concentration in H_2 flow, 1 bar pressure, 20 mL min^{-1} flow rate, catalyst pre-treatment at reaction temperature for 1 h in H_2 flow, 4 h time on stream.
b) Average conversion and product composition for 4 h time on stream.
c) C2 is ethene + ethane, PA is propanoic acid, EP is unconverted ethyl propanoate, other products are mainly butenes.
d) In N_2 flow; catalyst pre-treatment at reaction temperature for 1 h in N_2.
e) Ethene only formed.
f) Physical mixture of 7%Pt/C + CsPW or SiO_2 (1:19 w/w, 0.35% Pt content).
g) 21 h time on stream.
h) 10% of ethane and 90% of ethene formed.

Table 6.7 also shows the decomposition of EP in the presence of bifunctional catalyst Pt/C + CsPW under H_2; these results were obtained in the temperature range of 100-200 °C. In this temperature range, the conversion of EP increased from 3 to 97%. The results at 180 °C allow us to compare EP decomposition through acid-catalysed and metal-acid-catalysed pathways, i.e., with CsPW and Pt/C + CsPW catalysts. Pt/C alone (applied as Pt/C + SiO_2) in the absence of CsPW was inactive in EP decomposition (0.6% EP conversion). Addition of Pt/C to CsPW under

N_2 had practically no effect either; neither conversion nor product selectivity were affected as compared to the acid-catalysed reaction with CsPW, except for the formation of small amount of ethane in addition to ethene. Under H_2, the Pt/C + CsPW catalyst gave ethane instead of ethene due to complete hydrogenation of the latter, but EP conversion was practically the same as in the acid-catalysed reaction with CsPW, indicating no effect of Pt on the reaction rate. This points to irreversibility of the acid-catalysed decomposition of EP (Scheme 6.4) under reaction conditions studied.

6.4.3 Catalyst performance stability

At 180 ^{o}C, CsPW catalyst suffered from deactivation, with EP conversion decreasing from 88 to 74% in 4 h on stream (Figure 6.5). Initially white, the catalyst turned brown, indicating coke formation (2.0% of carbon was found in the spent catalyst), which probably caused the observed catalyst deactivation. The same reaction under H_2 gave similar conversion and product selectivity, and again catalyst deactivation took place (there was 1.2% carbon content in the spent catalyst).

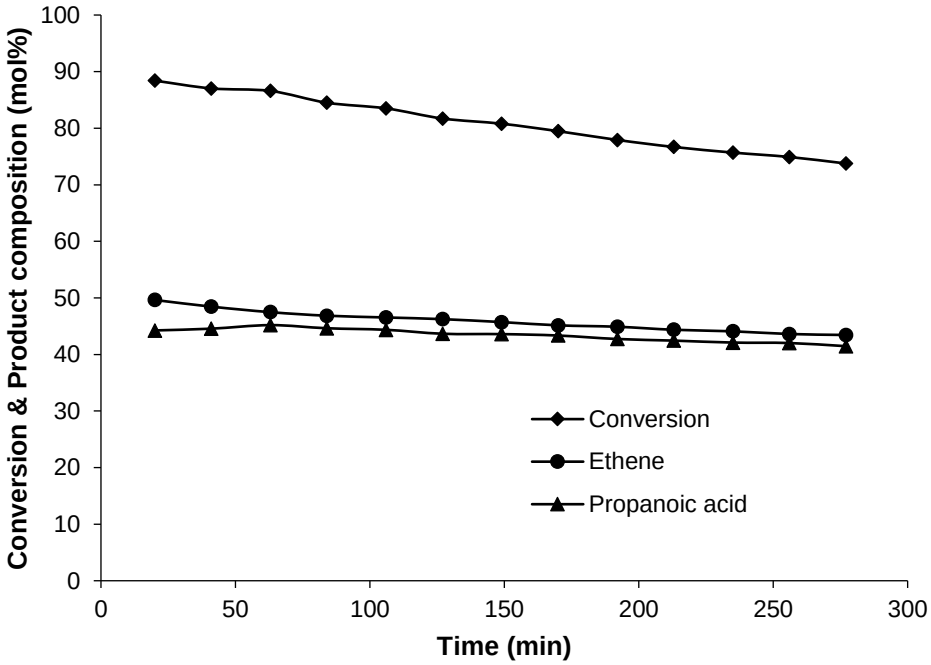

Figure 6.5 Ethyl propanoate decomposition over CsPW (0.20 g catalyst weight, 180 ^{o}C, 0.85% ethyl propanoate concentration in N_2 flow, 20 mL min^{-1} flow rate, catalyst pre-treatment at 180 ^{o}C/1 h in N_2 flow).

At the same temperature, 180 ^{o}C, the Pt/C + CsPW catalyst under H_2 had much better performance stability than CsPW alone; the Pt/C + CsPW catalyst showed no deactivation during 4 h on stream (Figure 6.6, cf. Figure 6.5), with an average EP conversion of 92%, which was close to the initial EP conversion with CsPW under N_2 (88%). Moreover, no deactivation of Pt/C + CsPW was observed in extended stability testing for 21 h at 170 ^{o}C (Figure 6.7). From these results it is evident that Pt itself under N_2 or H_2 is not active in the decomposition of EP in the temperature range studied, but addition of Pt to CsPW in the presence of H_2 improves catalyst resistance to deactivation. The latter can be explained by reduction of catalyst coking due to hydrogenation of alkene coke precursors.

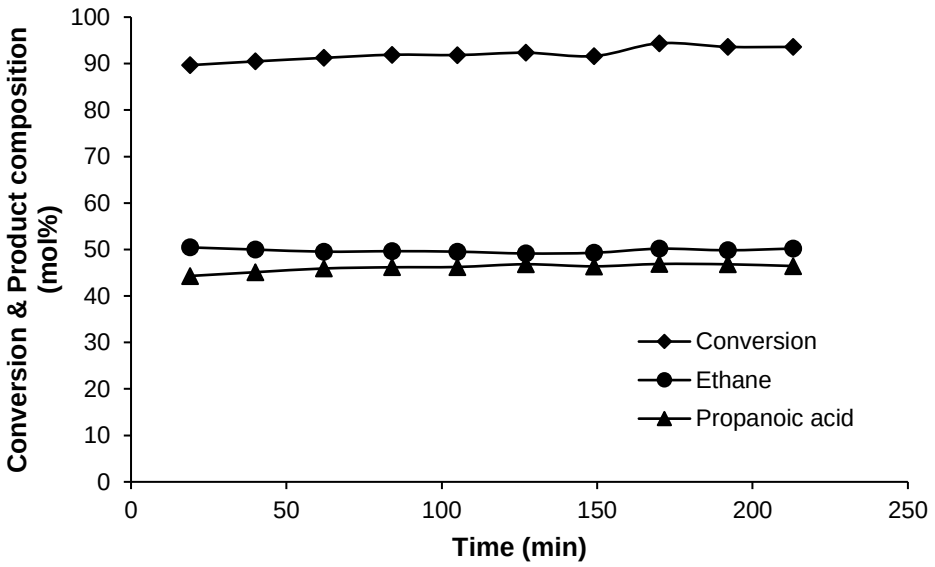

Figure 6.6 Ethyl propanoate hydrogenation over 7%Pt/C+CsPW (1:19 w/w, 0.35% Pt content) (0.20 g catalyst weight, 180 ^{o}C, 0.85% ethyl propanoate concentration in H_2 flow, 20 mL min^{-1} flow rate, catalyst pre-treatment at 180 ^{o}C/1 h in H_2 flow).

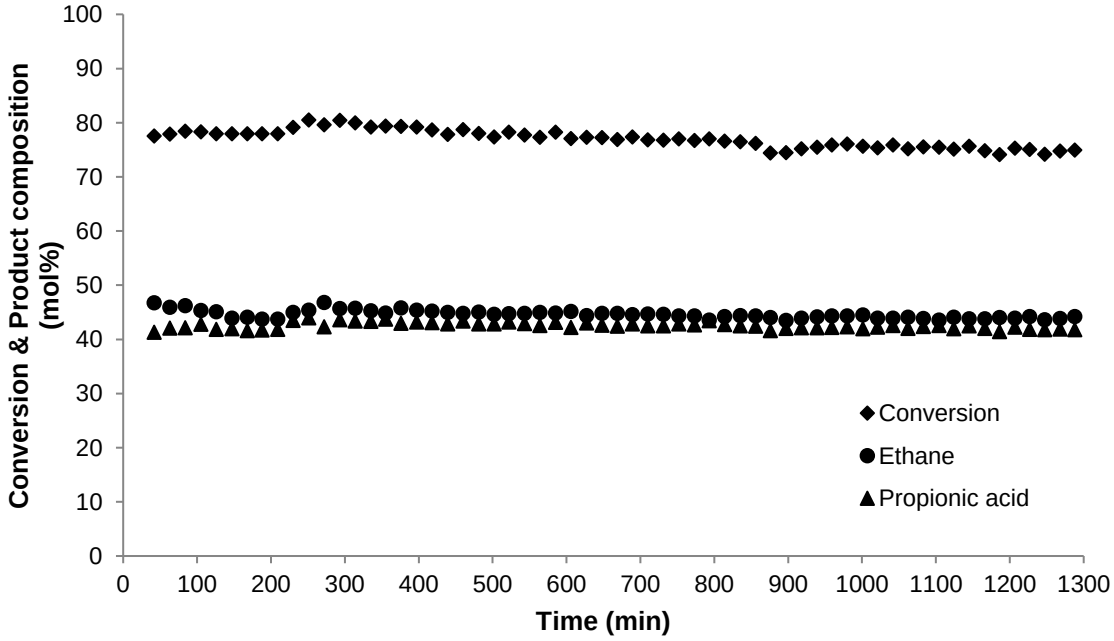

Figure 6.7 Ethyl propanoate decomposition over 7%Pt/C+CsPW (1:19 w/w, 0.35% Pt content) in flowing H_2 (0.20 g catalyst weight, 170 ^{o}C, 0.85% ethyl propanoate concentration in H_2 flow, 20 mL min^{-1} flow rate, catalyst pre-treatment at 170 ^{o}C/1 h in H_2 flow).

6.4.4 Kinetic studies

Kinetics of the CsPW-catalysed decomposition of EP was studied under differential conditions (EP conversion $X < 0.1$) at 130 ^{o}C under N_2; at such conditions, no catalyst deactivation was observed during catalyst testing (4 h time on stream). The reaction was found to be first order in EP in the ester partial pressure range of 1-8 kPa (Figure 6.8). It obeyed the Arrhenius equation with apparent activation energy E_a = 72.3 kJ mol^{-1} in the temperature range of 100-130 ^{o}C (Figure 6.9). This E_a value indicates that the reaction occurred without diffusion limitations, as in the case of DPE decomposition.

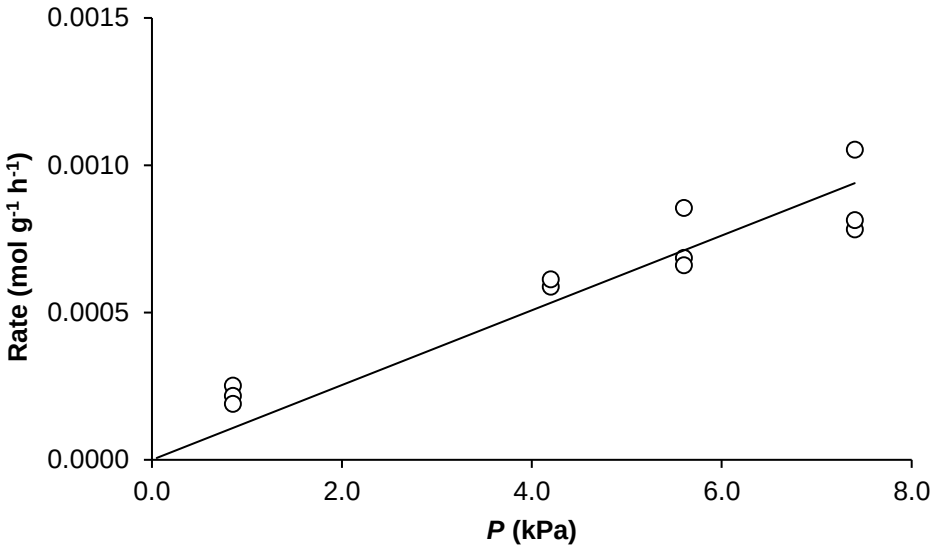

Figure 6.8 Effect of ethyl propanoate partial pressure range of 1-8 kPa on the rate of ethyl propanoate decomposition over CsPW (0.20 g catalyst weight, 130 ^{o}C, 20 ml min^{-1} flow rate).

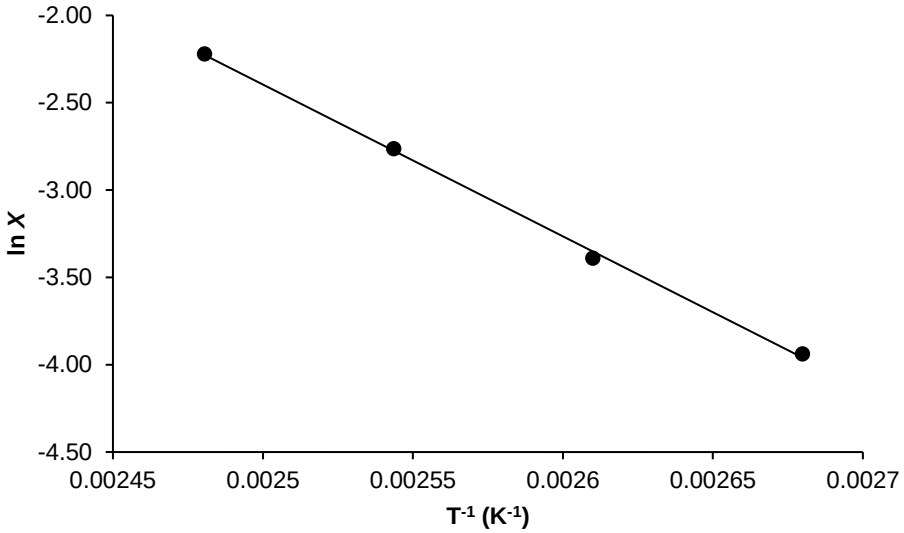

Figure 6.9 Arrhenius plot for ethyl propanoate decomposition over CsPW (*X* is the conversion of ethyl propanoate; 0.20 g catalyst weight, 0.85% ethyl propanoate concentration in N_2 flow, 20 mL min^{-1} flow rate, 100-130 ^oC temperature range; E_a = 72.3 kJ mol^{-1}).

TOF values for the acid-catalysed EP decomposition with the HPA catalysts listed in Table 3.2 are given in Table 6.8. These values were obtained at 130 ^oC under differential conditions, with proton site densities determined as in the case of DPE decomposition.

Table 6.8 Rates of ethyl propanoate decomposition over HPA catalysts.[a]

Catalyst	Conversion[b] (%)	10^4 Rate[c] (mol $h^{-1}g^{-1}$)	TOF[d] (h^{-1})
15%HPW/ZrO_2	0.017	0.34	0.22
15%HPW/Nb_2O_5	0.026	0.51	0.33
15%HPW/TiO_2	0.073	1.46	0.94
15%HSiW/SiO_2	0.116	2.31	1.11
15%HPW/SiO_2	0.101	2.02	1.30
$Cs_{2.5}H_{0.5}PW$	0.109	2.17	2.86
$Cs_{2.25}H_{0.75}PW$	0.311	6.22	5.60
HSiW	0.207	4.14	9.97
HPW	0.184	3.67	18.9

a) Reaction conditions: 130 ^oC, 0.20 g catalyst weight, 0.85% ethyl propanoate concentration in N_2 flow, 20 mL min^{-1} flow rate, catalyst pre-treatment at 130 ^oC/1 h in N_2 flow, 4 h time on stream.

b) Average conversion for 4 h time on stream.

c) Rate = XF/W, where X is the conversion, F is the molar flow rate of ethyl propanoate and W is the catalyst weight.

d) TOF calculated as the reaction rate per surface proton site.

A good activity/acid strength linear correlation (R^2 = 0.924) was obtained for the acid-catalysed EP decomposition (Figure 6.10), as for the decomposition of DPE. This relationship indicates that all HPA catalysts studied, both bulk and supported, operate through the same mechanism of surface catalysis.

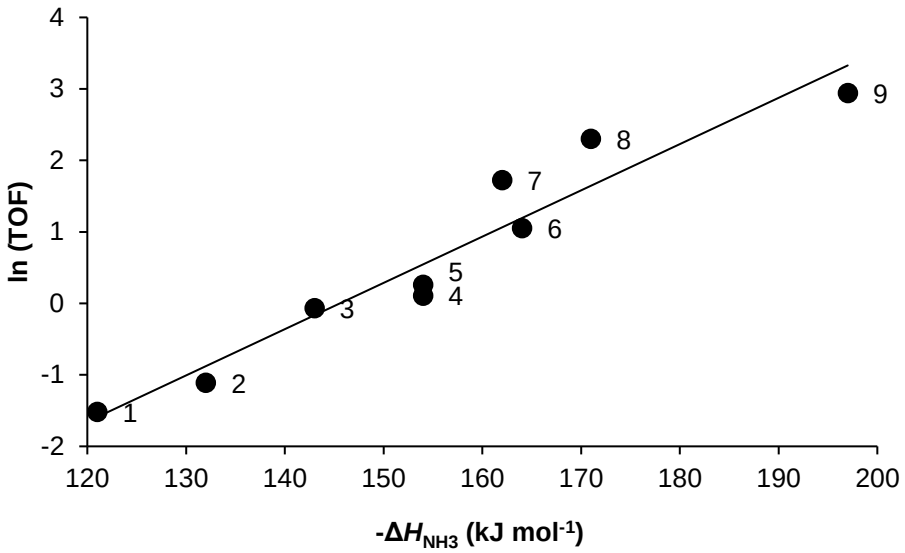

Figure 6.10 Plot of ln (TOF) (TOF in h^{-1}) versus catalyst acid strength (initial enthalpy of NH_3 adsorption) for ethyl propanoate decomposition over HPA catalysts (130 ^{o}C, 0.20 g catalyst weight, 0.85% ethyl propanoate concentration in N_2 flow, 20 mL min^{-1} flow rate): (1) 15%HPW/ZrO_2, (2) 15%HPW/Nb_2O_5, (3) 15%HPW/TiO_2, (4) 15%HSiW/SiO_2, (5) 15%HPW/SiO_2, (6) $Cs_{2.25}H_{0.75}PW$, (7) $Cs_{2.5}H_{0.5}PW$, (8) HSiW, (9) HPW.

6.5 Conclusion

Here, we have investigated the deoxygenation and decomposition of ethers and esters, including the aromatic ether anisole, the aliphatic diisopropyl ether (DPE) and the aliphatic ester ethyl propanoate (EP), using bifunctional metal-acid catalysis at a gas-solid interface in the presence and absence of hydrogen. The bifunctional catalysts comprise Pt, Ru, Ni and Cu as the metal components and $Cs_{2.5}H_{0.5}PW_{12}O_{40}$ (CsPW) as the acid component, with the main focus on the Pt–CsPW catalyst. It has been demonstrated that bifunctional metal-acid catalysis in the presence of H_2 is more efficient for ether and ester deoxygenation in comparison to the corresponding monofunctional metal and acid catalysis. Also it has been found that metal- and acid-catalysed pathways play a different role in these reactions. Hydrodeoxygenation of anisole is a model for the deoxygenation of lignin; with Pt-CsPW, it occurs with almost 100% yield of cyclohexane

under very mild conditions at 60-100 ^{o}C and 1 bar H_2 pressure. In this reaction, Pt-catalysed hydrogenation plays the key role, with a relatively moderate assistance of acid catalysis, further increasing the cyclohexane selectivity. The preferred catalyst formulation is a uniform physical mixture of Pt/C or Pt/SiO_2 with excess CsPW, with a Pt content of 0.1-0.5%, which provides much higher activity and better catalyst stability to deactivation as compared to the Pt/CsPW catalyst prepared by impregnation of platinum onto CsPW. The Pt/C + CsPW mixed catalyst has the highest activity in anisole deoxygenation for a gas-phase catalyst system reported so far. On the other hand, the aliphatic ether DPE decomposes readily over CsPW via acid-catalysed pathway (E1 mechanism) without metal assistance to give propene and isopropanol, with propene selectivity increasing with reaction temperature at the expense of isopropanol. Platinum alone (Pt/C), in the absence of CsPW, is inactive in this reaction, either under H_2 or N_2. However, in the presence of Pt-CsPW under H_2, DPE decomposition is significantly accelerated, yielding the more thermodynamically favorable product propane instead of propene. Decomposition of the EP aliphatic ester is also very efficient via acid-catalysed pathway without metal assistance to yield ethene and propanoic acid. Addition of Pt to CsPW under H_2 causes hydrogenation of ethene to ethane but does not affect the rate of EP decomposition. Nevertheless, in EP decomposition, the Pt-CsPW bifunctional catalyst under H_2 shows much better performance stability compared to the CsPW acid catalyst, which can be attributed to reduction of catalyst coking in the presence of Pt and H_2. Kinetics of the acid-catalysed decomposition of DPE and EP has been studied with a wide range of tungsten HPA catalysts. Good linear relationships between the logarithm of turnover reaction rate and the HPA catalyst acid strength represented by ammonia adsorption enthalpies have been demonstrated, which can be used to predict the activity of other Brønsted acid catalysts in these reactions.

6.6 References

1. M. A. Alotaibi, E. F. Kozhevnikova, I. V. Kozhevnikov, J. Catal. 293 (2012) 141.
2. M. A. Alotaibi, E. F. Kozhevnikova, I. V. Kozhevnikov, Chem. Commun. 48 (2012) 7194.
3. A. M. Alsalme, P. V. Wiper, Y. Z. Khimyak, E. F. Kozhevnikova, I. V. Kozhevnikov, J. Catal. 276 (2010) 181.
4. G. C. Bond, S. J. Frodsham, P. Jubb, E. F. Kozhevnikova, I. V. Kozhevnikov, J. Catal. 293 (2012) 158.
5. W. Alharbi, E. Brown, E. F. Kozhevnikova, I. V. Kozhevnikov, J. Catal. 319 (2014) 174.
6. W. Alharbi, E. F. Kozhevnikova, I. V. Kozhevnikov, ACS Catal. 5 (2015) 7186.
7. M. A. Alotaibi, E. F. Kozhevnikova, I. V. Kozhevnikov. App. Catal. A 447– 448 (2012) 32.
8. J. A. Widegren, R. G. Finke, J. Mol. Catal. A 198 (2003) 198, 317.
9. A. G. Sergeev, J. F. Hartwig, Science 332 (2011) 439.
10. A. G. Sergeev, J. D. Webb, J. F. Hartwig, J. Am. Chem. Soc. 134 (2012) 20226.
11. X. L. Zhu, L. L. Lobban, R. G. Mallinson, D. E. Resasco, *J. Catal*. 281 (2011) 21.
12. W. Lee, Z. Wang, R. J. Wu, A. Bhan, J. Catal. 2014, 319, 44.
13. Y. Yang, C. Ochoa-Hernandez, V. A. de la Pena O'Shea, P. Pizarro, J. M. Coronado, D. P. Serrano, Appl. Catal. B 145 (2014) 91.
14. S. Jin, Z. Xiao, C. Li, X. Chen, L. Wang, J. Xing, W. Li, C. Liang, Catal. Today 234 (2014) 125.
15. Q. Meng, H. Fan, H. Liu, H. Zhou, Z. He, Z. Jiang, T. Wu, B. Han, ChemCatChem 7 (2015) 2831.
16. K. Alharbi, W. Alharbi, E. F. Kozhevnikova, I. V. Kozhevnikov, ACS Catal. 6 (2016) 2067.
17. D. D. Wagman, W. H. Evans, V. B. Parker, R. H. Schumm, I. Halow, S. M. Bailey, K. L. Churney, R. L. J. Nuttall, Phys. Chem. Ref. Data 11 (1982) 1.
18. J. Chao, R. C. Wilhoit, B. J. J. Zwolinski, Phys. Chem. Ref. Data 2 (1973) 427.
19. J. Chao, B. J. J. Zwolinski, Phys. Chem. Ref. Data 4 (1975) 251.
20. CRC Handbook of Chemistry and Physics; Haynes, W. M., ed.; CRC Press, 2012.
21. http://webbook.nist.gov/cgi/cbook.cgi?ID=C67630&Mask=1#Thermo-Gas (accessed 11/01/2016).
22. P. B. Weisz, C. D. Prater, Adv. Catal. 6 (1954) 143.
23. M. Boudart, Chem. Rev. 95 (1995) 661.
24. E. F. Kozhevnikova, I. V. Kozhevnikov, J. Catal. 224 (2004) 164.

25. J. Macht, M. Janik, M. Neurock, E. Iglesia, J. Am. Chem. Soc. 130 (2008) 10369.
26. T. Okuhara, N. Mizuno, M. Misono, Adv. Catal. 41 (1996) 113.
27. I. V. Kozhevnikov, Catalysis by Polyoxometalates, Wiley & Sons, Chippenham, 2002, 65.
28. R. A. Y. Jones, Physical and Mechanistic Organic Chemistry; Cambridge University Press: Cambridge, 1979, 227.

7. Conclusion

The aim of this study was to examine the gas phase hydrodeoxygenation (HDO) of a wide range of oxygenated compounds, such as ketones, ethers and esters, over bifunctional metal acid catalysis under mild conditions. These catalysts comprise Pt, Ru, Ni and Cu metals supported on heteropoly acids (HPA), particularly Cs salt of Keggin-type HPA ($H_3PW_{12}O_{40}$), $Cs_{2.5}H_{0.5}PW_{12}O_{40}$ (CsPW), which possesses strong proton acidity and high surface area. Therefore the main focus in our research was on the Pt–CsPW catalyst. Another target of this study was to investigate the effect of gold additives on activity and performance stability in HDO of a ketone, 3-pentanone, over Pt-CsPW. A variety of techniques were used to characterise these catalysts. These include BET, TGA, gas chemisorption, ammonia adsorption calorimetry. STEM-EDX, XRD, ICP, element analysis (C, H analysis) and FTIR.

In the HDO of ketones we found that:

- The hydrogenation of ketones on supported metal catalysts (e.g. Pt/C and Pd/C) to form alcohols is feasible, however, further hydrogenation to alkanes is rather difficult to achieve on such catalysts. The ketone-to-alkane hydrogenation can be achieved much more easily using bifunctional metal-acid catalysts.
- The bifunctional catalysed HDO of ketones to form alkanes in gas phase occurs via a sequence of steps involving hydrogenation of ketone to alcohol on metal sites followed by dehydration of alcohol to alkene on acid sites and finally hydrogenation of alkene to alkane on metal sites (Scheme 7.1).
- Catalyst activity was found to decrease in the order of metals: Pt > Ru >> Ni > Cu.
- 0.5%Pt/CsPW was demonstrated to be versatile catalyst for the hydrogenation of aliphatic ketones, giving almost 100% alkane yield at 100 ^{o}C and 1 bar pressure.

- Evidence was provided that the reaction with Pt/CsPW at 100 ^{o}C is limited by ketone-to-alcohol hydrogenation, whereas at lower temperatures (≤ 60 ^{o}C) by alcohol dehydration resulting in alcohol formation as the main product.
- The catalyst comprising of a physical mixture of 7%Pt/C + CsPW was found to be highly efficient as well, which indicates that the reaction is not limited by migration of intermediates between metal and acid sites in the bifunctional catalyst.
- The mixed 7%Pt/C + CsPW catalyst showed better performance stability in acetophenone hydrogenation (as an aromatic ketone) compared to the impregnated Pt/CsPW catalyst, which suffered from deactivation.

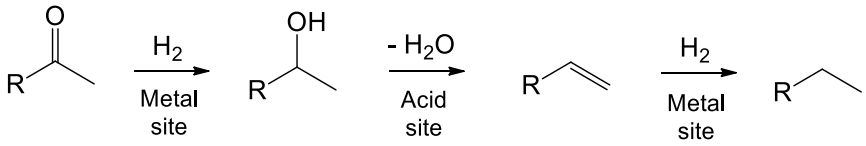

Scheme 7.1 Ketone hydrogenation via bifunctional metal-acid catalysis.

<u>In the investigation of the effect of gold additives on activity and performance stability in HDO of ketone, 3-pentanone, over Pt-CsPW, we found that:</u>

- Addition of gold increased the turnover rate of 3-pentanone HDO at Pt sites and decreased the rate of catalyst deactivation, although the gold itself was inert in this reaction.
- The activity enhancement also indicates the preference of the PtAu/CsPW catalysts toward hydrogenation of C=O bonds over C=C bonds in comparison with the unmodified Pt/CsPW.
- The Au enhancement appeared to be strongly dependent on catalyst formulation as well on the catalyst preparation method:
    - Carbon-supported Pt and Au physically mixed with CsPW solid acid failed to show any enhancement, whereas the metals directly supported onto CsPW did display the enhancement effect. This indicates importance of close proximity between

metal and proton active sites in the bifunctional metal-acid catalysts. This might also indicate a special role of the acidic CsPW polyoxometalate support, however there is no direct evidence for that as yet.

  - PtAu catalysts prepared by co-impregnation of metal precursors showed stronger enhancement effect in comparison with the catalysts prepared by sequential impregnation.

- STEM-EDX and XRD analysis indicates the presence of bimetallic nanoparticles with a wide range of Pt/Au atomic ratios in the PtAu/CsPW catalysts.
- The catalyst enhancement can be attributed to the two previously documented Au alloy effects, i.e., ensemble and ligand effects. These effects can modify the geometry and electronic state of Pt active sites to enhance their activity toward C=O bond hydrogenation and reduce catalyst poisoning.
- Overall, the results obtained confirm the view that the addition of Au is a promising methodology to enhance the HDO of biomass-derived feedstock using platinum group metal catalysts.

<u>In the HDO of ethers and esters, including the aromatic ether anisole, the aliphatic diisopropyl ether (DPE) and the aliphatic ester ethyl propanoate (EP), we found that:</u>

- Bifunctional metal-acid catalysis in the presence of H_2 was more efficient in comparison to the corresponding monofunctional metal and acid catalysis. Also we found that metal- and acid-catalysed pathways play a different role in these reactions.

<u>In the HDO of anisole we found that:</u>

- HDO of anisole with Pt-CsPW occurred with almost 100% yield of cyclohexane under very mild conditions at 60-100 ^{o}C and 1 bar H_2 pressure.

- In this reaction, Pt-catalysed hydrogenation played the key role, with a relatively moderate assistance of acid catalysis, further increasing the cyclohexane selectivity.
- The preferred catalyst formulation was a uniform physical mixture of Pt/C or Pt/SiO_2 with excess CsPW, with a Pt content of 0.1-0.5%, which provided much higher activity and better catalyst stability to deactivation as compared to the Pt/CsPW catalyst prepared by impregnation of platinum onto CsPW.
- The Pt/C + CsPW mixed catalyst showed the highest activity in anisole deoxygenation for a gas-phase catalyst system reported so far.

<u>In the decomposition of the aliphatic ether DPE:</u>

- DPE decomposed readily over CsPW via acid-catalysed pathway (E1 mechanism) without metal assistance to give propene and isopropanol, with propene selectivity increasing with reaction temperature at the expense of isopropanol.
- Platinum alone (Pt/C), in the absence of CsPW, was inactive in this reaction, either under H_2 or N_2. However, in the presence of Pt-CsPW under H_2, DPE decomposition was significantly accelerated, yielding the more thermodynamically favorable product propane instead of propene.

<u>In the decomposition of EP aliphatic ester:</u>

- Decomposition of the EP was very efficient via acid-catalysed pathway without metal assistance to yield ethene and propanoic acid.
- Addition of Pt to CsPW under H_2 caused hydrogenation of ethene to ethane but did not affect the rate of EP decomposition. Nevertheless, in EP decomposition, the Pt-CsPW bifunctional catalyst under H_2 showed much better performance stability compared to the CsPW acid catalyst, which can be attributed to reduction of catalyst coking in the presence of Pt and H_2.

- Kinetics of the acid-catalysed decomposition of DPE and EP was studied with a wide range of tungsten HPA catalysts. Good linear relationships between the logarithm of turnover reaction rate and the HPA catalyst acid strength represented by ammonia adsorption enthalpies was demonstrated, which can be used to predict the activity of other Brønsted acid catalysts in these reactions.

Future research on the HDO of organic oxygenates may be aimed at better understanding of reaction mechanisms. This can be achieved through catalyst characterisation and mechanistic studies. Another important issue is catalyst deactivation, which hampers the application of HDO. Therefore, investigation into catalyst deactivation and regeneration could lead to significant improvement of the HDO methodology.

7.1 References

1. M. A. Alotaibi, E. F. Kozhevnikova, I. V. Kozhevnikov, Chem. Commun. 48 (2012) 7194.
2. M. A. Alotaibi, E. F. Kozhevnikova, I. V. Kozhevnikov, J. Catal. 293 (2012) 141.
3. K. Alharbi, E. F. Kozhevnikova, I. V. Kozhevnikov, Appl. Catal. A 504 (2015) 457.
4. O. Poole, K. Alharbi, D. Belic, E. F. Kozhevnikova, I. V. Kozhevnikov, Appl. Catal. B 202 (2017) 446.
5. K. Alharbi, W. Alharbi, E. F. Kozhevnikova, I. V. Kozhevnikov, ACS Catal. 6 (2016) 2067.